2009

Modeling, identification and analysis of tractor and single axle towed implement system

Manoj Karkee
Iowa State University

Modeling, identification and analysis of tractor and single axle towed implement system

by

Manoj Karkee

A dissertation submitted to the graduate faculty

in partial fulfillment of the requirements for the degree of

DOCTOR OF PHILOSOPHY

Co-majors: Agricultural Engineering; Human Computer Interaction

Program of Study Committee:
Brian L. Steward, Major Professor
James E. Bernard
Stuart J. Birrell
Amy L. Kaleita
Lie Tang

Iowa State University

Ames, Iowa

2009

TABLE OF CONTENTS

LIST OF FIGURES

LIST OF TABLES

LIST OF VARIABLES

α	side slip angle or the angle between the direction the tire is going and the direction it is facing. The velocity vector to the right of the tire is positive and reverse is negative.
α_0	steady state side slip angle
γ	yaw rate
δ	steering angle
λ	angle between tractor heading and implement heading
σ	relaxation length
φ	heading angle
a	distance between front axle and CG of tractor
b	distance between rear axle and CG of tractor
c	distance between hitch point and CG of tractor
C_α	cornering stiffness
d	distance between hitch point and CG of implement
e	distance between rear axle and CG of implement
F	force
I_v, d_v and K_v	steering unit actuator parameters
I_z	yaw moment of inertia
i, j, and k	tractor body fixed orthogonal unit vectors.
L	wheelbase
l	distance of hitch point from rear wheel
$\overline{M}'$	Global sensitivity measure
m	mass
N	normal load to a tire
n	size of state (square) matrix A
p	parameter vector
Q	LQR controlled output penalty matrix
R	LQR control effort penalty matrix

R’	tire radius
r	turn radius of rear wheel
S	local sensitivity measure
U	system input
u	longitudinal velocity
$u_c(t)$	steering unit actuator input
V	velocity vector representing velocities in x, y and z axes
v	lateral velocity
ω	vector of three rotational speeds about x, y and z coordinate axes
X-Y-Z	world coordinates
X_c	control state vector
x’-y’-z’	vehicle coordinates
y	position of CG in y- axis of the world co-ordinate system

ACKNOWLEDGEMENTS

These past four years have been extremely exciting and challenging at the same time. These were the years when I learned perhaps the most valuable things in my life, not just those concepts written in the textbooks, but also those valuable life lessons. Many people helped me acquire these outstanding experiences and helped me be here with this dissertation. I would like to take this opportunity to extend my heartfelt gratitude and appreciation to all of them.

First and the foremost, I would like to extend my heartiest gratitude to my major professor, Dr. Brian Steward. I was fortunate to have a mentor like him who was always available and willing to help and support me; not only when I was doing well but also when I was facing setbacks. He was always there to guide, encourage and inspire me during both the smooth times and the rough times. His creativity, dynamism, knowledge and experience made so many difficult things possible; including this dissertation. I am also grateful to my POS committee members: Dr. James Bernard, Dr. Stuart Birrell, Dr. Amy Kaleita and Dr. Lie Tang for their efforts and contributions.

I would like to thank my colleague Dr. Samsuzana Abd Aziz for her creative inputs in the times they needed the most. I also want to thank James Bosserd II, another colleague, who provided valuable assistance in getting my early days in Iowa going, both personally and professionally. Many thanks to Kalyan Kappagantula and Zachery Kemp II for sharing so many memorable moments with me during the long hours of development and testing work in the VRAC office suite and Virtual Reality labs. I am also grateful to Dr. Atul Kelker for his guidance and contributions in the real-time simulation and visualization work.

I am also grateful to Dr. Matthew Darr, ABE faculty, for his guidance in constructing data collection equipment and Ryan Burnley, John Deere Urbandale, for helping me collect the experimental data, explain the results and letting me use his data collection equipments for many months. I would also like to thank Simon Nelson for helping me carry out the last field experiments.

At this moment, I would also like to recognize and appreciate the unconditional love and sacrifice of my mother Bhadrashila, my four brothers and my three sisters who have always been highly supportive of my never ending quest for new and advanced degrees. Specially, I want to dedicate this dissertation to my father Thir Bahadur, who had been the primary source of inspiration, strength and motivation for the first 27 years of my life; and he will remain the same forever even though he is not with me anymore. I would like to express my heartiest gratitude for his patience in helping me grow up and then letting me be educated. I was unable to grow as quickly and be educated fast enough to bring this moment to you as an ample source of smile on your face. Forgive me, if you are able to see me down from the heaven.

Last but not least, special thanks to my wife Rojee for her infinite love, patience, encouragement and support during these long and monotonous years for her while I have been dealing with the instability of graduate studies. I would not be here if it was not for you, and your understanding and sacrifice on the way to where I am today can never be paid off.

ABSTRACT

Increased and sustained agricultural productivity is a key to meet the globally increasing demands for food and energy. Automation of agricultural machinery is one of the ways to improve the efficiency and productivity of various field operations. Because a field implement performs most of these operations, accurate implement guidance is needed to reduce production cost, increase yield, and improve sustainability. Model-based guidance controller design and virtual prototyping techniques can be used in automatic guidance controller development to improve the accuracy and robustness of the guidance controller while reducing the development time and cost. Hence, development and analysis of accurate tractor and implement system models are needed to support automatic tractor and implement guidance controller development. Real-time vehicle model simulation capability allows engineers and users to intuitively interact with the realistic virtual prototypes and to evaluate the performance of physical hardware. As the model complexity is increased to improve the model accuracy and/or fidelity, the computational need will also increases thus increasing the challenge to meet real-time constraints. In this regard, it is important to minimize the computational load to a Virtual Reality (VR)-based real-time dynamics model simulation system.

In this dissertation, various strategies were investigated to reduce the computational burden on the dynamics model simulation so that real-time simulation could be achieved for increasingly complex models. A distributed architecture was developed for a virtual reality-based off-road vehicle real-time simulator to distribute the overall computational load of the system across multiple machines. Multi-rate model simulation was also used to simulate

various system dynamics with different integration time steps so that the computational power can be distributed more intelligently.

It is also important to study the trade-off between the model accuracy/fidelity and model complexity. Three different tractor-and-single-axle-towed-implement system models with varying degrees of fidelity, namely a kinematic model, a dynamic model, and a dynamic model with tire relaxation length, were developed, and the simulated transient and steady state responses were compared at various forward velocities and input frequencies. Both open and closed loop system characteristics were studied. Field experiments were also carried out to characterize the input-output relationship of the tractor-implement steering system. The responses from all three models were similar at lower forward velocities and with low frequency steering inputs (< 0.2 Hz). However, when the system was operated at higher forward velocities or with higher frequency steering inputs, the responses from the three models varied substantially. In this case, the dynamic model with tire relaxation length best represented the experimental system responses.

The system model contained various uncertain or varying parameters. It was important to understand and quantify the effect of parameter variation on system responses. Sensitivity analysis was used to identify the effect of variation in tire cornering stiffness, tire relaxation length, and implement inertial parameters on simulated system responses. Overall, the system was most sensitive to the tire cornering stiffness and least sensitive to the implement inertial parameters. In general, the uncertainty in the input parameters and the output variables were related in a non-linear fashion. At 4.5 m/s forward velocity, a 10% uncertainty in cornering stiffness caused a 2% average output uncertainty whereas a 50% uncertainty in cornering stiffness caused a 20% output uncertainty. Finally, a parameter

identification method was used to estimate the uncertain model parameters from measured field data. The accuracy of the model responses improved substantially when the model was simulated with the estimated parameters.

It was concluded that a dynamic model with tire relaxation length will represent a tractor and single axle towed implement system with reasonable accuracy. The study also helped improve the understanding of the relative importance of various model parameters, which will help to more judiciously allocate resources for estimating system parameters. Moreover, the analysis indicated that various vehicle parameters can be estimated with reasonable accuracy using a dynamic model, experimental data, and a parameter estimation method. The work will provide a framework for off-road vehicle and implement simulation through which engineers and scientists can determine to which parameters the system is most sensitive and how a model would perform with estimated model parameters.

CHAPTER 1. OVERVIEW

1.1 Introduction

Globally increasing demand for food, water and energy is one of the greatest challenges for the agricultural and natural resources scientists and engineers. Because arable land area is limited and shrinking due to increasing industrialization, urbanization, and soil degradation, improved and sustainable agricultural productivity becomes vital to meet the competing demands for food, water and energy. Agricultural production has very narrow profit margins and a slight improvement in productivity and efficiency will be a considerable help to farmers and growers who continuously labor to feed an increasing global population and fulfill increasing energy demands (Rekow, 2001). Efficient machinery systems have been and can be instrumental in improving the productivity and sustainability of farming systems.

Automation technologies is one important means for improving the agricultural efficiency and productivity and can be used to reduce energy and chemical inputs in such processes as tillage, planting, weed and pest control, soil and plant nutrient management, harvesting, processing, transporting and storage. Automating agricultural machinery system is particularly important to field operations such as tillage, planting, chemical input application, and harvesting. Accurate guidance of a tractor and an implement would result in a reduced row overlap in the farm, which will reduce the field operation time, input material, and fuel consumption thus reducing the production cost (Rekow, 2001) and improving the timeliness of field operations. In addition to the reduced row overlap, accurate implement

guidance also reduces row skips, improves accuracy of nutrients and chemicals application (Reid et al., 2000), and promotes more uniform utilization of inputs (Pierce and Nowak, 1999). As a result, precision implement guidance helps reduce the possibility of crop damage, reduce soil compaction and rutting, minimize the adverse effects of the overlapped or unwanted application of nutrients and chemicals, and improve the yield and sustainability of farming systems (Wright et al., 2006). .

Off-road vehicle automation technology has been developed for several decades. The use of the automatic guidance technology in the farms of North America has been growing steadily over the past several years (Whipker and Akridge, 2008). However, most of the automatic guidance controllers proposed or developed in the past used position and/or heading feedback from only the tractor mounted sensor(s) (Stombaugh et al., 1999; Bell, 2000, Reid et al., 2000). Because many field operations are performed using field implements, accurate guidance of the implement is equally or even more important than guiding the tractor (Karkee et al., 2007; Katupitiya and Eaton, 2008). Hence, a combined tractor and implement guidance system is one of the important guidance needs of the 21st century farm (Bevly, 2001; Pota et al., 2007).

Agricultural vehicles and implements must be operated in a semi-controlled environment as compared with the controlled environment associated with a factory in a manufacturing context. This environment is highly variable along both temporal and spatial dimensions (Scarlett, 2001; Hall and Lima, 2001). Spatially, the environment varies in terms of farm relief, terrain conditions, soil type and soil conditions (Katupitiya and Eaton, 2008; Metz, 1993). Temporally, soil and terrain conditions can vary substantially depending on the history of weather and farming activities.

In such an uncertain and unstructured environment, accuracy and robustness of agricultural guidance controllers should be improved to achieve precise field operations (Katupitiya and Eaton, 2008). To achieve an acceptable cultivator incursion probability with the use of an automatically steered vehicle, 1.5 cm guidance accuracy is required (Rekow, 2001). Because the goals that a guidance controller has to meet are challenging, it is essential to understand the dynamic behavior of the tractor and implement systems in various operating and field conditions to improve the accuracy, robustness and overall performance of the implement automatic guidance controller (Shim and Ghike, 2007; Pearson and Bevly, 2007; Rekow, 2001). In this regard, a tractor and implement model that can represent realistic steering behavior is essential to understand the system behavior and to develop a reliable guidance controller to follow complex field trajectories (Pearson and Bevly, 2007).

In addition, accurate off-road vehicle system models are becoming increasingly important as mechatronic engineers increasingly rely on model-based controller design and virtual prototyping (Karkee and Steward, 2008). Model-based controller design is a technique that uses a system model to represent the actual plant and wraps controller dynamics around the model. An analytical and simulation-based iterative design procedure is used to test controller accuracy and performance before developing physical prototypes and testing the controller with the actual physical system under real-world conditions (Zavala et al., 2004). With this approach, a relatively low cost simulation environment (as compared with the cost of physical prototyping and field tests) can be used to perform extensive tests on the control algorithm being developed.

Virtual Prototyping (VP) is defined differently across disciplines and industries. In manufacturing, VP may be referred to a process of developing, representing, analyzing, and

testing a soft or digital product model of an actual or planned physical product using simulation and realistic visualization tools (Pratt, 1995; Choi and Chan, 2004). For virtual prototyping to be useful in dynamic systems design and development, it should include three components: a dynamic systems modeling and simulation environment, a 3D geometric model, and a user interaction component. In recent years, Virtual Reality (VR) technology has been playing a key role in virtual prototyping, particularly in the area of providing a realistic environment for users to interact with the simulation system. Some literature have even defined VR to be an integrated component of VP (Gowda et al.,1999; Howard and Vance; 2007). Gowda et al. (1999) states "virtual prototyping is a relatively new technology which involves the use of virtual reality and other computer technologies to create digital prototypes." VR is a computer simulation of a system and its environment, which enables user to perform various system operations interactively in a realistic alternate world (Morris, 1992). VR technology uses computer graphics hardware and software to display a virtual environment allowing users to immersively interact with the system (Aguinis et al., 2001). VR-based simulation of dynamics models provides benefits of rapid prototyping, easier hardware and software controller performance testing, and convenience for studying user's perception and interaction with the new design (Cremer et al., 1996; Schulz et al., 1998; Kang et al., 2004; Castillo-Effen et al., 2005).

Collectively, model-based controller design and VP techniques provide control engineers a soft environment for automatic guidance controller design, prototype development, and performance testing early in the design cycle before going to the farm for extended field tests. The iterative guidance controller design process can be performed rapidly, which reduces the controller design cycle and development costs while decreasing

time to market. These techniques also help identify the critical problems very early in the controller development process. However, the effectiveness of these techniques depends on the accuracy of underlying system model. Hence, the development of accurate and realistic vehicle models that can be simulated in real-time has become very important (Shim and Ghike, 2007).

Real-time model simulation capability will add value to the model-based controller design and VP of dynamic systems by providing a realistic system with which engineers and users can interact. A system is said to be a real-time system if the correctness of the system responses depends on both the accuracy and timeliness of the computation (Stankovic, 1988). For real-time systems, even though a computation generates the correct system responses, the responses could be regarded as unsuccessful if they lag physical time (Glinsky and Wainer, 2002). Real-time simulation is important for intuitive interactions and qualitatively evaluations of system responses (Antonya and Talaba, 2007). Real-time simulation capability will also be valuable for operator-and-hardware-in-loop simulations. As off-road vehicle models become increasingly complex, improving model fidelity and accuracy requires increased computational resources. When computational requirements are high, real-time simulation may not be achieved, which will limit the usefulness of virtual prototyping.

In this research, various strategies were investigated to reduce the computational burden on the VR-based dynamics model simulation so that real-time simulation can be achieved for increasingly complex models. First, a distributed simulation architecture was developed for off-road vehicle dynamic models to distribute the overall computational load of the system across multiple machines. Second, a multi-rate model simulation technique was used to simulate various system dynamics with different integration time steps so that the

computational power can be distributed more intelligently. It is also important to study the trade-off between the model accuracy/fidelity and model complexity. Three different models of varying degrees of fidelity for a tractor and single axle towed implement system were developed and a comparative analysis of the accuracies of these models and experimental responses was performed to gain a better understanding of dynamic behavior of the system.

The trajectory of an off-road vehicle system depends on the lateral tire forces. Because the development of lateral tire force is highly dependent on soil parameters like internal friction angle, cohesion, cone index, and tire-soil friction, off-road vehicle responses will vary with different soil types (eg. clay, sand or loam), soil condition (e.g. density and moisture content), and soil surface cover (eg. bare soil, vegetation or stover) (Crolla and El-Razaz, 1987; Metz, 1993). Similarly, the responses also vary with variation in tire construction, size, inflation pressure and normal load (Schwanghart, 1968; Krick, 1973; Schwanghart and Rott, 1984; Raheman and Singh, 2004). It may be hard to estimate these variables accurately, and it is also hard to find a widely accepted model to relate these variables to the tire lateral force. The cornering stiffness coefficient, which is the slope of the lateral tire force as a function of side slip angle at zero side slip, is the parameter often used to represent the combined effect of these variables (Metz, 1993). Because the soil-tire parameters are uncertain, varying, and/or inaccurate, the cornering stiffness parameter also tends to be highly uncertain. Vehicle tire relaxation length, which is defined as the distance a tire rolls before the steady state side slip angle is reached, is another parameter that could be highly uncertain (Bevly et al., 2002). In the case of implements such as a grain cart or a sprayer, implement mass and moment of intertia (MI) may also be uncertain or may vary substantially over time.

These uncertain parameters will have an effect on the simulated response of the system, which often leads to unrealistic system responses and limits practitioners' confidence in the models and model-based studies (Kioustsioukis, et al. 2004). It is important to understand and quantify the effect of these parameter uncertainties or variations on the system response (Fales, 2004). Sensitivity analysis is one approach to identify and quantify these relationships (Xu and Gertner, 2007), which may help understand the accuracy of the model-based responses in representing the experimental system responses. A sensitivity analysis technique was presented in this research to identify the effect of system parameter uncertainty/variation on the system responses and to identify the most critical system parameters of a tractor and single axle towed implement system.

For the analytical models to be useful, their accuracy in representing the reality of the system has to be assessed extensively. When it comes to the model accuracy, two kinds of accuracies have to be considered; the accuracy of the mathematical representation of the system and the accuracy of the parameters used in the mathematical representation. Even though the two elements are independent of each other, they play a collective role in defining the accuracy of the model responses. The tractor and towed implement model will contain various soil-tire parameters that are difficult to measure accurately in the field. When the system responses are sensitive to model parameters, inaccuracies in the parameters will substantially affect the accuracy of the model responses. As a final component of this dissertation, a parameter estimation method was used along with the experimental data to improve the accuracy of various model parameters so that the accuracy of the model responses could be improved substantially.

This research work will provide a framework for off-road vehicle and implement simulation through which engineers and scientists can determine the parameters to which the system is most sensitive and how would a model performs with the estimated model parameters. This analysis will help engineers understand the relative significance of various system parameters so that more resources can be allocated to accurately estimate those parameters to which the system is most sensitive. The work will also provide a foundation for the development of effective and efficient implement guidance controller and for further research activities in the area of precision implement guidance (Pota et al., 2007). In addition, this study will be useful in real-time tractor and implement system simulation and virtual prototyping.

1.2 Research Questions

The following are the research questions the proposed work will attempt to answer:

I. A tractor and implement system will be operated in various field and operating conditions. How does the system behave over a range of forward velocities and input frequencies?

II. There are various system parameters that are uncertain and/or time-varying. To which parameters are the simulated model responses more sensitive? How do those uncertainties and variations affect the performance of a tractor and towed implement system?

III. Various model parameters such as the cornering stiffness coefficient and tire relaxation length will be highly uncertain. Can experimental data help improve the

estimation accuracy of those parameters and improve accuracy of the simulated response?

1.3 Research Objectives

The overall goal of the proposed research is to gain a better understanding of tractor and towed implement system dynamic behavior through model-based and experimental studies. To achieve this goal while answering the specific research questions outlined in the previous section, the work will focus on the study of the lateral dynamics of a tractor and wheeled implement (single axle grain cart) system. A single axle grain cart, which was available for experimental studies, was selected because it represents the general behavior of various wheeled implements while offering simplicity to the modeling and experimental data collection. More importantly, the cart was selected because it is an important field implement that will be used with various emerging automation techniques such as coordinated and autonomous guidance, which will improve the efficiency and productivity of various agricultural operations. The following are the specific objectives.

I. Investigate the steering responses of tractor and single axle towed implement system based on three models of varying degrees of fidelity and experimental data over a range of forward velocities,
II. Evaluate the effect of parameter uncertainties on the system responses and identify the parameters to which the model responses are most sensitive, and
III. Investigate a method for estimating the model parameters using experimental data and evaluate the performance of the analytical model.

1.4 Previous Work

Over the past several years, a virtual reality-based real-time hardware-and-operator-in-loop off-road vehicle simulation architecture was developed by a team of ISU researchers in collaboration with engineers of a major off-road equipment manufacturer (Ch. 4). The architecture provided a generic off-road vehicle modeling and simulation environment where new models can be added with minimal effort. Various models were developed for agricultural and construction machines including a tractor, a wheel loader and a backhoe. A PID controller was also developed for tractor automatic guidance. This project provided a good motivation and background to continue the work in off-road vehicle modeling, analysis and simulation. The experience with this project helped the team perceive the knowledge gap of how the uncertainties and/or variations in system parameters affect the steering responses of various off-road vehicles. Understanding the dynamics of a tractor and a towed implement system through model-based and experimental studies was found to be a particularly important problem, which will be essential to develop accurate and robust implement guidance controller.

To build a background for this research, a kinematic model-based PID guidance controller was developed for a tractor and single axle towed implement system and the transient and steady state performance were investigated using simulation results (Karkee et al., 2007). This work showed a promise for model-based implement guidance controller development and highlighted the importance of accurate tractor and implement system models. The work also helped identify the need to understand the relationship between the model complexity, which relates to the real-time computational requirement for real-time simulation, and the model fidelity and accuracy. Therefore, the work was continued to

develop and analyze tractor and single axle towed implement models of varying complexity and fidelity. To complement the analytical model-based studies, experimental trajectory data was collected in September, 2008 and again in July, 2009 using different types of steering inputs. The experimental data were used as a reference to compare three different models of varying degrees of fidelity, to estimate various model parameters, and validate model responses.

1.5 Organization of the Dissertation

This dissertation will follow the following organizational structure. An introduction to the research context was presented in this dissertation chapter (Ch. 1). Chapter Two will present a background to the general theories surrounding the dissertation work including the principles and concepts of vehicle dynamics, system identification, and sensitivity analysis. These principles and theories will be used in the subsequent chapters to develop various research methodologies. Three analytical models of a tractor and single axle towed implement system will be presented in Chapter Three. These models include a kinematic model, a dynamic model, and a dynamic model with tire relaxation length. This chapter will also develop steady state equations of the dynamic model and introduce the steering unit dynamics. Three papers submitted to peer-reviewed journals and one paper written for submission were developed based on the proposed research work. The dissertation will contain four major chapters (Ch. 4 – Ch. 7) to include those papers. The first research paper (Ch. 4) will introduce the general motivation behind this work and present different strategies on achieving real-time simulation with complex vehicle dynamics model and realistic virtual reality visualization. Analytical model-based analysis and comparison with experimental data

will be included in the second research paper (Ch. 5). This paper will focus on the effect of forward vehicle velocity on the system responses in open and closed loop configurations. Frequency responses will also be studied. The work done in the area of dynamic model sensitivity analysis and a study of the effect of the model parameter uncertainties on the system responses will be included in the third research paper (Ch. 6). System parameter estimation and model validation will be included in the fourth research paper presented in Ch. 7. General conclusions derived from the work and recommendations for the future work will be added as the final chapter (Ch. 8) of the dissertation.

References

Aguinis, H., C. A. Henle, and J. C. Beaty (2001). Virtual Reality Technology: A new Tool for Personal Selection. *International Journal of Selection and Assessment*, 9(1/2), 70-83.

Antonya, C., and D. Talaba (2007). Design evaluation and modification of mechanical systems in virtual environments. *Virtual Reality,* 11:275-285.

Bell, T. (2000). Automatic tractor guidance using carrier-phase differential GPS. *Computers and Electronics in Agriculture,* 25:53-66.

Bevly, D. M. (2001). High speed, dead reckoning, and towed implement control for automatically steered farm tractors using GPS. *PhD dissertation*, Stanford University.

Bevly, D. M., J. C. Gerdes, and B. W. Parkinson (2002). A new yaw dynamic model for improved high speed control of a farm tractor. *Journal of Dynamic Systems, Measurement, and Control*, 124: 659-667.

Choi, S. H., A. M. M. Chan (2004). A virtual prototyping system for rapid product development. *Computer-Aided Design,* 36: 401–412.

Castillo-Effen, M. W., C. Castillo, W. A. Moreno, and K. P. Valavanis (2005). Modeling and visualization of multiple autonomous heterogeneous vehicles. *In: Proceedings of the IEEE International Conference on Systems, Man and Cybernetics,* The Hague, The Netherlands, Oct 10-12, 2005.

Cremer, J., J. Kearney, Y. Papelis (1996) Driving simulation: challenges for VR technology. *IEEE Computer Graphics and Applications*, 16(5), 16-20

Crolla, D. A.; A. S. A. El-Razaz (1987). A review of the combined lateral and longitudinal force generation of tyres on deformable surfaces. *Journal of Terramechanics*, 24(3), 199-225.

Glinsky, E., and G. Wainer (2002). Definition of real-time simulation in the CD++ toolkit. *In Proceedings of the Summer Computer Simulation Conference*, July 14-18, San Diego, CA.

Gowda, S., S. Jayaram, and U. Jayaram (1999). Architectures for internet-based collaborative virtual prototyping. *Proceedings of the 1999 ASME Design Tehcnical Conference and Computers in Engineering Conference,* DETC99/CIE-9040, Las Vegas, Nevada, September 11-15.

Hall, S. G. and M. Lima (2001). Problem-solving approaches and philosophies in biological engineering: challenges from technical, social, and ethical arenas. *Transactions of the ASAE*, 44(4): 1037-1041.

Howard, B. M., and J. M. Vance (2007). Desktop haptic virtual assembly using physically based modelling. *Virtual Reality,* 11:207-215.

Kang, H. S., M. K. Abdul Jalil, and M. Mailah (2004). A PC-based driving simulator using virtual reality technology. *In: Proceedings of ACM SIGGRAPH international conference on Virtual Reality continuum and its applications in industry*, Singapore, June 16-18, 2004.

Karkee, M., B. L. Steward, and S. A. Aziz (2007). Distributed virtual reality assisted steering controller design for Off-road vehicle and implement tracking. *ASABE Paper No. 073006*. ASAE, St. Joseph, MI.

Karkee M., and B. L. Steward (2008). Open and Closed Loop System Characteristics of a Tractor and an Implement Dynamic Model. *ASABE Paper No. 084761*. ASABE, St. Joseph, MI; 2008.

Katupitiya, J., and R. Eaton (2008). Precision autonomous guidance of agricultural vehicles for future autonomous farming. *ASAE Paper # 084687.* ASABE, St. Joseph, MI.

Kioustsioukis, I., S. Tarantola, A. Saltelli, D. Gatelli (2004). Uncertainty and global sensitivity analysis of road transport emission estimates. *Atmospheric Environment,* 38:6609-6620.

Krick, G (1973). Behaviour of tyres driven in soft ground with side slip. *Journal of Terramechanics*, 9(4), 9-30.

Metz, L. D. (1993). Dynamics of four-wheel-steer off-highway vehicles. *SAE Paper No. 930765.* Warrendale, PA: SAE.

Morris, C. (1992). Academic press dictionary of science and technology. *Academic Press Inc.,* San Diego, USA.

Pearson, P., and D. V. Bevly (2007). Modeling and validation of hitch loading effects on tractor yaw dynamics. *Journal of Terramechanics,* 44: 439-450.

Pierce, F. J., P. Nowak (1999). Aspects of precision agriculture. *Advances in Agronomy*, 67: 1-70.

Pota, H., J. Katupitiya, and R. Eaton (2007). Simulation of a tractor-implement model under the influence of lateral disturbances. *IEEE Conference on Decision and Control,* New Orleans, LA, December 12-14, 2007.

Pratt, M. J. (1995). Virtual prototypes and product models in mechanical engineering. *Virtual Prototyping—Virtual Environments and the Product Design Process*, Chapman and Hall, London; 1995.

Raheman, H., and R. Singh (2004). Steering forces on undriven tractor wheel. *Journal of Terramechanics,* 40, 161-178.

Reid, J. F., Q. Zhang, N. Noguchi, and M. Dickson (2000). Agricultural automatic guidance research in North America. *Computers and Electronics in Agriculture*, 25: 155-167.

Rekow, A. (2001). System identification, adaptive control and formation driving of farm tractors. *PhD Dissertation,* Stanford University, USA.

Scarlett, A. J. (2001). Integrated control of agricultural tractors and implements: a review of potential opportunities relating to cultivation and crop establishment. *Computers and Electronics in Agriculture*, 30:167-191.

Schulz, M., T. Reuding, and T. Ertl (1998) Analyzing engineering simulations in a virtual environment. *IEEE Computer Graphics and Applications*, 18(6), 46 – 52

Schwanghart, H. (1968). Lateral forces of steered tyres in loose soil. *Journal of Terramechanics*, 5(1), 9-29.

Schwanghart, H., and K. Rott (1984). The influence of the tire tread on the rolling resistance and steering forces on undriven wheels. *In Proc. 8th International Conference of the Society of Terrain Vehicle Systems*, 855-888. Cambridge, UK: ISTVS.

Shim, T., and C. Ghike (2007). Understanding the limitations of vehicle model for roll dynamics study. *Vehicle System Dynamics-International Journal of Vehicle Mechanics and Mobility,* 45(3): 191-216.

Stankovic, J. 1988. Misconceptions about real time computing: a serious problem for next generation systems. *IEEE Computer Graphics and applications*, 21(10): 10-19.

Stombaugh, T. S., E. R. Benson, and J. W. Hummel (1999). Guidance control of agricultural vehicles at high field speeds. *Transactions of ASAE,* 42(2): 537-544.

Whipker, L. D., and J. T. Akridge (2008). Precision agricultural services dealership survey results. *Center for Food and Agricultural Business Department of Agricultural Economics, Purdue University,* Working Paper #08-09, September.

Wright, D. L., J. J. Marois and J. R. Rich (2006). Sustainability Aspects of Precision Agriculture for Row Crops in Florida and the Southeast U.S. *Series of the Agronomy Department, Florida Cooperative Extension Service, Institute of Food and Agricultural Sciences*, University of Florida, SS-AGR-184.

Xu, C., and G. Gertner (2007). Extending a global sensitivity analysis technique to models with correlated parameters. *Computational Statistics and Data Analysis*, 51, 5579-5590.

Zavala, C., P. Sanketi, D. Lamberson, A. R. Girard, and J. K. Hedrick (2004). Model-based real-time embedded control software for automotive torque management. *In proceedings of Real-Time and Embedded Technology and Applications Symposium (RTAS)*, May 25 - May 28, 2005, Le Royal Meridien, King Edward, Toronto, Canada.

CHAPTER 2. BACKGROUND

The work presented in this dissertation will be based on the fundamental principles and concepts of off-road vehicle dynamics. The work will extend on the depth and breadth analyzing the experimental and model-based responses to understand the steering dynamics behaviors of a tractor and single axle towed implement system. The system will be further studied to understand how the possible uncertainties in the system parameters will affect the system responses and to investigate if vehicle system model and experimental trajectory data can be used to estimate some of the system parameters which otherwise are difficult to measure in the field. This chapter will introduce the important principles and concepts in vehicle steering dynamics, sensitivity analysis, and parameter estimation to build a background on which the research methodologies will be developed to answer the research questions outlined in Chapter 1. First, the fundamentals of off-road vehicle steering dynamics will be introduced in Section 2.1. Section 2.2 will present the concepts and methods of parameter sensitivity analysis and Section 2.3 will provide an overview of parameter identification techniques.

2.1 Vehicle Dynamics

Vehicle dynamics refer to the position, velocity and/or acceleration responses of a conveyance in all possible degrees of freedom to various system inputs. In the broadest sense, a conveyance may include ships, airplanes, railroad trains, track laying vehicles as well as rubber tire ground vehicles (Gillespie, 1992). A ground vehicle can be classified as either an on-road or an off-road vehicle based on its primary area of operation, though the

fundamental principles of on-road and off-road vehicle dynamics are common. In general, an off-road vehicle may include all types of ground vehicles that primarily operate on unpaved land surfaces such as golf course turf, a limestone mine, a rugged forest land, a construction site, or an agricultural field. In some literature, the term *off-road vehicle* has been used to represent a relatively narrow set of recreational vehicles such as dune buggies, all-terrain vehicles, or four-wheel-drive pickup trucks that are capable of driving in both on and off-paved surfaces. Other vehicles such as agricultural tractors, loaders and bulldozers, which do not meet the public highway regulations of size and speed and operate mostly on unpaved surfaces, are generally termed as *off-highway* vehicles. However, the term *off-road vehicle* has also been used to indicate vehicles used in agricultural, construction, mining, and forestry industries (Schonberg et al., 1996; Granot, 2002; Guo and Zhang, 2002). This latter definition of *off-road vehicle* is used in this dissertation.

When the breadth of vehicle dynamics is considered, it is not possible to cover all background concepts in a dissertation chapter. In the context of this dissertation, only the horizontal cornering or directional dynamics of an off-road vehicle are considered and will be included in this subsection. Inherently, horizontal cornering dynamics are coupled with forward (along the vehicle's longitudinal axis), upward (along vehicle's vertical axis), pitch, and roll dynamics. In this work, forward velocity was assumed to be constant and the terrain surface was assumed to be flat so that the horizontal cornering dynamics could be decoupled from the whole system. A similar approach has commonly been used in research into the modeling, analysis and development of automatic guidance controller technology (O'Connor et al., 1996; O'Connor, 1997; Bell, 1999; Stombaugh et al., 1999; Bevly, 2001; Deng and Kang, 2003; Feng et al., 2005). Under these assumptions, the vehicle dynamics investigated

in this research included vehicle lateral and yaw position, velocity and/or acceleration responses to various steering inputs.

To study vehicle dynamics, a vehicle, which literally consists of thousands of components, is represented as a lumped mass located at its center of gravity (CG). This assumption is valid because the components move together as a single object when applied different steering, acceleration, and/or brake inputs (Gillespie, 1992). Two types of coordinate systems are used to define the vehicle motion: the vehicle coordinate system and the world coordinate system. In the vehicle coordinate system defined by Society of Automotive Engineers (SAE) Standard J670e, the vehicle CG is used as the origin with the x-axis pointing forward along the vehicle's longitudinal axis and the y-axis emerging from the right side of the vehicle. Yaw rate is defined as the rate of an angular rotation about the vertical axis. This coordinate system will be useful in defining forces, accelerations and velocities of the vehicle. In the world coordinate system, an arbitrary point in the world is selected as an origin. Geographic north is generally selected as positive X-axis and geographic east is selected as positive Y-axis. Vehicle position and heading are defined using the world coordinate systems. Heading angle is measured clockwise from the positive x-axis, which is also the geographic north, in general.

2.1.1 Vehicle Kinematic Model

In a vehicle kinematic model, the steered tires of a vehicle are assumed to be traveling in the direction they are facing. With this assumption, the system responses will have no acceleration states and the fidelity of transient behaviors will be compromised. In addition, the responses of a vehicle to a steering input are determined by only the geometric parameters. A prototypical example of an off-road vehicle is a farm tractor (Fig 2.1). Often

this type of vehicle can be represented with just one tire each in front and rear axle resulting in a so called bicycle vehicle model (Fig 2.2). The bicycle vehicle model neglects the load transfer between right and left wheels. This approach is widely used in off-road vehicle modeling as the effect of lateral load transfer on the lateral tire force development will not be substantial for a typical off-road velocity operation in flat terrain (O'Connor, 1997; Stombaugh et al., 1999; Bevly, 2001; Feng et al., 2005). Only front wheel steering was included in this analysis.

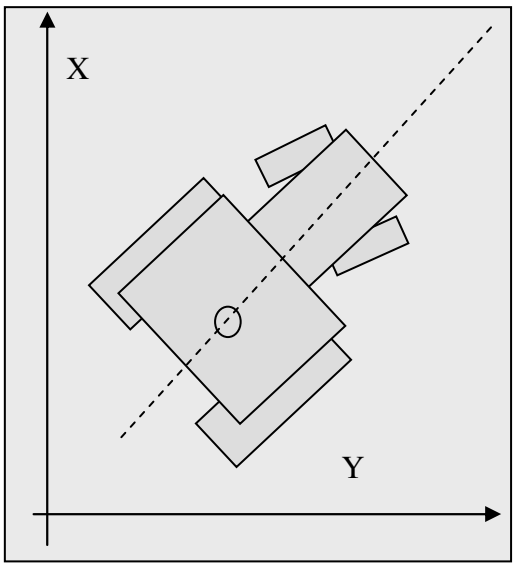

Fig. 2.1: Simplified representation of a tractor in a two dimensional world coordinate system.

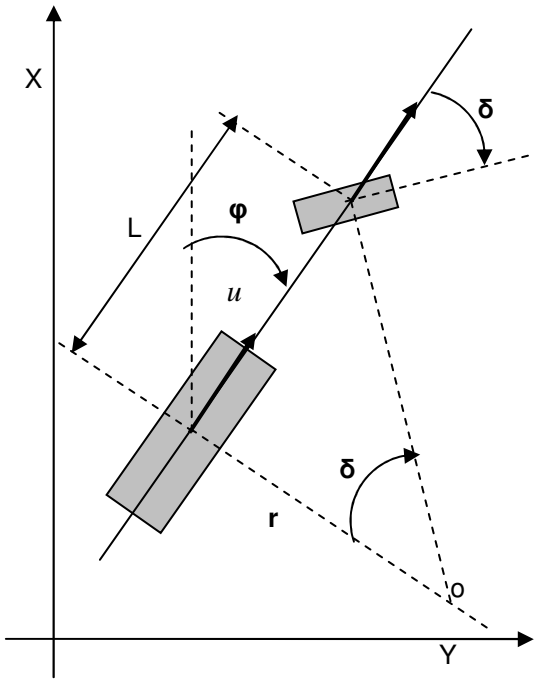

Fig. 2.2: Top view a vehicle modeled as a bicycle with geometric variables labeled. X-Y represents the world coordinate system.

Using the relationship between various geometric variables, the velocity of the vehicle CG in the world coordinate is given by,

$$\dot{x} = u\cos\varphi \qquad (2.1a)$$

$$\dot{y} = u\sin\varphi \qquad (2.2b)$$

where, u is the vehicle forward velocity and φ is the vehicle heading angle (i.e. angle between the world coordinate x-axis and the vehicle longitudinal axis). Assume that angle φ is small. This assumption will be valid when the model is used to follow a smooth trajectory with small absolute heading changes about a straight line. The assumption will be acceptable when the model is used to design a straight line path following controller. With more general applications of the model, φ should not be assumed to be small. This assumption is used to

linearize the model so that various analyses such as pole zero map analysis and Bode plot analysis can be performed easily. With this assumption,

$$\dot{x} = u \tag{2.1}$$

and,

$$\dot{y} = u\varphi \tag{2.2}$$

We also have,

$$\dot{\varphi} = \frac{u}{r} = \frac{u}{L}\tan\delta \tag{2.3a}$$

$\because r = \frac{L}{\tan\delta}$, where r is the turn radius, δ is the front steering angle, L is the wheel-base or the distance between front and rear axle (Fig. 2.2).

With the small angle linearization, Eq. 2.3a becomes,

$$\dot{\varphi} = \frac{u}{r} = \frac{u}{L}\delta \tag{2.3}$$

Eqs. 2.1, 2.2 and 2.3 represent the vehicle kinematic model consisting of the vehicle CG position and vehicle heading states defined in the world coordinate system. The model is restricted to small steering angle and small absolute changes in the heading angle about a straight line. Eqs. 2.1, 2.2 and 2.3 should be replaced by 2.1a, 2.2a and 2.3a for more general trajectory operations.

2.1.2 Vehicle Dynamic Model

In a vehicle dynamic model, tire lateral forces are used to excite the lateral and yaw dynamics of the system. Newton's second law of motion is applied to construct the force and moment balance so that the lateral and yaw dynamics model equations can be established.

Summation of forces in the y-direction of the vehicle coordinate system and summation of moments about the vehicle CG will give the following dynamic vehicle model equations (Fig. 2.3).

$$m(\dot{v} + ur) = F_{y,f} + F_{y,r} \tag{2.4}$$

$$I\dot{r} = aF_{y,f} - bF_{y,r} \tag{2.5}$$

where, m is vehicle mass, v is lateral velocity, $F_{y,f}$ is front tire lateral force, $F_{y,r}$ is rear tire lateral force, I is vehicle yaw moment of inertia (MI), a is the distance between the front axle and the vehicle CG and b is the distance between the rear axle and the vehicle CG.

The vehicle CG trajectory in the world coordinate system is then defined by,

$$\dot{x} = u\cos\varphi - v\sin\varphi \tag{2.6a}$$

$$\dot{y} = u\sin\varphi + v\cos\varphi \tag{2.7a}$$

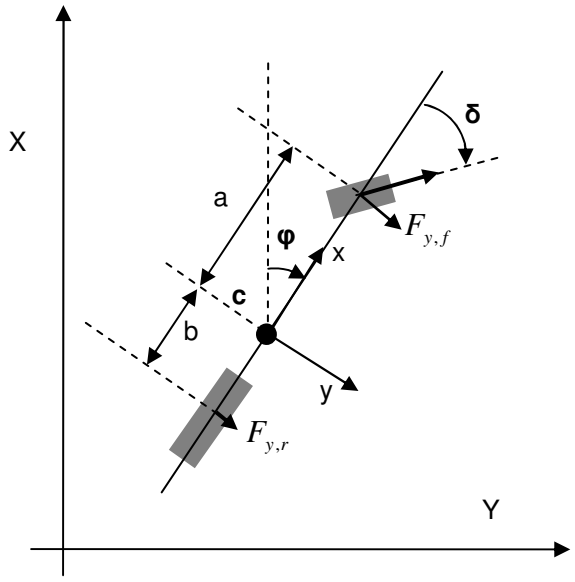

Fig. 2.3: Dynamics of a vehicle. X-Y constitutes the world coordinate system whereas x-y constitutes the vehicle coordinate system.

As discussed above, angle φ can be assumed to be small. With this assumption, equation 2.6 becomes

$$\dot{x} = u - v\varphi$$

which after further linearization about zero lateral velocity v and zero heading angle φ becomes

$$\dot{x} = u \tag{2.6}$$

and,

$$\dot{y} = u\varphi + v \tag{2.7}$$

where,

$$\dot{\varphi} = r \tag{2.8}$$

2.1.3 Lateral Tire Force

It was assumed in the kinematic model that the vehicle tires will move in the direction they are facing. In reality, a vehicle tire, when subjected to a steering side force, does not move to the direction it is facing resulting to an angular difference between the two directions (Wong, 2001). This angle of difference is called the side slip angle (Fig. 2.4). Vehicle tires go through some level of deformation when they move to a direction different than the direction they are facing (Fig. 2.4a). This deformation produces sheer stress in the tire-ground contact patch. In case of off-road vehicle systems, the ground surface is most often a soil surface. The stress developed in the soil-tire interface causes some level of lateral soil deformation as well (Metz, 1993). The lateral soil deformation releases part of the shear stress developed in the interface, and the resultant shear stress will generate a force at the contact patch called lateral tire force or cornering force (Crolla and El-Razaz, 1987). This force will act in the direction perpendicular to the wheel's longitudinal axis (Fig. 2.4a).

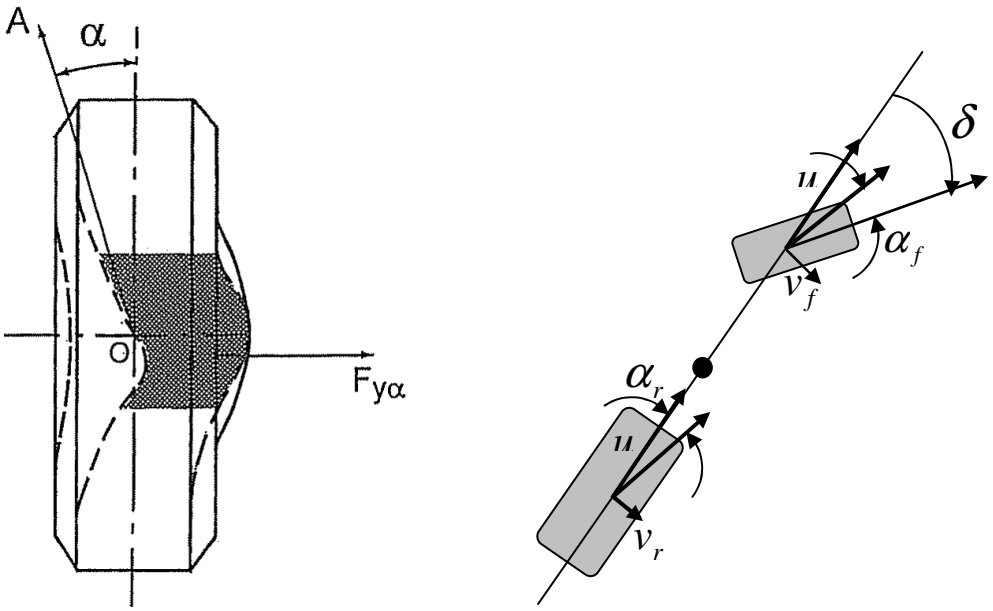

a) b)

Fig. 2.4: Behavior of a tire subject to a side force. a) Top view of a deformed tire under the application of a side force (Wong, 2001), b) Front and rear tire side slip angles for a bicycle vehicle model. A side slip angle is defined as the angle between the direction a tire is moving and the direction it is facing.

In addition to tire and lateral soil deformation, the phenomena such as tire soil friction and soil sinkage effects also affect the characteristics of lateral tire force development (Metz, 1993). Because most of these phenomena are dependent on soil properties such as internal friction angle, cohesion, cone index, and tire-ground surface friction, the lateral tire forces and thus the off-road vehicle responses will vary with different soil types (eg. clay, sand or loam), soil condition (e.g. soil shear strength, density, moisture content), and soil surface cover (eg. bare soil, vegetation or stover) (Crolla and El-Razaz, 1987). In addition, the responses may vary with the variation in tire construction, size, inflation pressure and normal

load (Schwanghart, 1968; Krick, 1973; Schwanghart and Rott, 1984; Raheman and Singh, 2004). Empirical and semi-empirical models have been proposed to describe the relationship between tire side slip angle and the tire lateral force coefficient (LFC; Fig. 2.5), which indirectly account for the variation in soil and tire parameters (Schwanghart and Rott, 1984; Crolla and El-Razaz, 1987; Metz, 1993). LFC is defined as the ratio between the lateral tire force and the normal load on the tire. When the steering input applied to the vehicle and the vehicle forward velocity are relatively small, the lateral forces require to laterally accelerate and yaw the vehicle will be small. In this case, the tire side slip angles will also be small and a linearized tire model will be a good approximation to the non-linear models. In the linear approximation, the slope of the non-linear model curve at origin called the cornering coefficient (C_c) is used to relate the side slip angle to the LFC.

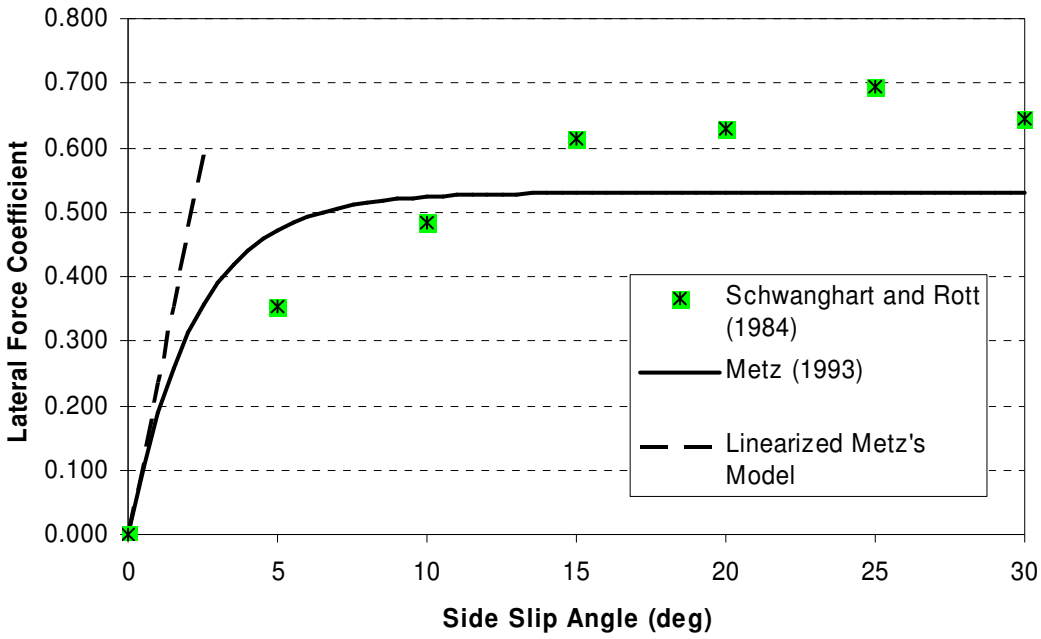

Fig. 2.5: A vehicle tire lateral force coefficient (LFC) for a corn field with various tire models. When the side slip angle is smaller than 2°, the linear model approximates the non-liner model fairly accurately.

Frequently, another coefficient called the cornering stiffness coefficient is used instead of the cornering coefficient, which is calculated as,

$$C_\alpha = N * C_c \tag{2.9}$$

where, N is the normal tire load and C_α is the cornering stiffness coefficient.

Based on this linear model, the lateral force developed by the tire is then given by,

$$F_y = -C_\alpha \alpha \tag{2.10}$$

where, α is the tire side slip angle. By definition (Fig. 2.4b), the front tire side slip angle can be calculated as,

$$\tan\left[\delta - \left(-\alpha_f\right)\right] = \frac{v_f}{u} \tag{2.11}$$

and the rear tire side slip angle is calculated as,

$$\tan\left(\alpha_r\right) = \frac{v_r}{u} \tag{2.12}$$

For small side slip angles,

$$\alpha_f + \delta = \frac{v_f}{u}$$

$$\text{or, } \alpha_f = \frac{v_f}{u} - \delta$$

$$\text{or, } \alpha_f = \frac{v + ar}{u} - \delta \quad \because v_f = v + ar \tag{2.13}$$

$$\text{and, } \alpha_r = \frac{v_r}{u} \tag{2.14}$$

$$\text{or, } \alpha_r = \frac{v - br}{u} \qquad \because v_r = v - br \tag{2.15}$$

From eqs. 2.4, 2.10, 2.13 and 2.15,

$$m\dot{v} + mur = -C_{\alpha,f}\frac{v+ar}{u} + C_{\alpha,f}\delta - C_{\alpha,r}\frac{v-br}{u}$$

From eqs. 2.5, 2.10, 2.13 and 2.15,

$$I\dot{r} = -aC_{\alpha,f}\frac{v+ar}{u} + aC_{\alpha,f}\delta + bC_{\alpha,r}\frac{v-br}{u}$$

Rearranging the terms results in two state equations,

$$\dot{v} = -\frac{1}{mu}\left(C_{\alpha,f} + C_{\alpha,r}\right)v - \frac{1}{mu}\left(aC_{\alpha,f} - bC_{\alpha,r} + mu^2\right)r + \frac{C_{\alpha,f}}{m}\delta \tag{2.16}$$

$$\dot{r} = -\frac{1}{Iu}\left(aC_{\alpha,f} - bC_{\alpha,r}\right)v - \frac{1}{Iu}\left(a^2C_{\alpha,f} + b^2C_{\alpha,r}\right)r + \frac{aC_{\alpha,f}}{I}\delta \tag{2.17}$$

Eqs. 2.16, 2.17, 2.6, 2.7, and 2.8 represent the yaw-plane dynamics model of a front wheel steered vehicle. This model was developed using a small angle assumption and bicycle approach. Therefore the responses will be valid for only small side slip angles operations in flat terrain. In general, this model can be used to represent any kind of two axle wheeled ground vehicles. The set of geometric and inertial parameters used in the model will differentiate the vehicles being represented. The model can be used to simulate the vehicle responses with different field conditions by adjusting the cornering stiffness parameters C_α as desired. The model can also be used as a plant in designing and testing automatic guidance controllers. Other possible applications could be operator-and-hardware-in-loop real-time simulation and virtual prototyping. However, eqs. 2.6 and 2.7 should be replaced by 2.6a and 2.7a in those general applications. The model development process demonstrated in this section will be used in Chapter 3 to develop a complete tractor and single axle grain cart system dynamics model.

2.2 Sensitivity Analysis

Sensitivity analysis is used to quantify the dependence of the system behavior on various system parameter variations (Rodriguez-Fernandez and J.R. Banga, 2009). The system could be a dynamic system represented by a set of differential equations, a static system represented by a set of algebraic equations or a hybrid system represented by a set of differential-algebraic equations (DAE). By principle, a sensitivity analysis method calculates the rate of change in the system output(s) with respect to changes in the system input parameter(s). If the rate of change of an output variable is large with respect to (w.r.t.) a parameter, the output is said to be more sensitive to that parameter and if the rate of change is small, it is said to be less sensitive. The aggregated sensitivities across the system outputs may be used as a measure of system's sensitivity to the parameters of interest. The results from a system sensitivity analysis can be used in a variety of ways. Some of the important applications of sensitivity analysis include (Isukapalli, 1999; Rodriguez-Fernandez and Banga, 2009).

- Validating system models and evaluating their applicability.
- Suggesting the accuracy to which the parameters must be estimated.
- Understanding the behavior of the system being modeled.
- Suggesting new experiments or guiding future data collection efforts.

Various sensitivity analysis techniques have been proposed in the literature to calculate sensitivity measures or indices. Based on the scope of the sensitivity measures, these methods can be classified into local and global sensitivity analysis methods. *Local sensitivity analysis* focuses on the estimation of system sensitivity in the vicinity of a predefined point in the parameter space. A partial derivative of the system model with

respect to (w.r.t.) a parameter at a particular location in the parameter space is a good example of a local sensitivity measure. This measure will be valuable in studying the parameter uncertainty about a nominal point or a point of interest. On the other hand, *global sensitivity analysis* covers the entire expected parameter range to define an overall sensitivity of the system to a parameter of interest. This type of sensitivity is important to identify the overall ranking of parameters within the parameter space as the method accounts for the interaction between correlated parameters (Kucherenko et al., 2009).

Based on the mathematical formulation of sensitivity measures, sensitivity analysis methods can broadly be classified into

1) variance-based methods,

2) screening methods, and

3) derivative-based methods.

In the variance-based methods, the contribution of a model parameter to the output variance is estimated (Kioutsioukis et al., 2004). Some of the widely used variance based methods are Fourier Amplitude Sensitivity Test (FAST) (Cukier et al., 1973; McRae et al., 1982), the extended FAST (Saltelli et al., 1999) and the method of Sobol (Sobol, 1993). The drawback of the variance-based methods is their computational inefficiency requiring a large number of function evaluations to calculate the sensitivity with a reasonable accuracy (Kucherenko et al., 2009). Screening methods are used to qualitatively rank the model parameters from the most influential to the least influential order. These methods are computationally attractive, but are less accurate (Kucherenko et al., 2009). The method of Morris (Morris, 1991) is one of such methods.

Derivative-based methods take the first order differentiation of the model outputs with respect to the model parameters. Local and global sensitivity measures are defined based on those derivatives. Jang and Han (1995) and Kucherenko et al. (2009), among others, have proposed and used derivative-based methods. Kucherenko et al. (2009) used the method to analyze sensitivity of seven algebraic equations and compared the results with those from the method of Sobol and Morris. The derivative-based sensitivity analysis method was more accurate than the screening method and was computationally efficient than the variance based methods. In addition, derivative-based method provides both local and global sensitivity measures within the same framework. Because both local and global sensitivities are of interest, the derivative-based sensitivity analysis method will be used in this dissertation to study the sensitivity of a tractor and single axle towed implement model to various system parameters. Moreover, derivative-based sensitivity analysis method is preferred over other methods in analyzing dynamic models (Jang and Han, 1997; Park et al., 2003; Ruta and Wojcicki, 2003; Eberhard et al., 2007). Hence this method will be an appropriate choice to study the tractor and towed implement dynamic system model. In the following subsection, the derivative-based sensitivity analysis method is explained with the help of a vehicle model.

2.2.1 Derivative-based Sensitivity Analysis

The first step in a derivative-based sensitivity analysis is to take a partial derivative of the system model with respect to various model parameters to define a first order derivative-based sensitivity. When the derivative is evaluated at a particular location in the parameter space, it is called a derivative-based local sensitivity. The derivative can also be evaluated over the entire variation of the input parameters to get an aggregated sensitivity measure

called the global sensitivity. The concept of derivative-based sensitivity analysis is further elaborated with the example of the vehicle dynamic model developed in sections 2.1.2 and 2.1.3. The model equations for the lateral vehicle dynamics are,

$$\dot{v} = -\frac{1}{mu}\left(C_{\alpha,f} + C_{\alpha,r}\right)v - \frac{1}{mu}\left(aC_{\alpha,f} - bC_{\alpha,r} + mu^2\right)r + \frac{C_{\alpha,f}}{m}\delta \tag{2.20}$$

$$\dot{r} = -\frac{1}{Iu}\left(aC_{\alpha,f} - bC_{\alpha,r}\right)v - \frac{1}{Iu}\left(a^2C_{\alpha,f} + b^2C_{\alpha,r}\right)r + \frac{aC_{\alpha,f}}{I}\delta \tag{2.21}$$

$$\dot{\varphi} = r \tag{2.22}$$

$$\dot{y} = u\varphi + v \tag{2.23}$$

The equation can be represented as,

$$\dot{z} = \begin{bmatrix} \dot{v} \\ \dot{r} \\ \dot{\varphi} \\ \dot{y} \end{bmatrix} = \begin{bmatrix} -\frac{1}{mu}\left(C_{\alpha,f} + C_{\alpha,r}\right)v - \frac{1}{mu}\left(aC_{\alpha,f} - bC_{\alpha,r} + mu^2\right)r + \frac{C_{\alpha,f}}{m}\delta \\ -\frac{1}{Iu}\left(aC_{\alpha,f} - bC_{\alpha,r}\right)v - \frac{1}{Iu}\left(a^2C_{\alpha,f} + b^2C_{\alpha,r}\right)r + \frac{aC_{\alpha,f}}{I}\delta \\ r \\ v + u\varphi \end{bmatrix} \tag{2.24}$$

In general form, the dynamic system such as eq. 2.24 can be represented as,

$$\dot{z} = f(z, p, t) \tag{2.25}$$

where, p is the model parameter vector given by,

$$p = \begin{bmatrix} a & b & m & I & C_{\alpha,f} & C_{\alpha,r} \end{bmatrix}^T$$

The derivative-based state sensitivities with respect to these parameters can be represented as (Jang and Han, 1997),

$$\frac{\partial \dot{z}}{\partial p} = \frac{\partial f}{\partial z} \cdot \frac{\partial z}{\partial p} + \frac{\partial f}{\partial p} \tag{2.26}$$

In this sensitivity equation, $\frac{\partial z}{\partial p}$ is the state sensitivity matrix and $\frac{\partial f}{\partial z}$ is the state matrix, A, given by,

$$A = \begin{bmatrix} -\frac{1}{mu}\left(C_{\alpha,f} + C_{\alpha,r}\right) & -\frac{1}{mu}\left(aC_{\alpha,f} - bC_{\alpha,r} + mu^2\right) & 0 & 0 \\ -\frac{1}{Iu}\left(aC_{\alpha,f} - bC_{\alpha,r}\right) & -\frac{1}{Iu}\left(a^2C_{\alpha,f} + b^2C_{\alpha,r}\right) & 0 & 0 \\ 1 & 0 & 0 & u \\ 0 & 1 & 0 & 0 \end{bmatrix}$$

Assuming only the sensitivities with respect to $C_{\alpha,f}$ and $C_{\alpha,r}$ are desired, the term $\frac{\partial f}{\partial p}$ is given by:

$$\frac{\partial f}{\partial p} = \begin{bmatrix} \frac{\partial f}{\partial C_{\alpha,f}} & \frac{\partial f}{\partial C_{\alpha,r}} \end{bmatrix}^T \tag{2.27}$$

where,

$$\frac{\partial f}{\partial C_{\alpha,f}} = \begin{bmatrix} -\frac{1}{mu}v - \frac{a}{mu}r + \frac{1}{m}\delta \\ -\frac{a}{Iu}v - \frac{a^2}{Iu}r + \frac{a}{I}\delta \\ 0 \\ 0 \end{bmatrix} \tag{2.28}$$

and $$\frac{\partial f}{\partial C_{\alpha,r}} = \begin{bmatrix} -\frac{1}{mu}v + \frac{b}{mu}r \\ \frac{a}{Iu}v - \frac{b^2}{Iu}r \\ 0 \\ 0 \end{bmatrix} \tag{2.29}$$

The local sensitivity of the individual system states at a given point in the parameter is given by equation 2.26. The overall local sensitivities can be calculated by averaging the individual state sensitivities. To calculate the global sensitivity, an uncertainty or variation range for each parameter is defined. For example, the cornering stiffness parameters can be assumed to vary by ±100% about the nominal values. Then, a number of points are selected

from the parameter space to calculate the global sensitivity. One way to select points could be to divide the parameter space into regular grids. If a grid size of 5% of the parameter range is assumed, the whole parameter space will consists of 20*20 = 400 points for the parameter space defined by the front and rear cornering stiffness parameters. Local sensitivities are calculated at each of the 400 points and then averaged to get the global sensitivity. This method of local and global sensitivity analysis will be used in this dissertation (Chap. 6) to study the sensitivity of a tractor and single axle towed implement model to various system parameters.

2.3 System Identification

System identification is a process of defining or improving a mathematical representation or a model of a physical system from experimental input/output data (Juang, 1994). Engineers work with systems and processes governed by physical, chemical, biological, economic and/or physiological principles. To understand the behavior, modify the functionality, and control the operation of these systems or processes, they must be represented in an understandable way, which is most often a set of mathematical equations called a system model (Van den Bosch and Van der Klauw, 1994). However, often times these systems and processes are very complex and the underlying physical, chemical, biological or other principles are unknown or are difficult to define from first principles. In such situations, it will be valuable to develop dynamic models from the experimental data using system identification processes.

For continuous systems, a generalized system identification process can be used to identify the system dynamics described by the input-output data (Fig. 2.6). As the preparation

for the system identification data collection, the system of interest is first broken down into various subsystems in such a way that each subsystem has a range of continuous operation (if possible). Then, inputs and outputs of interest are identified for each subsystem before actual data collection can be started. The next step in the system identification process is to capture *good* and *sufficient* input-output experimental data. The meaning of *good* and *sufficient* data may vary from system to system. Generally, a good set of data should include a wide range of input frequencies to excite all possible system frequencies, should be sampled at a rate twice as fast as the highest input frequency, above the Nyquist sampling rate, and should include both transient and steady state responses. To have a sufficient set of experimental data, experiments should be conducted with different combinations of inputs for a multiple input system and all output signals must be acquired.

The next step is to select a system identification method from the set of time domain techniques (eg. Observer-Kalman Filter Identification Algorithm or OKID) or frequency domain techniques (e.g. Eigensystem Realization Algorithm or ERA). Further details on these system identification techniques can be found in Ljung, (1999), Juang (1994), and Van den Bosch and Van der Klauw (1994) among others.

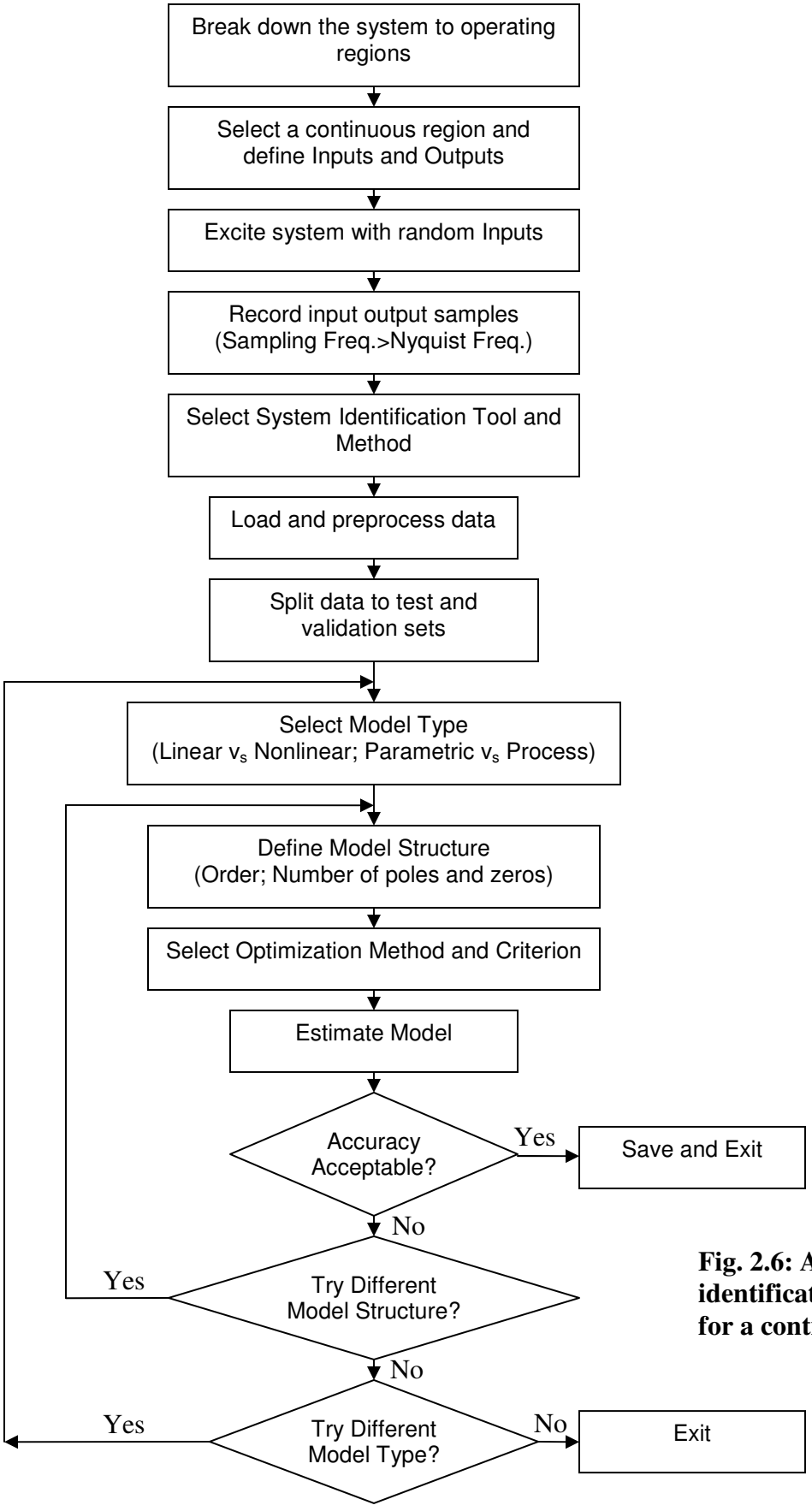

Fig. 2.6: A generic system identification flow chart for a continuous system.

Based on the availability of data and the method selected, a Fast Fourier Transform (FFT) or an inverse FFT may have to be used to convert the time domain data to frequency domain or vice-versa. Next, the experimental data is divided into test and validation sets so that the identified models can be validated against the data that has not been used in the identification process. Then, various model structures, model order and optimization methods (see sub-section 2.3.1) are tested iteratively to identify a model. At the end of each iteration, model performance will be evaluated, and if the performance does not meet the requirements, the process is repeated. Once the model with desired accuracy is identified, the model representation can be changed as per the requirement. For example, based on the identification method selected, the identified model may be in discrete time representation, which may have to be converted to continuous time representation for further analysis.

Sometimes, identifying a dynamic model from just the input-output data becomes difficult without knowing the underlying physical phenomenon particularly when the system consists of non-linearities and discontinuities. In other situations, the mathematical representation could either be available or developing one could be relatively straight forward, but estimating/measuring parameters associated with those models could be challenging. In such situations, it may be more beneficial to use experimental data to improve a system model rather than to identify one. A system identification technique is applied in several ways to improve the overall accuracy of an analytical model. The *overall accuracy* refers to the accuracy of the model responses in representing the actual responses considering both the accuracy of the mathematical structure of the model and the accuracy of the model parameters. The following three bullet points are the widely used techniques to improve the overall model accuracy (Juang, 1994).

- Estimation of uncertain model parameters using experimental data,
- Refinement of analytical model structure, and
- Identification and addition of a noise model.

System identification can be used to estimate model parameters which may otherwise be difficult to estimate accurately. This technique will help to improve the accuracy of the model responses in representing the experimental responses of the system. System identification methods can also be used to iteratively refine the mathematical representation of the model so that the model-based responses will represent the experimental responses more accurately. Finally, a noise model can be estimated from the experimental data and added to the system. The noise model will describe the input-output noise contained in the experimental data so that the model-based responses will represent the experimental responses more accurately. In this research, a parameter identification method was used to estimate various uncertain parameters of the tractor and single axle grain cart system model. In the following sub-section, this parameter identification method is introduced in more details.

2.3.1 Parameter Identification Method

If a mathematical representation of a physical system is available, a parameter identification method can be used to estimate various model parameters from the experimental data. This so-called white box system identification technique will be useful in many scenarios including when the system is non-linear and discontinuous. This method also provides an opportunity to estimate model parameters that could otherwise be difficult or even impossible to estimate with reasonable accuracy if no model exists. Parameter estimation using experimental data is essential to improve the overall accuracy of the model

and model-based studies. To discuss the process of parameter identification, a simple mass-spring-damper system is introduced as follows (Fig. 2.7).

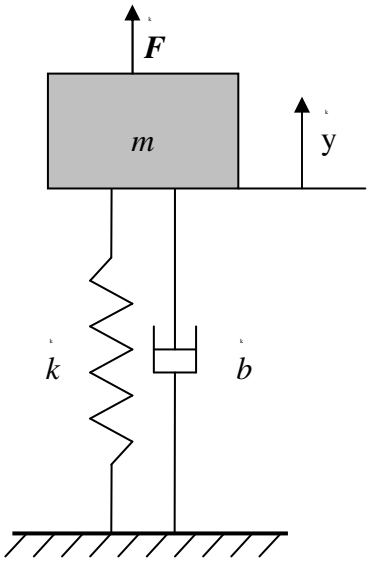

Fig. 2.7: A mass-spring-damper system; *m* is the mass, *k* is the spring constant, and *b* is the damping coefficient.

A free-body analysis will lead to the following second order dynamic model relating the vertical force F to the vertical position y, measured from the equilibrium position, for the mass m.

$$m\ddot{y} + b\dot{y} + ky = F \tag{2.18}$$

Now, we have a dynamic model of the system developed from first principles. It may not be difficult to measure the mass m but it could be difficult to measure the spring constant k and the damping coefficient b of the system with reasonable accuracy. However, if some input force $\boldsymbol{F}$ can be applied to the system and the vertical position y of the mass can be measured for a sufficiently long time, parameters b and k can be estimated so that the model-based response best represents the experimental response. Assuming the mass-spring-damper system has underdamped dynamics, the step input transient response will oscillate about the

steady state value (Fig. 2.8). The dynamics of the above example were simulated with some arbitrary values of *b* and *k* with white noise of zero mean and a standard deviation of 0.02 m added to the output as measurement noise. Assuming that the parameters *b* and *k* were unknown, an initial guess of b = 0.5 N-s/m and k = 8 N/m was made. The simulated model response with the initial parameter values was substantially different than the measured responses (Fig. 2.8a).

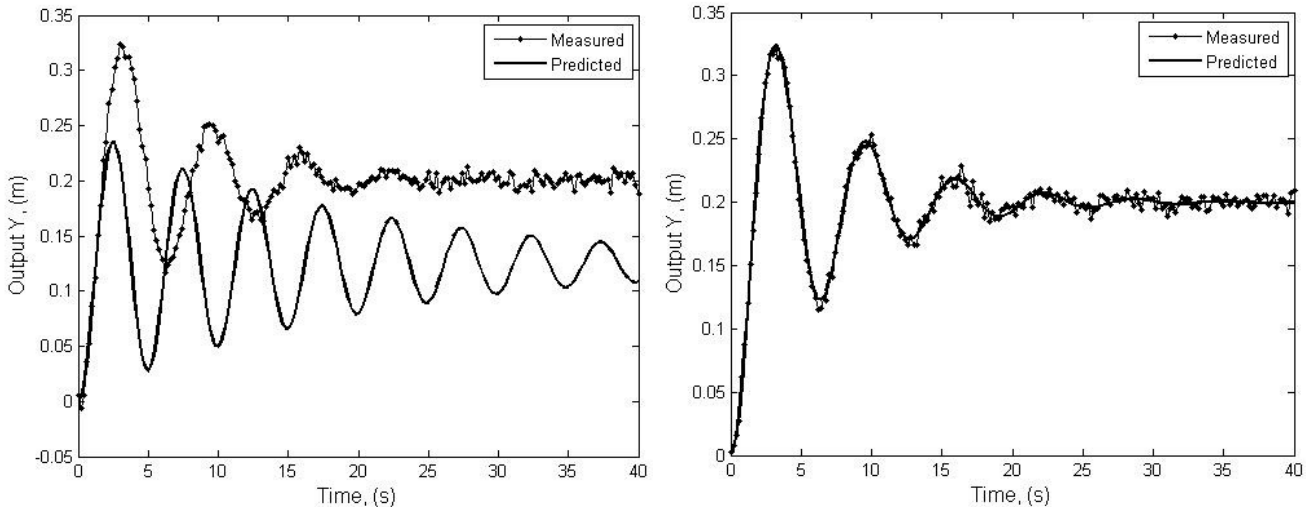

a) **b)**

Fig. 2.8: Measured v_s predicted output; a) with initial guesses of parameter *b* and *k,* and (b) with parameters estimated using the PEM.

Parameter identification method is an iterative optimization process used to adjust the model parameters so that the model response will closely represent the experimental response. Given the initial values for the unknown parameters, an optimization technique was used to adjust the parameters so that the difference between the predicted and actual output(s) was minimized. Because the objective of the optimization process is to minimize the prediction error, the method is called Prediction Error Minimization (PEM) method. Various

optimization techniques are available in the literature. In the PEM paradigm, only a specific case of the optimization problem, minimization, is encountered. Gradient decent, which is also called steepest decent, is a widely used first-order search method for minimizing a function. This method finds the direction of the steepest slope at the current location in the search surface and moves down the hill by a small step each time. Most often, the move size will be proportional to the extent of the slope called the gradient. The Gauss-Newton and Levenberg-Marquardt methods are also widely used to solve minimization problems. For further reading on optimization and search methods, the reader is referred to Elster (1993), Nocedal and Wright (2006) and Yang (2008) among others.

The function being optimized is called an objective function. In this example, an RMSE was used as the objective function as given by,

$$\varepsilon = \sqrt{\frac{\sum_{t=t_1}^{t_N} \left(y(t) - \hat{y}(t, \hat{k}, \hat{b}) \right)^2}{N}} \tag{2.19}$$

where, t is simulation time, t_1 is simulation start time, t_N is simulation end time, N is number of simulation steps, $y(t)$ is measured output, and $\hat{y}(t, \hat{k}, \hat{b})$ is predicted output.

The optimization routine minimizes this objective function with respect to parameters k and b. In this example, the model parameter values were set to b being 1.5 N-s/m and k was 5 N/m. Levenberg-Marquardt optimization method was used to minimize the objective function, which resulted to the final estimates of b = 1.48 N-s/m and k = 5.05 N/m. The model response with the estimated parameters represented the measured response reasonably accurately (Fig. 2.8b). The numerical solution of the objective function also showed that the estimated parameters corresponded to the minimum value of the objective function (Fig. 2.9).

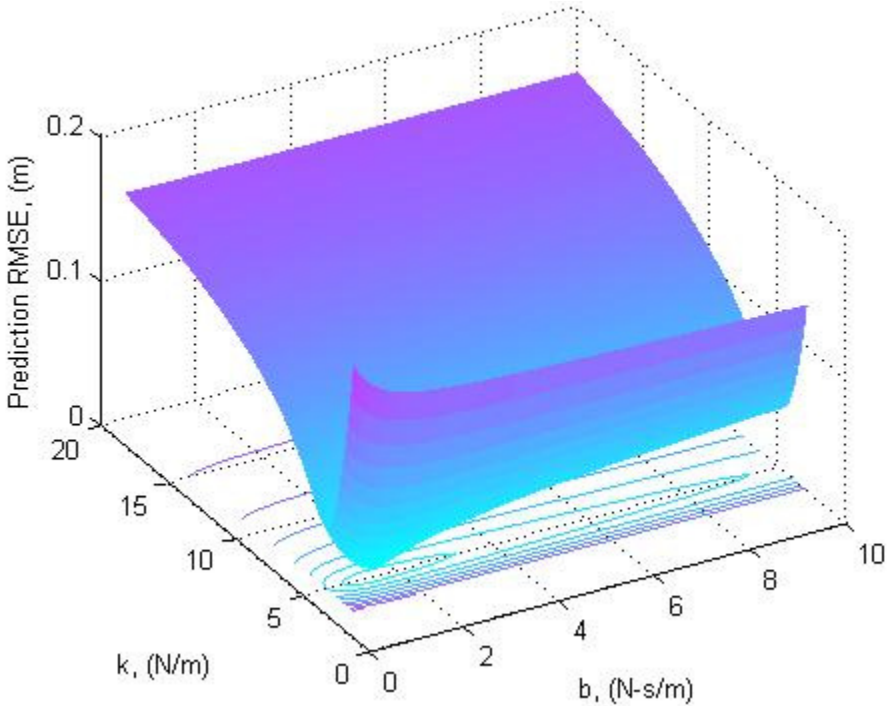

Fig. 2.9: The PEM objective function over a parameter space defined by the ranges of the parameters *b* and *k*.

References

Bell, T. (1999). Precision robotic control of agricultural vehicles on realistic farm trajectory. *PhD dissertation,* Stanford University.

Crolla, D. A., and A. S. A. El-Razaz (1987). A review of the combined lateral and longitudinal force generation of tyres on deformable surfaces. *Journal of Terramechanics*, 24(3), 199-225.

Cukier, R. I., C. M. Fortuin, K. E. Shuler, A. G. Petschek, and J. H. Schaibly (1973). Study of the sensitivity of coupled reaction system to uncertainties in rate coefficients - I: Theory. *Journal of Chemical Physics*, 59, 3873-3878.

Deng, W., and X. Kang (2003). Parametric study on vehicle-trailer dynamics for stability control. *SAE Transactions, Journol of Passenger Cars*, 2003, 411-1419.

Eberhard, P., W. Schiehlen; and J. Sierts (2007). Sensitivity analysis of inertial parameters in multibody dynamics simulations. *Twelfth IFToMM World Congress*, Besancon, France, June 18-21, 2007.

Elster, K. H. (1993). Modern Mathematical Methods of Optimization. Hoboken, NJ: *Wiley-VCH Publications*.

Feng, L., Y. He, Y. Bao, and H. Fang (2005). Development of trajectory model for a tractor-implement system for automated navigation applications. *Instrumentation and Measurement Technology Conference*, Ottawa, Canada, May 17-19, 2005.

Gillespie, T. D. (1992). Fundamentals of vehicle dynamics. Warrendale, P. A., USA: *Society of Automotive Engineers Inc*.

Granot, R. (2002). Architecture for human supervised autonomously controlled off-road equipment. *Proc of Automation Technology for Off-Road Equipment (ATOE) Conference,* July 6-7, 2002. Chicago, IL, USA.

Guo, L. S., and Q. Zhang (2002). A wireless LAN for collaborative off-road vehicle automation. *Proc of Automation Technology for Off-Road Equipment (ATOE) Conference*, July 6-7, Chicago, IL, USA.

Isukapalli, S. S. (1999). Uncertainty analysis of transport-transformation models. PhD Dissertation, The State University of New Jersey.

Jang, J. H., and C. S. Han (1997). The state sensitivity analysis of the front wheel steering vehicle. *KSME International Journal,* 11(6), 595-604.

Juang, J. N. (1994). Applied system identification. Englewood Cliffs, NJ: *Prentice-Hall.*

Kioutsioukis, I., S. Tarantola; A. Saltelli; and D. Gatelli (2004). Uncertainty and global sensitivity analysis of road transport emission estimates. *Atmospheric Environment*, 38, 6609-6620.

Krick, G. (1973). Behaviour of tyres driven in soft ground with side slip. *Journal of Terramechanics*, 9(4), 9-30.

Kucherenko, S., M. Rodriguez-Fernandez; C. Pantelides; N.Shah (2009). Monte Carlo evaluation of derivative-based global sensitivity measures. *Reliability Engineering and System Safety,* article in press.

Ljung, L (1999). System Identification: Theory for the User, Englewood Cliffs, NJ: *Prentice-Hall*.

McRae, G. J., J. W. Tilden, and J. H. Seinfield (1982). Global sensitivity analysis-a computational implementation of the Fourier amplitude sensitivity test (FAST). *Computational Chemical Engineering*, 6, 15-25.

Metz, L. D. (1993). Dynamics of four-wheel-steer off-highway vehicles. *SAE Paper No. 930765.* Warrendale, PA: SAE.

Morris, M. D. (1991). Factorial sampling plan for preliminary computational experiments. *Technometrics,* 33, 161-174.

Nocedal, J., and S. J. Wright (2006). Numerical Optimization. . New York, N.Y., USA: *Springer*.

O'Connor, M., T. Bell, G. Elkaim, and B. Parkinson (1996). Automatic steering of farm vehicles using GPS. *Third International Conference on Precision Agriculture. Minneapolis*, MN, June 23–26.

O'Connor, M. L (1997). Carrier-phase differential GPS for automatic control of land vehicles. *PhD thesis*, Stanford University.

Park, T. J., C. S. Han, and J. H. Jang (2003). Dynamic sensitivity analysis for the pantograph of a high-speed rail vehicle. *Journal of Sound and Vibration*, 266, 235-260.

Raheman, H., and R. Singh (2004). Steering forces on undriven tractor wheel. *Journal of Terramechanics*, 40, 161-178.

Rodriguez-Fernandez, M., and R. Banga (2009). Global sensitivity analysis of a biochemical pathway model. *Advances in Soft Computing, Springer-Verlag,* Berlin, Heidelberg.

Ruta, P., Z. Wojcicki (2003). Sensitivity analysis applied to a dynamic railroad model. *Journal of Sound and Vibration*, 266, 1-13.

Saltelli, A., S. Tarantola, and K. Chan (1999): A quantitive model-independent method for global sensitivity analysis of model output. *Technometrics,* 41(1), 39-56.

Schonberg, T., M. Ojala, J. Suomela, A. Torpo, and A. Halme (1996). Positioning an autonomous off-road vehicle by using fused DGPS and inertial navigation. *International Journal of Systems Science*, 27(8): 745 – 752.

Schwanghart, H. (1968). Lateral forces of steered tyres in loose soil. *Journal of Terramechanics*, 5(1), 9-29.

Schwanghart, H., and K. Rott (1984). The influence of the tire tread on the rolling resistance and steering forces on undriven wheels. *In Proc. 8th International Conference of the Society of Terrain Vehicle Systems,* 855-888. Cambridge, UK: ISTVS.

Sobol, I. M. (2001). Global sensitivity indices for nonlinear mathematical models and their Monte Carlo estimates. *Mathematics and Computer Simulations*, 55, 271-280.

Van den Bosch, P., and A. Van der Klauw (1994). Modeling, Identification and Simulation of Dynamical Systems. London, UK: *Taylor & Francis LLC*.

Wong, J. Y. (2001). Theory of ground vehicles. New York, N.Y., USA.: *John Wiley & Sons Ltd.*

Yang, X. S. (2008). Introduction to Mathematical Optimization: From Linear Programming to Metaheuristics. Cambridge, UK: *Cambridge International Science Publishing.*

CHAPTER 3. VEHICLE MODELS

3.1 Introduction

Various tractor and trailer steering models have been proposed in the literature for both off-road (Bell, 1999; Feng et al., 2005) and on-road (El-Gindy, 1989; Torishu et al. 1992; Deng and Kang, 2003) operations. Several models with varying degrees of fidelity and complexity were developed in this work for a tractor and grain cart system (Fig. 3.1). The tractor and implement rigid bodies were linked by a revolute joint at the hitch point (Feng et al., 2005). The tractor and the implement velocities were coupled to each other using the constraint caused by the joint. The system was constrained to only allow yawing and lateral motion with a constant forward tractor velocity. Common vehicle dynamics symbols were used to describe the dynamics of the tractor-and-implement system (see the list of the variables).

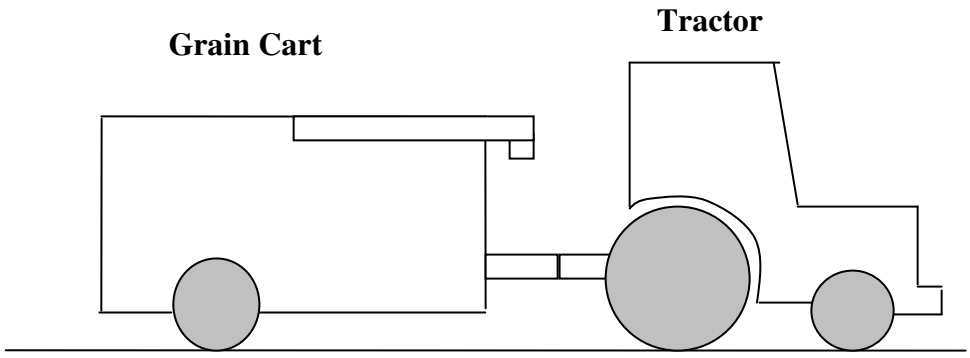

(a)

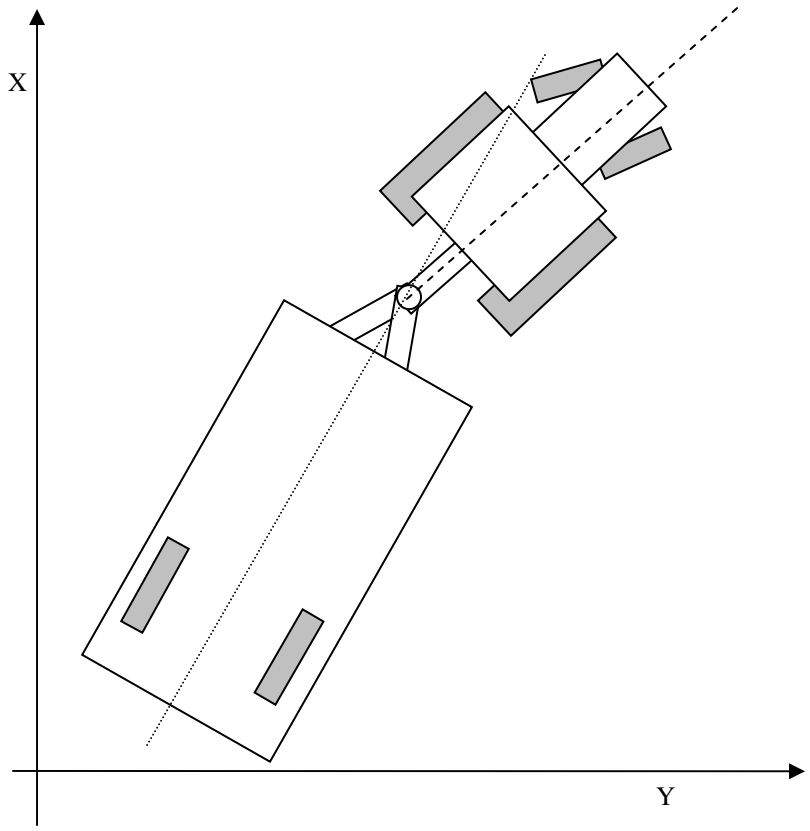

(b)

Fig. 3.1: A tractor and grain cart system geometry; a) side view, b) top view.

Subscript and superscript notations were used to specify various attributes associated with the vehicle dynamics variables used in this Chapter (Table 3.1). One superscript was used to denote whether the variable was related to the tractor or to the implement. There were two subscripts used in the notation. The first subscript specified the coordinate axis to which the variable was corresponded. The second subscript specified the location in the vehicle system to which the variable corresponded. The first and second subscripts were separated by a comma.

Table 3.1: Subscript and superscript notation for the vehicle dynamics variables.

Notation	Symbol	Description
Superscript	t	Tractor
	I	Implement
Subscript 1	x	x-axis
	y	y-axis
	z	z-axis
Subscript 2	f	front wheel
	r	rear wheel
	c	center of gravity
	p	hitch point

3.2 Kinematic Model

A kinematic steering model of the tractor and single axle towed implement system was used to simulate the motion of the system on an agricultural field with front wheel steering angle input (Fig. 3.2). It was called a kinematic model because the model did not include the physical quantities like mass and a dynamic force balance in the equations of motion. The motion of the system was described using only the geometric variables of the system. Therefore, it was assumed that the vehicle tires will all move in the direction they are facing, that is, there is no lateral tire slip in this model. The kinematic model represents the dominant steering dynamics of the tractor and the implement while providing a model that is easily comprehended and not complex. Additional dynamics will add higher order responses to the system, which will be included in the dynamic model and the dynamic model with tire relaxation length that follow in subsequent sections.

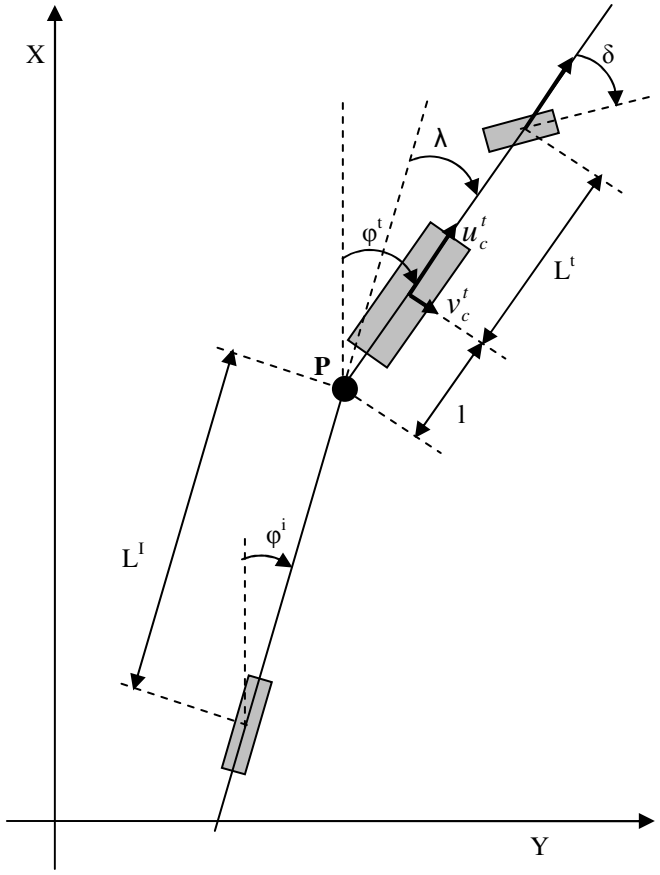

Fig. 3.2: Bicycle representation of the top view of a tractor and single axle towed implement system. X-Y defines the world coordinated system.

Based on the kinematic relationships of a bicycle tractor model (Fig. 3.3), the velocity of the tractor in x and y-directions of the global co-ordinate system is given by,

$$\dot{x}_c^t = u_c^t \cos\varphi^t - v_c^t \sin\varphi^t \tag{3.1}$$

$$\dot{y}_c^t = v_c^t \cos\varphi^t + u_c^t \sin\varphi^t \tag{3.2}$$

where, $v_c^t = b\dot{\varphi}^t$

And, yaw rate is given by,

$$\dot{\varphi}^t = \frac{u_c^t}{r} = \frac{u_c^t}{L^t}\tan\delta \tag{3.3}$$

$$\because r = \frac{L^t}{\tan\delta}$$

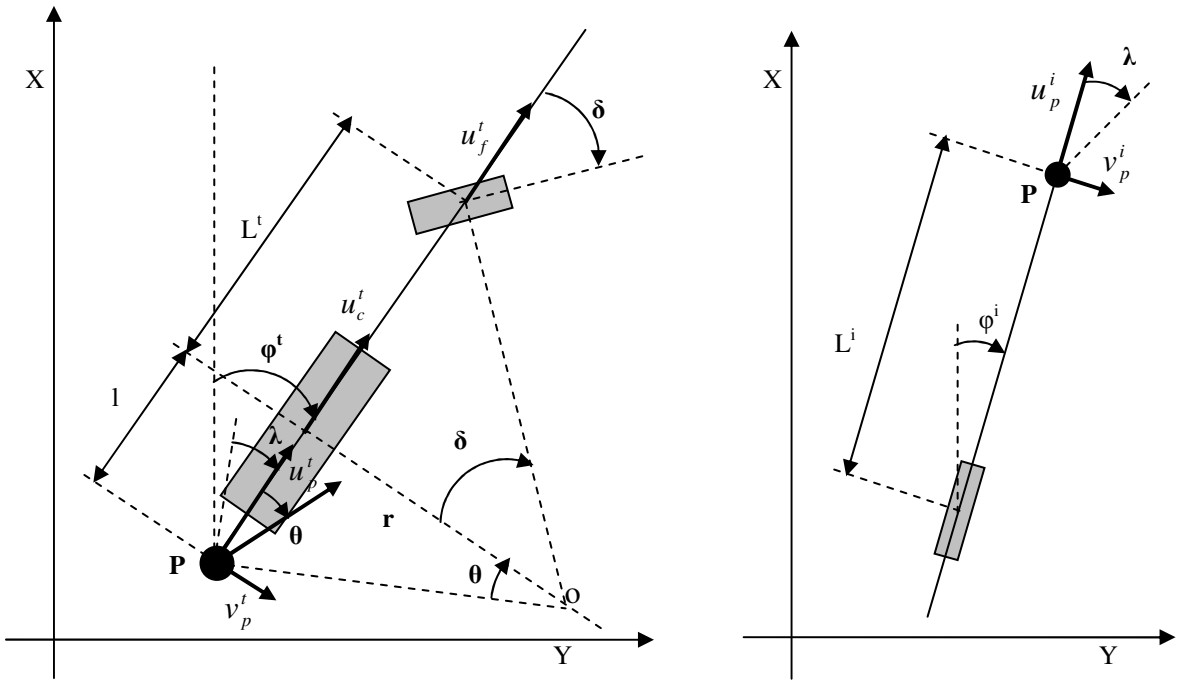

a) b)

Fig. 3.3: Resolving velocities at hitch point; a) velocities at the hitch point of the tractor, b) velocities at the pivot point of the towed implement

Because the tractor yaw motion is centered at the rear wheel axle, the hitch point will have a lateral velocity in the direction opposite to the lateral velocity of the CG. The lateral velocity caused by this motion is given by,

$$v_p^t = u_p^t \tan\theta \qquad (3.4)$$

where, θ = angle between the resultant velocity and forward velocity at hitch point

or, $$v_p^t = u_p^t \frac{l}{r} = \frac{u_p^t l}{L^t}\tan\delta = \frac{u_c^t l}{L^t}\tan\delta \quad \because r = \frac{L^t}{\tan\delta} \qquad (3.5)$$

$$\because u_p^t = u_c^t$$

Based on the kinematics of the bicycle tractor and implement model (Fig. 3.3), longitudinal and lateral velocities of the implement at hitch point are given by,

$$u_p^i = u_p^t \cos\lambda - v_p^t \sin\lambda = u_c^t \cos\lambda - v_p^t \sin\lambda \tag{3.6}$$

$$v_p^i = u_p^t \sin\lambda + v_p^t \cos\lambda = u_c^t \sin\lambda + v_p^t \cos\lambda \tag{3.7}$$

And, yaw rate of the implement is given by

$$\begin{aligned}\dot{\varphi}^i &= \frac{v_p^i}{L^i} \\ &= \frac{1}{L^i}\left(u_c^t \sin\lambda - v_p^t \cos\lambda\right) \\ &= \frac{1}{L^i} u_c^t \sin\lambda - \frac{u_c^t l}{L^t L^i} \tan\delta \cos\lambda \\ &= \frac{1}{L^i} u_c^t \sin\lambda - \frac{l}{L^t L^i} u_c^t \tan\delta \cos\lambda \end{aligned} \tag{3.8}$$

One can assume angles λ, δ, and φ^t are small since for a small steering angles, both λ and δ will remain small. The assumption of a small heading angle, φ^t, will be valid when the model is used to follow a smooth trajectory with small absolute heading changes about a straight line. This assumption will be acceptable when the model is used to design a straight line path following controller; with more general application of the model, then φ^t should not be assumed small. These assumptions are used to linearize the model so that various analytical analyses could be performed. With these assumptions, the state equations (Eqs. 3.2, 3.3 and 3.8) become,

$$\dot{y}_c^t = u_c^t \varphi^t + v_c^t \tag{3.9}$$

$$\dot{\varphi}^t = \frac{u_c^t}{L^t}\delta \tag{3.10}$$

$$\dot{\varphi}^i = \frac{1}{L^i} u_c^t \lambda - \frac{l}{L^t L^i} u_c^t \delta \tag{3.11}$$

where, $\lambda = \varphi^t - \varphi^i$ (3.12)

Using eq. (3.12), eq. (3.13) can be re-written as,

$$\dot{\varphi}^i = \frac{u_c^t}{L^i} \varphi^t - \frac{u_c^t}{L^i} \varphi^i - \frac{u_c^t l}{L^t L^i} \delta \tag{3.13}$$

Using eqs. 3.9, 3.10 and 3.13, the state space form representation of the system is,

$$\begin{aligned} \dot{X} &= AX + BU \\ Y &= CX + DU \end{aligned} \tag{3.14}$$

where,

$$\dot{X} = \begin{bmatrix} \dot{y}_c^t \\ \dot{\varphi}^t \\ \dot{\varphi}^i \end{bmatrix}, \quad X = \begin{bmatrix} y_c^t \\ \varphi^t \\ \varphi^i \end{bmatrix}, \quad U = \begin{bmatrix} \delta \end{bmatrix}$$

$$A = \begin{bmatrix} 0 & u_c^t & 0 \\ 0 & 0 & 0 \\ 0 & \frac{u_c^t}{L^i} & -\frac{u_c^t}{L^i} \end{bmatrix} \tag{3.15}$$

$$B = \begin{bmatrix} 0 & \frac{u_c^t}{L^t} & -\frac{u_c^t l}{L^t L^i} \end{bmatrix}^T \tag{3.16}$$

To get all three states as outputs,

$$C = \begin{bmatrix} 1 & 0 & 0 \\ 0 & 1 & 0 \\ 0 & 0 & 1 \end{bmatrix} \tag{3.17}$$

$$D = \begin{bmatrix} 0 & 0 & 0 \end{bmatrix}^T \tag{3.18}$$

This kinematic model (Eq. 3.14) represented the three positional states of the system, which constituted the dominant dynamics of the tractor and the single axle towed implement system. Both tractor heading and position dynamics have pure integrators, which means the dynamics are neutrally stable.

The system eqs. 3.9, 3.10 and 3.11 can also be represented in transfer function form as follows,

$$\frac{\Psi(s)}{\Delta(s)} = \frac{u_c^t}{L^t s} \tag{3.19}$$

$$\frac{Y(s)}{\Delta(s)} = \frac{u_c^t}{L^t s^2} \tag{3.20}$$

$$\frac{\Psi_I(s)}{\Delta(s)} = \frac{\frac{u_c^t l}{L^i}\left(-s + \frac{u_c^t}{l}\right)}{L^t s\left(s + \frac{u_c^t}{L^i}\right)} \tag{3.21}$$

The transfer function relating the tractor heading to the steering angle has one pole at the origin (Eq. 3.19). The heading angle will thus have a ramp response for a step steering angle. Similarly, the transfer function relating tractor position to steering angle has two poles at the origin (Eq. 3.20), and will thus have a parabolic response to a step input. The implement heading transfer function also has one pole at the origin (Eq. 3.21). The implement heading dynamics have another pole at $-V/L_I$, which shows that the implement angle will exhibit a first-order response with a time constant of L_I/V and follow the path of the tractor when pulled forward by the tractor. In addition, this transfer functions has a zero in the right-half plane at V/L_H, which is due to the fact that the pivot point of the implement (or the hitch point) is located behind the tractor rear axle (Bell, 1999).

These three positional states will also remain in the dynamic and dynamic with tire relaxation length models to be developed in the following subsections. The simulated responses from this kinematic model will be compared with those of the other models and also with experimental responses. This work will help identify the operating conditions where this model will be a realistic representation of vehicle-cart trajectories.

3.3 Dynamic Model

In this study, a dynamic steering model was developed for a tractor-and- single-axle-towed-implement system (called tractor-and-implement system in the text to follow, Fig. 3.4). The model development approach was similar to that of Feng et al. (2005) but had some important differences in the approach which were necessary for this research. One difference was that the tractor and implement CGs were used as the reference points in this model where as hitch point was used as the reference point in Feng et al. (2005). In addition, the world-coordinate lateral position was also added in this model, which is required to perform the closed loop analysis. Both this model and the Feng model took a "bicycle" approach meaning that the lateral forces in the left and right wheels were assumed to be equal and summed together. Front wheel steering was used. As mentioned before, the system was constrained to only allow yaw and lateral motion with a constant forward tractor velocity. The model thus included lateral velocity and yaw rate states for the tractor and a yaw rate state for the implement, which were driven by the lateral tire forces related to tire side slip.

Tractor front tire, tractor rear tire and implement tire longitudinal and side forces were used to define the lateral (along y-axis) and longitudinal (along x-axis) forces in the vehicle co-ordinate system (Fig. 3.4). The world and vehicle coordinate systems used in this

work were described in Chap. 2.1. The lateral tire forces were used to establish force balance in y-axis of the tractor and implement vehicle coordinate system and yaw moment balance about the tractor and implement CGs. Therefore, proceeding with the mathematical development of the model, starting from the definition of the forces acting on the system as shown graphically in Fig. 3.4:

$$F_{x,f}^{t} = F_{x,f}^{t}\cos\delta - F_{y,f}^{t}\sin\delta \tag{3.22}$$

$$F_{y,f}^{t} = F_{x,f}^{t}\sin\delta + F_{y,f}^{t}\cos\delta \tag{3.23}$$

$$F_{x,p}^{t} = -F_{x,p}^{i}\cos\lambda - F_{y,p}^{i}\sin\lambda \tag{3.24}$$

$$F_{y,p}^{t} = F_{x,p}^{i}\sin\lambda - F_{y,p}^{i}\cos\lambda \tag{3.25}$$

Similarly, from definition of the velocity vectors at various locations on the system (fig. 3-5), the two following equation are derived which are similarly to eqs. 3.6 and 3.7 of the kinematic model:

$$u_{p}^{i} = u_{p}^{t}\cos\lambda - v_{p}^{t}\sin\lambda \tag{3.26}$$

$$v_{p}^{i} = u_{p}^{t}\sin\lambda + v_{p}^{t}\cos\lambda \tag{3.27}$$

3.3.1. Tractor Motion

We have, based Newton's second law, for the translational tractor motion,

$$F^{t} = m^{t}\dot{V}_{c}^{t} \tag{3.28}$$

where,

$$F^{t} = F_{x}^{t}i + F_{y}^{t}j + F_{z}^{t}k \tag{3.29}$$

$$V_{c}^{t} = V_{x}^{t}i + V_{y}^{t}j + V_{z}^{t}k \tag{3.30}$$

and i, j, and k are tractor body fixed orthogonal unit vectors. The coordinate system used in this motion analysis was described in chapter 2.1.

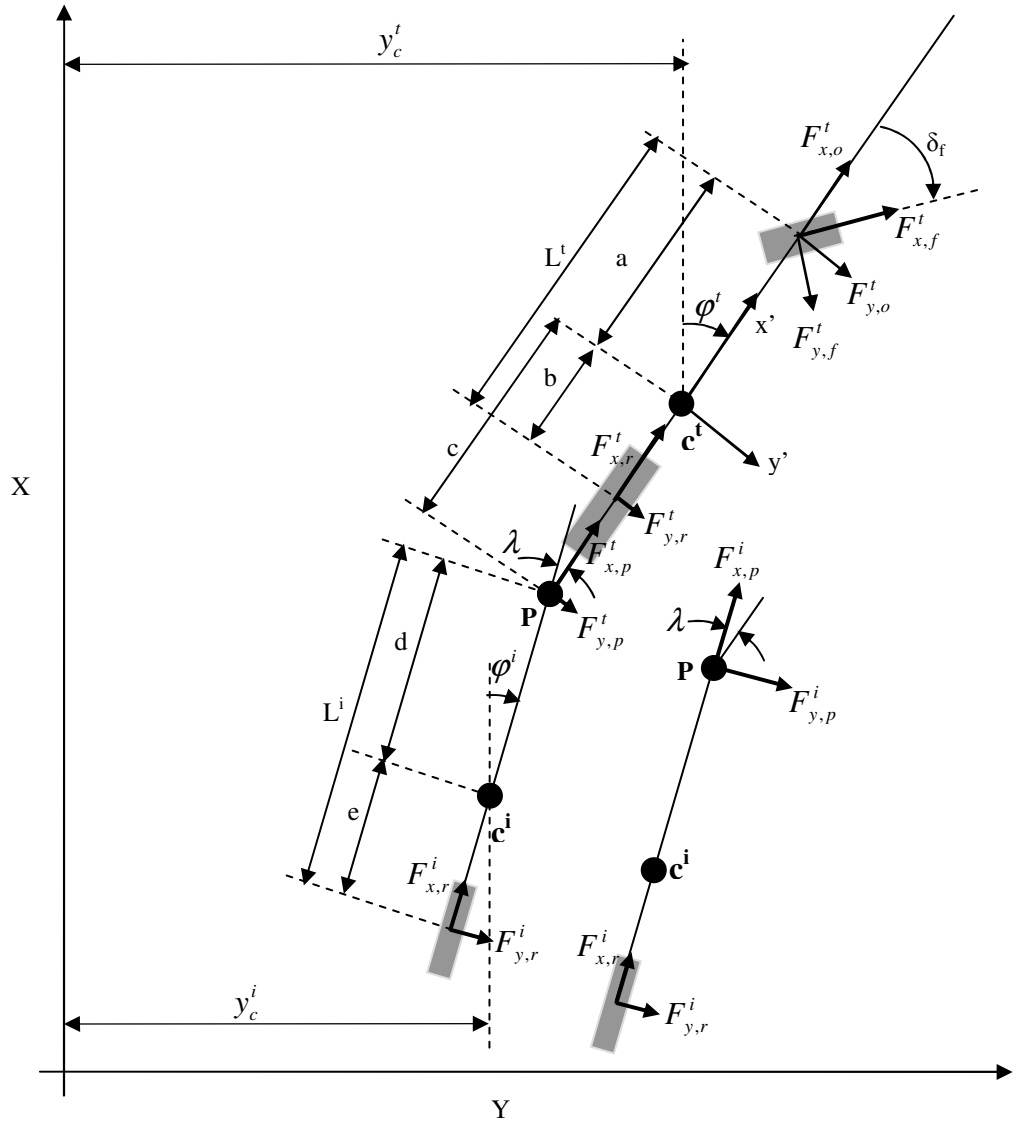

Fig. 3.4: Forces at different locations of the dynamic bicycle model of a tractor-and-implement system. X-Y represents the world coordinate system and x'-y' represents the vehicle coordinate system.

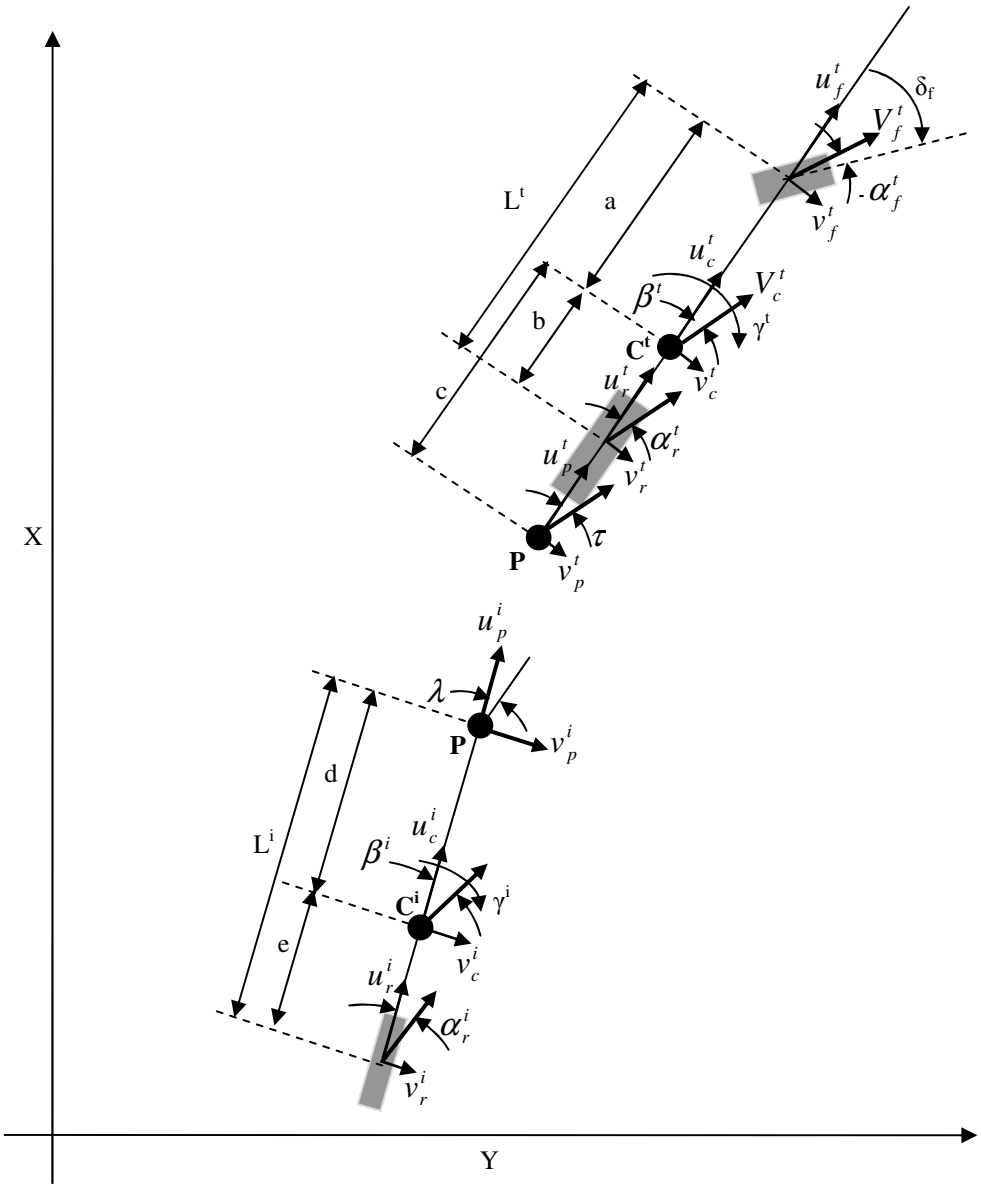

Fig. 3.5: Velocities at different locations of the dynamic bicycle model of a tractor-and-implement system. X-Y represents the world coordinate system and x'-y' represents the vehicle coordinate system.

The total acceleration at the CG of a body experiencing the six degree of freedom motion will be the sum of the centripetal acceleration and tangential acceleration (Greenwood, 1965), which can be written as:

$$\dot{V}_c^t = \left(\dot{V}_c^t\right)_r + \varpi^t \times V_c^t \tag{3.31}$$

where centripetal acceleration is given by,

$$\left(\dot{V}_c^t\right)_r = \dot{V}_x^t i + \dot{V}_y^t j + \dot{V}_z^t k \tag{3.32}$$

and tangential acceleration is given by the definition of the cross product:

$$\varpi^t \times V_c^t = \begin{vmatrix} i & j & k \\ \varpi_x & \varpi_y & \varpi_z \\ V_{x,c}^t & V_{y,c}^t & V_{z,c}^t \end{vmatrix} \tag{3.33}$$

$$= \left(\varpi_y^t V_{z,c}^t - \varpi_z^t V_{y,c}^t\right) i + \left(\varpi_z^t V_{x,c}^t - \varpi_x^t V_{z,c}^t\right) j + \left(\varpi_x^t V_{y,c}^t - \varpi_y^t V_{x,c}^t\right) k$$

$$\therefore \dot{V}_c^t = \dot{V}_x^t i + \dot{V}_y^t j + \dot{V}_z^t k + \left(\varpi_y^t V_{z,c}^t - \varpi_z^t V_{y,c}^t\right) i + \left(\varpi_z^t V_{x,c}^t - \varpi_x^t V_{z,c}^t\right) j + \left(\varpi_x^t V_{y,c}^t - \varpi_y^t V_{x,c}^t\right) k \tag{3.34}$$

From eqs. 3.28, 3.29 and 3.34, the force balance in y-direction of the vehicle coordinate system is given by,

$$F_y^t = m^t \left(\dot{V}_{y,c}^t + \varpi_z^t V_{x,c}^t - \varpi_x^t V_{z,c}^t\right) \tag{3.35}$$

Neglecting roll, pitch and z-direction velocities,

$$\begin{aligned} &\varpi_x^t = \varpi_y^t = 0 \\ &V_{z,c}^t = 0 \end{aligned} \tag{3.36}$$

$$F_y^t = m^t \left(\dot{V}_{y,c}^t + \varpi_z^t V_{x,c}^t\right) \tag{3.37}$$

Let,

$$\begin{aligned} &V_{x,c}^t = u_c^t \\ &V_{y,c}^t = v_c^t \\ &\varpi_z^t = \gamma^t \end{aligned} \tag{3.38}$$

$$\therefore F_y^t = m^t \left(\dot{v}_c^t + u_c^t \gamma^t\right) \tag{3.39}$$

For the rotational tractor motion, based again on Newton's law, we have,

$$M^t = I^t \dot{\varpi}^t \tag{3.40}$$

For yaw plane motion,

$$M^t_{z,c} = I^t_{z,c} \dot{\varpi}^t_z \tag{3.41}$$

$$or,\ M^t_{z,c} = I^t_{z,c} \dot{\gamma}^t \tag{3.42}$$

The sum of lateral forces applied to the system is:

$$F^t_y = F^t_{y,f} + F^t_{y,r} + F^t_{y,p}$$

$$= F^t_{x,f} \sin\delta + F^t_{y,f} \cos\delta + F^t_{y,r} + F^t_{y,p} \tag{3.43}$$

and the sum of moments due to the applied force is:

$$M^t_{z,c} = F^t_{y,f} a - F^t_{y,r} b - F^t_{y,p} c$$

$$= a\left(F^t_{x,f} \sin\delta + F^t_{y,f} \cos\delta\right) - bF^t_{y,r} - cF^t_{y,p} \tag{3.44}$$

From eq. 3.39 and 3.43

$$m^t\left(\dot{v}^t_c + u^t_c \gamma^t\right) = F^t_{x,f} \sin\delta + F^t_{y,f} \cos\delta + F^t_{y,r} + F^t_{y,p} \tag{3.45}$$

From eq. 3.42 and 3.44

$$I^t_{z,c} \dot{\gamma}^t = a\left(F^t_{x,f} \sin\delta + F^t_{y,f} \cos\delta\right) - bF^t_{y,r} - cF^t_{y,p} \tag{3.46}$$

3.3.2. Single Axle Towed Implement Motion

The tractor and towed implement rigid bodies were linked by a revolute joint at the hitch point, which provided a velocity coupling between the tractor and the implement. To describe the implement motion, the velocity at the tractor CG can be transferred to the hitch point, resolved into the velocities in implement coordinate axes, and then transferred to the implement CG to define the velocity of the implement CG.

The velocity at the hitch point *p* of the tractor experiences both translational and rotational motion which is the sum of the velocity of the CG and the velocity of *p* with respect to the CG (Greenwood, 1965). The relative velocity of *p* with respect to the CG is given by,

$$\left(V_p^t\right)_r = \varpi \times R_p$$

Therefore, the total velocity of *p* is given by,

$$\because V_p^t = V_c^t + \varpi \times R_p \tag{3.47}$$

where, R_p is the distance vector between the tractor CG and the hitch point *p* given by,

$$R_p = \begin{bmatrix} -c \\ 0 \\ 0 \end{bmatrix} \tag{3.48}$$

$$\therefore V_p^t = \begin{bmatrix} V_{x,c}^t \\ V_{y,c}^t \\ V_{z,c}^t \end{bmatrix} + \begin{bmatrix} \varpi_x^t \\ \varpi_y^t \\ \varpi_z^t \end{bmatrix} \times \begin{bmatrix} -c \\ 0 \\ 0 \end{bmatrix}$$

$$= \begin{bmatrix} V_{x,c}^t \\ V_{y,c}^t \\ V_{z,c}^t \end{bmatrix} + \begin{bmatrix} 0 \\ -c\varpi_z^t \\ -c\varpi_y^t \end{bmatrix}$$

$$= \begin{bmatrix} V_{x,c}^t \\ V_{y,c}^t - c\varpi_z^t \\ V_{z,c}^t - c\varpi_y^t \end{bmatrix} \tag{3.49}$$

For yaw plane motion:

$$V_{x,p}^t = V_{x,c}^t$$

or, $u_p^t = u_c^t$ (3.50)

$$V_{y,p}^{t} = V_{y,c}^{t} - c\varpi_{z}^{t}$$

or, $v_{p}^{t} = v_{c}^{t} - c\gamma^{t}$ (3.51)

From Eqs. 3.26 and 3.50 and 3.51,

$$u_{p}^{i} = u_{c}^{t}\cos\lambda - \left(v_{c}^{t} - c\gamma^{t}\right)\sin\lambda \quad (3.52)$$

From eqs. 3.27 and 3.50 and 2.51,

$$v_{p}^{i} = u_{c}^{t}\sin\lambda + \left(v_{c}^{t} - c\gamma^{t}\right)\cos\lambda \quad (3.53)$$

Using eq. 3.49 again to transfer tractor hitch pin velocities to implement CG,

$$u_{c}^{i} = u_{p}^{i} = u_{c}^{t}\cos\lambda - \left(v_{c}^{t} - c\gamma^{t}\right)\sin\lambda \quad (3.54)$$

$$v_{c}^{i} = v_{p}^{i} - d\gamma^{i} = u_{c}^{t}\sin\lambda + \left(v_{c}^{t} - c\gamma^{t}\right)\cos\lambda - d\gamma^{i} \quad (3.55)$$

Taking the derivative with respect to time:

$$\dot{u}_{c}^{i} = \dot{u}_{c}^{t}\cos\lambda - u_{c}^{t}\sin\lambda\dot{\lambda} - \left(\dot{v}_{c}^{t} - c\dot{\gamma}^{t}\right)\sin\lambda - \left(v_{c}^{t} - c\gamma^{t}\right)\cos\lambda\dot{\lambda} \quad (3.56)$$

$$\dot{v}_{c}^{i} = \dot{u}_{c}^{t}\sin\lambda + u_{c}^{t}\cos\lambda\dot{\lambda} + \left(\dot{v}_{c}^{t} - c\dot{\gamma}^{t}\right)\cos\lambda - \left(v_{c}^{t} - c\gamma^{t}\right)\sin\lambda\dot{\lambda} - d\dot{\gamma}^{i} \quad (3.57)$$

Now, using equation 3.29 for the single axle towed implement

$$F_{x}^{i} = m^{i}\left(\dot{u}_{c}^{i} - v_{c}^{i}\gamma^{i}\right) \quad (3.58)$$

$$F_{y}^{i} = m^{i}\left(\dot{v}_{c}^{i} + u_{c}^{i}\gamma^{i}\right) \quad (3.59)$$

The total longitudinal force applied to the implement body is the sum of the forces generated by the implement tire and the interaction force at the hitch point (Fig. 3.4), which is given by:

$$F_{x}^{i} = F_{x,p}^{i} + F_{x,r}^{i} \quad (3.60)$$

or, $F_{x,p}^{i} = F_{x}^{i} - F_{x,r}^{i}$

$$\text{or, } F^i_{x,p} = m^i\left(\dot{u}^i_c - v^i_c\gamma^i\right) - F^i_{x,r} \tag{3.61}$$

Using equation 3.61, 3.55 and 3.56,

$$F^i_{x,p} = m^i\left[\left\{\dot{u}^t_c\cos\lambda - u^t_c\sin\lambda\dot{\lambda} - \left(\dot{v}^t_c - c\dot{\gamma}^t\right)\sin\lambda - \left(v^t_c - c\gamma^t\right)\cos\lambda\dot{\lambda}\right\} - \gamma^i\left\{u^t_c\sin\lambda + \left(v^t_c - c\gamma^t\right)\cos\lambda - d\gamma^i\right\}\right] - F^i_{x,r} \tag{3.62}$$

Assuming a small angle λ, $\sin\lambda = 0, \cos\lambda = 1$. This assumption will be valid for small steering input operations as λ remains small for small steering angle inputs. Now eq. 3.62 becomes:

$$F^i_{x,p} = m^i\left(\dot{u}^t_c - \left(v^t_c - c\gamma^t\right)\dot{\lambda} - \left(v^t_c - c\gamma^t - d\gamma^i\right)\gamma^i\right) - F^i_{x,r} \tag{3.63}$$

Similarly, the total lateral forces applied to the implement is given by,

$$F^i_y = F^i_{y,p} + F^i_{y,r} \tag{3.64}$$

$$\text{or, } F^i_{y,p} = F^i_y - F^i_{y,r}$$

$$\text{or, } F^i_{y,p} = m^i\left(\dot{v}^i_c + u^i_c\gamma^i\right) - F^i_{y,r} \tag{3.65}$$

Using equation 3.65, 3.54 and 3.57

$$F^i_{y,p} = m^i\left[\begin{array}{l}\left\{\dot{u}^t_c\sin\lambda + u^t_c\cos\lambda\dot{\lambda} + \left(\dot{v}^t_c - c\dot{\gamma}^t\right)\cos\lambda - \left(v^t_c - c\gamma^t\right)\sin\lambda\dot{\lambda} - d\dot{\gamma}^i\right\} \\ + \gamma^i\left\{u^t_c\cos\lambda - \left(v^t_c - c\gamma^t\right)\sin\lambda\right\}\end{array}\right] - F^i_{y,r} \tag{3.66}$$

Again, assuming small angle λ, $\sin\lambda = 0, \cos\lambda = 1$

$$F^i_{y,p} = m^i\left(u^t_c\dot{\lambda} + \left(\dot{v}^t_c - c\dot{\gamma}^t\right) - d\dot{\gamma}^i + u^t_c\gamma^i\right) - F^i_{y,r} \tag{3.67}$$

From Eqs. (3.54) and (3.55); using the same small angle assumption,

$$u^i_c = u^t_c \tag{3.68}$$

$$v^i_c = \left(v^t_c - c\gamma^t\right) - d\gamma^i \tag{3.69}$$

We have, for the yaw plane rotational implement motion,

$$M^{i}_{z,c} = I^{i}_{z,c}\dot{\gamma}^{i} \tag{3.70}$$

$$M^{i}_{z,c} = F^{i}_{y,p}d - F^{i}_{y,r}e \tag{3.71}$$

$$\therefore I^{i}_{z,c}\dot{\gamma}^{i} = m^{i}d\left\{\left(u^{t}_{c}\dot{\lambda} + \left(\dot{v}^{t}_{c} - c\dot{\gamma}^{t}\right) - d\dot{\gamma}^{i} + u^{t}_{c}\gamma^{i}\right)\right\} - (d+e)F^{i}_{y,r} \tag{3.72}$$

$$or,\ I^{i}_{z,c}\dot{\gamma}^{i} = m^{i}du^{t}_{c}\dot{\lambda} + m^{i}d\dot{v}^{t}_{c} - m^{i}cd\dot{\gamma}^{t} - m^{i}d^{2}\dot{\gamma}^{i} + m^{i}du^{t}_{c}\gamma^{i} - (d+e)F^{i}_{y,r}$$

$$or,\ I^{i}_{z,c}\dot{\gamma}^{i} + m^{i}d^{2}\dot{\gamma}^{i} - m^{i}d\dot{v}^{t}_{c} + m^{i}cd\dot{\gamma}^{t} = m^{i}du^{t}_{c}\dot{\lambda} + m^{i}du^{t}_{c}\gamma^{i} - (d+e)F^{i}_{y,r}$$

$$\text{or,}\ \left(I^{i}_{z} + m^{i}d^{2}\right)\dot{\gamma}^{i} - m^{i}d\dot{v}^{t}_{c} + m^{i}cd\dot{\gamma}^{t} = m^{i}du^{t}_{c}\dot{\lambda} + m^{i}du^{t}_{c}\gamma^{i} - (d+e)F^{i}_{y,r} \tag{3.73}$$

3.3.3. Combining Tractor and Implement Equations

From Eqs. 3.45, 3.25, 3.63 and 3.66, the following equation is derived:

$$m^{t}\left(\dot{v}^{t}_{c} + u^{t}_{c}\gamma^{t}\right) = F^{t}_{x,f}\sin\delta + F^{t}_{y,f}\cos\delta + F^{t}_{y,r} + \left\{m^{i}\left(\dot{u}^{t}_{c} - \left(v^{t}_{c} - c\gamma^{t}\right)\dot{\lambda} - \left(v^{t}_{c} - c\gamma^{t} - d\gamma^{i}\right)\gamma^{i}\right) - F^{i}_{x,r}\right\}\sin\lambda - \left\{m^{i}\left(u^{t}_{c}\dot{\lambda} + \left(\dot{v}^{t}_{c} - c\dot{\gamma}^{t}\right) - d\dot{\gamma}^{i} + u^{t}_{c}\gamma^{i}\right) - F^{i}_{y,r}\right\}\cos\lambda \tag{3.74}$$

Assuming small angles δ and λ, which is valid for small steering angle operations,

$$m^{t}\left(\dot{v}^{t}_{c} + u^{t}_{c}\gamma^{t}\right) = F^{t}_{y,f} + F^{t}_{y,r} - \left\{m^{i}\left(u^{t}_{c}\dot{\lambda} + \left(\dot{v}^{t}_{c} - c\dot{\gamma}^{t}\right) - d\dot{\gamma}^{i} + u^{t}_{c}\gamma^{i}\right) - F^{i}_{y,r}\right\} \tag{3.75}$$

$$m^{t}\dot{v}^{t}_{c} + m^{t}u^{t}_{c}\gamma^{t} = F^{t}_{y,f} + F^{t}_{y,r} + F^{i}_{y,r} - m^{i}u^{t}_{c}\dot{\lambda} - m^{i}\dot{v}^{t}_{c} + m^{i}c\dot{\gamma}^{t} + m^{i}d\dot{\gamma}^{i} - m^{i}u^{t}_{c}\gamma^{i}$$

$$m^{t}\dot{v}^{t}_{c} + m^{i}\dot{v}^{t}_{c} - m^{i}c\dot{\gamma}^{t} - m^{i}d\dot{\gamma}^{i} = F^{t}_{y,f} + F^{t}_{y,r} + F^{i}_{y,r} - m^{i}u^{t}_{c}\dot{\lambda} - m^{t}u^{t}_{c}\gamma^{t} - m^{i}u^{t}_{c}\gamma^{i}$$

$$\left(m^{t} + m^{i}\right)\dot{v}^{t}_{c} - m^{i}c\dot{\gamma}^{t} - m^{i}d\dot{\gamma}^{i} = F^{t}_{y,f} + F^{t}_{y,r} + F^{i}_{y,r} - m^{i}u^{t}_{c}\dot{\lambda} - m^{t}u^{t}_{c}\gamma^{t} - m^{i}u^{t}_{c}\gamma^{i} \tag{3.76}$$

From Eqs. 3.46, 3.25, 3.63 and 3.66, the following equation is derived:

$$I_{z,c}^{t}\dot{\gamma}^{t} = a\left(F_{x,f}^{t}\sin\delta + F_{y,f}^{t}\cos\delta\right) - bF_{y,r}^{t} - c\begin{bmatrix}\left\{m^{i}\left(\dot{u}_{c}^{t} - \left(v_{c}^{t} - c\gamma^{t}\right)\dot{\lambda} - \left(v_{c}^{t} - c\gamma^{t} - d\gamma^{i}\right)\gamma^{i}\right) - F_{x,r}^{i}\right\}\sin\lambda \\ -\left\{m^{i}\left(u_{c}^{t}\dot{\lambda} + \left(\dot{v}_{c}^{t} - c\dot{\gamma}^{t}\right) - d\dot{\gamma}^{i} + u_{c}^{t}\gamma^{i}\right) - F_{y,r}^{i}\right\}\cos\lambda\end{bmatrix} \tag{3.77}$$

Again, for the small steering angle operation,

$$I_{z,c}^{t}\dot{\gamma}^{t} = aF_{y,f}^{t} - bF_{y,r}^{t} + c\left\{m^{i}\left(u_{c}^{t}\dot{\lambda} + \left(\dot{v}_{c}^{t} - c\dot{\gamma}^{t}\right) - d\dot{\gamma}^{i} + u_{c}^{t}\gamma^{i}\right) - F_{y,r}^{i}\right\} \tag{3.78}$$

$$I_{z,c}^{t}\dot{\gamma}^{t} = aF_{y,f}^{t} - bF_{y,r}^{t} + m^{i}cu_{c}^{t}\dot{\lambda} + m^{i}c\dot{v}_{c}^{t} - m^{i}c^{2}\dot{\gamma}^{t} - m^{i}cd\dot{\gamma}^{i} + m^{i}cu_{c}^{t}\gamma^{i} - cF_{y,r}^{i}$$

$$I_{z,c}^{t}\dot{\gamma}^{t} + m^{i}c^{2}\dot{\gamma}^{t} - m^{i}c\dot{v}_{c}^{t} + m^{i}cd\dot{\gamma}^{i} = aF_{y,f}^{t} - bF_{y,r}^{t} - cF_{y,r}^{i} + m^{i}cu_{c}^{t}\dot{\lambda} + m^{i}cu_{c}^{t}\gamma^{i}$$

$$\left(I_{z}^{t} + m^{i}c^{2}\right)\dot{\gamma}^{t} - m^{i}c\dot{v}_{c}^{t} + m^{i}cd\dot{\gamma}^{i} = aF_{y,f}^{t} - bF_{y,r}^{t} - cF_{y,r}^{i} + m^{i}cu_{c}^{t}\dot{\lambda} + m^{i}cu_{c}^{t}\gamma^{i} \tag{3.79}$$

We have,

$$\dot{\lambda} = \gamma^{t} - \gamma^{i} \tag{3.80}$$

From Eq. 3.76 and 3.80,

$$\left(m^{t} + m^{i}\right)\dot{v}_{c}^{t} - m^{i}c\dot{\gamma}^{t} - m^{i}d\dot{\gamma}^{i} = F_{y,f}^{t} + F_{y,r}^{t} + F_{y,r}^{i} - m^{i}u_{c}^{t}\left(\gamma^{t} - \gamma^{i}\right) - m^{t}u_{c}^{t}\gamma^{t} - m^{i}u_{c}^{t}\gamma^{i}$$

$$\left(m^{t} + m^{i}\right)\dot{v}_{c}^{t} - m^{i}c\dot{\gamma}^{t} - m^{i}d\dot{\gamma}^{i} = F_{y,f}^{t} + F_{y,r}^{t} + F_{y,r}^{i} - m^{i}u_{c}^{t}\gamma^{t} + m^{i}u_{c}^{t}\gamma^{i} - m^{t}u_{c}^{t}\gamma^{t} - m^{i}u_{c}^{t}\gamma^{i}$$

$$\left(m^{t} + m^{i}\right)\dot{v}_{c}^{t} - m^{i}c\dot{\gamma}^{t} - m^{i}d\dot{\gamma}^{i} = F_{y,f}^{t} + F_{y,r}^{t} + F_{y,r}^{i} - (m^{i} + m^{t})u_{c}^{t}\gamma^{t} \tag{3.81}$$

From Eq. 3.79 and 3.80,

$$\left(I_{z}^{t} + m^{i}c^{2}\right)\dot{\gamma}^{t} - m^{i}c\dot{v}_{c}^{t} + m^{i}cd\dot{\gamma}^{i} = aF_{y,f}^{t} - bF_{y,r}^{t} - cF_{y,r}^{i} + m^{i}cu_{c}^{t}\left(\gamma^{t} - \gamma^{i}\right) + m^{i}cu_{c}^{t}\gamma^{i}$$

$$\left(I_{z}^{t} + m^{i}c^{2}\right)\dot{\gamma}^{t} - m^{i}c\dot{v}_{c}^{t} + m^{i}cd\dot{\gamma}^{i} = aF_{y,f}^{t} - bF_{y,r}^{t} - cF_{y,r}^{i} + m^{i}cu_{c}^{t}\gamma^{t} - m^{i}cu_{c}^{t}\gamma^{i} + m^{i}cu_{c}^{t}\gamma^{i}$$

$$\left(I_{z}^{t} + m^{i}c^{2}\right)\dot{\gamma}^{t} - m^{i}c\dot{v}_{c}^{t} + m^{i}cd\dot{\gamma}^{i} = aF_{y,f}^{t} - bF_{y,r}^{t} - cF_{y,r}^{i} + m^{i}cu_{c}^{t}\gamma^{t} \tag{3.82}$$

From Eq. 3.73 and 3.80,

$$\left(I_{z}^{i} + m^{i}d^{2}\right)\dot{\gamma}^{i} - m^{i}d\dot{v}_{c}^{t} + m^{i}cd\dot{\gamma}^{t} = m^{i}du_{c}^{t}\left(\gamma^{t} - \gamma^{i}\right) + m^{i}du_{c}^{t}\gamma^{i} - (d + e)F_{y,r}^{i}$$

$$\left(I_z^i + m^i d^2\right)\dot{\gamma}^i - m^i d\dot{v}_c^t + m^i cd\dot{\gamma}^t = m^i du_c^t\gamma^t - m^i du_c^t\gamma^i + m^i du_c^t\gamma^i - (d+e)F_{y,r}^i$$

$$\left(I_z^i + m^i d^2\right)\dot{\gamma}^i - m^i d\dot{v}_c^t + m^i cd\dot{\gamma}^t = m^i du_c^t\gamma^t - (d+e)F_{y,r}^i \tag{3.83}$$

3.3.4. Tire Forces

We have, based the definition of the force vectors acting on the tractor front tire, assuming small angles and a linear tire model (See Chap 2.1.3), which is valid for small side slip angles,

$$F_{y,f}^t = -C_{\alpha,f}^t \tan\alpha_f^t \approx -C_{\alpha,f}^t\alpha_f^t \tag{3.84}$$

From the definition of the front slip angle, α_f^t , and assuming a small angle, which is valid for the small steering and slip angles,

$$\tan\left[\delta - \left(-\alpha_f^t\right)\right] \approx \delta - \left(-\alpha_f^t\right) = \frac{v_f^t}{u_f^t} \tag{3.85}$$

where, $v_f^t = v_c^t + a\gamma^t$ and $u_f^t = u_c^t$

$$\therefore \delta - \left(-\alpha_f^t\right) = \frac{v_c^t + a\gamma^t}{u_c^t}$$

$$\therefore -\left(-\alpha_f^t\right) = \frac{v_c^t + a\gamma^t}{u_c^t} - \delta$$

$$\therefore \alpha_f^t = \frac{v_c^t + a\gamma^t}{u_c^t} - \delta \tag{3.86}$$

From 3.84 and 3.86,

$$F_{y,f}^t = -C_{\alpha,f}^t\frac{v_c^t + a\gamma^t}{u_c^t} + C_{\alpha,f}^t\delta \tag{3.87}$$

For the tractor rear tires, the lateral force is given by:

$$F_{y,r}^{t} = -C_{\alpha,r}^{t} \tan \alpha_{r}^{t} \approx -C_{\alpha,r}^{t} \alpha_{r}^{t} \tag{3.88}$$

$$\tan \alpha_{r}^{t} \approx \alpha_{r}^{t} = \frac{v_{r}^{t}}{u_{r}^{t}} = \frac{v_{c}^{t} - b\gamma^{t}}{u_{c}^{t}} \tag{3.89}$$

$$\therefore F_{y,r}^{t} = -C_{\alpha,r}^{t} \frac{v_{c}^{t} - b\gamma^{t}}{u_{c}^{t}} \tag{3.90}$$

For the implement tires, the lateral force is given by:

$$F_{y,r}^{i} = -C_{\alpha,r}^{i} \tan \alpha_{r}^{t} \approx -C_{\alpha,r}^{i} \alpha_{r}^{i} \tag{3.91}$$

And, slip angle is given by,

$$\tan(-\lambda + \alpha_{r}^{i}) \approx \alpha_{r}^{i} - \lambda = \frac{v_{r}^{i}}{u_{r}^{i}} = \frac{v_{c}^{i} - e\gamma^{i}}{u_{c}^{i}} \tag{3.92}$$

We know from equations 3.68 and 3.69 that:

$$u_{c}^{i} = u_{c}^{t}$$

and that

$$v_{c}^{i} = \left(v_{c}^{t} - c\gamma^{t}\right) - d\gamma^{i}$$

$$\therefore \alpha_{r}^{i} = \frac{v_{c}^{t} - c\gamma^{t} - (d+e)\gamma^{i}}{u_{c}^{t}} + \lambda \tag{3.93}$$

From equations 3.91 and 3.93,

$$F_{y,r}^{i} = -C_{\alpha,r}^{i} \frac{v_{c}^{t} - c\gamma^{t} - (d+e)\gamma^{i}}{u_{c}^{t}} - C_{\alpha,r}^{i} \lambda \tag{3.94}$$

We also know from eq. 3.12,

$$\lambda = \varphi^{t} - \varphi^{i} \tag{3.95}$$

Using eqs. 3.81, 3.87, 3.90, 3.94 and 3.95,

$$\left(m^t + m^i\right)\dot{v}_c^t - m^i c\dot{\gamma}^t - m^i d\dot{\gamma}^i = -C_{\alpha,f}^t \frac{v_c^t + a\gamma^t}{u_c^t} + C_{\alpha,f}^t \delta - C_{\alpha,r}^t \frac{v_c^t - b\gamma^t}{u_c^t}$$

$$- C_{\alpha,r}^i \frac{v_c^t - c\gamma^t - (d+e)\gamma^i}{u_c^t} - C_{\alpha,r}^i \lambda - (m^i + m^t) u_c^t \gamma^t$$

or,

$$\left(m^t + m^i\right)\dot{v}_c^t - m^i c\dot{\gamma}^t - m^i d\dot{\gamma}^i = -C_{\alpha,f}^t \frac{v_c^t}{u_c^t} - C_{\alpha,f}^t \frac{a\gamma^t}{u_c^t} - C_{\alpha,r}^t \frac{v_c^t}{u_c^t} + C_{\alpha,r}^t \frac{b\gamma^t}{u_c^t}$$

$$- C_{\alpha,r}^i \frac{v_c^t}{u_c^t} 2C_{\alpha,r}^i \frac{c\gamma^t}{u_c^t} + C_{\alpha,r}^i \frac{(d+e)\gamma^i}{u_c^t} - (m^i + m^t) u_c^t \gamma^t - C_{\alpha,r}^i \lambda + C_{\alpha,f}^t \delta$$

or,

$$\left(m^t + m^i\right)\dot{v}_c^t - m^i c\dot{\gamma}^t - m^i d\dot{\gamma}^i = -\frac{C_{\alpha,f}^t}{u_c^t} v_c^t - \frac{C_{\alpha,r}^t}{u_c^t} v_c^t - \frac{C_{\alpha,r}^i}{u_c^t} v_c^t - \frac{aC_{\alpha,f}^t}{u_c^t} \gamma^t$$

$$+ \frac{bC_{\alpha,r}^t}{u_c^t} \gamma^t + \frac{cC_{\alpha,r}^i}{u_c^t} \gamma^t - (m^i + m^t) u_c^t \gamma^t + \frac{2(d+e)C_{\alpha,r}^i}{u_c^t} \gamma^i - C_{\alpha,r}^i \lambda + C_{\alpha,f}^t \delta$$

or,

$$\left(m^t + m^i\right)\dot{v}_c^t - m^i c\dot{\gamma}^t - m^i d\dot{\gamma}^i = -\frac{1}{u_c^t}\left(C_{\alpha,f}^t + C_{\alpha,r}^t + C_{\alpha,r}^i\right) v_c^t$$

$$- \frac{1}{u_c^t}\left(aC_{\alpha,f}^t - bC_{\alpha,r}^t - cC_{\alpha,r}^i + (m^i + m^t) u_c^{t\,2}\right)\gamma^t + \frac{(d+e)C_{\alpha,r}^i}{u_c^t} \gamma^i - C_{\alpha,r}^i \varphi^t + C_{\alpha,r}^i \varphi^i + C_{\alpha,f}^t \delta \tag{3.96}$$

Using Eqs. 3.82, 3.87, 3.90, 3.94 and 3.95:

$$\left(I_z^t + m^i c^2\right)\dot{\gamma}^t - m^i c\dot{v}_c^t + m^i cd\dot{\gamma}^i = a\left(-C_{\alpha,f}^t \frac{v_c^t + a\gamma^t}{u_c^t} + C_{\alpha,f}^t \delta\right) - b\left(-C_{\alpha,r}^t \frac{v_c^t - b\gamma^t}{u_c^t}\right)$$

$$- c\left(-C_{\alpha,r}^i \frac{v_c^t - c\gamma^t - (d+e)\gamma^i}{u_c^t} - C_{\alpha,r}^i \lambda\right) + m^i c u_c^t \gamma^t$$

or,

$$\left(I_z^t + m^i c^2\right)\dot{\gamma}^t - m^i c\dot{v}_c^t + m^i cd\dot{\gamma}^i = -aC_{\alpha,f}^t \frac{v_c^t + a\gamma^t}{u_c^t} + aC_{\alpha,f}^t \delta + bC_{\alpha,r}^t \frac{v_c^t - b\gamma^t}{u_c^t}$$

$$+ cC_{\alpha,r}^i \frac{v_c^t - c\gamma^t - (d+e)\gamma^i}{u_c^t} + cC_{\alpha,r}^i \lambda + m^i cu_c^t \gamma^t$$

or,

$$\left(I_z^t + m^i c^2\right)\dot{\gamma}^t - m^i c\dot{v}_c^t + m^i cd\dot{\gamma}^i = -aC_{\alpha,f}^t \frac{v_c^t}{u_c^t} - aC_{\alpha,f}^t \frac{a\gamma^t}{u_c^t} + bC_{\alpha,r}^t \frac{v_c^t}{u_c^t} - bC_{\alpha,r}^t \frac{b\gamma^t}{u_c^t} + cC_{\alpha,r}^i \frac{v_c^t}{u_c^t}$$

$$- cC_{\alpha,r}^i \frac{c\gamma^t}{u_c^t} + m^i cu_c^t \gamma^t - cC_{\alpha,r}^i \frac{(d+e)\gamma^i}{u_c^t} + cC_{\alpha,r}^i \lambda + aC_{\alpha,f}^t \delta$$

or,

$$\left(I_z^t + m^i c^2\right)\dot{\gamma}^t - m^i c\dot{v}_c^t + m^i cd\dot{\gamma}^i = -\frac{1}{u_c^t}\left(aC_{\alpha,f}^t - bC_{\alpha,r}^t\right)v_c^t + \frac{cC_{\alpha,r}^i}{u_c^t} v_c^t - \frac{1}{u_c^t}\left(a^2 C_{\alpha,f}^t + b^2 C_{\alpha,r}^t + c^2 C_{\alpha,r}^i\right)\gamma^t$$

$$+ m^i cu_c^t \gamma^t - \frac{c(d+e)C_{\alpha,r}^i}{u_c^t}\gamma^i + cC_{\alpha,r}^i \lambda + aC_{\alpha,f}^t \delta$$

or,

$$- m^i c\dot{v}_c^t + \left(I_z^t + m^i c^2\right)\dot{\gamma}^t + m^i cd\dot{\gamma}^i = -\frac{1}{u_c^t}\left(aC_{\alpha,f}^t - bC_{\alpha,r}^t - cC_{\alpha,r}^i\right)v_c^t$$

$$-\frac{1}{u_c^t}\left(a^2 C_{\alpha,f}^t + b^2 C_{\alpha,r}^t + c^2 C_{\alpha,r}^i - m^i cu_c^{t\,2}\right)\gamma^t - \frac{c(d+e)C_{\alpha,r}^i}{u_c^t}\gamma^i + cC_{\alpha,r}^i \varphi^t - cC_{\alpha,r}^i \varphi^i + aC_{\alpha,f}^t \delta \tag{3.97}$$

Using Eqs. 3.83, 3.87, 3.90, 3.94 and 3.95:

$$\left(I_z^i + m^i d^2\right)\dot{\gamma}^i - m^i d\dot{v}_c^t + m^i cd\dot{\gamma}^t = m^i du_c^t \gamma^t - (d+e)\left(-C_{\alpha,r}^i \frac{v_c^t - c\gamma^t - (d+e)\gamma^i}{u_c^t} - C_{\alpha,r}^i \lambda\right)$$

or,

$$\left(I_z^i + m^i d^2\right)\dot{\gamma}^i - m^i d\dot{v}_c^t + m^i cd\dot{\gamma}^t = m^i du_c^t \gamma^t + (d+e)C_{\alpha,r}^i \frac{v_c^t}{u_c^t} - (d+e)C_{\alpha,r}^i \frac{c\gamma^t}{u_c^t}$$
$$-(d+e)C_{\alpha,r}^i \frac{(d+e)\gamma^i}{u_c^t} + (d+e)C_{\alpha,r}^i \lambda$$

or,

$$-m^i d\dot{v}_c^t + m^i cd\dot{\gamma}^t + \left(I_z^i + m^i d^2\right)\dot{\gamma}^i = \frac{(d+e)C_{\alpha,r}^i}{u_c^t} v_c^t + \left(m^i du_c^t - \frac{c(d+e)C_{\alpha,r}^i}{u_c^t}\right)\gamma^t$$
$$-\frac{(d+e)^2 C_{\alpha,r}^i}{u_c^t}\gamma^i + (d+e)C_{\alpha,r}^i \varphi^t - (d+e)C_{\alpha,r}^i \varphi^i$$

(3.98)

3.3.5. Model Equations

Collecting the equations for the three velocity states of the dynamic model (eqs. 3.96, 3.97 and 3.98) results in:

$$\left(m^t + m^i\right)\dot{v}_c^t - m^i c\dot{\gamma}^t - m^i d\dot{\gamma}^i = -\frac{1}{u_c^t}\left(C_{\alpha,f}^t + C_{\alpha,r}^t + C_{\alpha,r}^i\right)v_c^t$$
$$-\frac{1}{u_c^t}\left(aC_{\alpha,f}^t - bC_{\alpha,r}^t - cC_{\alpha,r}^i + (m^i + m^t)u_c^{t\,2}\right)\gamma^t + \frac{(d+e)C_{\alpha,r}^i}{u_c^t}\gamma^i - C_{\alpha,r}^i \varphi^t + C_{\alpha,r}^i \varphi^i + C_{\alpha,f}^t \delta$$

(3.99)

$$-m^i c\dot{v}_c^t + \left(I_z^t + m^i c^2\right)\dot{\gamma}^t + m^i cd\dot{\gamma}^i = -\frac{1}{u_c^t}\left(aC_{\alpha,f}^t - bC_{\alpha,r}^t - cC_{\alpha,r}^i\right)v_c^t$$
$$-\frac{1}{u_c^t}\left(a^2 C_{\alpha,f}^t + b^2 C_{\alpha,r}^t + c^2 C_{\alpha,r}^i - m^i cu_c^{t\,2}\right)\gamma^t - \frac{c(d+e)C_{\alpha,r}^i}{u_c^t}\gamma^i + cC_{\alpha,r}^i \varphi^t - cC_{\alpha,r}^i \varphi^i + aC_{\alpha,f}^t \delta$$

(3.100)

$$-m^i d\dot{v}_c^t + m^i cd\dot{\gamma}^t + \left(I_z^i + m^i d^2\right)\dot{\gamma}^i = \frac{(d+e)C_{\alpha,r}^i}{u_c^t} v_c^t + \left(m^i d u_c^t - \frac{c(d+e)C_{\alpha,r}^i}{u_c^t} \right)\gamma^t$$
$$-\frac{(d+e)^2 C_{\alpha,r}^i}{u_c^t}\gamma^i + (d+e)C_{\alpha,r}^i\varphi^t - (d+e)C_{\alpha,r}^i\varphi^i$$

(3.101)

The tractor position in the x and y axes of the world coordinate system is given by,

$$\dot{x}_c^t = u_c^t \cos\varphi^t - v_c^t \sin\varphi^t \tag{3.102a}$$

$$\dot{y}_c^t = v_c^t \cos\varphi^t + u_c^t \sin\varphi^t \tag{3.103a}$$

Linearizing the position in x- and y-axis about a zero tractor heading angle and zero lateral velocity, which will be valid when the model is used to follow a smooth trajectory with absolute heading changes about a straight line is very small.

$$\dot{y}_c^t = u_c^t \tag{3.102}$$

$$\dot{y}_c^t = v_c^t + u_c^t\varphi^t \tag{3.103}$$

The tractor and implement heading angles are,

$$\dot{\varphi}^t = \gamma^t \tag{3.104}$$

$$\dot{\varphi}^i = \gamma^i \tag{3.105}$$

In matrix form, using eqs. 3.99-3.100 and 3.103-3.105,

$$M\dot{X} = NX + PU \tag{3.106}$$

where,

$$M = \begin{bmatrix} (m^t + m^i) & -m^i c & -m^i d & 0 & 0 & 0 \\ -m^i c & (I_z^t + m^i c^2) & m^i cd & 0 & 0 & 0 \\ -m^i d & m^i cd & (I_z^i + m^i d^2) & 0 & 0 & 0 \\ 0 & 0 & 0 & 1 & 0 & 0 \\ 0 & 0 & 0 & 0 & 1 & 0 \\ 0 & 0 & 0 & 0 & 0 & 1 \end{bmatrix}$$

$$N = \begin{bmatrix} -\frac{1}{u_c^t}\left(C_{\alpha,f}^t + C_{\alpha,r}^t + C_{\alpha,r}^i\right) & -\frac{1}{u_c^t}\left(aC_{\alpha,f}^t - bC_{\alpha,r}^t - cC_{\alpha,r}^i + (m^t + m^i)u_c^{t\,2}\right) & \frac{(d+e)C_{\alpha,r}^i}{u_c^t} & 0 & -C_{\alpha,r}^i & C_{\alpha,r}^i \\ -\frac{1}{u_c^t}\left(aC_{\alpha,f}^t - bC_{\alpha,r}^t - cC_{\alpha,r}^i\right) & -\frac{1}{u_c^t}\left(a^2 C_{\alpha,f}^t + b^2 C_{\alpha,r}^t + c^2 C_{\alpha,r}^i - m^i cu_c^{t\,2}\right) & -\frac{c(d+e)C_{\alpha,r}^i}{u_c^t} & 0 & cC_{\alpha,r}^i & -cC_{\alpha,r}^i \\ \frac{(d+e)C_{\alpha,r}^i}{u_c^t} & \left(m^i du_c^t - \frac{c(d+e)C_{\alpha,r}^i}{u_c^t}\right) & -\frac{(d+e)^2 C_{\alpha,r}^i}{u_c^t} & 0 & (d+e)C_{\alpha,r}^i & -(d+e)C_{\alpha,r}^i \\ 1 & 0 & 0 & 0 & u_c^t & 0 \\ 0 & 1 & 0 & 0 & 0 & 0 \\ 0 & 0 & 1 & 0 & 0 & 0 \end{bmatrix}$$

$$P = \begin{bmatrix} C_{\alpha,f}^t \\ aC_{\alpha,f}^t \\ 0 \\ 0 \\ 0 \\ 0 \end{bmatrix}, \quad \dot{X} = \begin{bmatrix} \dot{v}_c^t \\ \dot{\gamma}^t \\ \dot{\gamma}^i \\ \dot{y}_c^t \\ \dot{\varphi}^t \\ \dot{\varphi}^i \end{bmatrix}, \quad X = \begin{bmatrix} v_c^t \\ \gamma^t \\ \gamma^i \\ y_c^t \\ \varphi^t \\ \varphi^i \end{bmatrix}, \quad U = [\delta]$$

To transform the model to the set of coupled, 1st order ODEs needed for a state model (eq. 3.14), the following matrix operations are used:

$$A = M^{-1}N$$

$$B = M^{-1}P$$

To obtain all the state variables as outputs:

$$C = \begin{bmatrix} 1 & 0 & 0 & 0 & 0 & 0 \\ 0 & 1 & 0 & 0 & 0 & 0 \\ 0 & 0 & 1 & 0 & 0 & 0 \\ 0 & 0 & 0 & 1 & 0 & 0 \\ 0 & 0 & 0 & 0 & 1 & 0 \\ 0 & 0 & 0 & 0 & 0 & 1 \end{bmatrix}, \; D = \begin{matrix} 0 \\ 0 \\ 0 \\ 0 \\ 0 \\ 0 \end{matrix}$$

As represented by eq. 3.105, the dynamic tractor and single axle towed implement model consisted of six states. The three positional states of this model were the same states represented by the kinematic model developed in the previous subsection. However, this model included three higher order states (velocity states) in addition to the positional states. This model has a relatively higher degree of fidelity and complexity as compared to the kinematic model. In chapter 4, the responses from this model will also be compared with the responses from the other models and also with measured experimental responses, which will help to identify the operating conditions where this model will be useful.

3.4 Dynamic Model with Tire Relaxation Length

Relaxation length is defined as the distance a tire rolls before the steady state side slip angle is reached and is an important dynamic mode of an agricultural vehicle steering system. A tire can not generate the steady state lateral force instantaneously, and the delay is incorporated as a delay in the side slip angle. A first order model is given by (Bevly et. al., 2002),

$$\dot{\alpha} = \frac{u}{\sigma}(\alpha_0 - \alpha) \tag{3.107}$$

where σ is relaxation length and α_0 is the steady state side slip angle of the tire.

Now for the front tractor tire:

$$\dot{\alpha}_f^t = \frac{u_c^t}{\sigma_f^t}\left(\frac{v_c^t + a\gamma^t}{u_c^t} - \delta - \alpha_f^t\right) \tag{3.108}$$

$$\dot{\alpha}_f^t = \frac{v_c^t}{\sigma_f^t} + \frac{a\gamma^t}{\sigma_f^t} - \frac{u_c^t}{\sigma_f^t}\delta - \frac{u_c^t}{\sigma_f^t}\alpha_f^t \tag{3.109}$$

Similarly, for the rear tractor tire:

$$\dot{\alpha}_r^t = \frac{u_c^t}{\sigma_r^t}\left(\frac{v_c^t - b\gamma^t}{u_c^t} - \alpha_r^t\right) \tag{3.110}$$

$$\dot{\alpha}_r^t = \frac{v_c^t}{\sigma_r^t} - \frac{b\gamma^t}{\sigma_r^t} - \frac{u_c^t}{\sigma_r^t}\alpha_r^t \tag{3.111}$$

and for the implement tire:

$$\dot{\alpha}_r^i = \frac{u_c^t}{\sigma_r^i}\left(\frac{v_c^t - c\gamma^t - (d+e)\gamma^i}{u_c^t} + \lambda - \alpha_r^i\right) \tag{3.112}$$

$$\dot{\alpha}_r^i = \frac{v_c^t}{\sigma_r^i} - \frac{c\gamma^t}{\sigma_r^i} - \frac{(d+e)\gamma^i}{\sigma_r^i} + \frac{u_c^t}{\sigma_r^i}\lambda - \frac{u_c^t}{\sigma_r^i}\alpha_r^i \tag{3.113}$$

Because, $\lambda = \varphi^t - \varphi^i$ (eq. 3.12)

$$\dot{\alpha}_r^i = \frac{v_c^t}{\sigma_r^i} - \frac{c\gamma^t}{\sigma_r^i} - \frac{(d+e)\gamma^i}{\sigma_r^i} + \frac{u_c^t}{\sigma_r^i}\varphi^t - \frac{u_c^t}{\sigma_r^i}\varphi^i - \frac{u_c^t}{\sigma_r^i}\alpha_r^i \tag{3.114}$$

Using eqs. 3.81, 3.82 and 3.83, velocity states in terms of α can be written as,

$$(m^t + m^i)\dot{v}_c^t - m^i c\dot{\gamma}^t - m^i d\dot{\gamma}^i = -(m^i + m^t)u_c^t\gamma^t - C_{\alpha,f}^t\alpha_f^t - C_{\alpha,r}^t\alpha_r^t - C_{\alpha,r}^i\alpha_r^i \tag{3.115}$$

$$(I_z^t + m^i c^2)\dot{\gamma}^t - m^i c\dot{v}_c^t + m^i cd\dot{\gamma}^i = m^i cu_c^t\gamma^t - aC_{\alpha,f}^t\alpha_f^t + bC_{\alpha,r}^t\alpha_r^t + cC_{\alpha,r}^i\alpha_r^i \tag{3.116}$$

$$\left(I_z^i + m^i d^2\right)\dot{\gamma}^i - m^i d\dot{v}_c^t + m^i cd\dot{\gamma}^t = m^i du_c^t\gamma^t + (d+e)C_{\alpha,r}^i\alpha_r^i \tag{3.117}$$

The positional states, as given by 3.103, 3.104, 3.105 are

$$\dot{y}_c^t = v_c^t + u_c^t\varphi^t \tag{3.118}$$

$$\dot{\varphi}^t = \gamma^t \tag{3.119}$$

$$\dot{\varphi}^i = \gamma^i \tag{3.120}$$

In matrix form, using eqs. 3.109, 3.111, and 3.114 – 3.120,

$$M\dot{X} = NX + PU \tag{3.121}$$

where,

$$M = \begin{bmatrix} \left(m^t + m^i\right) & -m^i c & -m^i d & 0 & 0 & 0 & 0 & 0 & 0 \\ -m^i c & \left(I_z^t + m^i c^2\right) & m^i cd & 0 & 0 & 0 & 0 & 0 & 0 \\ -m^i d & m^i cd & \left(I_z^i + m^i d^2\right) & 0 & 0 & 0 & 0 & 0 & 0 \\ 0 & 0 & 0 & 1 & 0 & 0 & 0 & 0 & 0 \\ 0 & 0 & 0 & 0 & 1 & 0 & 0 & 0 & 0 \\ 0 & 0 & 0 & 0 & 0 & 1 & 0 & 0 & 0 \\ 0 & 0 & 0 & 0 & 0 & 0 & 1 & 0 & 0 \\ 0 & 0 & 0 & 0 & 0 & 0 & 0 & 1 & 0 \\ 0 & 0 & 0 & 0 & 0 & 0 & 0 & 0 & 1 \end{bmatrix}$$

$$N=\begin{bmatrix} 0 & -u_c^t\left(m^t+m^i\right) & 0 & -C_{\alpha,f} & -C_{\alpha,r} & -C_{\alpha,i} & 0 & 0 & 0 \\ 0 & m^i c u_c^t & 0 & -aC_{\alpha,f} & bC_{\alpha,r} & cC_{\alpha,f} & 0 & 0 & 0 \\ 0 & m^i d u_c^t & 0 & 0 & 0 & (d+e)C_{\alpha,i} & 0 & 0 & 0 \\ \frac{1}{\sigma_f^t} & \frac{a}{\sigma_f^t} & 0 & -\frac{u_c^t}{\sigma_f^t} & 0 & 0 & 0 & 0 & 0 \\ \frac{1}{\sigma_r^t} & -\frac{b}{\sigma_r^t} & 0 & 0 & -\frac{u_c^t}{\sigma_r^t} & 0 & 0 & 0 & 0 \\ \frac{1}{\sigma_r^i} & -\frac{c}{\sigma_r^i} & -\frac{(d+e)}{\sigma_r^i} & 0 & 0 & -\frac{u_c^t}{\sigma_r^i} & 0 & \frac{u_c^t}{\sigma_r^i} & -\frac{u_c^t}{\sigma_r^i} \\ 1 & 0 & 0 & 0 & 0 & 0 & 0 & u_c^t & 0 \\ 0 & 1 & 0 & 0 & 0 & 0 & 0 & 0 & 0 \\ 0 & 0 & 1 & 0 & 0 & 0 & 0 & 0 & 0 \end{bmatrix}$$

$$P=\begin{bmatrix} 0 \\ 0 \\ 0 \\ -\frac{u_c^t}{\sigma_f^t} \\ 0 \\ 0 \\ 0 \\ 0 \\ 0 \end{bmatrix}, \qquad \dot{X}=\begin{bmatrix} \dot{v}_c^t \\ \dot{\gamma}^t \\ \dot{\gamma}^i \\ \dot{\alpha}_f^t \\ \dot{\alpha}_r^t \\ \dot{\alpha}_r^i \\ \dot{y}_c^t \\ \dot{\varphi}^t \\ \dot{\varphi}^i \end{bmatrix}, \qquad X=\begin{bmatrix} v_c^t \\ \gamma^t \\ \gamma^i \\ \alpha_f^t \\ \alpha_r^t \\ \alpha_r^i \\ y_c^t \\ \varphi^t \\ \varphi^i \end{bmatrix}, \qquad U=\begin{bmatrix}\delta\end{bmatrix}$$

The dynamic model with tire relaxation length (Eq. 3.121) was the highest fidelity model developed and used in this work. This model included the three tire relaxation length states in addition to the three positional states and three velocity states represented by the dynamic model developed in the previous subsection. The responses from this model will also be compared with the experimental and other model-based responses. In addition, this model will be used to perform the parameter estimation study and parameter sensitivity analysis presented in the subsequent chapters of this dissertation.

3.5 Steering Dynamics

A steering unit can not reach the commanded steering wheel angle instantaneously. This steering delay has to be modeled to make the simulation response of the agricultural equipment realistic. The steering valve dynamics can be represented by (Bevly et al., 2002; Stombaugh, 1999),

$$\ddot{\delta} = \frac{d_v}{I_v}\dot{\delta} + \frac{K_v}{I_v}u_c(t) \tag{3.122}$$

where d_v is the damping constant, K_v is the input gain and I_v is the inertial constant, all of the steering system. For simplicity, the steering linkage relationship was neglected in developing this steering dynamics equation. In chapter 4, the steering dynamics will be used to study the closed loop characteristics of the three models developed in the previous subsections.

3.6 Steady State Equations

One of the objectives of this research was to estimate and understand the variability of uncertain model parameters using the experimental data. Three cornering stiffness parameters and three tire relaxation length parameters were considered in the parameter estimation study. Steady state equations were derived to simplify the parameter estimation method because the tire relaxation length parameters drop out of the steady state model, and the parameter estimation method then only must estimate three cornering stiffness parameters.

Steady state equations will be developed with the assumption that the first derivative of the positional states will be zero or some constant. With this assumption, at steady state,

the yaw and lateral accelerations will be zero, tractor lateral velocity will be constant, tractor and implement yaw-rates will be constant and equal, and the angle between the tractor and the implement will also be constant. Because the kinematic model equations (Eqs. 3.9, 3.10 and 3.13) do not include velocity states or they are already zero, the model itself was a steady state model. For the dynamic model, the velocity states were equaled to zero to derive the steady state dynamic model equations as follows,

From Eq. 3.76,

$$F_{y,f}^{t} + F_{y,r}^{t} + F_{y,r}^{i} - m^{t}u_{c}^{t}\gamma^{t} - m^{i}u_{c}^{t}\gamma^{i} = 0 \tag{3.122}$$

From Eq. 3.79 and 3.80,

$$aF_{y,f}^{t} - bF_{y,r}^{t} - cF_{y,r}^{i} + m^{i}cu_{c}^{t}\gamma^{i} = 0 \tag{3.123}$$

From Eq. 3.73 and 3.80,

$$m^{i}du_{c}^{t}\gamma^{i} - (d+e)F_{y,r}^{i} = 0 \tag{3.124}$$

From eq 3.80

$$\gamma^{t} - \gamma^{i} = 0 \tag{3.125}$$

Using eqs. 3.122, 3.123, 3.87, 3.90, 3.94

$$C_{\alpha,f}^{t}\frac{v_{c}^{t}+a\gamma^{t}}{u_{c}^{t}} + C_{\alpha,f}^{t}\delta - C_{\alpha,r}^{t}\frac{v_{c}^{t}-b\gamma^{t}}{u_{c}^{t}} - C_{\alpha,r}^{i}\frac{v_{c}^{t}-c\gamma^{t}-(d+e)\gamma^{i}}{u_{c}^{t}} - C_{\alpha,r}^{i}\lambda - m^{t}u_{c}^{t}\gamma^{t} - m^{i}u_{c}^{t}\gamma^{i} = 0$$

or,

$$-C_{\alpha,f}^{t}\frac{v_{c}^{t}}{u_{c}^{t}} - C_{\alpha,f}^{t}\frac{a\gamma^{t}}{u_{c}^{t}} - C_{\alpha,r}^{t}\frac{v_{c}^{t}}{u_{c}^{t}} + C_{\alpha,r}^{t}\frac{b\gamma^{t}}{u_{c}^{t}} - C_{\alpha,r}^{i}\frac{v_{c}^{t}}{u_{c}^{t}} + C_{\alpha,r}^{i}\frac{c\gamma^{t}}{u_{c}^{t}} + C_{\alpha,r}^{i}\frac{(d+e)\gamma^{i}}{u_{c}^{t}} - m^{t}u_{c}^{t}\gamma^{t} - m^{i}u_{c}^{t}\gamma^{i} - C_{\alpha,r}^{i}\lambda + C_{\alpha,f}^{t}\delta = 0$$

or,

$$-C^t_{\alpha,f}\frac{v^t_c}{u^t_c}-C^t_{\alpha,r}\frac{v^t_c}{u^t_c}-C^i_{\alpha,r}\frac{v^t_c}{u^t_c}-C^t_{\alpha,f}\frac{a\gamma^t}{u^t_c}+C^t_{\alpha,r}\frac{b\gamma^t}{u^t_c}+C^i_{\alpha,r}\frac{c\gamma^t}{u^t_c}-m^tu^t_c\gamma^t+C^i_{\alpha,r}\frac{(d+e)\gamma^i}{u^t_c}-m^iu^t_c\gamma^i-C^i_{\alpha,r}\lambda+C^t_{\alpha,f}\delta=0$$

$$-\frac{1}{u^t_c}\left(C^t_{\alpha,f}+C^t_{\alpha,r}+C^i_{\alpha,r}\right)v^t_c-\left(\frac{aC^t_{\alpha,f}}{u^t_c}-\frac{bC^t_{\alpha,r}}{u^t_c}-\frac{cC^i_{\alpha,r}}{u^t_c}+m^tu^t_c\right)\gamma^t+\left(\frac{(d+e)C^i_{\alpha,r}}{u^t_c}-m^iu^t_c\right)\gamma^i-C^i_{\alpha,r}\lambda=-C^t_{\alpha,f}\delta$$

$$-\frac{1}{u^t_c}\left(C^t_{\alpha,f}+C^t_{\alpha,r}+C^i_{\alpha,r}\right)v^t_c-\left(\frac{aC^t_{\alpha,f}}{u^t_c}-\frac{bC^t_{\alpha,r}}{u^t_c}-\frac{cC^i_{\alpha,r}}{u^t_c}-\frac{(d+e)C^i_{\alpha,r}}{u^t_c}+m^iu^t_c+m^tu^t_c\right)\gamma^t-C^i_{\alpha,r}\lambda=-C^t_{\alpha,f}\delta$$

(3.126)

Using eqs. 3.123, 3.125, 3.87, 3.90, 3.94,

$$a\left(-C^t_{\alpha,f}\frac{v^t_c+a\gamma^t}{u^t_c}+C^t_{\alpha,f}\delta\right)-b\left(-C^t_{\alpha,r}\frac{v^t_c-b\gamma^t}{u^t_c}\right)-c\left(-C^i_{\alpha,r}\frac{v^t_c-c\gamma^t-(d+e)\gamma^i}{u^t_c}-C^i_{\alpha,r}\lambda\right)++m^icu^t_c\gamma^i=0$$

$$\text{or, }-aC^t_{\alpha,f}\frac{v^t_c+a\gamma^t}{u^t_c}+aC^t_{\alpha,f}\delta+bC^t_{\alpha,r}\frac{v^t_c-b\gamma^t}{u^t_c}+cC^i_{\alpha,r}\frac{v^t_c-c\gamma^t-(d+e)\gamma^i}{u^t_c}+cC^i_{\alpha,r}\lambda+m^icu^t_c\gamma^i=0$$

or,

$$-aC^t_{\alpha,f}\frac{v^t_c}{u^t_c}-aC^t_{\alpha,f}\frac{a\gamma^t}{u^t_c}+bC^t_{\alpha,r}\frac{v^t_c}{u^t_c}-bC^t_{\alpha,r}\frac{b\gamma^t}{u^t_c}+cC^i_{\alpha,r}\frac{v^t_c}{u^t_c}-cC^i_{\alpha,r}\frac{c\gamma^t}{u^t_c}-cC^i_{\alpha,r}\frac{(d+e)\gamma^i}{u^t_c}+m^icu^t_c\gamma^i+cC^i_{\alpha,r}\lambda=-aC^t_{\alpha,f}\delta$$

or,

$$-\frac{1}{u^t_c}\left(aC^t_{\alpha,f}-bC^t_{\alpha,r}\right)v^t_c+\frac{cC^i_{\alpha,r}}{u^t_c}v^t_c-\frac{1}{u^t_c}\left(a^2C^t_{\alpha,f}+b^2C^t_{\alpha,r}+c^2C^i_{\alpha,r}\right)\gamma^t-\frac{c(d+e)C^i_{\alpha,r}}{u^t_c}\gamma^i+m^icu^t_c\gamma^i+cC^i_{\alpha,r}\lambda=-aC^t_{\alpha,f}\delta$$

or,

$$-\frac{1}{u^t_c}\left(aC^t_{\alpha,f}-bC^t_{\alpha,r}-cC^i_{\alpha,r}\right)v^t_c-\frac{1}{u^t_c}\left(a^2C^t_{\alpha,f}+b^2C^t_{\alpha,r}+c^2C^i_{\alpha,r}\right)\gamma^t-\left(\frac{c(d+e)C^i_{\alpha,r}}{u^t_c}-m^icu^i_c\right)\gamma^i+cC^i_{\alpha,r}\lambda=-aC^t_{\alpha,f}\delta$$

$$-\frac{1}{u^t_c}\left(aC^t_{\alpha,f}-bC^t_{\alpha,r}-cC^i_{\alpha,r}\right)v^t_c-\frac{1}{u^t_c}\left(a^2C^t_{\alpha,f}+b^2C^t_{\alpha,r}+c^2C^i_{\alpha,r}+c(d+e)C^i_{\alpha,r}-m^icu^{i^2}_c\right)\gamma^t+cC^i_{\alpha,r}\lambda=-aC^t_{\alpha,f}\delta$$

(3.127)

Using eqs. 3.124, 3.125, 3.87, 3.90, 3.94,

$$m^i du_c^t \gamma^i - (d+e)\left(- C_{\alpha,r}^i \frac{v_c^t - c\gamma^t - (d+e)\gamma^i}{u_c^t} - C_{\alpha,r}^i \lambda \right) = 0$$

$$\text{or}, m^i du_c^t \gamma^i + (d+e) C_{\alpha,r}^i \frac{v_c^t}{u_c^t} - (d+e) C_{\alpha,r}^i \frac{c\gamma^t}{u_c^t} - (d+e) C_{\alpha,r}^i \frac{(d+e)\gamma^i}{u_c^t} + (d+e) C_{\alpha,r}^i \lambda = 0$$

$$\text{or}, \frac{(d+e) C_{\alpha,r}^i}{u_c^t} v_c^t - \frac{c(d+e) C_{\alpha,r}^i}{u_c^t} \gamma^t - \left(\frac{(d+e)^2 C_{\alpha,r}^i}{u_c^t} - m^i du_c^t \right) \gamma^i + (d+e) C_{\alpha,r}^i \lambda = 0$$

$$\frac{(d+e) C_{\alpha,r}^i}{u_c^t} v_c^t - \left(\frac{c(d+e) C_{\alpha,r}^i}{u_c^t} + \frac{(d+e)^2 C_{\alpha,r}^i}{u_c^t} - m^i du_c^t \right) \gamma^t + (d+e) C_{\alpha,r}^i \lambda = 0 \tag{3.128}$$

Eqs. 2.126 – 3.128 represented the steady state equations for the dynamic model (Eqs. 3.114 - 3.119). A simulation was performed with the parameters of a MFWD tractor (model 7930, Deere and Co., Moline, IL) and a single axle 500 bu (18 m^3) grain cart (model 500, Alliance Product Group, Kalida, OH) system. As seen in the yaw-rate responses to a 10° step steering angle input (Fig. 3.6), the steady state responses of the dynamic model and the dynamic model with tire relaxation length will be the same. This result was expected because the relaxation length terms will just vanish at steady state operation. Hence, the steady state equations for the dynamic model with tire relaxation length will also be the same as eqs. 3.126 – 3.128. The dynamic model with tire relaxation length (Fig. 3.6a) showed a substantially underdamped yaw-rate response, which is unlikely to happen in the reality. This result was expected as the tire relaxation length may not be appropriate at small forward velocity (Rajamani, 2006). The kinematic model yaw-rate response does not have any transient behavior as the model does not include the velocity states. The step steering steady state yaw-rates increased systematically with all three models when the forward velocity was

increased. The steady state turning radius also increased with the forward velocity (Fig. 3.7). This result showed that the tractor and single axle towed implement model was understeered.

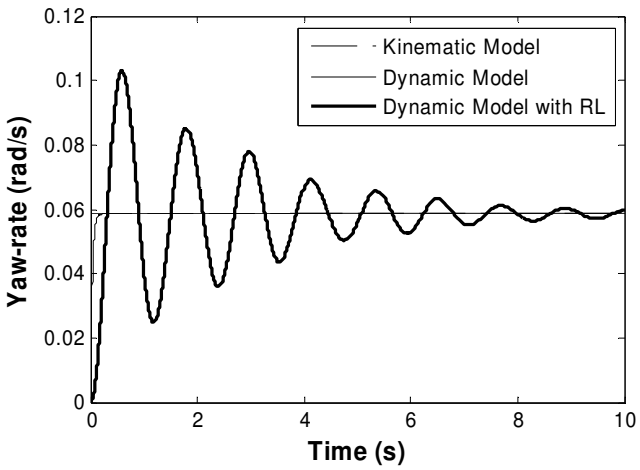

a) at 1.0 m/s

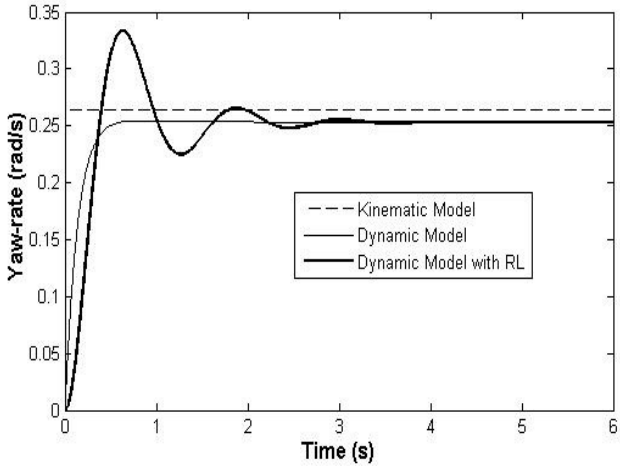

b) at 4.5 m/s

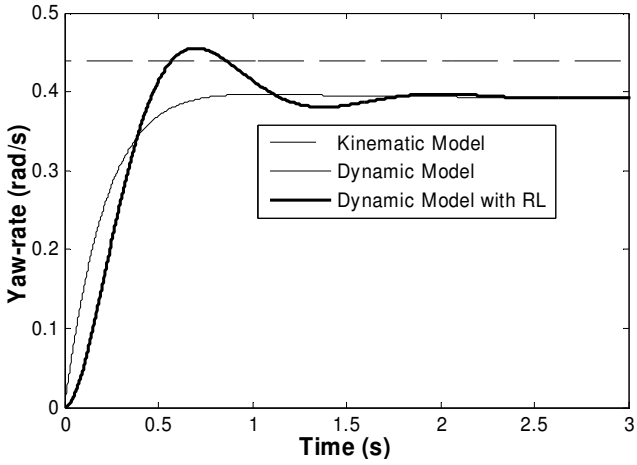

c) at 7.5 m/s

Fig. 3.6: Step steering input (10°) tractor yaw-rate simulated responses of three models at various forward velocities; a) 1.0 m/s, b) 4.5 m/s and c) 7.5 m/s. The kinematic model has a constant simulated response as it does not include the velocity states. Dynamic model and dynamic model with tire relaxation length have different transient responses, but the same steady state responses as the effect of relaxation length vanished at steady state.

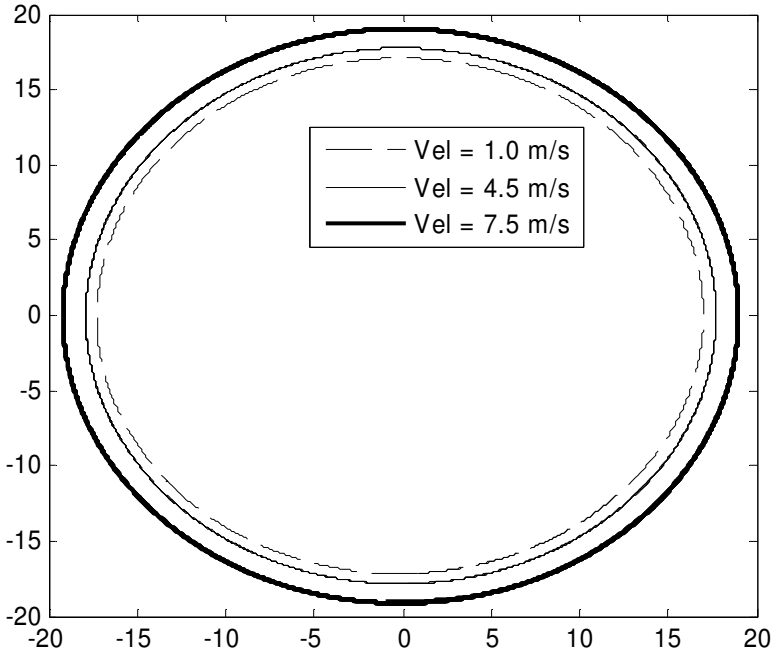

Fig. 3.7: Step steering input (10°) tractor CG trajectories with the dynamic model with tire relaxation length. The x and y positional states were not linearized in these simulations. The steady state turning radius increased as the forward velocity increased; showing that the tractor and single axle towed implement system is an understeer vehicle.

These steady state equations (Eqs. 3.126 - 3.128) can be solved for the tractor lateral velocity, the tractor yaw rate and the angle between tractor and implement longitudinal axes. These equations will be used in Chapter Five to estimate three cornering stiffness parameters of the tractor and single axle towed implement system from the experimental data. The steady state equations simplified the parameter estimation method by providing a set of simpler algebraic equations to the optimization routine.

References

Bell, T. (1999). Precision robotic control of agricultural vehicles on realistic farm trajectory. *PhD dissertation,* Stanford University.

Bevly, D. M., J. C. Gerdes, and B. W. Parkinson (2002). A new yaw dynamic model for improved high speed control of a farm tractor. *Journal of Dynamic Systems, Measurement, and Control*, 124: 659-667.

El-Gindy, M. (1989). Directional response of a tractor towing a semitrailer. *International Journal of Vehicle Design,* 10(2): 211-226.

Deng, W., and X. Kang (2003). Parametric study on vehicle-trailer dynamics for stability control. *SAE Transactions, Journal of Passenger Cars*, 2003, 411-1419.

Feng, L., Y. He, Y. Bao, and H. Fang (2005). Development of trajectory model for a tractor-implement system for automated navigation applications. *Instrumentation and Measurement Technology Conference*, Ottawa, Canada, May 17-19.

Greenwood, D. T. (1965). Principles of Dynamics. Engleswood Cliffs, NJ, *Prentice Hall*.

Rajamani, R. (2006). Vehicle dynamics and control. New York, N.Y., USA: *Springer.*

Torishu, R, S. W. Mugucia, and J. Takeda (1992). The kinematics and open-loop characteristics of tractor-trailer combinations. *Journal of Faculty of Agriculture*, Iwate University 20: 299-314.

CHAPTER 4. MODELING AND REAL-TIME SIMULATION ARCHITECTURES FOR VIRTUAL PROTOTYPING OF OFF-ROAD VEHICLES

A paper submitted to *Virtual Reality*

Manoj Karkee, Brian L. Steward, Atul G. Kelkar, Zachary T. Kemp II

Abstract

Virtual Reality (VR)-based simulation environment has evolved as a useful design and analysis tool at an early stage in the design for evaluating performance of human-operated agricultural and construction machinery. Detecting anomalies in the design before building physical prototypes and expensive testing leads to significant cost savings. The efficacy of such simulation environment depends on how realistically the simulation mimics the real-life operation of the machinery. It is therefore necessary to achieve real-time simulation of the dynamics of such machines with operator-in-the-loop functionality. Such simulation often leads to a substantial computational burden. A distributed architecture was developed for off-road vehicle dynamic models and 3D graphics visualization to distribute the overall computational load of the system across multiple machines. Multi-rate model simulation was also used to simulate various system dynamics with different integration time steps so that the computational power can be distributed more intelligently. This architecture consisted of three major components: a dynamic model simulator, a virtual reality simulator for 3D graphics, and an interface to the controller and input hardware devices. Several off-road vehicle dynamics models were developed with varying degrees of fidelity, as well as automatic guidance controller models and controller area network interface to embedded

controllers and user input devices. The simulation architecture reduced the computational load to an individual machine and increased the real-time simulation capability with complex off-road vehicle system models and controllers. This architecture provides an environment to test virtual prototypes of the vehicle systems in real-time and the opportunity to test the functionality of newly developed controller software and hardware.

Keywords: real-time simulation, distributed architecture, virtual reality, vehicle dynamics models, multi-rate simulation

4.1 Introduction

Globalization has put tremendous pressure on U. S. manufacturers to reduce the cost of manufacturing goods while maintaining product quality and reliability to remain ahead in the competition. In particular, manufacturers of off-road machinery face a difficult challenge as the cost of design, development, and prototyping is very high due to the size and complexity of their products. A major portion of this cost involves the time taken to design and build the prototype machines and iterate through the design process based on the evaluation of the prototype. A long product development cycle time can cause significant delays in the introduction of a product to the market and a loss of first to market position. In addition, modern off-highway machines are truly mechatronic machines in the sense that they are based on several engineering technologies including mechanisms, fluid power (hydraulics), electronics and embedded control. The design of such machine requires substantial amounts of systems integration, and thus early virtual prototyping and hardware-in-the-loop (HIL) testing is necessary for system design.

The advancement of the virtual reality (VR) technology offers exciting possibilities in this regard. In manufacturing, VR technology can be used to rapidly develop digital prototypes of the planned or existing products. VR-based digital prototyping, also called virtual prototyping, offers a realistic and flexible presentation of, and interaction with the digital prototypes (Sastry and Boyd, 1998; Howard and Vance, 2007). The main goal of virtual prototyping is to provide an immersive and interactive virtual environment for the design engineers and product users to examine the accuracy of and usability of the design, which is achieved through immersive displays, haptics, and other sensory input devices (Sastry and Boyd, 1998). Virtual prototyping offers a faster and low cost environment to test the new product designs or modifications to ensure that minimal problems occur at the production stage. The reduced physical prototyping and production life cycle will substantially reduce the product development time and cost while improving the product quality (Savall et al. 2002, Howard and Vance, 2007).

Models of product system dynamics and simulation are essential components of the virtual prototyping (De Sa and Zachmann, 1999; Antonya and Talaba, 2007; Howard and Vance, 2007). To fully utilize virtual prototypes, these prototypes must be based on high-fidelity dynamic simulation, which not only includes, at times, a complete nonlinear model of the entire machine, but also has realistic controller and operator interfaces. High-fidelity dynamic model simulation and realistic visualization helps design engineers understand the behavior of the new or existing off-road vehicle systems so that modifications or iterations through the product design and development cycles can be accelerated. In addition to rapid virtual prototyping, dynamic model simulation and VR visualization provide the benefits of easier and low cost modeling and testing environment and convenience for studying user's

perception and interaction with the new design (Cremer et al., 1996; Schulz et al., 1998; Kang et al., 2004; Castillo-Effen et al., 2005).

Various virtual prototyping applications using system dynamics model simulation and VR have been proposed in the literature to aid in the design, test and manufacture of various vehicle system products (Cremer et al., 1996; Sastry and Boyd, 1998; Schulz et al., 1998; Fales et al., 2005; Antonya and Talaba, 2007; Howard and Vance, 2007). The National Advanced Driving Simulator (NADS) facility at the University of Iowa (Cremer et al., 1996) provided an operator-in-the-loop simulation system which has been used in transportation studies, virtual prototyping and medical research. Schulz et al. (1998) developed an environment for visualizing car-body virtual prototypes. Cuadrado et al. (2004) developed a virtual prototype of a car to evaluate the trajectory responses and optimize the vehicle design. A multi-body system dynamics model was used to simulate the physical behavior of the system. Castillo-Effen et al. (2005) proposed a distributed architecture for modeling and visualization of multiple vehicles. Eberhard and Li (2006) also developed several simulation systems based on the VR and multi-body system dynamics. Antonya and Talaba (2007) developed a VR-based product evaluation and modification environment for mechanical systems.

In the area of virtual assembly, Johnson and Vance (2001) developed an assembly system using a physics engine to simulate the motion of virtual objects. Kim and Vance (2002) expanded this system with haptic capability, and Howard and Vance (2007) modified the system to develop a haptics based desktop virtual assembly system. Similar virtual assembly systems were developed by Jayaram et al. (1999), Coutee and Bras (2002), Wan et al. (2004), and Zhu et al. (2004). VR has also provided an environment for simulating tele-

operation and monitoring of robots and autonomous vehicles (Lin and Kuo, 1997; Gracanin el al., 1999) and an interactive environment for vehicle controller design and performance evaluation (Eberhard and Li, 2006). However, generality and flexibility of adding new devices or machines to the simulation system was not emphasized in most of these developments, which may limit the wider applicability of the system. In addition, it is important that off-road vehicle simulation and visualization systems include operator-and-controller-hardware-in-the-loop capability, which is essential to test the performance of new software and hardware controller devices in various field conditions that may be very difficult or expensive to find in the real world.

In hardware and operator in the loop simulation and VR visualization, real-time dynamics simulation is required to allow users to intuitively interact with the realistic virtual prototypes and to evaluate the performance of physical hardware. However, achieving a real-time simulation goal becomes challenging when the high-fidelity dynamic model simulation is required along with the realistic virtual reality visualization (Antonya and Talaba, 2007, Howard and Vance, 2007). In most of the systems mentioned above, real-time simulation was not achieved or was limited to moderately-sized dynamic models. To meet these requirements and facilitate virtual prototyping of off-road vehicle systems, there is a need to develop a generic and flexible modeling, simulation and visualization system. The overall goal of this work was to develop a generic and flexible real-time VR-based simulation system for off-road dynamics models with operator and hardware in the loop configuration. The specific objectives were to:

- Develop a general-purpose, real-time, dynamic simulator for off-road vehicles in a virtual reality (VR) environment with controller-hardware-and-operator-in-the-loop capability,
- Provide *plug and play* type functionality for simulation architecture requiring minimal effort to switch between models and controllers, and
- Enhance the real-time capability of the simulation using distributed and multi-rate simulation techniques.

4.2 Real-time Simulation Architecture

A system is said to be a real-time system if the correctness of the system responses depends on both the accuracy and timeliness of the computation (Stankovic, 1988). For real-time systems, even though a computation generates the correct system responses, the responses could be regarded as unsuccessful if they lag physical time (Glinsky and Wainer, 2002). A real-time VR-based simulation is required to enable the user to visualize and perceive the effect of their actions during the simulation in real-time (Antonya and Talaba, 2007). The primary goal of this work was to provide a real-time simulation environment to the users, which is also flexible, extendable and scalable. As mentioned before, this goal of real-time VR-based simulation of off-road vehicles is challenging because of the heavy computational load required. To achieve this goal, a distributed vehicle simulation and visualization architecture (Fig. 4.1) was developed. The architecture consisted of three components: a vehicle dynamics model and model simulator, a VR geometric model and visualization system and an interface to controller and input hardware devices. The

architecture provided the flexibility of distributing different components of the system across multiple processors to harness more computational capacity for the simulation.

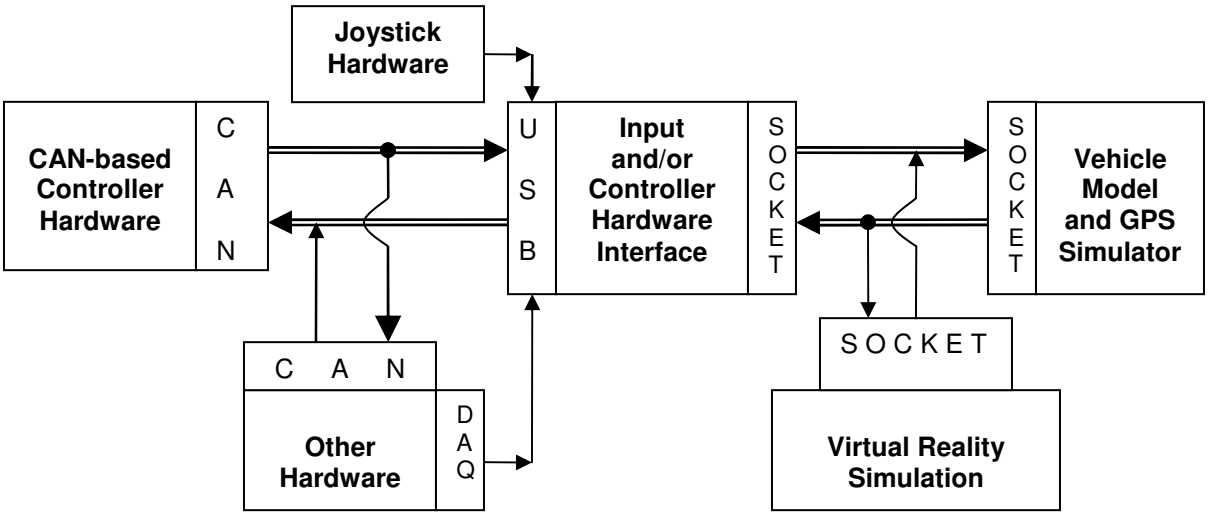

Fig. 4.1: Generic distributed VR-based simulation architecture for off-road vehicle system dynamics models. The block diagram shows the communication paths and messages among the software and hardware components incorporated in system.

All three components of the simulation architecture were implemented in such a way that the modeling, simulation and visualization systems were highly flexible to allow modifications without major programming efforts (Castillo-Effen et al., 2005). Existing technologies were surveyed to identify the best candidates for the implementation to meet the following three primary requirements.

1) *Modifiable:* Easy to modify the visualization environment as well as swappability between available geometric and dynamic models
2) *Portable* across multiple environments
3) *Extendable*: Easy to extend the system to include more dynamic models and additional hardware interfaces

4.2.1 Modeling and Simulation Environment and Dynamics Modeling

Matlab Simulink (The Mathworks, Natick, MA) was used for the dynamic system model development. Matlab Simulink offered several desirable features such as:

- block-diagram based modeling, which allowed to model a system with multiple hierarchical subsystems essential for cleaner and generalized modeling (eg. swappable subsystems),
- facility to include C/C++ code allowing easier socket programming and machine synchronization,
- facility to automatically translate Simulink block diagrams into low level code and to build into executables, consequently accelerating the simulation speed.

To enable dynamic simulations to be seamlessly integrated into current and future VR applications, a modular environment was adopted for the vehicle dynamics modeling. This modeling environment was based on a system of data buses defining the interfaces between vehicle sub-systems and the encapsulation of the vehicle sub-systems into swappable model blocks. The I/O bus was designed to eliminate the need for the user of the system to manually make connections between dynamic model blocks. Through the data buses, all signals were routed using Simulink tags, which acted as *wireless* links between model blocks. Each model block in this environment was a subsystem with a self-contained set of inputs and outputs connected to buses. Thus, this modeling environment fostered a modular environment so that users without detailed modeling expertise can still assemble vehicle dynamics models and run simulations. This environment not only presented a cleaner appearance and simpler modeling environment, but also enabled model component swappability for dynamic system models of vehicles and components. Using the available set of subsystem model blocks with

varying complexity, users can easily optimize the model complexity to match available computational power and meet the need of the real-time simulation. Users can also develop their own models and add to the library with minimal effort.

Off-road vehicle sub-system models were developed and incorporated into a *model block library* (Fig. 4.2). The library included a preliminary set of sub-system models for a wheel loader, an agricultural tractor and towed implement, and a backhoe loader. The subsystem models included were chassis models, drive train models, linkage models, hydraulic models, navigation controller models, steering controller models, a VR interface, a hardware interface, and an internal data bus. The interfacing subsystems were developed using C-language code within the Simulink S-function builder blocks. Transmission Control Protocol/Internet Protocol (TCP/IP) sockets were used as the communication channels.

Alternative models developed for a particular sub-system were categorized into the common groups in the model block library. Different blocks from the same category can be swapped in and out of a vehicle system model without any changes to the system. Using the simulation architecture and the model block library, the set-up of the dynamics for an off-road vehicle simulation was a simple process consisting of the following three steps.

1. Select one instance of each category of required blocks and ‘Setting/Communication Bus’ block from the library.
2. Place each of these blocks in a Simulink Workspace.
3. Compile with Real-time Workshop and produce an executable.

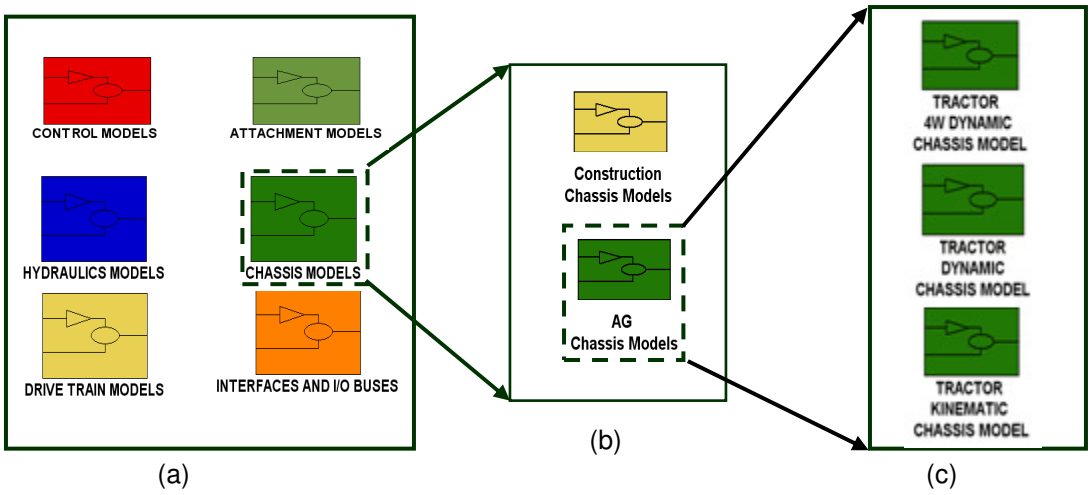

Fig. 4.2: Generic modeling and simulation environment for off-road vehicle systems; a) library of generic model blocks, b) available vehicle chassis models, and c) available chassis models for a tractor.

4.2.2 VR Visualization

The second component of the architecture was the VR visualization system. For an off-road vehicle visualization system to be widely adaptable, it should provide an environment with the following features:

- Seamless handling of low level details like culling, texture mapping, and rendering.
- Scalable from a desktop to a six sided VR CAVE visualization systems.
- Feel of realism and interactivity such as immersion, and walking through the scene.
- Ease of manipulating the scene such as swapping different scene and vehicle models, setting initial location and orientation of the scene.

VR technology was used to visualize the off-road vehicle systems (Fig. 4.3a) because it offered all of the required features. The visualization system was based on a hierarchy of several programming tools and libraries (Fig. 4.3b). VR Juggler (Infiscape Corporation,

Ames, IA) was the backbone of this visualization system, which provided a generic virtual reality development platform. The VR Juggler-based visualizations can be scalable from a desktop VR to a fully immersive VR. Open Scene Graph (OSG) (AI2, Universidad Politecnica de Valencia, Spain) was used as the computer graphics engine.

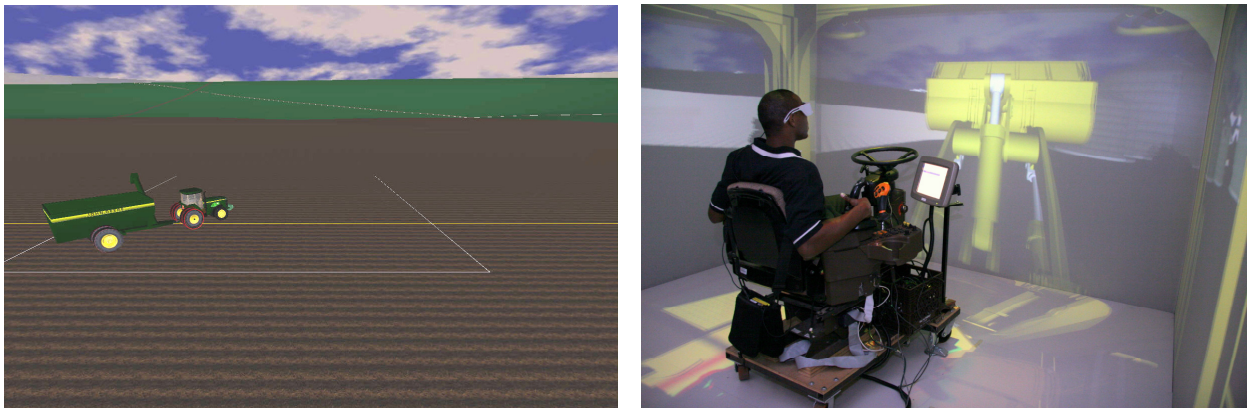

a) **b)**

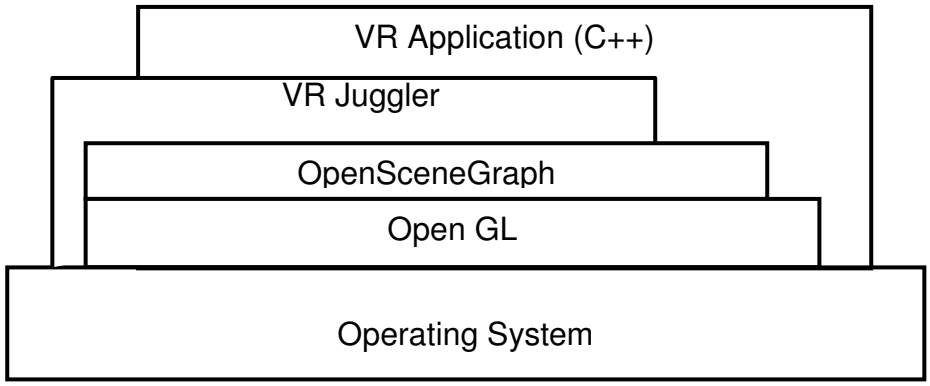

c)

Fig. 4.3: Off-road vehicle VR visualization system, a) the virtual farm scene with an example machine, b) operator in the loop interface for real-time simulation with a four sided CAVE VR visualization (Virtual Reality Application Center, Iowa State University), and c) the software hierarchy.

A generic application structure was developed for the VR visualization based on a XML parameter file. Visualization and communication-related parameters were read from a

user defined parameter file, which provided the flexibility and simplicity in selecting the required vehicle geometries and setting the initial position and orientation of the vehicles in the virtual scene. The capability to switch geometric models of vehicle parts, implements, and attachments during run-time was also implemented so that the design reviews can be performed conveniently. A shared application data structure was implemented to synchronize the communication between dynamics simulator and the clustering nodes used in the immersive VR.

Incorporation of the real terrain into the VR visualization system was essential for studying vehicle dynamic behavior and safety scenarios in realistic terrains. Publicly available digital elevation models (DEM) provided by the United States Geological Survey (USGS) were incorporated into the virtual world. DEMs represent the elevation data using regularly gridded points over the field. ArcGIS (ESRI, Redlands, CA) was used to convert gridded elevations into polygonal representation in VRML format before importing it to the OSG. The VR application implemented terrain following by collision detection of each vehicle wheel with the virtual world terrain.

4.2.3 Hardware Interface

The third component of the simulation architecture was the interface between the vehicle model simulator and the controller and operator input hardware. Visual C++ was used to develop the interfacing program in Windows platform. The interface was capable of communicating with Controller Area Network (CAN)-based hardware. CAN is an asynchronous serial network used in vehicle systems, which was designed to allow controllers and other electronic units to communicate among each other without requiring a

host computer (Bosch, 1991). Because CAN bus is a common resource to all the nodes connected to it, a priority-based arbitration and scheduling, also called Carrier Sense Multiple Access with Collision Avoidance (CSMA/CA), is used to meet the deadlines of each unit in spite of the competition for the communication medium (Livani et al. 1999). CAN specifications for data transfer requires an arbitration or identifier field to specify a source address and global priority among the nodes. The specification allows 0 to 8 byte CAN message transmitted in the data field (Fig. 4.4).

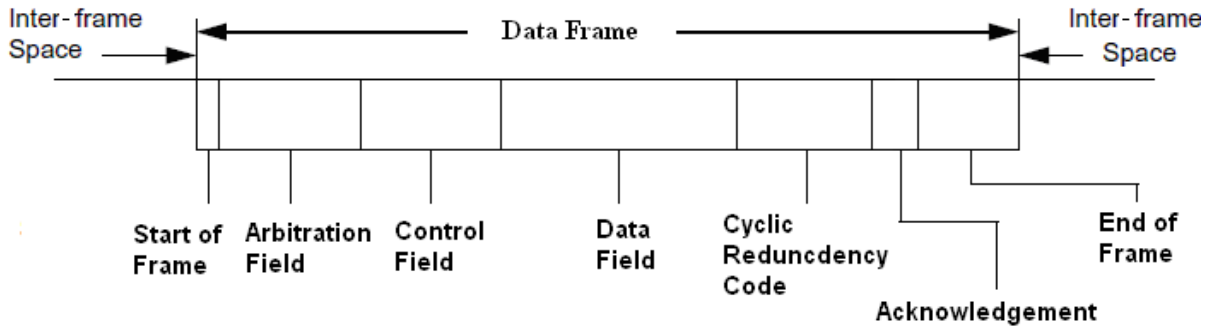

Fig. 4.4: CAN data frame structure. Arbitration field, also known as identifier, is used to resolve the conflict when two or more nodes in the network send messages at the same time.

CAN protocol allows only a message-based communication meaning that the messages are broadcasted to the bus without specifying any destination address. A CAN node has to scan through all the CAN messages in the bus to find out the useful messages to this node. The standard supports up to 1Mbits/s data transfer rate (Pazul, 2009). The interface program developed in this work simulated a virtual CAN node to read and write required CAN messages. The interface also incorporated a Data Acquisition (DAQ) system to sense various physical hardware signals. Joystick devices were also interfaced to provide additional user inputs. The interface communicated to the system dynamics simulator through a TCP/IP

socket and to the hardware through the USB ports. A CAN to USB adaptor (LAWICEL AB, Sweden) was used to provide a hardware interface to the CAN-based hardware.

4.2.4 Communication Scheme

The three components of the distributed simulation architecture communicated to each other using a client-server TCP/IP sockets. The system dynamics model simulator was designated as the server to establish socket communication as this component was required to communicate with both the hardware interface and VR visualization system. Two server sockets were implemented in the vehicle system model blocks; one responsible to receive data from the hardware interface and the other from the VR visualization system. One client socket was created each in the hardware interface and the VR visualization systems. A generic packet structure was defined for each communication channel (model simulator to VR, VR to model simulator, model simulator to hardware interface, and hardware interface to model simulator) to provide a common communication protocol required to simulate various off-road vehicle systems.

At the start of a simulation, the vehicle model simulator started a server socket and waited for the connection request from the hardware. Similarly, another server socket waited for the VR visualization system. Once the connections were made, handshaking was performed to identify and initialize the data communication among the components. Then the information produced by the vehicle model simulator (e.g. position, attitude, yaw-rate) was sent to both the hardware interface and the VR visualization. Using this information, the interface generated messages in the format that CAN-based hardware recognizes and sent them over the CAN network to the hardware. The CAN-based hardware can scan and parse

the messages and generate required signals. The interface was also responsible for acquiring user inputs through hardware data acquisition systems and forward the signals to the vehicle model simulator.

The VR visualization system received the required information from the model simulator and applied corresponding transformations/mapping to the appropriate objects in the virtual environment. The VR visualization system was also responsible for estimating and sending vehicle attitude information back to the vehicle model simulator to simulate the vertical, roll and pitch chassis dynamics. In this communication scheme, each component in the architecture sent one data packet every 20 ms. This speed was sufficient to communicate with user input devices and other hardware whose practical frequency/data-rate, often, was about 5 Hz. The speed was also enough to visualize the system with reasonable refresh rate (~50 frames per second). As the data rate required was not very demanding, the Ethernet communication medium used in this architecture provided the required bandwidth without any problem.

4.3 Case Studies

4.3.1 Multi-rate simulation

Real-time simulation is necessary for virtual prototyping in off-road vehicle systems design and development. The distributed simulation architecture harnessed the computational power of multiple processors to increase the real-time simulation capability for off-road vehicle models. However, as the model complexity is increased in the pursuit of higher

accuracy and fidelity, the dynamic model simulation alone may limit the real-time simulation capability.

Various strategies were investigated to reduce the computational burden on the dynamics model simulation so that real-time simulation can be achieved for increasingly complex models. Simulation speed can be increased by simplified rigid body dynamics, constraint maintenance, and velocity slow down compensation but the model accuracy and/or fidelity will be compromised (Howard and Vance, 2007). Selecting a suitable simulation time step was also found to be critical to achieve a good trade-off between the simulation speed and the accuracy of the simulation results.

When modeling and simulating the dynamics of mechatronic systems typical of off-road vehicles, models will tend to consist of sub-system models which have slower and faster dynamics and are often lightly coupled. One way to improve the real-time performance of these stiff dynamical systems is to simulate different subsystems at different rates, so that unnecessary computational burden is reduced (Fig. 4.5). The modular simulation architecture developed in this work offered a highly favorable modeling and simulation environment to implement multi-rate simulation. Multi-rate simulation also provided an opportunity to divide subsystem models into different machines to further increase the computational efficiency and thus the real-time capability.

Multi-rate simulation was implemented by creating two different model blocks containing relatively faster and slower dynamics in each model. Socket communication provided the required communication between two models. In this simulation approach, there were three different time steps to be determined; the time step for slower dynamics (T), the time step for faster dynamics (t), and rate at which the two models communicate (c). Because

faster dynamics require a smaller time step, the relationship $t<T$ is always true. It can also be assumed that the relation t<c<T will hold for the communication time step *c*. There is a trade-off in selecting these time steps. Larger time steps might lead to instability or loss of accuracy while smaller time steps might lead to slower simulations. The choice of *t* and *T* also depends on the solver or integrator used for each model. It is preferable to use the best possible solver for the faster dynamics model and a moderately accurate solver for the slower dynamics model. However, the solvers can be changed if they don't give rise to either the required accuracy or stability or real-time speed.

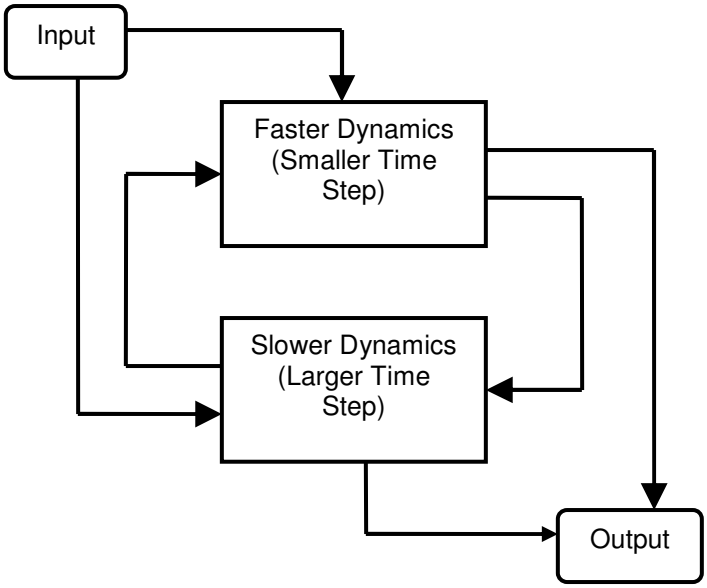

Fig. 4.5: Multi-rate simulation scheme. Faster and slower dynamics were separated and simulated with different time steps.

To choose the three time steps, first, a maximum value of a time step *s* was found with which the whole model ran without instabilities (Fig. 4.6). This value of s was used as the reference point for all the three time steps *t*, *c* and *T*. The initial estimates for *t* was anywhere between *s*/10 and s/5, and *c* and *T* were set equal to s. If the simulation was

numerically unstable with these time steps, the value of *t* was decreased until the system became stable. If the simulation was stable, c and T were increased together until the system became marginally stable. The time step *c* was fixed at that point and *T* was further increased until real-time simulation was reached without affecting the stability. If the real-time goal was not achieved, larger time step *t* and reduced order hydraulics solver were investigated.

In this case study, a backhoe loader model was developed using the library blocks developed in this work (Fig. 4.7a). The model consisted of a rear linkage dynamics, linkage hydraulics dynamics, interface to VR visualization, interface to the operator inputs, and vehicle ID. The user input interface program was developed to establish communication with USB based joysticks and received signals from the joysticks and sent this information back to the vehicle model via a TCP/IP socket. These joystick signals were used to provide steering, drive, brake and lift inputs required for the dynamic simulation. *Vehicle ID* block was required to inform the VR visualization system of the type of machine being simulated so that appropriate geometric models can be loaded and simulated.

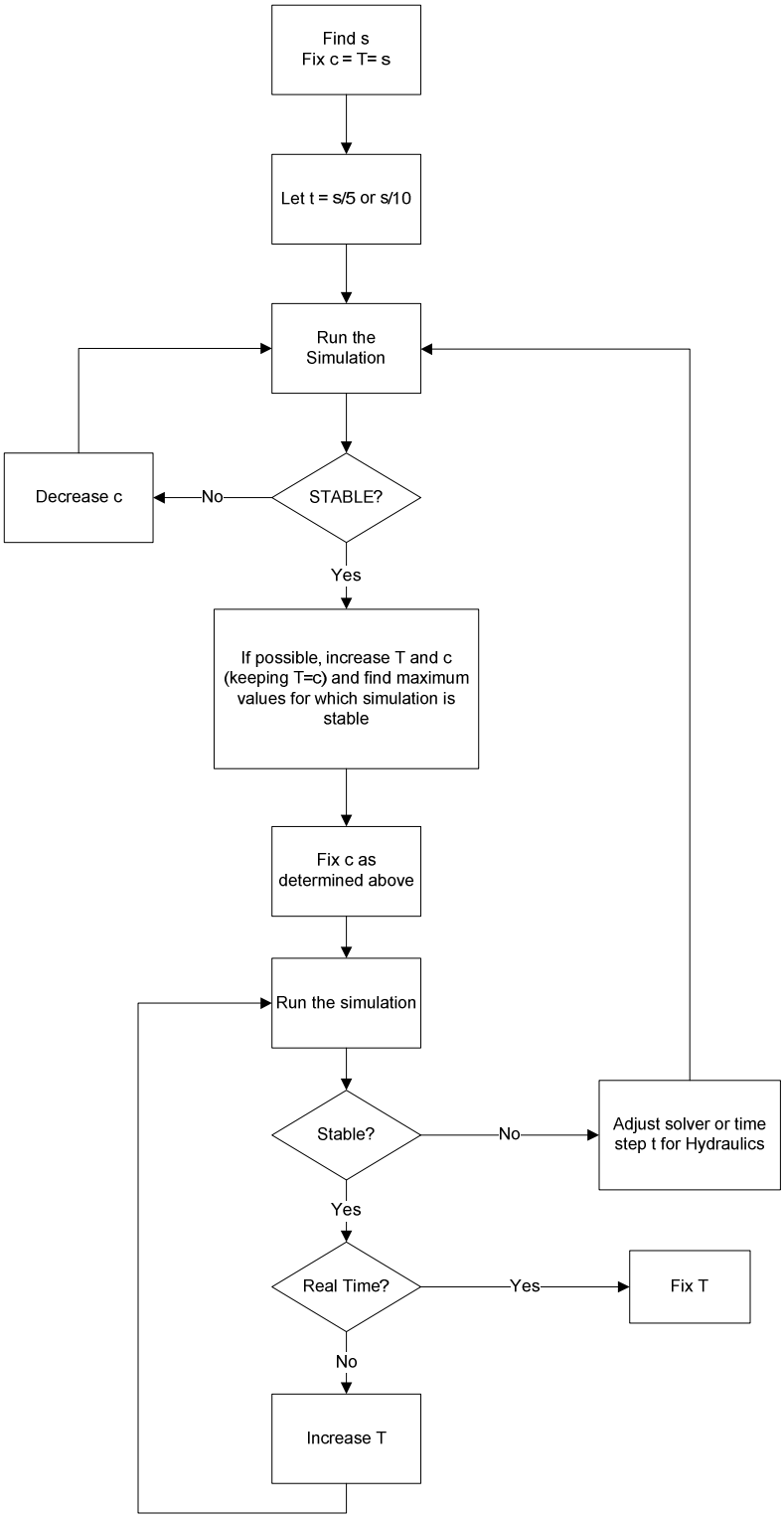

Fig. 4.6: Selecting the simulation time steps for the multi-rate simulation of a complex dynamics model.

For the loader model, the linkage and the linkage hydraulics were the two main components offering the possibility of the multi-rate simulation. The hydraulics dynamics required a smaller time step to run as compared to the loader linkage dynamics. A multi-rate simulation approach was implemented to improve the real-time simulation capability for this model (Fig. 4.7b). As mentioned before, there were two solvers and three time steps to be chosen to perform this multi-rate simulation. A fifth order solver/integrator (Simulink *ode5*) was suitable for the hydraulics block while a third order solver (Simulink *ode3*) was suited for the linkage block. The simulation time steps *s*, *t*, *c* and *T* were 0.005 s, 0.001 s (ode5 solver), 0.002 s and 0.008 s (ode3 solver) respectively.

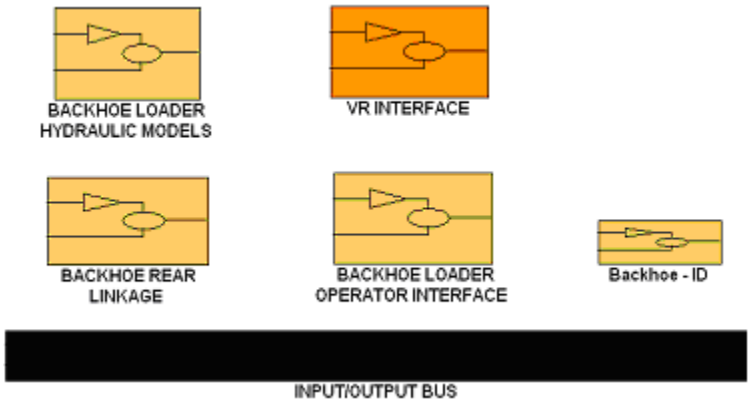

a)

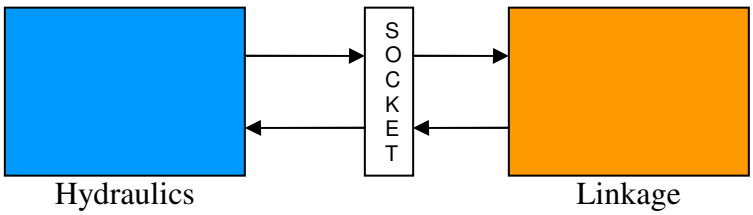

b)

Fig. 4.7: A wheel loader model developed using the model block library; a) top level view and b) multi-rate simulation with socket communication.

4.3.1.1 Discussion

Multi-rate simulation, in addition to the computational efficiency provided by the distributed architecture, provided a method to reduce the burden on the dynamics simulator due to unnecessarily small integration time step could be reduced. The following metric was used to compare the real-time performance of the single-rate and multi-rate simulations.

$$p(t_r) = \frac{1}{T}\int_o^T (t_s - t_r)dt_s \tag{4.1}$$

where, p = performance index, T = total simulation time, t_r = real-time, t_s = simulation time. The result indicated that the time deficit of the single rate simulation to meet the real-time goal was increasing exponentially with simulation time whereas that of the multi-rate simulation remained constant at a very low value over the entire simulation period (Fig. 4.8).

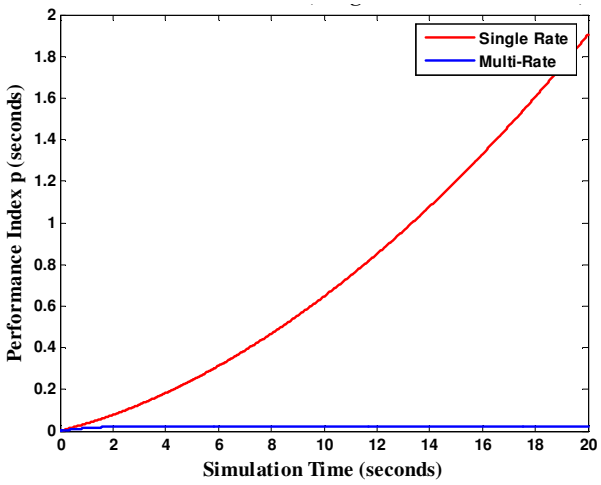

Fig. 4.8: Real-time simulation performance with the single rate and multi-rate simulation techniques.

This case study demonstrated that the multi-rate dynamics modeling can be used successfully to reduce the computational burden of the real-time VR-based simulation of off-road vehicle systems.

4.3.2 Operator and controller hardware in the loop simulation

The ability to test the performance of various software and hardware controllers in the virtual environment can reduce the development time and cost for the new controllers. Using the real-time VR-based simulation architecture, a Controller-Hardware-In-the-Loop (CHIL) simulation was implemented to incorporate CAN based navigation system and automatic steering controller hardware. In contrast to the classical concept of hardware-in-loop (HIL) system, which involves simulating a controller and putting a real machine in the loop, the CHIL system simulates the machine and puts the hardware controller in the loop. This scheme enabled the simulation study of the performance of newly developed controller hardware and software. The scheme also enabled the study of the vehicle dynamics models with the current controller hardware. The generic simulation architecture (see section 2) was used to perform this case study with the navigation and universal steering controller hardware units in the loop (Fig. 4.9).

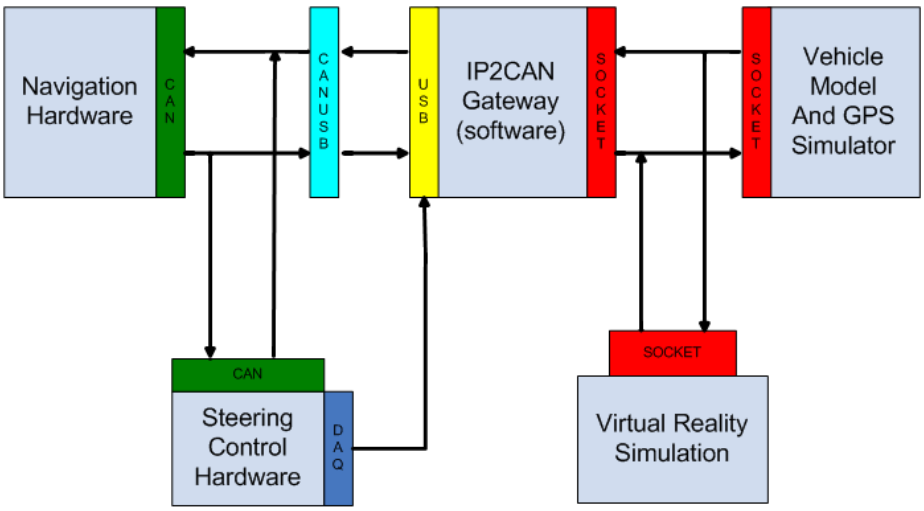

Fig. 4.9: An implementation of Controller-Hardware-In-the-Loop (CHIL) architecture using commercial navigation and steering controller hardware.

Various component models were selected from the model block library (see section 3.2) to construct a tractor and towed implement system model with CHIL configuration. The vehicle system model included a chassis model, a drive train model, an interface to the navigation controller hardware (including GPS simulator), an interface to the steering controller hardware, an interface to the VR visualization, an Input/Output bus and a Vehicle ID (Fig. 4.10). An implement model was also added to the system. *Vehicle ID* block was required to inform the VR visualization of the type of machine being simulated so that appropriate geometric models can be loaded and simulated. Three different tractor chassis models of varying fidelity were developed and included in the model block library. Using the model block library and the simulation environment, the three chassis models were swapped in and out alternatively to observe the simulation speed with each chassis model.

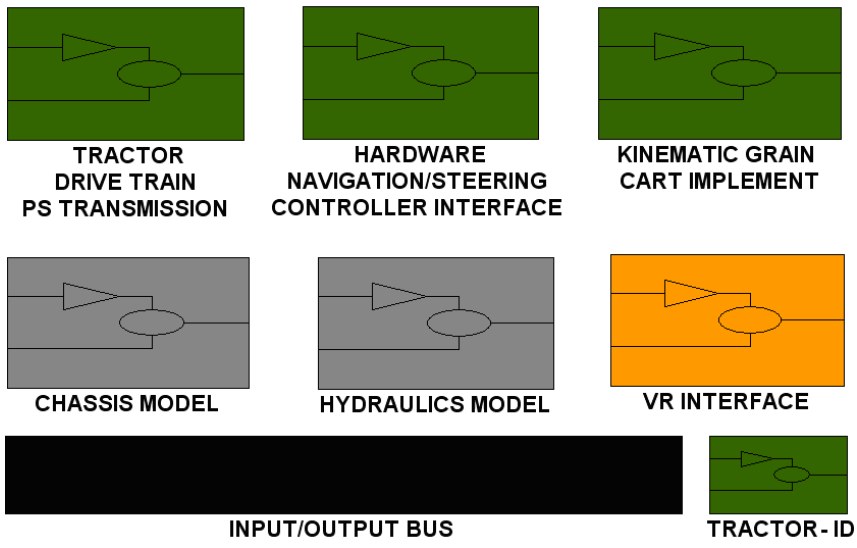

Fig. 4.10: Controller-Hardware-In-the-Loop (CHIL) simulation of an agricultural tractor: a Simulink model with interfaces to the controller hardware and steering unit

A Global Positioning System (GPS) simulator was included in the vehicle model block, which converted the vehicle position into latitude and longitude format. The vehicle

position, attitude and yaw-rate data produced by the model simulator were next sent to the interface software through a TCP/IP socket. An interface to Controller Area Network (CAN) called TCP/IP socket-to-CAN or the IP2CAN gateway was developed to communicate with the CAN-based hardware. The IP2CAN gateway managed the communication between the dynamic model and the hardware. The gateway received the vehicle position, attitude and yaw velocity information from the dynamic model simulator, converted it to the format that navigation hardware understands, and sent it out to the controller hardware over a CAN bus. The gateway was also responsible to receive the off-tracking and heading errors from the navigation controller hardware, convert the messages into the form the vehicle dynamics simulator understands and send them out to the dynamic simulator over the TCP/IP socket. The gateway program implemented a state logic structure to produce the required CAN messages to enable automatic steering function on the navigation controller hardware. A number of additional messages were necessary to establish a connection and interact with the navigation controller hardware through a simulated GPS receiver. If all the required messages were present in the CAN network, the navigation controller enabled the automatic steering functionality and started generating navigation error messages (off-tracking error and heading error). These errors were calculated and broadcasted over the CAN bus once for each set of position and attitude messages received by the navigation controller. The steering controller unit read and parsed these errors and applied them to generate the proper steering angle based on the controller implemented in the hardware.

The IP2CAN gateway was also responsible for reading in the steering angle from the hardware steering controller and sending that over to the model, which was used as an input steering angle to the vehicle dynamics. A hardware data acquisition (DAQ) system was

developed to acquire the steering angle signal. The vehicle model simulator, on the other end, received the steering angle and other input signals, and applied them to the vehicle system model thus completing the simulation loop.

4.3.2.1 Discussion

The CHIL simulation was successfully implemented using the distributed architecture and modular dynamics modeling and simulation environment. The simulation demonstrated that the architecture can be used to perform various controller and operator hardware-in-the-loop real-time VR-based simulations, which will be valuable to interactively test the performance of newly developed controllers for various off-road vehicle subsystems in various field conditions that may be very difficult or expensive to find in the real world. The VR visualization included field boundaries and the predefined path that an autonomous off-road vehicle is going to follow. The actual path followed by the vehicle can also be inserted. These path lines enabled a user to visually evaluate the performance of an autonomous vehicle guidance algorithm.

As mentioned before, the CHIL simulation was performed with tractor chassis model of varying fidelity and complexity. The models used were a kinematic model, a two wheel dynamic model and a four wheel dynamic model. The kinematic model and the four wheel dynamic model were respectively the simplest and the most complex models among the three models. As the model complexity increased, the computational time for each simulation cycle was increased substantially (Fig. 4.11). A desktop computer (model 7570, Dell, Round Rock, TX) with Pentium 4, 2.8 GHz, microprocessor running with 1 GB system memory and running Windows XP took approximately 100 times longer to finish a single simulation cycle of the four wheel dynamic chassis model as compared to that of the kinematic model. The

result helped to identify an appropriate chassis model to achieve a real-time simulation with the available computational resources.

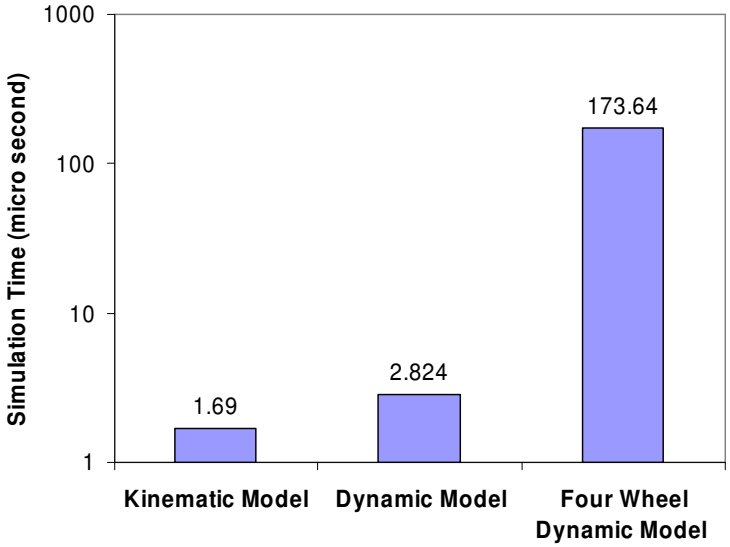

Fig. 4.11: Computational time for each simulation cycle of different tractor chassis model. The simulation time of the four wheel dynamic model was substantially higher than that of the kinematic and dynamic models.

4.4 Conclusions

Real-time simulation has become an essential element of VR-based simulation architecture with operator and hardware in the loop configuration. A flexible, scalable, and extendable off-road vehicle modeling, simulation and visualization architecture was developed for operator-and-hardware-in-the-loop off-road vehicle system dynamics models. The distributed architecture and multi-rate modeling technique were used to enhance the computational speed of the dynamic simulation with visualization in an immersive VR environment. The simulation architecture was designed to handle diverse interfacing hardware and software platforms. The architecture also provided a generic and cleaner

modeling, simulation and visualization environment. A plug and play modeling environment saved considerable set-up time between different simulation runs. Model block libraries were also developed for various off-road vehicle systems, which allowed users to select models with appropriate complexity to achieve real-time simulation with the available computational resources. Moreover, the case studies presented in this paper demonstrated the practicality, flexibility and versatility of the real-time VR-based hardware-and-operator-in-the-loop simulation architecture, which will be helpful in interactive product design evaluation and modification using virtual prototypes.

Models of different vehicle subsystems such as chassis, power train and guidance controller were developed and added to a model block library. The architecture allowed users to develop their own models and add to the library without much difficulty. Various blocks from the library can easily be selected to build a new vehicle system model. The blocks can be swapped in and out to a vehicle system model so that altering a vehicle system model becomes highly flexible. Some of the complex models were developed with multi-rate simulation capability. This distributed real-time VR-based simulation system can effectively be used in virtual prototyping of off-road vehicles and controllers, which can facilitate:

- Reducing number of product development and test cycles,
- Virtual testing of various controller hardware and software,
- Reducing risk associated with extended field tests/experiments particularly in difficult terrains,
- Reducing post processing and communication effort on modeling and simulation, and
- Developing methodologies for understanding customer behavior and perceptions.

Acknowledgements

The authors would like to thank Deere & Co. for their technical and financial support to this project.

References

Antonya, C., and D. Talaba (2007). Design evaluation and modification of mechanical systems in virtual environments. *Virtual Reality*, 11: 275-285.

Bosch, R. (1991). CAN specification version 2.0. *Rober Bousch GmbH, Postfach* 300240, D-7000 Stuttgart 30.

Castillo-Effen, M. W., C. Castillo, W. A. Moreno, and K. P. Valavanis (2005). Modeling and visualization of multiple autonomous heterogeneous vehicles. *In: Proceedings of the IEEE International Conference on Systems, Man and Cybernetics,* The Hague, The Netherlands, Oct 10-12, 2005.

Cremer, J., J. Kearney, and Y. Papelis (1996). Driving simulation: challenges for VR technology. *IEEE Computer Graphics and Applications*, 16(5): 16-20.

Coutee, A. S., and B. Bras (2002). Collision detection for virtual objects in a haptic assembly and disassembly simulation environment. *In: Proceedings of ASME Design Engineering Technical Conferences and Computer and Information in Engineering Conference*, Montreal, Quebec, Canada.

Cuadrado, J., M. Gonzalez, R. Gutierrez, and M. A. Naya (2004). Real time MBS formulations: towards virtual engineering. *In: Product Engineering, Eco-design Technologies and Green Energies,* Springer, Heidelberg, pp 253–272.

De Sa, A. G., and G. Zachmann (1999). Virtual reality as a tool for verification of assembly and maintenance processes. *Computer Graphics (Pergamon),* 23: 389–403.

Eberhard, P., and Z. Li (2006). Virtual reality simulation of multibody systems. *In: Proceedings of EUROMECH Colloquium*, 476, Ferrol, Spain.

Fales, R., E. Spencer, K. Chipperfield, F. Wagner, and A. Kelkar (2005). Modeling and control of a wheel loader with a human-in-the-loop assessment using virtual reality. *Journal of Dynamic Systems, Measurement, and Control,* 127: 415-423.

Glinsky, E., and G. Wainer (2002). Definition of real-time simulation in the CD++ toolkit. *In Proceedings of the Summer Computer Simulation Conference*, July 14-18, San Diego, CA.

Gracanin, D., M. Matijasevic, N.C. Tsourveloudis, and K. P. Valavanis (1999). Virtual reality testbed for mobile robots. *In: Proceedings of the IEEE International Symposium on Industrial Electronics*, Bled, Slovenia, July 12-16.

Howard, B. M., and J. M. Vance (2007). Desktop haptic virtual assembly using physically based modelling. *Virtual Reality,* 11: 207-215.

Jayaram, S., Y. Wang, H. Tirumali, K. Lyons, and P. Hart (1999). VADE: A Virtual Assembly Design Environment. *IEEE Computer Graphics and Applications,* 19: 44–50.

Johnson, T. C., and J. M. Vance (2001). The use of the Voxmap pointshell method of collision detection in virtual assembly methods planning. *In: Proceedings of the ASME Design Engineering Technical Conference*, Pittsburgh, PA.

Kang, H. S., M. K. Abdul Jalil, and M. Mailah (2004). A PC-based driving simulator using virtual reality technology. *In: Proceedings of ACM SIGGRAPH International Conference on Virtual Reality Continuum and Its Applications in Industry*, Singapore, June 16-18, 2004.

Kim, C. E., and J. M. Vance (2003). Using VPS (Voxmap PointShell) as the basis for interaction in a virtual assembly environment. *In: SME Design Engineering Technical Conferences and Computers and Information in Engineering Conference*, Chicago, IL, United States.

Lin, Q., and C. Kuo (1997). Virtual tele-operation of underwater robots. *In: Proceedings of the IEEE International Conference on Robotics and Automation,* Albuquerque, New Mexico, April 21-27.

Livani, M. A., J. Kaiser, and W. Jia (1999). Scheduling hard and soft real-time communication in a controller area network. *Control Engineering Practice*, 7: 1515-1523.

Pazul, K. (2009). Controller area network (CAN) basics. *Microchip Technology, Inc.* AN713. Available at: http://www.cl.cam.ac.uk/research/srg/HAN/Lambda/webdocs/an713.pdf. Accessed: 16 June, 2009.

Sastry, L., and D. R. S. Boyd (1998). Virtual environments for engineering applications. *Virtual Reality,* 3: 235-244.

Savall, J., D. Borro, J. J. Gil, and L. Matey (2002). Description of a haptic system for virtual maintainability in aeronautics. *In: Proceeding of 2002 IEEE/RSJ International Conference on Intelligent Robots and Systems*, Lausanne, Switzerland.

Schulz, M., T. Reuding, and T. Ertl (1998). Analyzing engineering simulations in a virtual environment. *IEEE Computer Graphics and Applications*, 18(6): 46 – 52.

Stankovic, J. 1988. Misconceptions about real time computing: a serious problem for next generation systems. *IEEE Computer Graphics and applications*, 21(10): 10-19.

Wan H., S. Gao, Q. Peng, G. Dai, and F. Zhang (2004). MIVAS: a multi-modal immersive virtual assembly system. *In: Proceedings of the ASME Design Engineering Technical Conference*, Salt Lake City, UT.

Zhu Z., S. Gao, H. Wan, Y. Luo, and W. Yang (2004). Grasp identification and multi-finger haptic feedback for virtual assembly. *In: Proceedings of the ASME Design Engineering Technical Conference*, Salt Lake City, UT.

CHAPTER 5. STUDY OF THE OPEN AND CLOSED LOOP CHARACTERISTICS OF A TRACTOR AND A SINGLE AXLE TOWED IMPLEMENT SYSTEM

A paper submitted to the *Journal of Terramechanics*

Manoj Karkee and Brian L. Steward

Abstract.

Accurate automatic guidance of towed implements is important for performing agricultural field operations and for gaining the ultimate benefit from such systems. The study of open and closed loop system responses of a the lateral dynamics of a vehicle-implement system can be helpful in the design of practical guidance controllers. Open loop analysis of the kinematic and dynamic models revealed that the higher order dynamics captured by the dynamic model had an impact on simulated responses at higher operating velocities and on higher input frequencies. In addition, a dynamic model with tire relaxation length dynamics was also studied. The various model responses were compared with the experimental responses. Closed loop system characteristics were studied by using a linear quadratic regulator (LQR) controller. The tractor position and heading and implement heading states along with respective rate states were fed back to close the loop. Steering dynamics were also added to the dynamic model closed loop analysis, which helped to achieve a realistic closed loop steering angle history. The closed loop system response became faster as the forward velocity was increased. These open and closed loop response analyses provided an

understanding about the system at various forward velocities, which will help to design and develop efficient and robust tractor and towed implement guidance controllers.

Keywords. dynamic vehicle model, implement guidance, automatic guidance, LQR controller, relaxation length

5.1 Introduction

Increased and sustained agricultural productivity is a key to meet the globally increasing demands for food and energy. Automation of agricultural machinery is one of the ways to improve the efficiency and productivity of various field operations such as tillage, planting, pest control, nutrient management, and harvesting. Accurate guidance of agricultural machinery while performing these field operations will result in reduced operation time, chemical inputs, and energy inputs thus reducing production costs and improving the timeliness of field operation (Rekow, 2001). Improved accuracy and reduced row overlap in field operation will also reduce the crop damage, soil compaction, and soil rutting as well as the adverse effects of overlapped application of nutrients and agricultural chemicals.

Off-road vehicle automation technology has been studied, developed and used in agriculture for several decades. A surge of relative position-based guidance system research occurred in the 1970's and 1980's (Julian, 1971; Gerris and Surbrook, 1984; Smith et al., 1985) and continued into the 1990's and new millennium (Choi et al., 1990; and Benson et al., 2001). Relative position-based guidance systems use a local coordinate system as a reference frame to define the navigation problem and uses relatively short range sensing techniques such as vision-based guidance (Reid and Searcy, 1987). In the mid and late 90's,

emboldened by the successful application of Global Positioning System (GPS) in navigating airplanes and marine vehicles, researchers started applying high accuracy GPS signals to automatically guide agricultural equipment (O'Connor et al., 1996; O'Connor, 1999; Bell, 1997; Stombaugh et al., 1999). In contrast to relative position sensors, GPS provided absolute position and bearing measurements of agricultural vehicles. Due to its global availability, accuracy and relatively low cost, GPS technology was key in bringing agricultural automation technology to a new level.

In the past decade, several researchers developed automatic steering controllers to guide agricultural vehicles along straight and curved paths (Stombaugh et al., 1999; Bell, 2000; Bevly et al., 2002). In addition, manufacturers have commercialized navigation and automatic guidance technologies, and the adoption of these technologies has been growing steadily in recent years (Whipker and Akridge, 2008). However, most automatic guidance controllers only use tractor mounted sensors. To extend agricultural automation, the capabilities of the automatic guidance systems must be extended to implements as well (Bevly, 2001; Pota et al., 2007). In the end, it is the implement which often performs the field operation and navigating the implement is equally or even more important than guiding the tractor (Karkee et al., 2007; Katupitiya and Eaton, 2008).

Some researchers have investigated guidance controllers for tractor and implement systems. O'Connor et al. and O'Connor (1996; 1999) developed an automatic steering controller based on a kinematic model of a tractor and towed two-wheel implement. They designed a hybrid controller to provide a fast response to large errors. Bell (1999) also developed a kinematic model of a tractor and towed implement system and designed an automatic tracking LQR controller. Takigawa et al. (1998) developed a trajectory control

method for an agricultural vehicle and a mounted implement system. The feedback controller was designed based on a kinematic vehicle model. Karkee et al. (2007) also developed a kinematic model-based integrated position and heading feedback controller for a tractor and single axle towed implement system. One common element in these tractor and implement tracking controller design studies was that all used a kinematic tractor and implement model. It was assumed in the kinematic model that the vehicle tires will move to the direction they are pointed. Because these models neglect important dynamics associated with tire side slip phenomenon, the performance of a guidance controller developed based on a kinematic vehicle steering model may degrade, particularly at higher operating velocities (Bevly et al., 2002).

Agricultural equipment must be operated in highly uncertain and variable environments. Accuracy and robustness of agricultural guidance controllers must achieve a required precision in such an uncertain and unstructured environment (Katupitiya and Eaton, 2008). To achieve an acceptable cultivator incursion probability with the use of an automatically steered vehicle, 1.5 cm guidance accuracy is required (Rekow, 2001). Because of such tight guidance controller design specifications, it is essential to understand the dynamic behavior of the tractor and implement systems in various operating and field conditions to improve the accuracy, robustness and overall performance of the implement automatic guidance controller (Shim and Ghike, 2007; Pearson and Bevly, 2007; Rekow, 2001). In this regard, a tractor and implement model that can represent realistic steering behavior is essential to understand the system behavior and to develop a reliable guidance controller to follow complex field trajectories (Pearson and Bevly, 2007).

In addition, accurate off-road vehicle system models are becoming increasingly important as mechatronic engineers increasingly rely on model-based controller design and virtual prototyping (Karkee and Steward, 2008). Model-based controller design is a technique that uses a system model to represent the plant and wraps a controller dynamics around the model. Analytical and simulation-based iterative procedures are used to improve the controller accuracy and performance before testing the controller with the actual physical system and developing physical prototypes (Zavala et al., 2004). Virtual Prototyping (VP) is defined differently across disciplines and industries. In manufacturing, VP is referred to as the process of developing, representing and analyzing a soft or digital product model of an actual or planned physical product using simulation and realistic visualization tools (Pratt, 1995; Choi and Chan, 2004). Collectively, model-based controller design and VP techniques will provide engineers a soft environment for guidance controller design, prototype development, and performance testing before extended field tests. The iterative procedure of guidance controller development can be performed very rapidly, which reduces the product development time and cost while increasing the timeliness of product marketing. The faster, easier and lower cost iterative procedure allows engineers to perform a large number of design iterations relatively quickly to improve the accuracy and robustness of the guidance controller.

Even though model-based controller design and VP techniques are promising, the effectiveness of these techniques depends on the accuracy of underlying system model. Hence, the development of accurate and realistic vehicle models has become vital (Shim and Ghike, 2007). It is also important to achieve real-time simulation capability when model-based controller design and VP techniques are used in guidance controller development so

that developers and users can intuitively interact with the virtual product. As off-road vehicle models become increasingly complex to improve the model fidelity and accuracy, the computational requirements also increase substantially, which may limit the real-time simulation capability and the usefulness of these techniques. In this regard, it is important to understand the benefits and drawbacks of off-road vehicle models of varying complexity and fidelity.

This work focused on developing three lateral dynamics models of varying degrees of fidelity for a tractor and single axle towed implement system and performing comparative analysis of these models. Experimental trajectory data was collected and used as the reference responses. A single axle grain cart was selected as the implement in this work because it represented the general behavior of a towed implement while offering a well defined system to be modeled. The study of this system will be important because various emerging automation techniques such as coordinated guidance and autonomous guidance will have to incorporate the tractor and grain cart systems. The system provides a good starting point in understanding tractor and towed implement lateral dynamics, which then can be extended to other towed implements or a chain of towed implements. The overall goal of this study was to gain a better understanding of dynamic behavior of a tractor and wheeled implement system through model-based and experimental studies. The specific objectives of the study were to:

- Compare the open loop characteristics of the three tractor and implement steering models over a range of forward velocities,
- Compare the model frequency responses with the experimental frequency response over a range of forward velocities, and

- Study the closed loop system responses in terms of settling time and maximum overshoot over a range of forward velocities

5.2 Materials and Methods

5.2.1 Tractor and Towed Implement System Models

Various tractor and towed implement models have been proposed in the literature for both off-road (Bell, 1999; Feng et al., 2005) and on-road (El-Gindy, 1989; Torishu et al. 1992; Deng and Kang, 2003) operations. In this study, a dynamic model was developed for a tractor and a single axle towed implement system. The tractor and the towed implement rigid bodies were linked by a revolute joint at the hitch point. The tractor and the implement velocities were coupled to each other through the constraint caused by the joint. The model was then extended by adding relaxation length dynamics to it. A kinematic model developed by Karkee et al. (2007) was also used to compare the models with varying degrees of fidelity. Common vehicle dynamics symbols were used to describe the dynamics of the tractor-and-implement system (for notation, see the list of the variables).

5.2.1.1 Kinematic Model

It was assumed in the *kinematic model* that the vehicle tires moved to the direction they were facing, that is, there was no tire side slip in the model. The kinematic model was the simplest model used in this study to compare the model-based and experimental responses. The tractor and towed implement kinematic model presented by Karkee et al. (2007) was restructured as follows.

$$\dot{y}_c^t = u_c^t \varphi^t \tag{5.1}$$

$$\dot{\varphi}^t = \frac{u_c^t}{L^t}\delta \tag{5.2}$$

$$\dot{\varphi}^i = \frac{u_c^t}{L^i}\varphi^t - \frac{u_c^t}{L^i}\varphi^i - \frac{u_c^t l}{L^t L^i}\delta \tag{5.3}$$

where the variables are defined in the list of variables.

5.2.1.2 Dynamic Model

A *dynamic model* was developed for a tractor-and- single-axle- towed-implement system (called tractor-and-implement system in the text to follow, Fig. 5.1). This model was similar to that developed by Feng et al. (2005), but differed by using the hitch point as the reference point instead of the tractor and implement CGs being the reference points. The world-coordinate lateral position was also added in this model, which is required to perform the closed loop automatic guidance analysis. This model took a "bicycle" approach meaning that the lateral forces in the left and right wheels were assumed to be equal and summed together. This assumption can be justified since the effect of lateral load transfer on overall cornering force will be small for small steering angle operation at typical farm velocities (<7.5 m/s). Front wheel steering was used, and the system was constrained to only allow yaw and lateral motion with a constant forward tractor velocity. The model thus included lateral velocity and yaw-rate states for the tractor and a yaw-rate state for the implement, all of which were driven by the lateral tire forces generated through tire side slip. Longitudinal forces due to traction and rolling resistance were neglected since small steering angle operations will limit interaction with lateral forces.

For a constant forward velocity, the yaw plane tractor lateral motion is given by (Greenwood, 1969),

$$m^t\left(\dot{v}_c^t + u_c^t\gamma^t\right) = F_{x,f}^t \sin\delta + F_{y,f}^t \cos\delta + F_{y,r}^t + F_{y,p}^t \tag{5.4}$$

Similarly, tractor yaw motion is given by,

$$I_{z,c}^{t}\dot{\gamma}^{t} = a\left(F_{x,f}^{t}\sin\delta + F_{y,f}^{t}\cos\delta\right) - bF_{y,r}^{t} - cF_{y,p}^{t} \tag{5.5}$$

Assuming small angle δ and further linearizing the equations,

$$m^{t}\left(\dot{v}_{c}^{t} + u_{c}^{t}\gamma^{t}\right) = F_{y,f}^{t} + F_{y,r}^{t} + F_{y,p}^{t} \tag{5.6}$$

$$I_{z,c}^{t}\dot{\gamma}^{t} = aF_{y,f}^{t} - bF_{y,r}^{t} - cF_{y,p}^{t} \tag{5.7}$$

The velocity at tractor CG can be transferred to the implement CG as,

$$u_{c}^{i} = u_{p}^{i} = u_{c}^{t}\cos\lambda - \left(v_{c}^{t} - c\gamma^{t}\right)\sin\lambda \tag{5.8}$$

$$v_{c}^{i} = v_{p}^{i} - d\gamma^{i} = u_{c}^{t}\sin\lambda + \left(v_{c}^{t} - c\gamma^{t}\right)\cos\lambda - d\gamma^{i} \tag{5.9}$$

Taking derivatives, the lateral acceleration is,

$$\dot{v}_{c}^{i} = \dot{u}_{c}^{t}\sin\lambda + u_{c}^{t}\cos\lambda\dot{\lambda} + \left(\dot{v}_{c}^{t} - c\dot{\gamma}^{t}\right)\cos\lambda - \left(v_{c}^{t} - c\gamma^{t}\right)\sin\lambda\dot{\lambda} - d\dot{\gamma}^{i} \tag{5.10}$$

Assuming a small angle λ and further linearizing the eqs. 5.8, 5.9 and 5.10 results in:

$$u_{c}^{i} = u_{c}^{t} \qquad (12) \quad v_{c}^{i} = \left(v_{c}^{t} - c\gamma^{t}\right) - d\gamma^{i} \tag{5.11}$$

$$\dot{v}_{c}^{i} = u_{c}^{t}\dot{\lambda} + \left(\dot{v}_{c}^{t} - c\dot{\gamma}^{t}\right) - d\dot{\gamma}^{i} \tag{5.12}$$

From the implement lateral motion:

$$F_{y,p}^{i} = m^{i}\left(u_{c}^{t}\dot{\lambda} + \left(\dot{v}_{c}^{t} - c\dot{\gamma}^{t}\right) - d\dot{\gamma}^{i} + u_{c}^{t}\gamma^{i}\right) - F_{y,r}^{i} \tag{5.13}$$

For a small angle λ, $F_{y,p}^{t} = F_{y,p}^{i}$. From Eqs. 5.6 and 5.7,

$$m^{t}\left(\dot{v}_{c}^{t} + u_{c}^{t}\gamma^{t}\right) = F_{y,f}^{t} + F_{y,r}^{t} - \left\{m^{i}\left(u_{c}^{t}\dot{\lambda} + \left(\dot{v}_{c}^{t} - c\dot{\gamma}^{t}\right) - d\dot{\gamma}^{i} + u_{c}^{t}\gamma^{i}\right) - F_{y,r}^{i}\right\} \tag{5.14}$$

$$I_{z,c}^{t}\dot{\gamma}^{t} = aF_{y,f}^{t} - bF_{y,r}^{t} + c\left\{m^{i}\left(u_{c}^{t}\dot{\lambda} + \left(\dot{v}_{c}^{t} - c\dot{\gamma}^{t}\right) - d\dot{\gamma}^{i} + u_{c}^{t}\gamma^{i}\right) - F_{y,r}^{i}\right\} \tag{5.15}$$

The yaw dynamics of the implement are given by,

$$I_{z,c}^{i}\dot{\gamma}^{i} = m^{i}d\left\{\left(u_{c}^{t}\dot{\lambda} + \left(\dot{v}_{c}^{t} - c\dot{\gamma}^{t}\right) - d\dot{\gamma}^{i} + u_{c}^{t}\gamma^{i}\right)\right\} - (d+e)F_{y,r}^{i} \tag{5.16}$$

where, $\lambda = \gamma^t - \gamma^i$ (5.17)

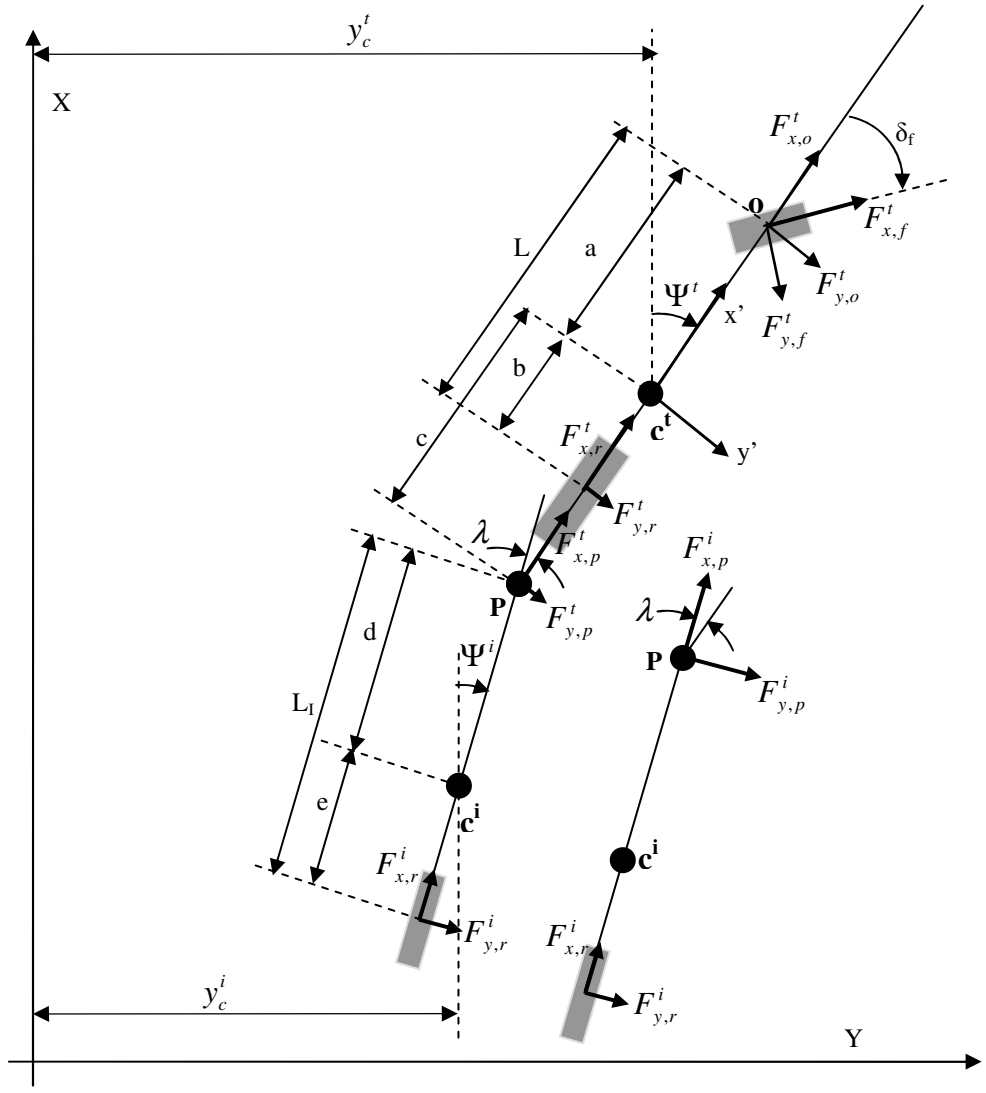

a)

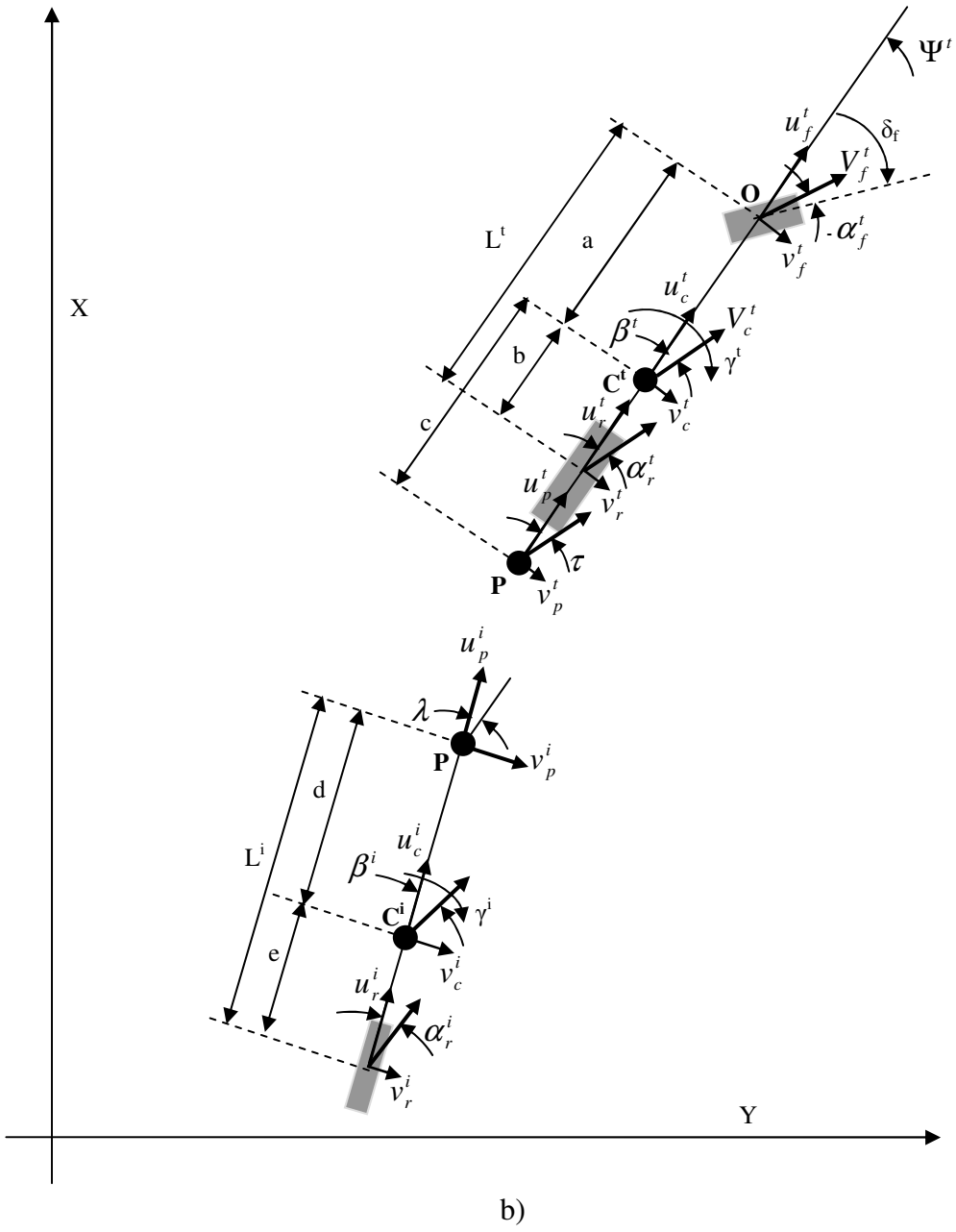

b)

Fig. 5.1: Dynamic bicycle model of a tractor-and-implement system; a) forces on the system, and b) velocities at different locations of the system.

We then have, based on a linear tire model (Wong, 2001),

$$\left(m^t + m^i\right)\dot{v}_c^t - m^i c\dot{\gamma}^t - m^i d\dot{\gamma}^i = -(m^i + m^t)u_c^t\gamma^t - C_{\alpha,f}^t\alpha_f^t - C_{\alpha,r}^t\alpha_r^t - C_{\alpha,r}^i\alpha_r^i \quad (5.18)$$

$$\left(I_z^t + m^i c^2\right)\dot{\gamma}^t - m^i c\dot{v}_c^t + m^i cd\dot{\gamma}^i = m^i cu_c^t\gamma^t - aC_{\alpha,f}^t\alpha_f^t + bC_{\alpha,r}^t\alpha_r^t + cC_{\alpha,r}^i\alpha_r^i \quad (5.19)$$

$$\left(I_z^i + m^i d^2\right)\dot{\gamma}^i - m^i d\dot{v}_c^t + m^i cd\dot{\gamma}^t = m^i du_c^t\gamma^t + (d+e)C_{\alpha,r}^i\alpha_r^i \quad (5.20)$$

From the definition of the tire side slip angle,

$$\alpha_f^t = \frac{v_c^t + a\gamma^t}{u_c^t} - \delta \quad (5.21)$$

$$\alpha_r^t = \frac{v_c^t - b\gamma^t}{u_c^t} \quad (5.22)$$

$$\alpha_r^i = \frac{v_c^t - c\gamma^t - (d+e)\gamma^i}{u_c^t} + \lambda \quad (5.23)$$

Eqs. 5.18 to 5.23, when combined, resulted in the three velocity state equations of the tractor-and-implement system model. The tractor CG lateral position, tractor heading, and implement heading were the other three model states with the following three state equations,

$$\dot{y}_c^t = v_c^t + u_c^t\varphi^t \quad (5.24)$$

$$\dot{\varphi}^t = \gamma^t \quad (5.25)$$

$$\dot{\varphi}^i = \gamma^i \quad (5.26)$$

5.2.1.3 Dynamic Model with Tire Relaxation Length

Relaxation length, which is defined as the distance a tire rolls before the steady state side slip angle is reached, is an important dynamic mode of an agricultural vehicle steering system. A tire can not generate the steady state lateral force instantaneously, and the delay is incorporated as a delay in the side slip angle. A first order model is given by Bevly et al. (2002),

$$\dot{\alpha} = \frac{u}{\sigma}(\alpha_0 - \alpha) \tag{5.27}$$

where σ is relaxation length and α_0 is the steady state side slip angle of the tire. The three tire side slip states of the system can then be represented as,

$$\dot{\alpha}_f^t = \frac{v_c^t}{\sigma_f^t} + \frac{a\gamma^t}{\sigma_f^t} - \frac{u_c^t}{\sigma_f^t}\delta - \frac{u_c^t}{\sigma_f^t}\alpha_f^t \tag{5.28}$$

$$\dot{\alpha}_r^t = \frac{v_c^t}{\sigma_r^t} - \frac{b\gamma^t}{\sigma_r^t} - \frac{u_c^t}{\sigma_r^t}\alpha_r^t \tag{5.29}$$

$$\dot{\alpha}_r^i = \frac{v_c^t}{\sigma_r^i} - \frac{c\gamma^t}{\sigma_r^i} - \frac{(d+e)\gamma^i}{\sigma_r^i} + \frac{u_c^t}{\sigma_r^i}\varphi^t - \frac{u_c^t}{\sigma_r^i}\varphi^i - \frac{u_c^t}{\sigma_r^i}\alpha_r^i \tag{5.30}$$

After including the tire relaxation length dynamics, a dynamic tractor-and-implement model with tire relaxation length was represented by eqs. 5.18 - 5.20 and 5.28-5.30. Similar to the dynamic model, the tractor CG lateral position, tractor heading, and implement heading states (Eqs. 5.24 - 5.26) were added to this model.

5.2.2 Field Data Collection

Tractor and towed implement trajectory field data was collected on Sep 19, 2008 in the Iowa State University (ISU) research farm located about eight miles west of the ISU central campus. The field was planted to oats in the 2008 summer season and was harvested before the tests. A John Deere MFWD tractor (model 7930, Deere and Co., Moline, IL) and a single axle 500 bu (18 m^3) grain cart (model 500, Alliance Product Group, Kalida, OH) were used in the experiment (Fig. 5.2).

Fig. 5.2: An experimental system with a MFWD tractor (model 7930, Deere and Co., Moline, IL) and a single axle 500 bu (18 m^3) grain cart (model 500, Alliance Product Group, Kalida, OH). Two RTK GPS receivers were mounted on the tractor and two were mounted on the implement.

An RTK GPS base station was set up in the farm about 100 m away from the test field. Two roaming RTK GPS receivers were mounted in the front and back of the tractor and two more units were mounted in the front and back of the implement. The GPS receivers and a wheel angle sensor were connected to a data acquisition computer through a CAN bus network. GPS messages were logged at 5 Hz, and the wheel angle was logged at 50 Hz. Inertial and geometric parameters of the experimental system were also measured (Table 5.1). Random steering angles (~3° to 8° in both directions) were provided to the system as an input and various RTK GPS messages were recorded to calculate the tractor and implement yaw-rates, CG positions and heading angles. Three replicates of the experimental data were collected at 1.0 m/s, 2.5 m/s and 4.5 m/s forward velocities. Even though the analytical study was conducted up to 7.5 m/s forward velocity, the field tests were difficult to perform at this velocity due to the oscillations caused by the uneven ground surface.

Table 5.1: Geometric and tire parameters of a JD 7930 tractor and a Parker 500 grain cart

Tractor		Implement	
Parameters	Values	Parameters	Values
a	1.7 m	D	3.62 m
b	1.2 m	E	0.1 m
c	2.1 m		
L^t	2.9 m	L^i	3.72 m
m^t	9391 kg	m^i	2127 kg
I_z^t	35709 kg-m^2	I_z^i	6402 kg-m^2
$C_{\alpha f}^t$	220 KN/rad*		
$C_{\alpha r}^t$	486 KN/rad*	$C_{\alpha r}^i$	167 KN/rad*
σ_f^t	0.75 m**	σ_r^i	0.75 m**
σ_r^t	1.0 m**		

**Calculated based on Metz (1993) and Schwanghart and Rott (1984)*

***Calculated based on Bevly et al.(2002)*

5.2.3 System Analysis

A set of agricultural tractor and grain cart parameters (Table 5.1) was used in the simulation of the three system models. Eigenvalue maps were used to compare the open loop characteristics of the kinematic model, dynamic model and dynamic model with tire relaxation length over a range of forward velocities. Bode gain and phase plots were used to compare the model-based and experimental frequency responses.

Closed loop system responses were also studied with the all three models. Before closing the loop around the system, it was important to test the controllability and the observability of the model with the parameters selected. The controllability matrix of the model had a full rank, which means that any state of the system can be driven to zero from an arbitrary initial value. The system was also observable with the assumption that the tractor

lateral position, tractor heading angle and implement heading angle were the measured variables. This characteristic provided an opportunity to estimate unmeasurable states and use a full state feedback closed loop system to be discussed in the following paragraphs.

A linear quadratic regulator (LQR) was used to study the closed loop characteristics of the tractor-and-implement system. Using all the states of the system model in the feed-back loop, the control law, with zero command input became,

$$u(t) = -Kx(t) \tag{5.31}$$

The controller gain K was found in such a way that minimized the objective function (Franklin et al., 2002),

$$J = \int_0^\infty \left(x^T Q x + u^T R u\right) dt \tag{5.32}$$

Matlab 'lqr' utility was used to find K and simulate the response of the closed loop system. Two matrices *R* and *Q* were used to establish a tradeoff between the control effort and the state errors. The control effort weight was varied over a range to see its effect on the closed loop system characteristics. To make the closed loop steering history more realistic, a steering unit delay was modeled and added to the closed loop systems (Stombaugh et al., 1999; Bevly et al., 2002).

$$\ddot{\delta} = \frac{d^v}{I^v}\dot{\delta} + \frac{K^v}{I^v}u_C(t) \tag{5.33}$$

where d^v is the damping constant, K^v is the input gain and I^v is the inertial constant, all of the steering system. In this work, the parameters used were $K^v = 10.0$, $I^v = 1$ and $d^v = 10.0$, which corresponded to the 0.1 s time constant used in Bosserd II (2007). Closed loop responses with all three models were studied over a range of forward velocities using an

eigenvalue maps, damping ratio plot, and settling distance plot. Closed loop simulations were performed with feedback system designed based on the kinematic model and the dynamic model with tire relaxation length. The dynamic model with tire relaxation length was modified including non-linearity in tire model and non-linearity in CG trajectory before using as the plant in the closed loop simulation. The non-linear tire model was given by:

$$F_y = NA\left(1 - e^{(-B\alpha)}\right) \tag{5.34}$$

where, N is the normal load to the tire. Parameters A and B depend on the soil type, soil condition and tire parameters (Metz, 1993). The non-linear tractor CG trajectory equations were given by:

$$\dot{x}_c^t = u_c^t \cos(\varphi^t) - v_c^t \sin(\varphi^t) \tag{5.35}$$

$$\dot{y}_c^t = u_c^t \sin(\varphi^t) + v_c^t \sin(\varphi^t) \tag{5.36}$$

This modified model will be called the *non-linear* model in the text to follow.

5.3 Results and Discussions

5.3.1 Open Loop System Analysis

The open loop characteristics of the three models were studied for a range of operating velocities (Fig. 5.3). The kinematic model was a third order model with two eigenvalues at the origin (Fig. 5.3 a). The three eigenvalues of this model represented the tractor lateral position, the tractor heading and the implement heading states. The two pure integrators represented the dynamics associated with the steering angle being integrated twice to get the lateral position. This model did not incorporate inertial dynamics of the system. The dynamic model represented the velocity states of the tractor-and-implement

system in addition to the positional states represented by the kinematic model (Fig. 5.3 b). This model also included two pure integrators, one each to transfer tractor and implement yaw-rate states to tractor and implement heading states. The dynamic model with tire relaxation length consisted of nine eigenvalues including three tire side slip states in addition to the six states represented by the dynamic model (Fig. 5.3 c). Similar to the dynamic model, two of the nine eigenvalues were located at origin.

At velocities lower than 4.5 m/s, the response of the dynamic model was not much different than that of the kinematic model as the locations of the dominant eigenvalues were not substantially different. At a velocity of 4.5 m/s, the non-zero eigenvalue of the kinematic model was located at -1.2 whereas the dominant non-zero eigenvalue of the dynamic model was located at -1.4. The remaining three dynamic model eigenvalues were located at -7.5 or further to the left on the real axis. When the forward velocity was increased to 7.5 m/s, the locations of the dominant non-zero eigenvalue of the two models moved apart substantially. The fourth eigenvalue of the dynamic model moved closer to origin and formed a conjugate pair at $-1.4 \pm 1.2j$. As the velocity increased, the dominant non-zero eigenvalue of both the kinematic and the dynamic models moved to the left on the real axis, thus decreasing the system settling time. This result was expected because the implement straightens sooner as the tractor moves faster in the forward direction.

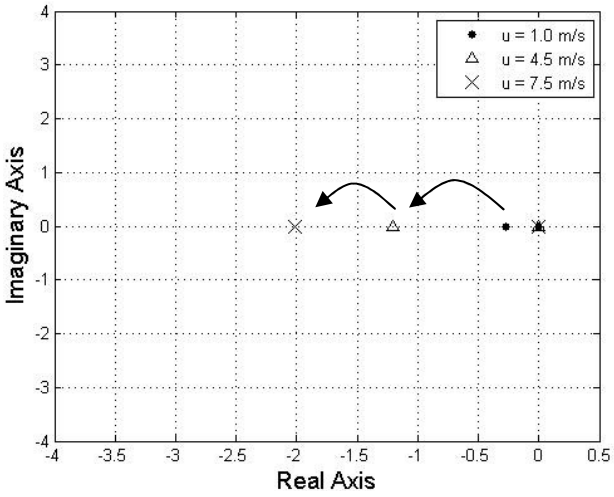

a) Kinematic model, two eigenvalues at origin

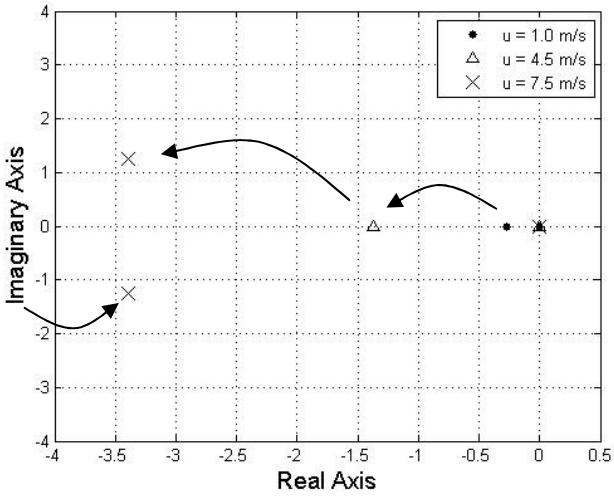

b) Dynamic model, two eigenvalues at origin

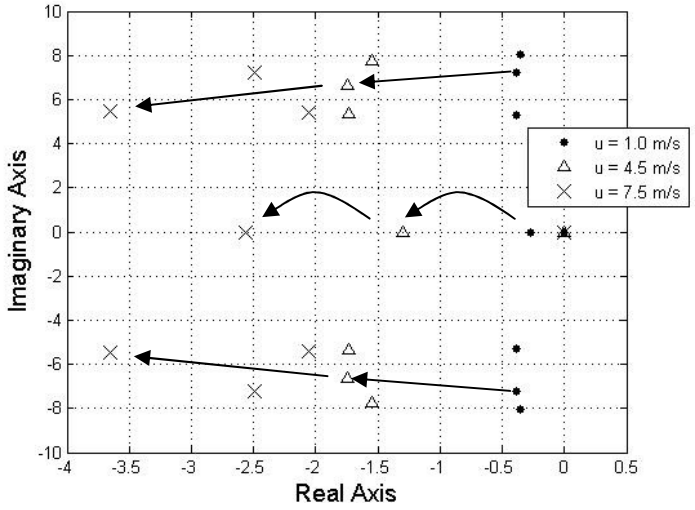

c) Dynamic model with tire relaxation length, three eigenvalues at the origin

Fig. 5.3: Dominant eigenvalues of the tractor-and-implement system for forward velocities of 0.5 m/s, 4.5 m/s and 7.5 m/s. a) kinematic model, b) dynamic model and c) dynamic model with tire relaxation length. All eigenvalues were real and negative, which showed that the systems were stable.

At lower velocities, the three dominating eigenvalues of the dynamic model represented the tractor lateral position, the tractor heading and the implement heading states.

Eigenvalues representing the velocity states (the tractor lateral velocity and the tractor and the implement yaw states) were further to the left (Fig. 5.3 b). The non-zero dominant pole of the dynamic model moved to the left faster than in the kinematic model as the velocity increased. The remaining faster eigenvalues of the dynamic model moved to the right with the increasing velocity. At a velocity of 7.5 m/s, the eigenvalues formed a complex conjugate pair causing the system to have underdamped dynamics. This result also indicated that the additional fidelity represented by the dynamic model comes into play at higher operating velocities.

In the dynamic model with tire relaxation length also, the positional states were clearly identifiable and dominated the system response. However, the tire side slip states coupled with the inertial states and formed complex conjugate pairs. As the velocity increased, the eigenvalues systematically moved further to the left while the imaginary parts of the complex conjugate pairs decreased slightly. This result indicated that the open loop system became faster and more damped as the operating velocity increased. At lower velocities, the three conjugate pairs formed by the side slip and the inertial states were highly underdamped and very close to the imaginary axis causing significant oscillation and overshoot in the system response. At a very low velocity, the model might be marginally unstable, which was unlikely to happen in the real agricultural vehicle. In agreement with the description in Rajamani (2006), this result indicated that a constant tire relaxation length may not represent the dynamics accurately over a range of the forward velocities.

To understand the steady state and transient responses of the kinematic model, dynamic model and dynamic model with tire relaxation length, tractor and implement yaw-rate Bode plots were calculated for a range of input frequencies and compared with the

experimental frequency response functions (Fig. 5.4 – Fig. 5.6). The forward velocities used were 1.0 m/s, 2.5 m/s and 4.5 m/s. As expected, gain and phase responses of the three models were similar at lower input frequencies at all forward velocities. The responses were dominated by the DC gains for frequencies less then 0.6 rad/s, which were –9.0 dB, 0.0 dB and 3.8 dB at 1.0 m/s, 2.5 m/s and 4.5 m/s forward velocities, respectively. The dynamic model gain decreased much faster than that of the kinematic model when the input frequency approached to the cutoff frequency of ~5 rad/s caused by the higher order dynamics. The kinematic model implement heading lagged the steering input for only a limited band of frequencies from about 0.1 to 10 rad/s. This lag was due to the hitch point being behind the rear axle of the tractor and higher order dynamics being neglected. The size and location of the frequency band where the implement heading response lagged the input depended on the distance between the hitch point and the tractor rear axle. The dynamic model heading phase lag increased rapidly in the frequency range from 1 rad/s to 100 rad/s at all velocities. However, both the kinematic and the dynamic model responses were substantially different from the experimental spectrum in the higher frequency range.

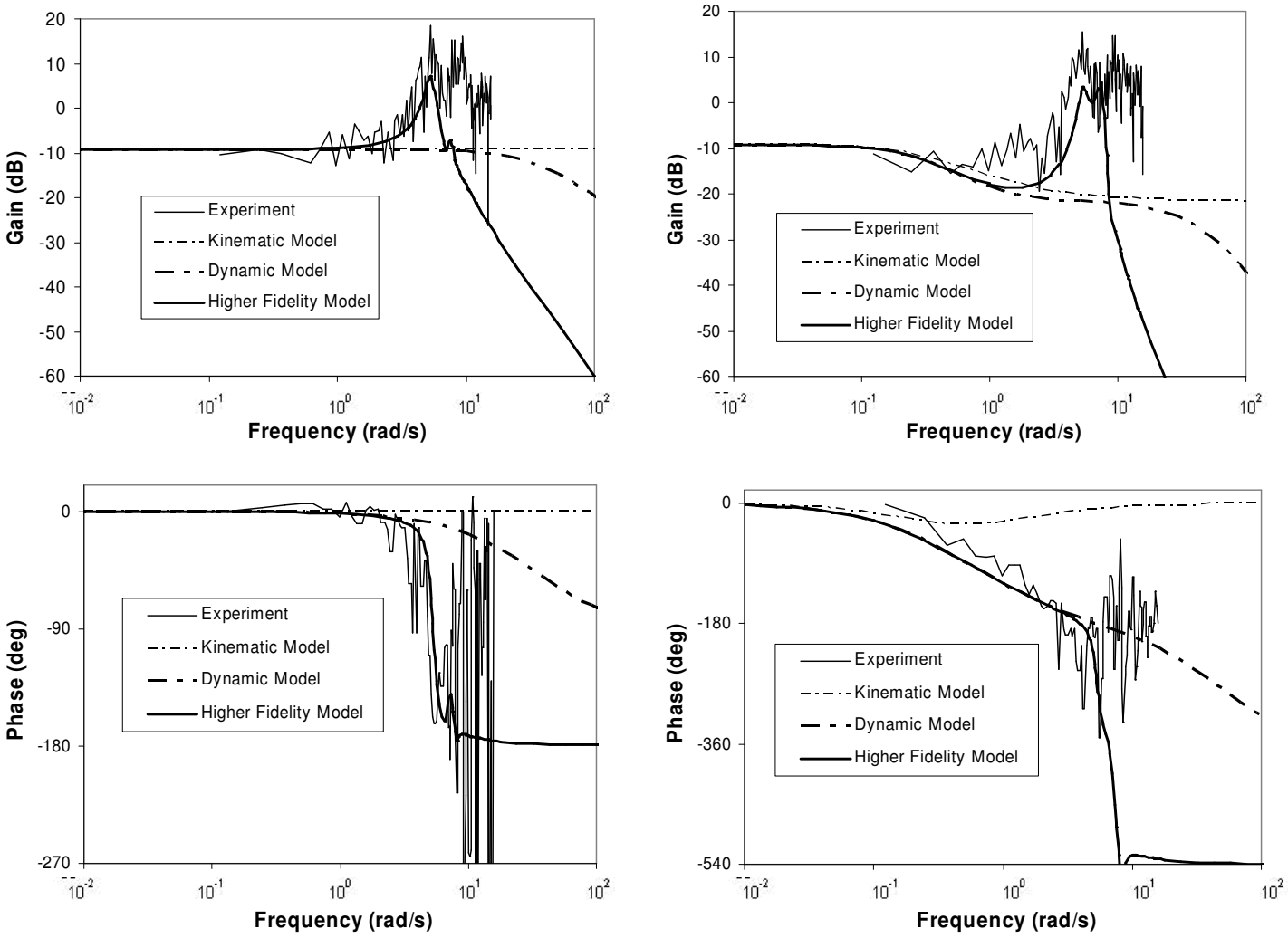

Fig. 5.4: Frequency response of the kinematic model, dynamic model, and dynamic model with tire relaxation length at 1.0 m/s forward velocity, a) tractor yaw-rate output gain and phase shift, b) implement yaw-rate output gain and phase shift.

The dynamic model with tire relaxation length tractor yaw-rate Bode plots indicated that second order dynamics dominated the response with a resonant frequency of about 5 rad/s. Implement yaw-rate plots revealed that sixth order dynamics dominated the response with the same resonance frequency. The implement yaw-rate response lagged the input by

about 200° at the point when the gain was still more than 0 db and the input frequency was about 1.0 rad/s.

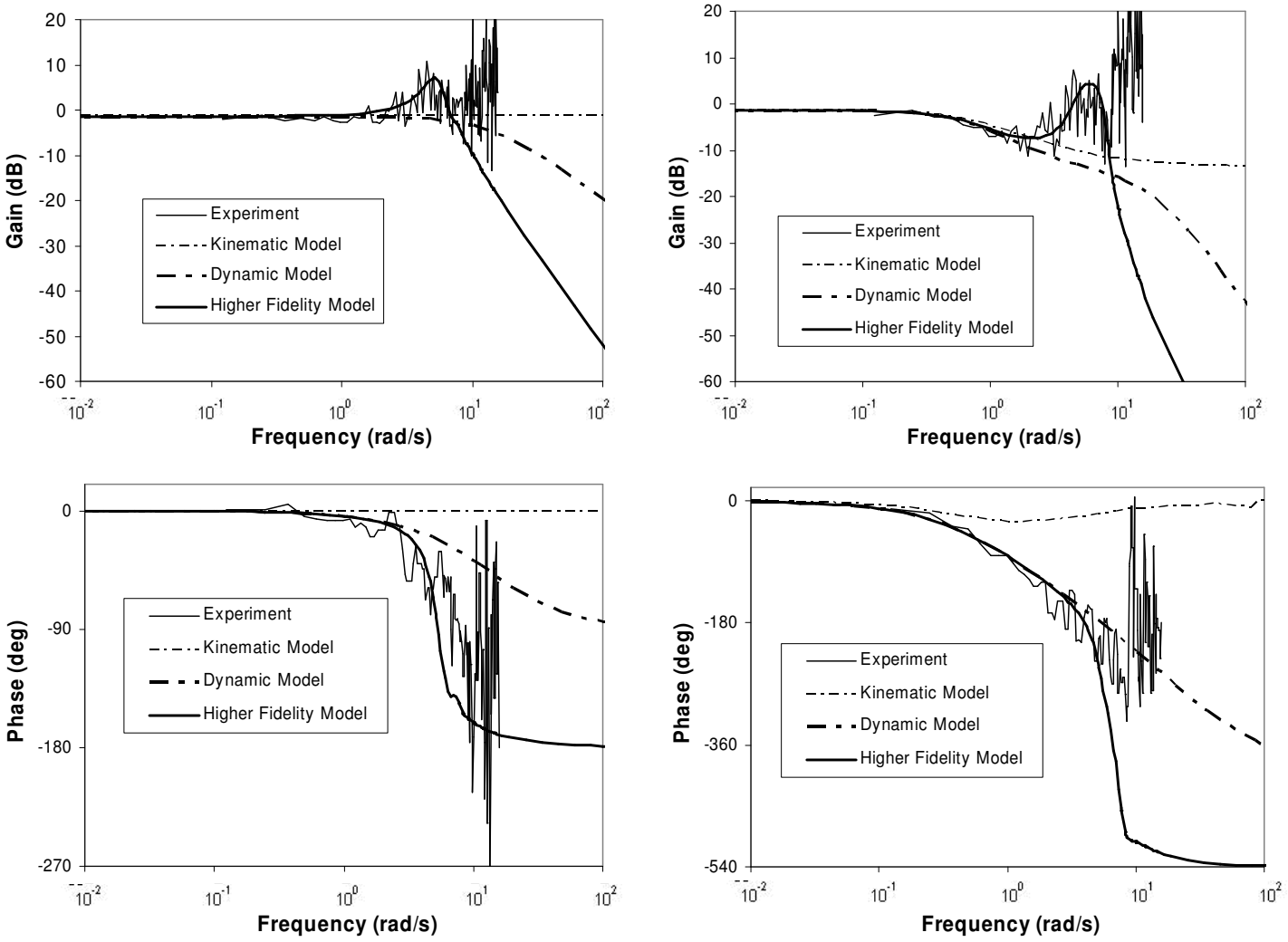

Fig. 5.5: Frequency response of the kinematic model, dynamic model, and dynamic model with tire relaxation length at 2.5 m/s forward velocity, a) tractor yaw-rate gain and phase shift, b) implement yaw-rate gain and phase shift.

The dynamic model with tire relaxation length showed a resonance phenomenon, which was not present in the kinematic and dynamic model responses. The output gain peak at the resonant frequency decreased as the forward velocity was increased (Fig. 5.4 - Fig.

5.6). These responses from the dynamic model with tire relaxation length represented the experimental data with a reasonable accuracy over a wide range of input frequencies at all three velocities. It should be noted that the random values in the experimental spectrum beyond ~8 rad/s were caused by the band limited input excitation.

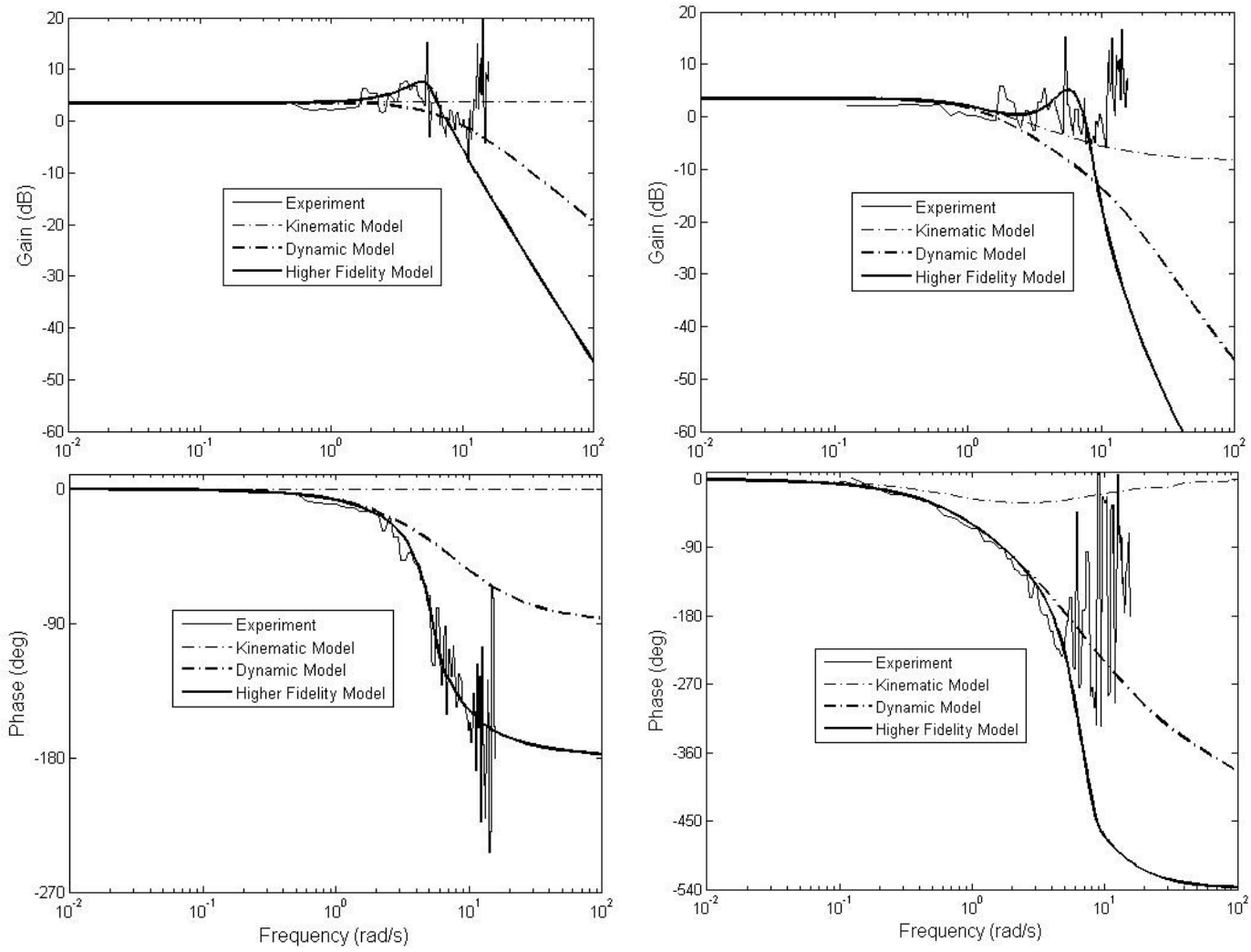

Fig. 5.6: Frequency response of the kinematic model, dynamic model, and dynamic model with tire relaxation length at 4.5 m/s forward velocity, a) tractor yaw-rate gain and phase shift, b) implement yaw-rate gain and phase shift.

5.3.2 Closed Loop System Analysis

Closed loop system responses were studied with all three tractor-and- implement system models. An LQR controller was used with a control effort penalty *R* of 800 and state error weight *Q* of 1. All eigenvalues of the closed loop systems were located in the left half plane for forward velocities from 0.5 m/s to 10 m/s, which indicated the closed loop system was stable in this range of velocities (Fig. 5.7 and Fig. 5.8). At each velocity, a conjugate pair of eigenvalues dominated the closed loop response with all three models. As the velocity increased, the closed loop eigenvalues moved to the left as in the open loop system. For the kinematic model, the real part of dominant closed loop eigenvalue pair was -0.08, -0.35 and -0.58 at 1.0 m/s, 4.5 m/s and 7.5 m/s forward velocities respectively, which corresponded to a settling times of 50 s, 11 s and 7 s (Fig. 5.7 a).

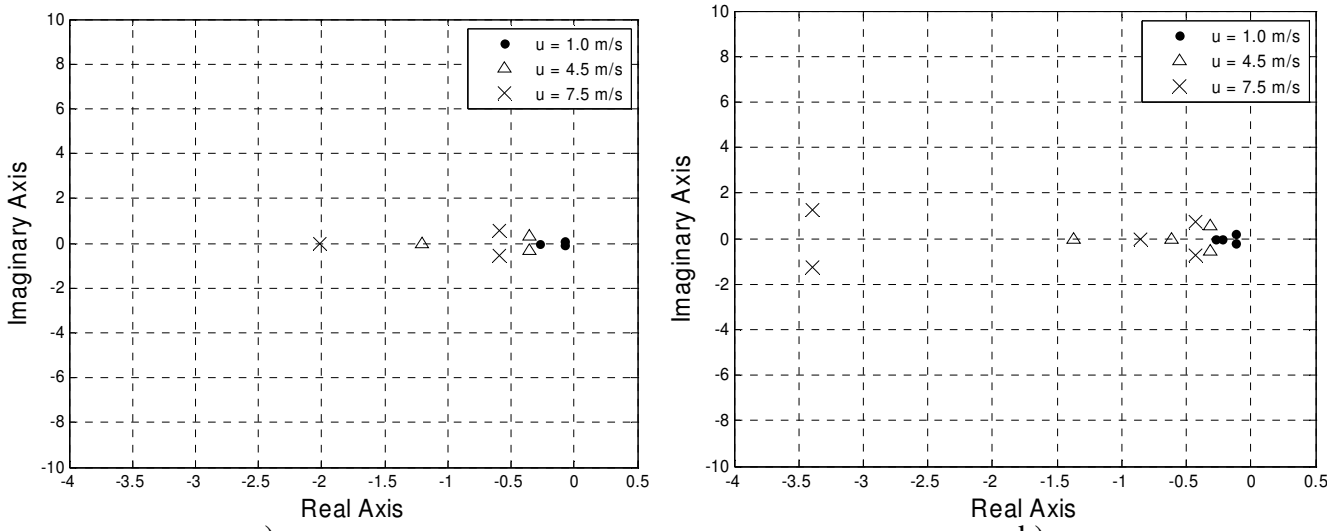

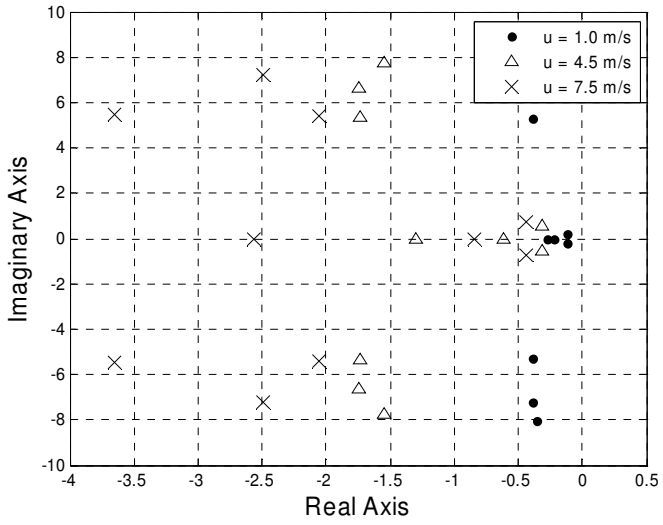

c)

Fig. 5.7: Eigenvalues of the state matrix Ac of the dynamic model with tire relaxation length closed loop system for forward velocities of 1.0 m/s, 4.5 m/s and 7.5 m/s; a) kinematic model, b) dynamic model, c) dynamic model with tire relaxation length. Control effort penalty *R* was 800. All eigenvalues were located in the left half plane, which showed the closed loop systems were stable in this range of velocities.

Similarly, the dynamic model based closed loop system contained the dominant eigenvalue pair at -0.12, -0.31 and -0.42 respectively at 1.0 m/s, 4.5 m/s and 7.5 m/s. The corresponding settling times were 33 s, 13 s and 10 s (Fig. 5.7 b). For the dynamic model with tire relaxation length, most of the eigenvalues were located close to the origin at 1.0 m/s forward velocity. Most of the complex conjugate eigenvalue pairs were highly underdamped. Meantime, there were two real eigenvalues nearby the dominating pair, which helped to improve the system damping (Fig. 5.7 c). With all three closed loop systems, the eigenvalues systematically moved to the left as the forward velocity was increased. Consequently, the closed loop systems became faster with the increasing velocity.

The closed loop characteristics of the dynamic model with tire relaxation length were further assessed using settling distance and damping ratio of the response over a range of operating velocities. The settling distance was about 24 m at 0.5 m/s and increased almost linearly over the velocity range from 0.5 m/s to 10 m/s (Fig. 5.8). Even though the settling time decreased as the velocity increased (Fig. 5.7), the decrease in settling time was not enough to offset the increase in velocity causing the settling distance to increase with velocity. The damping ratio associated with the dominant pair decreased slightly as the velocity increased, but the change was not substantial (Fig. 5.8). The damping ratios were quite small (~0.5) in the velocity range of 0.5 m/s to 10.0 m/s. However, there were two real eigenvalues located nearby the dominant conjugate eigenvalue pair. These real eigenvalues forced the system response to decay faster than indicated by the conjugate eigenvalue pair.

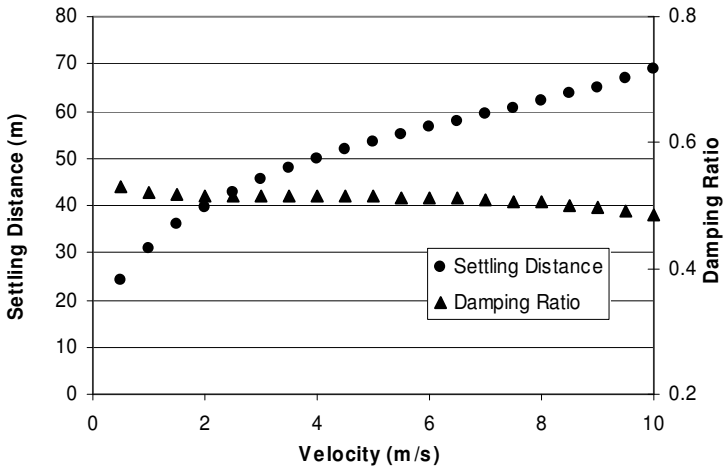

Fig. 5.8: Dominant settling distance and damping ratio of closed loop system response of the dynamic model with tire relaxation length over a range of forward velocities. The settling distance increased almost linearly with velocity. The damping ratio remained almost constant.

5.4 Simulation Results

The closed loop system responses were further assessed by simulating the closed loop system with the non-linear plant model. First, the closed loop system was simulated with the feedback system designed based on the kinematic model at 4.5 m/s forward velocity. In this case, the non-linear model-based simulated responses were unstable (Fig. 5.9 a). Similar behavior was observed by Bevly et al. (2002) when they used a kinematic model-based guidance controller with an actual farm tractor. This result was expected as one of the eigenvalues of the dynamic model with tire relaxation length closed loop system with the feedback system designed around the kinematic model had a small positive real part. However, the simulated closed loop responses with the feedback system designed based on the dynamic model with tire relaxation length were stable for a wide range of operating velocities (Fig. 5.9 b) and met the nominal performance specification of an off-road vehicle guidance system (Karkee et al., 2007). Because pure integrators were available in the system, the closed loop steady state errors were driven to zero without having an integrator in the feedback loop.

The performance of the controller designed around the dynamic model with tire relaxation length was assessed in terms of the settling time and the maximum overshoot. The settling time for the tractor tracking and heading errors was about 12 s to 13 s for a forward velocity of 4.5 m/s (Fig. 5.9 b and Fig. 5.10 a). Similarly, the implement heading error settling time was about 14 s (Fig. 5.10 b). These settling times were slightly higher than the settling time calculated from the dominant eigenvalues of the dynamic model with tire relaxation length. The discrepancy was because of the effect of other real eigenvalue(s)

which were located nearby the dominant conjugate eigenvalue pair and the non-linear tire and trajectory equations used in the simulation model.

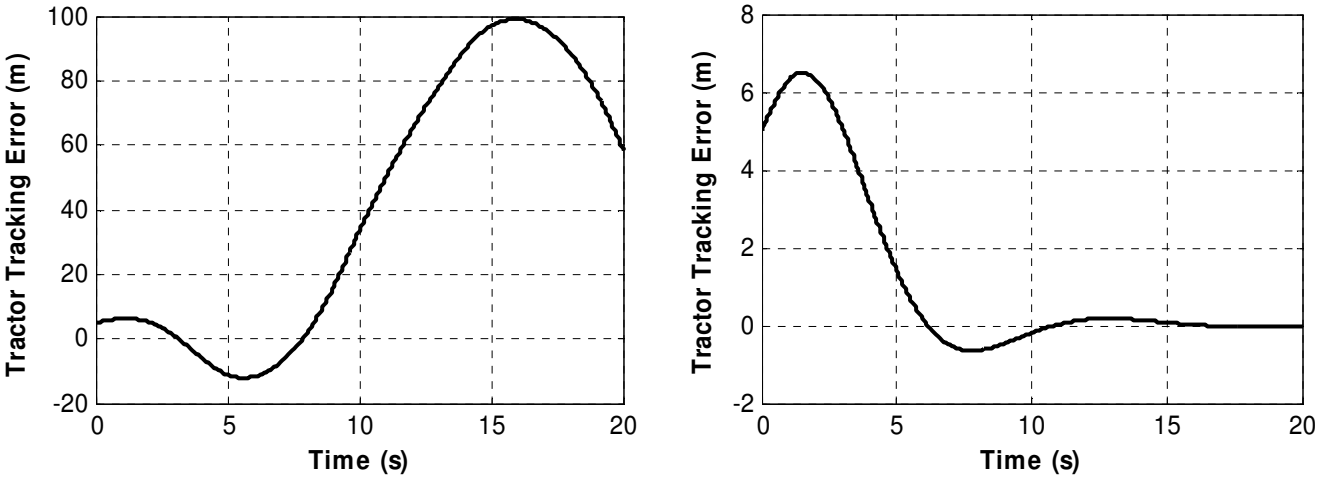

Fig. 5.9: Non-linear model-based closed loop simulation responses; a) tractor CG tracking error with the kinematic-model based feedback system, b) tractor CG tracking error with the feedback system designed based on dynamic model with tire relaxation length. The forward velocity was 4.5 m/s. The initial tractor tracking error was 5 m and initial tractor and implement heading errors were 20°.

Due to the relatively sluggish response at the beginning, the control effort of the LQR remained aggressive for some time, which resulted in some oscillation in the closed loop response. The dominant eigenvalue of the closed loop system showed that the response would have 15% maximum overshoot. However, the simulated tracking error showed only about 10% overshoot (Fig. 5.10 b). The overshoot was subsided due to the damping effect of first order system responses, which was close enough to affect the lightly damped dominant second order response as indicated by the linearized model (Fig. 5.7).

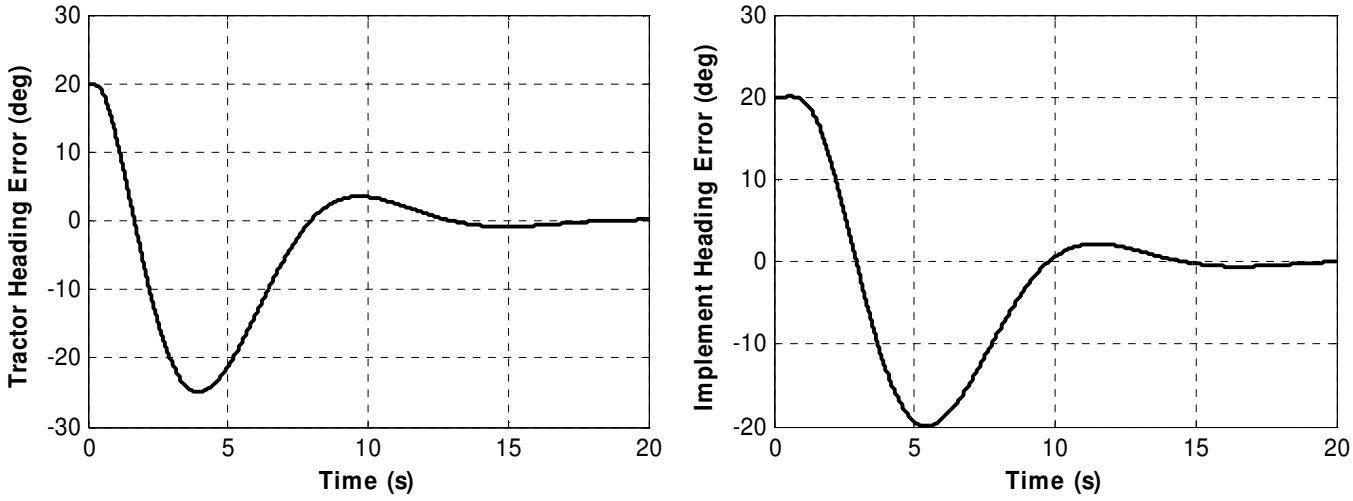

a) b)

Fig. 5.10: Non-linear model-based simulation responses of the closed loop system with the feedback system designed based on the dynamic model with tire relaxation length; a) tractor heading error, b) implement heading error. The forward velocity was 4.5 m/s, the initial tractor off-track error was 5 m and initial tractor and implement heading error was 20°.

The heading errors of the closed loop response went up to 24° and 20° respectively for the tractor and the implement for an initial heading error of 20° and tractor off-track error of 5 m (Fig. 5.9). In addition, the controller drove the steering angle to a maximum value of 11°. The small angle assumption for heading and steering angles used in the linearization of the model may not hold beyond 10°. Larger steering angle may also violate the assumption of a linear tire model. The heading and steering angles remained above 10° for some time (<5 s) in the transient period, which will have little effect on the steady state performance but may have some effect in the transient behavior. However, the maximum value of the heading and steering angles remained below 10° when the tractor initial off-track error was reduced to

3 m and the tractor and implement initial heading error was reduced to 10°. The characteristics of the dynamic model with tire relaxation length closed loop system in terms of stability, settling time and maximum overshoot were promising for the tractor and implement guidance system development (Stombaugh et al., 1999; Karkee et al., 2007).

5.5 Conclusions

The open loop and closed loop characteristics of a tractor and towed single axle implement system were studied based on various analytical models and experimental data. Both time responses and frequency responses were evaluated. An LQR controller was used to close the loop around the system. The open and closed loop response analysis performed in this work provided an understanding of the system characteristics at different operating velocities and helped understand the strengths and weaknesses of various system models. The work will be helpful to design and develop efficient and robust tractor and towed implement guidance controller. In addition, the work will help to select an appropriate model to meet the specific requirements of various applications such as model-based guidance controller design, virtual prototyping, and real-time simulation.

Specifically, we can conclude the following from this work.

- In the lower range of operating velocities (0 to ~ 4.5 m/s) and input frequencies (0 to ~1 rad/s), a kinematic model of the tractor and the implement represents the system dynamics as well as a dynamic model.
- A dynamic model with tire relaxation length dynamics is necessary to represent higher order dynamics of the system, which is essential when the field operation requires higher velocities or higher input frequencies.

- A dynamic model with tire relaxation length may be required to design a robust implement guidance controller.
- The settling distance of the LQR-based closed loop tractor and towed implement system increases as the forward velocity is increased.

Acknowledgements

This research was supported by Hatch Act and State of Iowa funds. Journal paper of the Iowa Agriculture and Home Economics Experiment Station, Ames, Iowa, Project No. 3612.

Notation and List of Variables

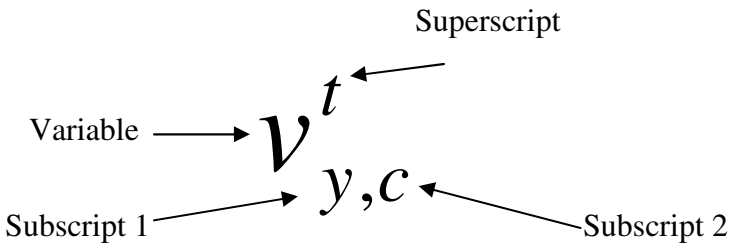

Variable: The variable itself.

Big or bold letter – vector or matrix, small letter – scalar

Superscript: Denotes whether the variable is related to tractor or implement.

t – tractor, i – implement

Subscript 1: Specifies the co-ordinate axis the variable corresponds to.

x – x axis, y – y axis, z – z axis

Subscript 2: Specifies the location the variable corresponds to.

f – front tire axle, r – rear tire axle, c – center of gravity, p – toe pin (hitch point)

List of variables

α	side slip angle or the angle between the direction the tire is going and the direction it is facing. The velocity vector to the right of the tire is positive and reverse is negative.
α_0	steady state side slip angle
γ	yaw-rate
δ	steering angle
λ	angle between tractor heading and implement heading
σ	relaxation length
φ	heading angle
a	distance between front axle and CG of tractor
b	distance between rear axle and CG of tractor
c	distance between hitch point and CG of tractor
C_α	cornering stiffness
d	distance between hitch point and CG of implement
e	distance between rear axle and CG of implement
F	force
I^v	Steering unit inertial constant
d^v	Steering unit damping constant
K^v	steering unit input gain
I_z	yaw moment of inertia

L	wheelbase
m	mass
n	size of state (square) matrix A
N	normal load to a tire
Q	LQR controlled output penalty matrix
R	LQR control effort penalty matrix
r	turn radius of rear wheel
u	longitudinal velocity
$u_c(t)$	steering unit actuator input
v	lateral velocity
X_c	control state vector
X-Y	world coordinates
x'-y'	vehicle coordinates
y	position of CG in y- axis of the world co-ordinate system

References

Bell, T. (1999). Precision robotic control of agricultural vehicles on realistic farm trajectory. *PhD dissertation,* Stanford University.

Bell, T. (2000) Automatic tractor guidance using carrier-phase differential GPS. Computers and Electronics in Agriculture, 25: 53-66.

Benson, E. R., J. F. Reid, and Q. Zhang (2001). Machine vision based steering system for agricultural combines. *ASAE Paper # 01-1159.* ASAE, St. Joseph, MI.

Bevly, D. M. (2001). High speed, dead reckoning, and towed implement control for automatically steered farm tractors using GPS. *PhD dissertation*, Stanford University.

Bevly, D. M., J. C. Gerdes, and B. W. Parkinson (2002). A new yaw dynamic model for improved high speed control of a farm tractor. *Journal of Dynamic Systems, Measurement, and Control*, 124: 659-667.

Bosserd II, J. A. (2007). Investigation of roll angle feed-forward control and look-ahead functions to improve automatic guidance on sloped terrain. *Master's Thesis*, Iowa State University.

Choi, C. H., D. C. Erbach, and R. J. Smith (1990). Navigational tractor guidance system. *Transactions of the ASAE,* 33(3): 699-706.

Choi, S. H., A. M. M. Chan (2004). A virtual prototyping system for rapid product development. *Computer-Aided Design,* 36: 401–412.

Deng, W., and X. Kang (2003). Parametric study on vehicle-trailer dynamics for stability control. *SAE Transactions, Journal of Passenger Cars*, 2003: 411-1419.

El-Gindy, M. (1989). Directional response of a tractor towing a semitrailer. *International Journal of Vehicle Design,* 10(2): 211-226.

Feng, L., Y. He, Y. Bao, and H. Fang (2005). Development of trajectory model for a tractor-implement system for automated navigation applications. *Instrumentation and Measurement Technology Conference*, Ottawa, Canada, May 17-19.

Franklin, G. F., J. D. Powell, and A. Emami-Naeini (2002). Feedback control of dynamic systems. Upper Saddle River, NJ, *Prentice Hall.*

Gerrish, J. B., and T. C. Surbrook (1984). Mobile robots in agriculture. *In Proc. of First International Conference on Robotics and Intelligent Machines in Agriculture*. ASAE, St. Joseph, MI. 30–41.

Greenwood, D. T. (1965). Principles of Dynamics. Engleswood Cliffs, NJ, *Prentice Hall*.

Julian, A. P. (1971). Design and performance of a steering control system for agricultural tractors. *J. Agric. Eng. Res.,* 16(3): 324-336.

Karkee, M., B. L. Steward, and S. A. Aziz (2007). Distributed virtual reality assisted steering controller design for Off-road vehicle and implement tracking. *ASABE Paper No. 073006*. ASAE, St. Joseph, MI.

Karkee, M., and B. L. Steward (2008). Open and Closed Loop System Characteristics of a Tractor and an Implement Dynamic Model. *ASABE Paper No. 084761*. ASABE, St. Joseph, MI.

Katupitiya, J., and R. Eaton (2008). Precision autonomous guidance of agricultural vehicles for future autonomous farming. *ASAE Paper # 084687*. ASAE, St. Joseph, MI.

Metz, L. D. (1993). Dynamics of four-wheel-steer off-highway vehicles. *SAE Paper No. 930765*. Warrendale, PA: SAE.

O'Connor, M., T. Bell, G. Elkaim, and B. Parkinson (1996). Automatic steering of farm vehicles using GPS. *Third International Conference on Precision Agriculture. Minneapolis*, MN, June 23–26.

O'Connor , M. L (1997). Carrier-phase differential GPS for automatic control of land vehicles. *PhD thesis*, Stanford University.

Pearson, P., and D. V. Bevly (2007). Modeling and validation of hitch loading effects on tractor yaw dynamics. *Journal of Terramechanics,* 44: 439-450.

Pota, H., J. Katupitiya, and R. Eaton (2007). Simulation of a tractor-implement model under the influence of lateral disturbances. *IEEE Conference on Decision and Control,* New Orleans, LA, December 12-14.

Pratt, M. J. (1995). Virtual prototypes and product models in mechanical engineering. *Virtual Prototyping—Virtual Environments and the Product Design Process*, Chapman and Hall, London.

Rajamani, R. (2006). Vehicle dynamics and control. New York, N.Y., USA: *Springer.*

Reid, J. F. and S. W. Searcy (1987). Vision-based guidance of an agricultural tractor. *IEEE Control Systems Magazine,* 7:43-49.

Rekow, A. (2001). System identification, adaptive control and formation driving of farm tractors. *PhD thesis,* Stanford University.

Schwanghart, H., and K. Rott (1984). The influence of the tire tread on the rolling resistance and steering forces on undriven wheels. *In Proc. 8th International Conference of the Society of Terrain Vehicle Systems*, 855-888. Cambridge, UK: ISTVS.

Shim, T., and C. Ghike (2007). Understanding the limitations of vehicle model for roll dynamics study. *Vehicle System Dynamics-International Journal of Vehicle Mechanics and Mobility,* 45(3): 191-216.

Smith, L. A., R. L. Scharfer, and R. E. Young (1985). Control algorithms for tractor-implement guidance. *Transactions of the ASAE,* 28(2): 415-419.

Stombaugh, T. S., E. R. Benson, and J. W. Hummel (1999). Guidance control of agricultural vehicles at high field speeds. *Transactions of ASABE,* 42(2): 537-544.

Takigawa, T., T. Konaka, M. Koike, R. Noguchi, and H. Hasegawa (1998). Trajectory control for agricultural autonomous vehicles (Part 1). *Journal of JSAM*, 60(2): 89-96.

Torishu, R, S. W. Mugucia, and J. Takeda (1992). The kinematics and open-loop characteristics of tractor-trailer combinations. *Journal of Faculty of Agriculture*, Iwate University 20: 299-314.

Whipker, L. D., and J. T. Akridge (2008). Precision agricultural services dealership survey results. *Center for Food and Agricultural Business Department of Agricultural Economics, Purdue University,* Working Paper #08-09, September.

Wong, J.Y. (2001). Theory of ground vehicles. New York, N.Y., USA: *John Wiley & Sons Ltd.*

Zavala, C., P. Sanketi, D. Lamberson, A. R. Girard, and J. K. Hedrick (2004). Model-based real-time embedded control software for automotive torque management. *In proceedings of Real-Time and Embedded Technology and Applications Symposium (RTAS)*, May 25 - May 28, 2005, Le Royal Meridien, King Edward, Toronto, Canada.

CHAPTER 6. LOCAL AND GLOBAL SENSITIVITY ANALYSIS OF A TRACTOR AND SINGLE AXLE TOWED IMPLEMENT DYNAMIC SYSTEM MODEL

A paper submitted to *Biosystems Engineering*

Manoj Karkee, Brian L. Steward

Abstract

Tractor and towed implement system models have become increasingly important for model-based guidance controller design, virtual prototyping, and operator-and-hardware-in-loop simulation. Various tractor and towed implement models which contain uncertain or time-varying parameters have been proposed in the literature. Sensitivity analysis was used to identify the effect of system parameter uncertainty/variation on system responses and to identify the most critical parameters of a tractor and single axle grain cart system. Both local and global sensitivity analyses were performed with respect to three tire cornering stiffness parameters, three tire relaxation length parameters, and two implement inertial parameters. Overall, the system was most sensitive to the tire cornering stiffness parameters and least sensitive to the implement inertial parameters. In general, the uncertainty in the input parameters and the system output responses were related in a non-linear fashion. With the nominal parameter values for a MFWD tractor, a single axle grain cart, and corn stubble surface conditions, a 10% uncertainty in cornering stiffness parameters caused a 2% average uncertainty in the system responses whereas a 50% uncertainty in cornering stiffness parameters caused a 20% average uncertainty at 4.5 m/s forward velocity. If a 5% average uncertainty in system responses is acceptable, the cornering stiffness parameters must be

estimated within 25% of actual/nominal values. The output uncertainty increased as the forward velocity increased.

Keywords. tractor and implement model, sensitivity analysis, sensitivity measures, parameter uncertainty

6.1 Introduction

Off-road vehicle system models are becoming increasingly important as mechatronic engineers increasingly rely on model-based controller design, virtual prototyping, and real-time hardware-and-operator-in-loop simulation in the design process (Karkee and Steward, 2009). As a tremendous amount of computational power has become available for numerical simulation, vehicle models have become increasingly complex often possessing dozens of model parameters. Accurate estimation of those parameters is often difficult because of the high variability in field conditions. Because uncertain parameter estimates will have an effect on simulated model responses, off-road vehicle simulations may often be unrealistic, limiting the applicability of the models and model-based studies (Kioutsioukis et al., 2004). It is important to understand and quantify the effect of these parameter uncertainties or variations on the system response (Fales, 2004). Sensitivity analysis is one approach to identify and quantify the relationships between input and output uncertainties (Xu and Gertner, 2007).

Sensitivity analysis evaluates the variation in dynamic model outputs with respect to (w.r.t.) variation in model parameters (Crosetto and Tarantola, 2001; Deif, 1986). Thus, sensitivity analysis can be used to perform uncertainty analysis, estimate model parameters, analyze experimental data, guide future data collection efforts, and suggest the accuracy to which the parameters must be estimated (Rodriguez-Fernandez and Banga, 2009).

Sensitivity analysis has been used to optimize vehicle system design (Jang and Han, 1995; Park et al., 2003). Jang and Han (1997) used a direct differentiation method for sensitivity analysis of on-road vehicle lateral dynamics with respect to (w.r.t.) tire cornering stiffness, location of vehicle center of gravity (CG), vehicle mass, and vehicle moment of inertia (MI) using a bicycle model of a front wheel steered vehicle. The study was performed at typical on-road vehicle velocities ranging from 9 m/s (20 mph) to 53 m/s (120 mph). Park et al. (2003) performed a dynamic sensitivity analysis for a pantograph of a rail vehicle. Dominant design variables were identified using derivative-based state sensitivity measures and were modified for optimal design. Ruta and Wojcicki (2003) also applied sensitivity analysis to a dynamic railroad track vibration model. They focused on developing an analytical solution for derivative-based sensitivity analysis of a system represented by a set of differential equations. Both first and second order derivatives were used to isolate a set of parameters to which the model outputs were the most sensitive. Eberhard et al. (2007) performed a vehicle model sensitivity analysis w.r.t. various design variables of a passenger car and found that vehicle dynamics were highly sensitive to MI and the CG location. The study was conducted at 10 m/s (~22 miles/hour) forward velocity. In off-road vehicle systems, the application of sensitivity analysis to understand the effect of uncertain parameters on a tractor and towed implement lateral dynamics is important to support the emerging farm automation technology such as implement guidance and coordinated guidance.

Various tractor and towed implement steering models have been proposed in the literature for both on-road (Chen and Tomizuka, 1995; Deng and Kang, 2003; Kim et al., 2007) and off-road (Feng et al., 2005; Karkee and Steward, 2009) operations. As suggested

by these models, the lateral dynamics of an off-road tractor and towed implement system depend on the lateral forces generated by soil-tire interactions. A vehicle tire, when subjected to a steering side force, does not move to the direction it is facing resulting to an angular difference between the two directions called the side slip angle (Wong, 2001). Vehicle tires go through some level of deformation when they move to a direction different than the direction they are facing. This deformation produces shear stress in the tire-soil interface. This shear stress causes some level of lateral soil deformation as well, which releases part of the shear stress developed in the interface (Metz, 1993). The resultant shear stress will generate a force at the contact patch called lateral tire force or cornering force (Crolla and El-Razaz, 1987).

In addition to tire and lateral soil deformation, the phenomena such as tire soil friction and soil sinkage effects also affect the characteristics of lateral tire force development (Metz, 1993). Because most of these phenomena are dependent on soil properties such as internal friction angle, cohesion, cone index, and tire-ground surface friction, the lateral tire forces and thus the off-road vehicle responses will vary with different soil types (eg. clay, sand or loam), soil condition (e.g. density and moisture content), and soil surface cover (eg. bare soil, vegetation or stover; Crolla and El-Razaz, 1987). In addition, the responses may vary with the variation in tire construction, size, inflation pressure and normal load (Schwanghart, 1968; Krick, 1973; Schwanghart and Rott, 1984; Raheman and Singh, 2004). It may be difficult to estimate these variables accurately, and it is also difficult to find a widely accepted model to relate these variables to the tire lateral force. The cornering stiffness coefficient, which is the slope of the lateral tire force as a function of side slip angle at zero side slip, is the parameter often used to represent the combined effect of these variables

(Metz, 1993). Because the soil-tire parameters are uncertain, varying, and/or inaccurate, the cornering stiffness parameter also tends to be highly uncertain. Vehicle tire relaxation length, which is defined as the distance a tire rolls before the steady state side slip angle is reached, is another parameter that could be highly uncertain (Bevly et al., 2002). In the case of implements such as grain carts or towed sprayers, implement mass and MI may also be uncertain or may vary substantially over time.

In this work, dynamic model sensitivity analysis was performed to quantify the dependence of tractor and single axle grain cart system responses on the uncertain model parameters. This analysis will increase understanding of the relative significance of these parameters so that more resources can be allocated to more accurately estimate those parameters to which the system is more sensitive. Specific objectives will be:

- to investigate the changes in sensitivities with the changes in vehicle forward velocity,
- to identify the parameters to which the model is most sensitive, and
- to evaluate the effect of parameter uncertainties on the system response uncertainty.

6.2 Methods

The sensitivity of a tractor and single axle grain cart steering system w.r.t. variation in various model parameters was analyzed using derivative-based sensitivity analysis method. A dynamic bicycle model of the system (Karkee and Steward, 2009) was adapted to perform the analysis. Grain cart mass and MI, tire cornering stiffness, and tire relaxation length parameters were assumed to have some level of uncertainty and/or variation over the field operation. Expanded ranges of these uncertain parameter values were used to define a

parameter space for the study. A numerical simulation-based approach was used to calculate local and global sensitivities w.r.t. those parameters.

6.2.1 Vehicle Model

A tractor and single axle towed implement model was required to study the sensitivity of the system states and outputs w.r.t. various system parameters. Karkee and Steward (2009) studied various models of a tractor and single axle grain cart system. Among the three models used, a dynamic bicycle model with tire relaxation length dynamics represented the system most accurately. While higher fidelity models could be used, this model represented the system lateral response reasonably accurately and included the most important system parameters. In this work, this model was used to study the sensitivity of the system w.r.t. eight system parameters including three tire cornering stiffness parameters, three tire relaxation length parameters and two implement inertial parameters. Common vehicle dynamics symbols were used to describe the dynamics of the system (see the list of the variables). This model is described by Eqs. 6.1 to 6.8:

$$\left(m^t + m^i\right)\dot{v}_c^t - m^i c\dot{\gamma}^t - m^i d\dot{\gamma}^i = -(m^i + m^t)u_c^t\gamma^t - C_{\alpha,f}^t\alpha_f^t - C_{\alpha,r}^t\alpha_r^t - C_{\alpha,r}^i\alpha_r^i \tag{6.1}$$

$$\left(I_z^t + m^i c^2\right)\dot{\gamma}^t - m^i c\dot{v}_c^t + m^i cd\dot{\gamma}^i = m^i cu_c^t\gamma^t - aC_{\alpha,f}^t\alpha_f^t + bC_{\alpha,r}^t\alpha_r^t + cC_{\alpha,r}^i\alpha_r^i \tag{6.2}$$

$$\left(I_z^i + m^i d^2\right)\dot{\gamma}^i - m^i d\dot{v}_c^t + m^i cd\dot{\gamma}^t = m^i du_c^t\gamma^t + (d+e)C_{\alpha,r}^i\alpha_r^i \tag{6.3}$$

$$\dot{\alpha}_f^t = \frac{v_c^t}{\sigma_f^t} + \frac{a\gamma^t}{\sigma_f^t} - \frac{u_c^t}{\sigma_f^t}\delta - \frac{u_c^t}{\sigma_f^t}\alpha_f^t \tag{6.4}$$

$$\dot{\alpha}_r^t = \frac{v_c^t}{\sigma_r^t} - \frac{b\gamma^t}{\sigma_r^t} - \frac{u_c^t}{\sigma_r^t}\alpha_r^t \tag{6.5}$$

$$\dot{\alpha}_r^i = \frac{v_c^t}{\sigma_r^i} - \frac{c\gamma^t}{\sigma_r^i} - \frac{(d+e)\gamma^i}{\sigma_r^i} + \frac{u_c^t}{\sigma_r^i}\varphi^t - \frac{u_c^t}{\sigma_r^i}\varphi^i - \frac{u_c^t}{\sigma_r^i}\alpha_r^i \tag{6.6}$$

$$\dot{\psi}^t = \gamma^t \tag{6.7}$$

$$\dot{\psi}^i = \gamma^i \tag{6.8}$$

Eqs. 6.1 – 6.8 can be represented in matrix form as,

$$M\dot{X} = NX + PU \tag{6.9}$$

where, the state vector is

$X = \begin{bmatrix} v_c^t & \gamma^t & \gamma^i & \alpha_f^t & \alpha_r^t & \alpha_r^i & \varphi^t & \varphi^i \end{bmatrix}^T$ and the input is $U = [\delta]$. Matrices M and N are give by,

$$M = \begin{bmatrix} (m^t + m^i) & -m^i c & -m^i d & 0 & 0 & 0 & 0 & 0 \\ -m^i c & (I_z^t + m^i c^2) & m^i cd & 0 & 0 & 0 & 0 & 0 \\ -m^i d & m^i cd & (I_z^i + m^i d^2) & 0 & 0 & 0 & 0 & 0 \\ 0 & 0 & 0 & 1 & 0 & 0 & 0 & 0 \\ 0 & 0 & 0 & 0 & 1 & 0 & 0 & 0 \\ 0 & 0 & 0 & 0 & 0 & 1 & 0 & 0 \\ 0 & 0 & 0 & 0 & 0 & 0 & 1 & 0 \\ 0 & 0 & 0 & 0 & 0 & 0 & 0 & 1 \end{bmatrix}$$

$$N = \begin{bmatrix} 0 & -(m^t + m^i)u_c^t & 0 & -C_{\alpha,f}^t & -C_{\alpha,r}^i & -C_{\alpha,r}^i & 0 & 0 \\ 0 & cm^i u_c^t & 0 & -aC_{\alpha,r}^t & bC_{\alpha,r}^t & cC_{\alpha,r}^i & 0 & 0 \\ 0 & dm^i u_c^t & 0 & 0 & 0 & (d+e)C_{\alpha,r}^i & 0 & 0 \\ \frac{1}{\sigma_f^t} & \frac{a}{\sigma_f^t} & 0 & -\frac{u_c^t}{\sigma_f^t} & 0 & 0 & 0 & 0 \\ \frac{1}{\sigma_r^t} & -\frac{b}{\sigma_r^t} & 0 & 0 & -\frac{u_c^t}{\sigma_r^t} & 0 & 0 & 0 \\ \frac{1}{\sigma_r^i} & -\frac{c}{\sigma_r^i} & -\frac{(d+e)}{\sigma_r^i} & 0 & 0 & -\frac{u_c^t}{\sigma_r^i} & 0 & 0 \\ 1 & 0 & 0 & 0 & 0 & 0 & 0 & 0 \\ 0 & 1 & 0 & 0 & 0 & 0 & 0 & 0 \end{bmatrix}$$

The tractor CG trajectory was calculated as follows.

$$\dot{x}_c^t = u_c^t \cos(\varphi^t) - v_c^t \sin(\varphi^t) \tag{6.10}$$

$$\dot{y}_c^t = u_c^t \sin(\varphi^t) + v_c^t \cos(\varphi^t) \tag{6.11}$$

The parameter values suggested by Karkee and Steward (2009) were used as the nominal values in this study (Table 6.1). The parameters were based on a MFWD tractor (model 7930, Deere and Co., Moline, IL) and a single axle 18 m^3 (500 bu) grain cart (model 500, Alliance Product Group, Kalida, OH).

Table 6.1: Dynamic bicycle model parameters for the JD 7930 tractor and Parker 500 grain cart system.

Tractor		Implement	
Parameters	Nominal Values	Parameters	Nominal Values
a	1.7 m	d	3.62 m
b	1.2 m	e	0.1 m
c	2.1 m		
m^t	9391 kg	m^i	2127 kg
I_z^t	35709 kg-m^2	I_z^i	6402 kg-m^2
$C_{\alpha f}^t$	220 KN/rad*		
$C_{\alpha r}^t$	486 KN/rad*	$C_{\alpha r}^i$	167 KN/rad*
σ_f^t	1.1 m**	σ_r^i	1.1 m**
σ_r^t	1.5 m**		

**Values based on the work of Metz (1993) and Schwanghart and Rott (1984).*

***Values based on the work of Bevly et al. (2002).*

As mentioned before, the front tire cornering stiffness $C_{\alpha f}^t$, rear-tire cornering stiffness $C_{\alpha r}^t$, implement tire cornering stiffness $C_{\alpha r}^i$, front tire relaxation length σ_f^t, rear tire relaxation length σ_r^t, implement tire relaxation length σ_f^i, implement mass m^i and implement moment of inertia I_z^i were considered to be uncertain or varying parameters. Cornering stiffness and relaxation length parameters were dependent on the soil-tire properties, which

can be highly uncertain. In case of the tractor and grain cart system model, the implement mass and MI could also vary substantially depending on the load on the cart. Implement CG was considered to be fixed assuming that the shape of the grain cart and the load on it are symmetrical about the implement lateral axis. Geometric parameters of the tractor and implement system, tractor mass, tractor MI and the tractor CG were also considered fixed as they can be known or estimated with reasonable accuracy. A range of parameter values was defined for each of the uncertain/varying model parameters (Table 6.2). These parameter ranges were used to define a parameter hyperspace used in the global sensitivity analysis. An uncertainty region of roughly ±100% about the nominal values (Table 6.1) was defined for cornering stiffness and tire relaxation length parameters. Because zero values for these parameters would fundamentally change the dynamic model, small positive numbers (~10% of the nominal values) were used as the minimum values. In case of the implement inertial parameters, the lowest limit roughly represented an empty grain cart (~10 m^3) and upper limit roughly represented a 35 m^3 grain cart with a full load of maize.

Table 6.2: Ranges of the uncertain parameters of the JD 7930 tractor and Parker 500 grain cart system dynamic model.

Tractor Parameters	Implement Parameters
$20 <= C_{\alpha f}^{t} <= 450$ KN/rad	$1100 <= m^{i} <= 7000$ kg
$50 <= C_{\alpha r}^{t} <= 980$ KN/rad	$3200 <= I_z^{i} <= 21000$ kg-m^2
$0.1 <= \sigma_f^{t} <= 2.2$ m	$10 <= C_{\alpha r}^{i} <= 340$ KN/rad
$0.15 <= \sigma_r^{t} <= 3.0$ m	$0.1 <= \sigma_r^{i} <= 2.2$ m

6.2.2 Sensitivity Analysis

Sensitivity is the measure of the variation in system responses w.r.t. to small perturbations in a system parameter. When using a dynamic model, the more a state/output

variable changes with a small change in a model parameter, the more sensitive it is to this parameter (Rodriguez-Fernandez and Banga, 2009). The sensitivity measure calculated at a particular location in the parameter space is called the local sensitivity. This measure will be valuable in studying the parameter uncertainty about a nominal point or a point of interest. The average sensitivity calculated over the entire parameter space is called the global sensitivity. This type of sensitivity is useful to identify the overall ranking of parameters in terms of their influence on the model responses within the parameter space as the method accounts for the interaction between model parameters (Kucherenko et al., 2009).

Various sensitivity analysis techniques have been proposed in the literature to calculate both local and global sensitivity measures or indices. Primarily, these techniques can be classified into three groups, namely variance-based methods, screening methods, and derivative-based methods. In the variance-based methods, the contribution of a model parameter to the output variance is estimated (Kioutsioukis et al., 2004). Some of the widely used variance based methods are Fourier Amplitude Sensitivity Test (FAST) (Cukier et al., 1973; McRae et al., 1982), the extended FAST (Saltelli et al., 1999) and the method of Sobol (Sobol, 1993). The drawback of the variance based methods is their computational inefficiency requiring a large number of function evaluations to calculate the sensitivity with a reasonable accuracy (Kucherenko et al., 2009). Screening methods are used to qualitatively rank the model parameters from the most influential to the least influential order. These methods are computationally attractive, but are less accurate (Kucherenko et al., 2009). The method of Morris (Morris, 1991) is one of such methods.

Derivative-based methods apply first order differentiation of the model outputs with respect to the model parameters. Local and global sensitivity measures are defined based on

those derivatives. Jang and Han (1995) and Kucherenko et al. (2009), among others, have proposed and used derivative-based methods. Kucherenko et al. (2009) used the method to analyze the sensitivity of seven algebraic equations to the equation parameter variations and compare the results with those from the method of Sobol and Morris. This method was more accurate than the method of Morris and was computationally more efficient than the Sobol's method. In addition, derivative-based methods provided both local and global sensitivity measures within the same framework. Because both local and global sensitivities were of interest, the derivative-based sensitivity analysis method was used in this work. Moreover, the derivative-based sensitivity analysis method was preferred over other methods in analyzing continuous-system dynamic models (Jang and Han, 1997; Park et al., 2003; Ruta and Wojcicki, 2003; Eberhard et al., 2007). In this work, some modifications were applied to the derivative-based formulation developed by Kucherenko et al. (2009) so that the sensitivity analysis of a complex dynamic model would be possible.

6.2.2.1 Local Sensitivity Measures

A dynamic system model such as one presented in section 2.1 can be represented as,

$$\dot{X} = f(X, p, t, u) \tag{6.12}$$

where, X is the state variable vector, p is the parameter vector t is time, and u is the input.

The local sensitivity of the system to a parameter p_i is defined as the partial derivative of the function f w.r.t. the parameter. The local sensitivity function about a nominal point p^* in the parameter space w.r.t. parameter p_i is then represented as,

$$S_i(p^*) = \left.\frac{\partial f}{\partial p_i}\right|_{p=p^*} \tag{6.13}$$

where, $i = 1, \ldots, n$ and n = size of parameter vector. As the point p^* moves in the parameter space, the local sensitivity measures will also change.

Because analytical solutions to the local sensitivity measure (Eq. 6.13) were difficult to obtain for the tractor and implement system used in this study, the sensitivities were calculated numerically using the simulated responses of the dynamic model (Ruta and Wojcicki, 2003). Six system variables, namely tractor lateral velocity and yaw-rate, implement yaw-rate, tractor CG position, tractor heading, and implement heading, were used in the analysis, which accounted for sensitivities of important state variables as well as output variables. The tractor and grain cart dynamic system (Eq. 6.9) was then represented in the state space form as,

$$\dot{X} = AX + BU \tag{6.14}$$

$$Y = CX + DU \tag{6.15}$$

where, $A = M^{-1}N$, $B = M^{-1}P$, C = identity matrix of size 8, and D=[0]. M and N were defined in Eq. 6.9.

First, the model was simulated with a 10° step steering input at the nominal point p^* in the parameter space. Even though applying a step is not possible in reality, a step was chosen of the mathematical convenience of the signal. The simulation was repeated at 1.0 m/s, 4.5 m/s and 7.5 m/s forward velocities to perform sensitivity analysis at those three velocities. The simulation time was twice the settling times of the slowest non-zero eigenvalue of the system model, which were 30 s, 6 s and 3 s at 1.0 m/s, 4.5 m/s and 7.5 m/s forward velocities respectively. With this simulation time, the sensitivity analysis accounted for both the transient and steady state sensitivities. The output responses from this simulation were used as the reference. Parameters of interest were then varied one at a time by 1% of the nominal values to get the perturbed output responses. Finally, the local sensitivity of an

individual output/state variable w.r.t. the parameters at the nominal point was calculated using the finite difference equation:

$$S_{ij}(p^*) = \frac{Y_j\left(p_1^*, \ldots\ldots\ldots, p_{i-1}^*, p_i^* + \Delta p_i^*, p_{i+1}^*, \ldots\ldots\ldots, p_n^*\right) - Y_j(p^*)}{\Delta p_i^*} \tag{6.16}$$

where, $j = 1, \ldots\ldots, m$; m = number of output or state variables; Δp_i^*= small change in the parameter of interest. The variable Y_j represented a time series data of an individual output response of the dynamic system. A root mean squared (RMS) change in the output variable over the simulation time was used to calculate the local sensitivity of an individual output/state variable. This local sensitivity measure was calculated w.r.t. all parameters of interest at various points in the parameter space.

The changes in input parameters were divided by the nominal values of the parameters to normalize the results as it was not appropriate to directly compare or average the output sensitivities w.r.t. various input parameters whose numerical ranges differed by several order of magnitude. Output variables were also of different orders of magnitudes. An approach to define the sensitivity in this case would also be to normalize the changes in the output variables by the nominal output values. However, because we were dealing with a dynamic system responses with zero crossings, the three state variables were normalized only after the RMS changes in output variables were calculated. In the case of the CG position, the distance between the end points of the reference and perturbed trajectories was normalized by the steady state turn radius of the reference trajectory. In the case of the heading angles, the heading difference at the end points of the reference and perturbed trajectories was normalized by the absolute heading difference between the start and end point of the

reference trajectory. The normalized sensitivity measures had units of percentage-of-output-response/percentage-of-input-parameter (or %/%).

Finally, the overall local sensitivity w.r.t. a parameter p_i was calculated using a mean over the output/state variables,

$$S_i = \frac{1}{m}\sum_{j=1}^{m} S_{ij} \tag{6.17}$$

6.2.2.2 Global Sensitivity Measures

A global sensitivity measure can be calculated by averaging the local sensitivities (Eq. 6.13) over the whole parameter space using (Kucherenko et al., 2009),

$$\overline{M}_i' = \int_{H^n} S_i dp \tag{6.18}$$

where, $\overline{M}_i'$ is the global sensitivity of the system w.r.t. the parameter p_i, H^n is the parameter space, and p is the parameter vector.

The 8-dimentional parameter space was defined by using ranges of uncertain model parameters about the nominal values (Table 6.2). A finite summation technique was applied to the model simulation-based local sensitivities (Eq. 6.16) to calculate the global sensitivities of the output/state variables w.r.t. each model parameter p_i,

$$\overline{M}'_{ij} = \frac{1}{n}\sum_{k=1}^{n} S_{ijk} \tag{6.19}$$

where, $k = 1,\ldots..,n$ and n = number of points in the parameter space. An overall global sensitivity measure was then calculated as

$$M'_i = \frac{1}{m}\sum_{j=1}^{m} M'_{ij} \tag{6.20}$$

A hyper space gridding was required to calculate the global sensitivity measures (Eq. 6.19 and Eq. 6.20). For an eight-dimensional parameter space used in this work, the

computational load was tremendously high when a small grid resolution was used. Therefore, the sensitivity analysis was started with a fairly large grid size, and it was gradually reduced to achieve a good tradeoff between the computational time and the accuracy achieved. The global sensitivities were also computed at 1.0 m/s, 4.5 m/s and 7.5 m/s forward velocities. The average global sensitivities of the system over a simulation period of twice the settling times were used to rank the parameters from high to low importance in terms of the estimation accuracy required (Sobol, 2001).

6.2.2.3 Parameter Uncertainty Analysis

Parameter uncertainty analysis was performed to study the effect of the model parameter uncertainties on the system responses. Monte Carlo simulation is one of the ways to analyze uncertainty propagation from the input parameters p_i to the output variables y_i (Istvan, 1999). In Monte Carlo simulation, sets of randomly generated numbers are used as inputs to iteratively evaluate a system model and generate the distribution of output variations (Wittwer, 2004). Depending on the existing knowledge and/or estimates of the variables, different types of distributions can be used to define the variation in the input parameters (Fig. 6.1).

Input parameters were assumed to be normally distributed. Because the system was most sensitive to cornering stiffness parameters, the analysis was performed with just three cornering stiffness parameters. The three cornering stiffness parameters varied together because the parameters were positively correlated. Monte Carlo simulations were performed at 1.0 m/s, 4.5 m/s and 7.5 m/s forward velocities with a set of 2500 cornering stiffness parameter values randomly selected from normal distributions. Then, the variations in the six individual output/state responses were averaged to generate the distribution of the output

variation. The same numerical simulation technique used in the sensitivity analysis method was used to evaluate the tractor and towed single axle grain cart model for the Monte Carlo simulation.

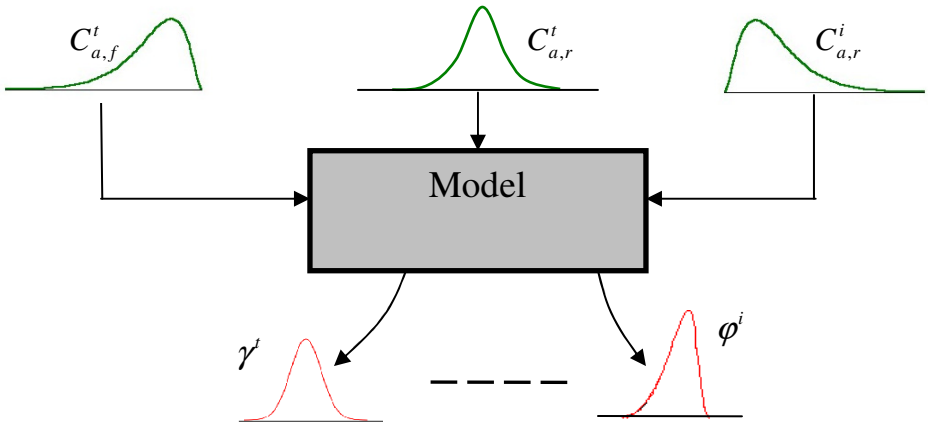

Fig. 6.1: Propagation of uncertainty from input variables/parameters to the output variables (adapted from Wittwer, 2004). Monte Carlo simulation can be used to iteratively evaluate the model and estimate the output uncertainties.

The uncertainty *u'* associated with a parameter or a variable can be quantitatively defined by the absolute or relative error about the estimated value (Ellison et al., 2000; Wittwer, 2004). In this work, uncertainties were represented by the relative error written as a percentage. For the normally distributed input parameters, the standard deviation, σ, was used to define the uncertainty as this was the most widely used uncertainty measure (Fig. 6.2a) (Ellison et al., 2000). With this uncertainty measure, 68% of the total estimates of an uncertain variable were used to define the level of uncertainty in the variable. Assuming that the estimated values of the tractor and single axle grain cart system parameters were normally distributed with means representing the expected parameter values, standard deviations of the distributions were used as the uncertainties in the input parameters. However, the distribution of the average output variation w.r.t. the normally distributed input

parameters did not follow a normal distribution at any forward velocities. In this case, a 68% interval in the central lobe of the output distribution was calculated leaving 16% samples of the distribution in each tail. Half of this interval was used as the uncertainty measure for the output responses (Fig. 6.2b). To model the relationship between input and output uncertainties (Grau, 2002), the uncertainty propagation study was performed with varying level of uncertainties in cornering stiffness parameters.

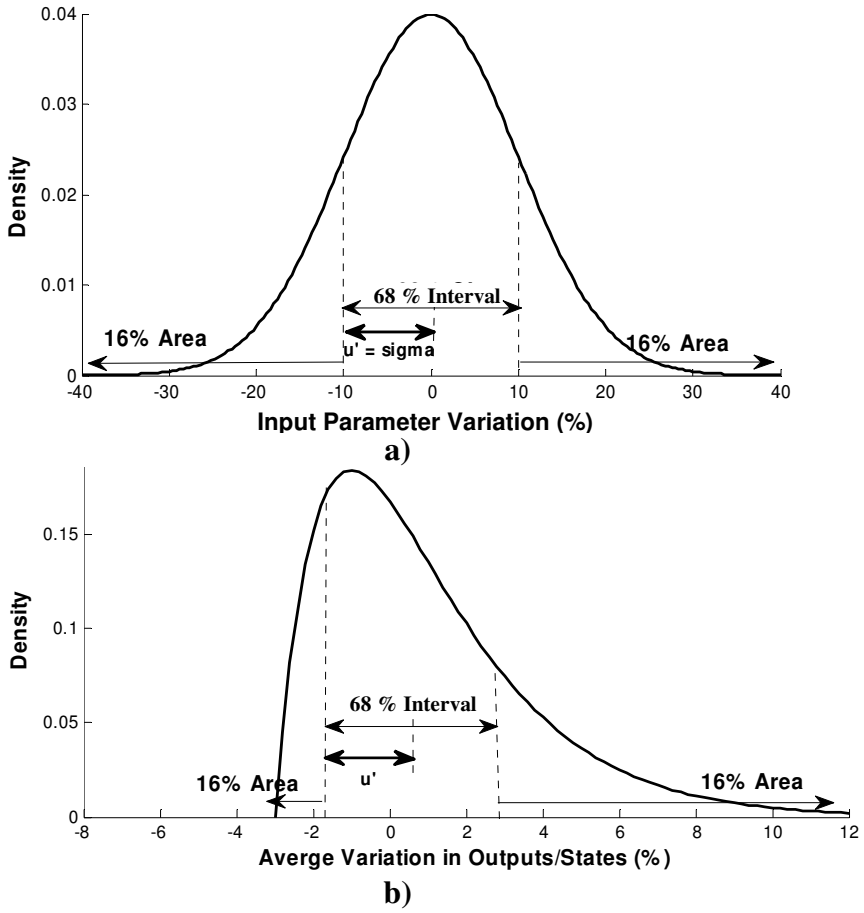

Fig. 6.2: Arbitrary probability distributions of an input parameter a) and an output/state variable b). For the normally distributed input parameter, standard deviation was used to define the input parameter uncertainty *u'* whereas half of the 68% interval was used to define the uncertainties associated with the output variables having distributions different than the normal distribution.

6.3 Results and Discussions

6.3.1 Local Sensitivity Analysis

The local sensitivities at the nominal point (Table 6.1) in the parameter space showed the effect of variations in the system parameters on the system responses (Fig. 6.3- Fig. 6.5). In general, lateral velocity and yaw-rate states were more sensitive to the input parameters at 1.0 m/s forward velocity than at 4.5 m/s and 7.5 m/s forward velocities. As expected, the implement mass, implement MI, and implement tire cornering stiffness parameters primarily influenced the implement yaw-rate and heading responses. The tractor CG position, tractor heading and implement heading outputs were most sensitive to the front and rear tire cornering stiffness parameters.

Local sensitivities w.r.t. implement inertial parameters were relatively small at all forward velocities with a maximum of 0.14 for the tractor lateral velocity (Fig. 6.3). Implement yaw-rate and tractor lateral velocity were the most sensitive states to both the implement mass and implement MI. This result was expected as the implement inertial parameters will have a higher influence on the implement dynamics, and the tractor lateral velocity was coupled with the implement yaw-rate state. Implement heading angle was relatively insensitive to the variation in implement mass (0.05 %/%) as well as to that of the implement MI. Because the implement MI influenced only the transient implement yaw-rate, the influence on the implement heading was diminished when the yaw-rate was integrated to get the heading angle. The implement yaw-rate sensitivities w.r.t. implement mass were 0.07 and 0.06 respectively at 1.0 m/s and 7.5 m/s forward velocities. The tractor lateral velocity sensitivity w.r.t. the implement MI was 0.06 at 1.0 m/s forward velocity. All other sensitivities w.r.t. both implement mass and MI were 0.05 or less.

In general, velocity response sensitivities (tractor lateral velocity, tractor yaw-rate and implement yaw-rate) w.r.t. tire cornering stiffness parameters decreased as the forward velocity increased to 4.5 m/s from 1.0 m/s and increased as the forward velocity increased to 7.5 m/s from 4.5 m/s (Fig. 6.4). However, the positional response sensitivities (tractor heading, implement heading and tractor position) increased consistently with increasing forward velocity. The velocity responses were more sensitive than the positional responses to tractor rear tire and implement tire cornering stiffness variations. All responses were equally sensitive to tractor front tire cornering stiffness variation. Sensitivities were observed as high as 0.4 to front tire cornering stiffness variation, 0.7 to rear tire cornering stiffness variation and 0.2 to implement tire cornering stiffness variation. In general, the system was more sensitive to the cornering stiffness parameters than to the other uncertain parameters (Fig. 6.3 and Fig. 6.5).

Tire relaxation lengths only influenced the velocity responses of the system (Fig. 6.5). The sensitivities were much higher at 1.0 m/s than at higher velocities. The lateral velocity and yaw-rate sensitivities to tire relaxation length variations were caused by the changes in the damped natural frequency of the underdamped transient responses as a relaxation length does not affect the steady state system responses. The changes in the natural frequency of the underdamped transient responses were mitigated when the lateral velocity and yaw-rate responses were integrated to get the position and heading responses. The tractor CG position, tractor heading and implement heading sensitivities w.r.t. relaxation length parameters were thus negligible even when the lateral velocity and yaw rate states were highly sensitive.

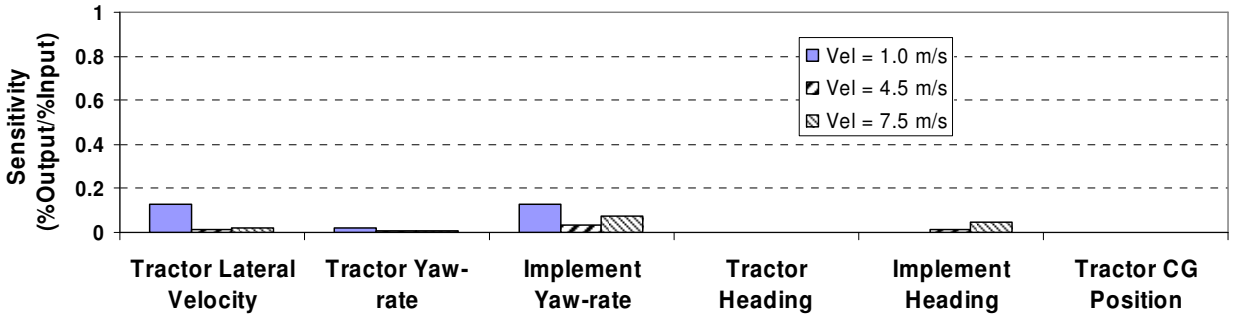

a) Local sensitivities of state variables w.r.t. implement mass

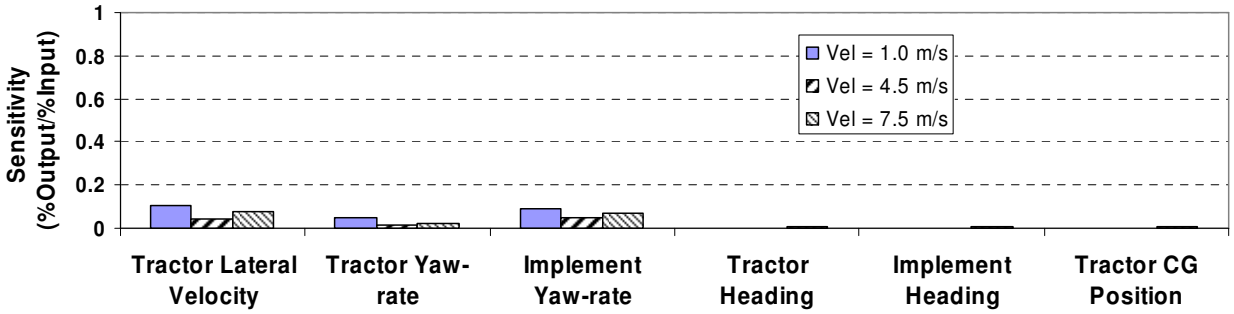

b) Local sensitivities of state variables w.r.t. implement MI

Fig. 6.3: Individual state/output local sensitivities at the nominal point in the parameter space w.r.t. a) implement mass, and b) implement MI. The sensitivities were calculated at 1.0 m/s, 4.5 m/s and 7.5 m/s forward velocities.

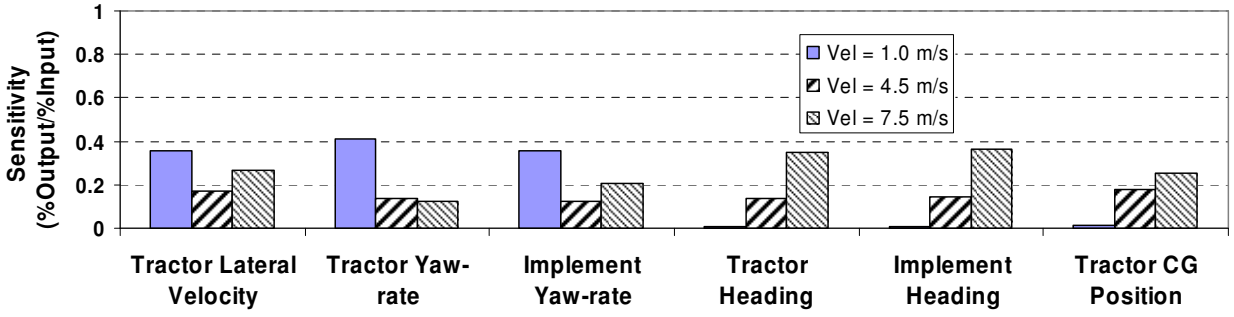

a) Local sensitivities of state variables w.r.t. front tire cornering stiffness

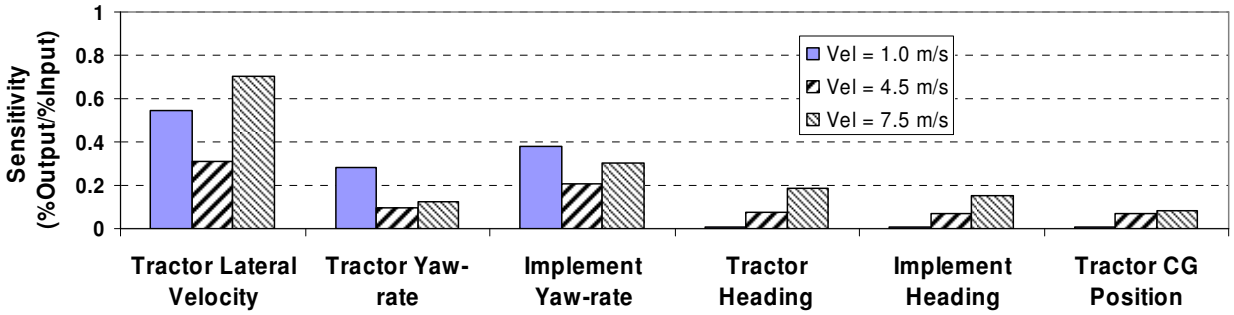

b) Local sensitivities of state variables w.r.t. rear tire cornering stiffness

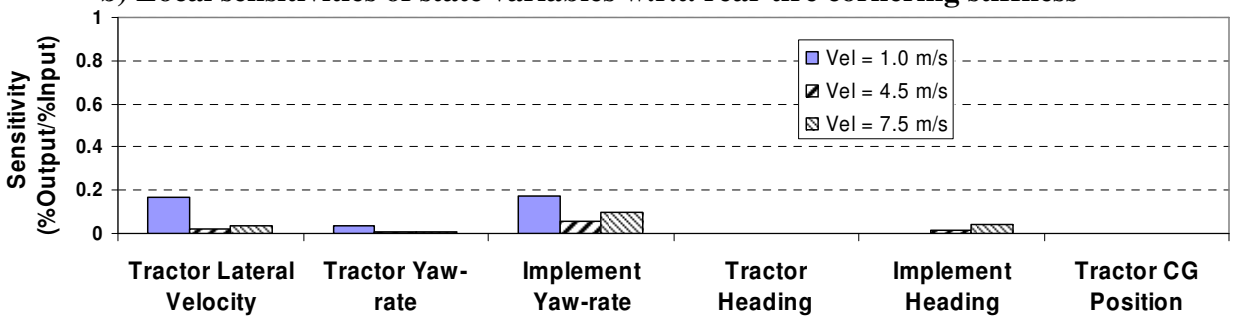

c) Local sensitivities of state variables w.r.t. implement tire cornering stiffness

Fig. 6.4: Individual state/output local sensitivities at the nominal point in the parameter space w.r.t. cornering stiffness parameters; a) front tire cornering stiffness, b) rear tire cornering stiffness, and c) implement tire cornering stiffness. The sensitivities were calculated at 1.0 m/s, 4.5 m/s and 7.5 m/s forward velocities.

As discussed above, the system velocity states were highly sensitive to all input parameters at 1.0 m/s forward velocity. The system responses were less damped at 1.0 m/s than at 4.5 m/s and 7.5 m/s forward velocities (Fig. 6.6), and the interaction between tire relaxation length and other parameters caused a larger change in undamped natural frequencies between the reference and perturbed responses at 1.0 m/s (Fig 6.6a). The increased natural frequency resulted to the higher system sensitivities at the low forward velocity. However, the highly underdamped yaw-rate response observed at 1.0 m/s (Fig. 6.6a) is unrealistic. This result suggests that the inclusion of tire relaxation length dynamics

into the model may not be appropriate at lower velocities and the sensitivities to run-length parameter variation obtained at 1.0 m/s may not be reliable.

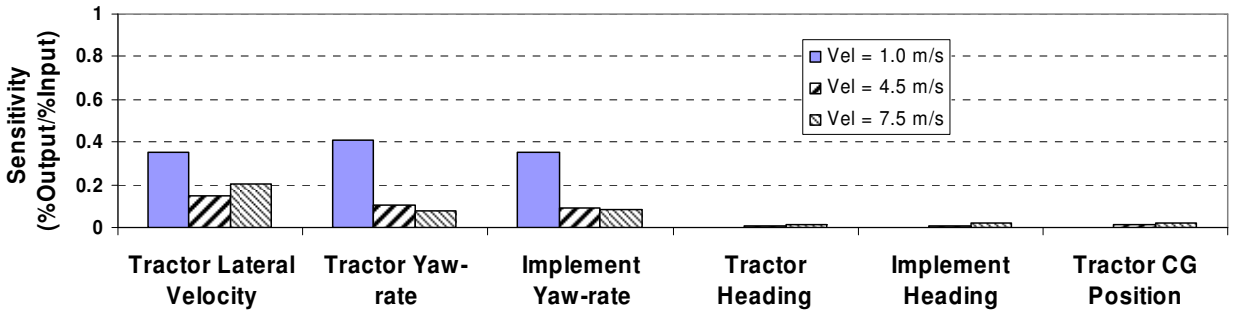

a) Local sensitivities of state variables w.r.t. front tire relaxation length

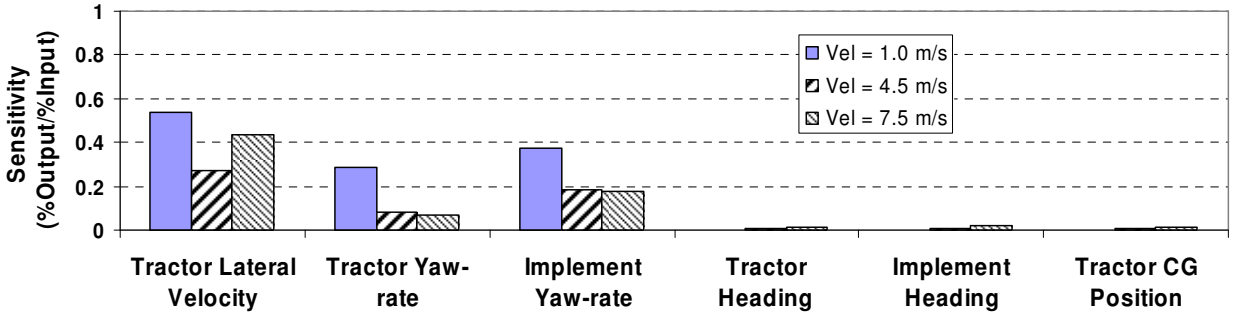

b) Local sensitivities of state variables w.r.t. rear tire relaxation length

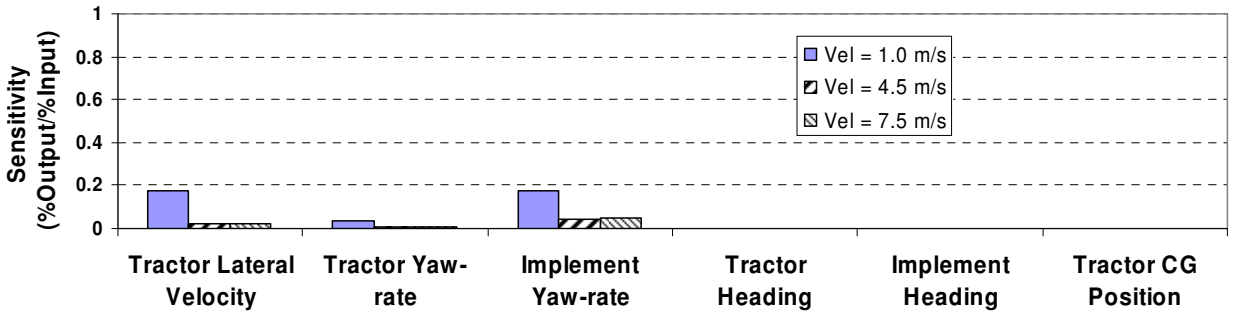

c) Local sensitivities of state variables w.r.t implement tire relaxation length

Fig. 6.5: Individual output/state local sensitivities at the nominal parameter point w.r.t. a) front tire relaxation length, b) rear tire relaxation length, and c) implement tire relaxation length. The sensitivities were calculated at 1.0 m/s, 4.5 m/s and 7.5 m/s forward velocities.

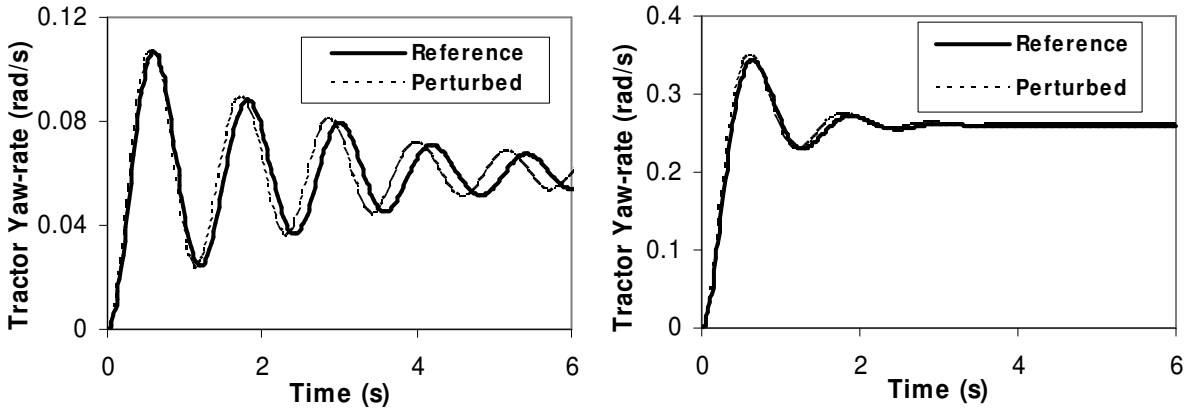

Fig. 6.6: Tractor yaw-rate time histories for the nominal parameters (reference) and 10% change in the rear tire relaxation length parameter (perturbed); a) at 1.0 m/s forward velocity, b) at 4.5 m/s forward velocity.

Similarly, the local sensitivities at 7.5 m/s forward velocity, in general, were higher as compared to those at 4.5 m/s forward velocity. This result was caused by the larger change in the steady state output responses at higher forward velocity as compared to the changes in the steady state responses at lower forward velocities (Fig. 6.7).

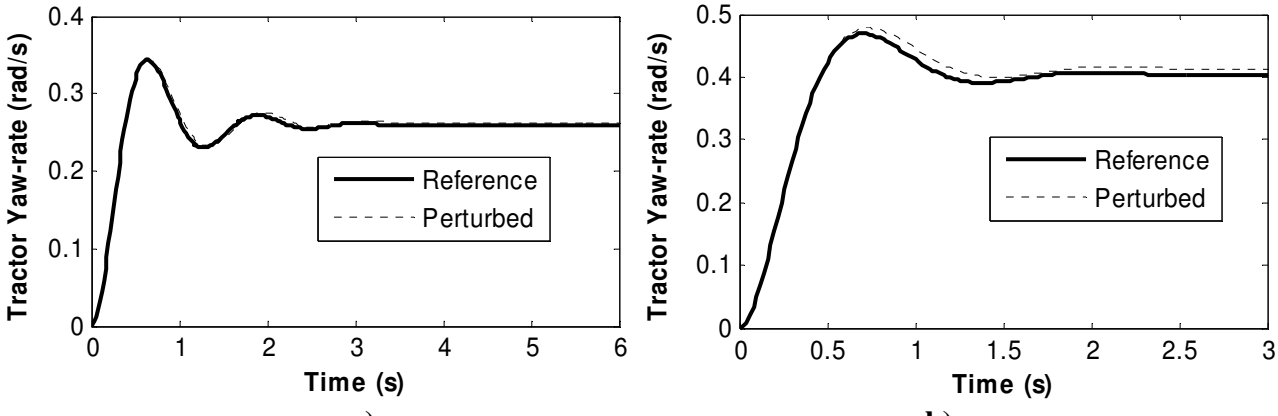

Fig. 6.7: Tractor yaw-rates for the nominal parameters (reference) and 10% change in the rear tire cornering stiffness (perturbed); a) at 1.0 m/s and b) at 4.5 m/s forward velocities.

At the nominal parameter point, the overall system was most sensitive to tractor front and rear tire cornering stiffness variations (Fig. 6.8). The front and rear tire relaxation lengths were the next two parameters to which the system response was most sensitive. The system was least sensitive to the implement mass and MI. At 1.0 m/s, the system was almost equally sensitive to cornering stiffness and corresponding relaxation length parameters. At 4.5 m/s and 7.5 m/s, however, the tractor-and-implement system was twice as sensitive to cornering stiffness parameters as it was to relaxation length parameters. The system was less sensitive to relaxation length at 4.5 m/s than at 1.0 m/s, and the sensitivity increased again when the velocity was increased to 7.5 m/s. The higher sensitivity at 1.0 m/s was expected for the reason discussed above (Fig. 6.6).

The system response was less sensitive to the cornering stiffness parameters at 4.5 m/s than it was at 1.0 m/s forward velocity. The average state sensitivity at 1.0 m/s was 0.2 w.r.t. both the front and rear tire cornering stiffness parameters. However, it dropped to 0.15 at 4.5 m/s forward velocity. When the forward velocity was increased to 7.5 m/s, the system became more sensitive to all three cornering stiffness parameters. At this velocity, the average state sensitivity increased to 0.26 w.r.t. both the front and rear tire cornering stiffness parameters. This result can be explained because the cornering stiffness parameters define the velocity state of the eigenvalues, which dominate the system response at higher forward velocities (Karkee and Steward, 2009). However, because the interaction between cornering stiffness and relaxation length parameters was substantial at lower velocities (Fig. 6.4), the system was highly sensitive to cornering stiffness parameters at 1.0 m/s forward velocity.

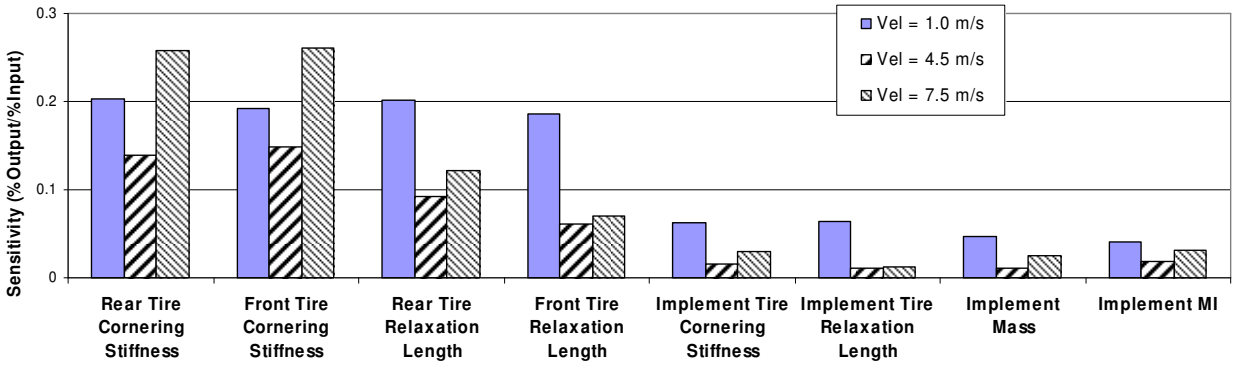

Fig. 6.8: Overall local sensitivities at nominal point in the parameter space with respect to various system parameters at 1.0 m/s, 4.5 m/s and 7.5 m/s forward velocities.

Similar trends were observed with the implement inertial parameters. The system was most sensitive to variations in implement mass and MI at 1.0 m/s. The average state sensitivity was about 0.05 w.r.t. both the implement mass and MI at 1.0 m/s. The sensitivity dropped to 0.02 at 4.5 m/s and increased slightly at 7.5 m/s. In general, the system was sensitive to all system parameters at 1.0 m/s forward velocity. As discussed before (Fig. 6.6), higher system sensitivity at the low forward velocity was caused by the substantial change in the system natural frequencies.

The interactions between input parameters were observed by computing local sensitivities at various points in the parameter space. At a sample point with small relaxation length parameters (10% of the nominal values), large implement inertial parameters (200% of the nominal values), and nominal cornering stiffness parameters, the interaction between relaxation length and other input parameters was not substantial even at 1.0 m/s forward velocity (Fig. 6.9).

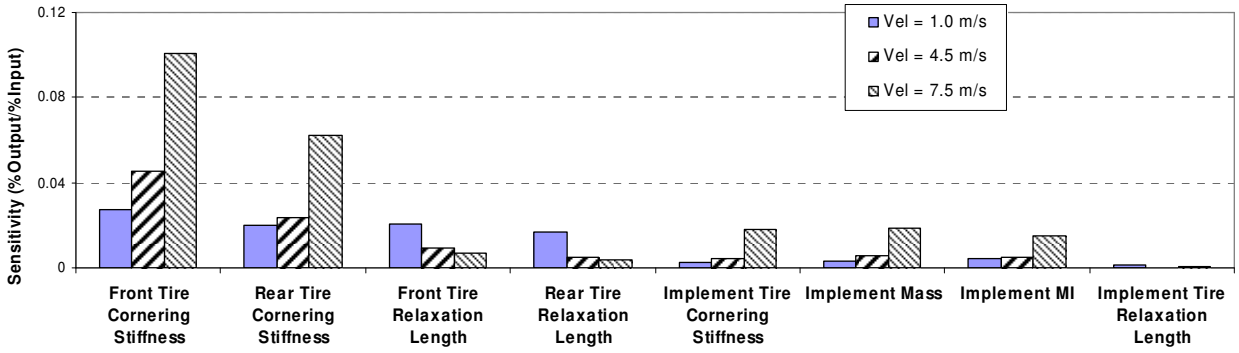

Fig. 6.9: Overall local sensitivities at a sample point in the parameter space with respect to various system parameters at 1.0 m/s, 4.5 m/s and 7.5 m/s forward velocities.

As expected, the sensitivities at 1.0 m/s w.r.t. cornering stiffness and implement inertial parameters were smaller at this point. The system sensitivities w.r.t. cornering stiffness parameters increased consistently as the forward velocity increased. At this point, the system was most sensitive to cornering stiffness parameters at all velocities. The front and rear tire relaxation length parameters were the second most influential parameters at 1.0 m/s and 4.5 m/s forward velocities whereas implement inertial parameters were the second most influential parameters at 7.5 m/s forward velocity.

6.3.2 Global Sensitivity Analysis

The local sensitivities at different points in the parameter space varied due to the interaction between the input parameters (Fig. 6.8 and Fig. 6.9). The overall system sensitivity within the parameter space was studied with global sensitivity measure. The grid resolution selected for the parameter hyperspace gridding had an effect on the computational load and accuracy of the global sensitivity calculation. As the resolution was decreased, the accuracy of the global sensitivity improved, but with an $O(N^8)$ increase in the computation time. The global sensitivities did not change much after when the resolution was decreased to

1/5th of the parameter range, i.e. when there were five grid points in each parameter axis. With this grid resolution, 390 thousand points in the parameter space were used to calculate global sensitivities w.r.t. various model parameters (Fig. 6.10).

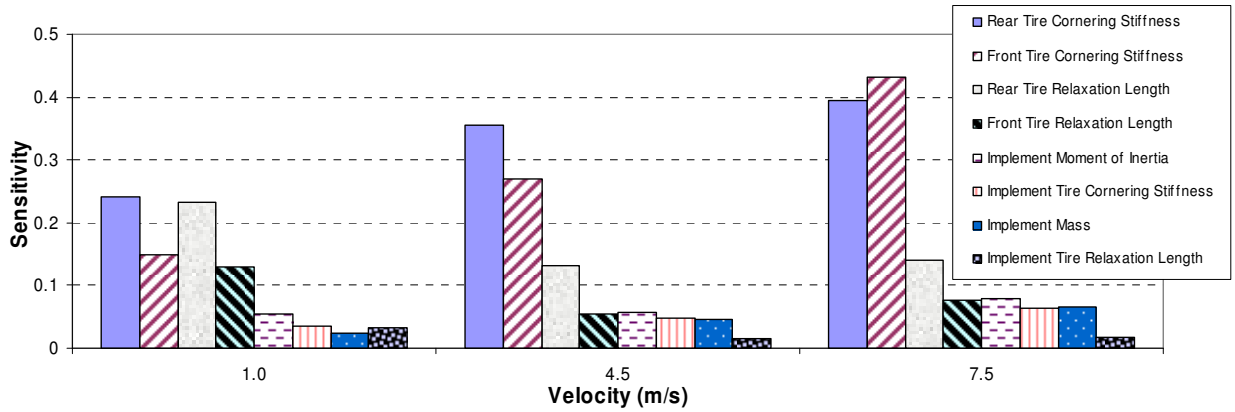

a) Categorized by velocity

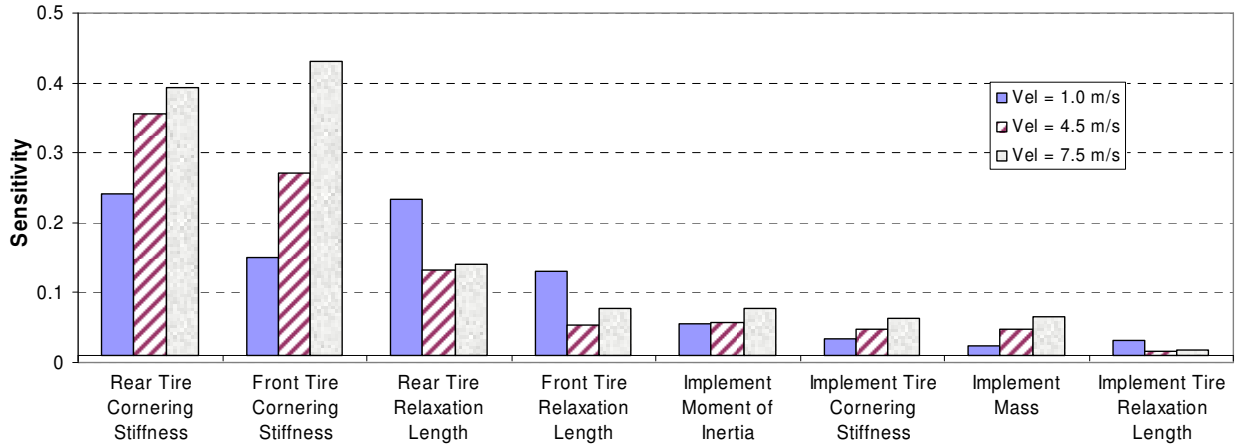

b) Categorized by parameter

Fig. 6.10: Average global sensitivities over 360,000 regularly gridded points in the parameter space, a) categorized by velocity, b) categorized by input parameter.

In terms of overall global sensitivities, generally the system was more sensitive to the cornering stiffness parameters than to the implement inertial parameters and the tire relaxation length parameters. At 1.0 m/s and 4.5 m/s, the system was most sensitive to the tractor rear tire cornering stiffness (Fig. 6.10a). The sensitivity w.r.t. the rear tire cornering

stiffness was 0.24 and 0.35 respectively at 1.0 m/s and 4.5 m/s forward velocities. At 7.5 m/s, the tractor front tire relaxation length was the most influential parameter with the system sensitivity of 0.43. At lower velocity, similar to the local sensitivities at the nominal point, the tire relaxation length parameters remained highly influential. At 1.0 m/s, the system was more sensitive to the tractor rear tire relaxation length then it was to the tractor front tire cornering stiffness. The second most influencing parameter at 4.5 m/s was the tractor front tire relaxation length whereas at 7.5 m/s the tractor rear tire cornering stiffness was the second most influencing parameter. Implement tire relaxation length was generally the least influencing parameter.

The system sensitivity to the variation in cornering stiffness parameters increased as the forward velocity increased (Fig. 6.10b). For example, the sensitivity w.r.t. the tractor front tire cornering stiffness was 0.15, 0.27 and 0.43 respectively at 1.0 m/s, 4.5 m/s and 7.5 m/s forward velocities. This result was expected as the higher order dynamics influenced by the cornering stiffness parameter dominate the system response as the forward velocity is increased. Similar trends were observed with the implement inertial parameters (implement mass and MI). However, the variation in the system sensitivities w.r.t. the inertial parameters was much smaller than the variation w.r.t. cornering stiffness parameters. The sensitivities w.r.t. implement MI was 0.05, 0.05 and 0.07 respectively at 1.0 m/s, 4.5 m/s and 7.5 m/s forward velocities. With respect to the relaxation length parameters, the system was most sensitive at 1.0 m/s. These sensitivities decreased substantially when the velocity increased to 4.5 m/s but did not change much when the velocity increased to 7.5 m/s from 4.5 m/s. With respect to the rear tire relaxation length, the sensitivities were 0.23, 0.13 and 0.14 at 1.0 m/s, 4.5 m/s and 7.5 m/s velocities respectively.

6.3.3 Parameter Uncertainty Analysis

The distributions of the average output variation were skewed to the right when the variation in the cornering stiffness parameters was normally distributed (Fig. 6.11). A goodness of fit test at 1% significance level did not support the hypothesis that the output variations were normally distributed. The distribution of the average output variation at 1.0 m/s was not very skewed about the reference output (skewness of 0.04), but followed an approximately uniform distribution (Fig. 6.11b). The skewnesses of the distributions at 4.5 m/s and 7.5 m/s forward velocities were 0.46 and 0.56 (Fig. 6.11c and Fig. 6.11d). In general, the uncertainty *u'* in output variables, as defined in section 2.3, increased as the forward velocity was increased. For a 10 % uncertainty in the cornering stiffness parameters, the output variables had an average of 1.5%, 2.0% and 4.0% uncertainties respectively at 1.0 m/s, 4.5 m/s and 7.5 m/s forward velocities.

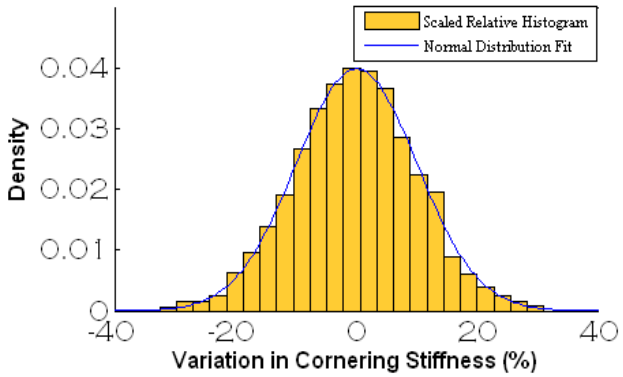

a) Cornering stiffness variation, *u'* = 10%

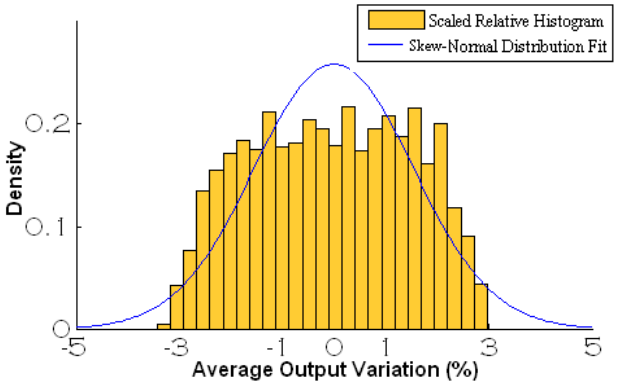

b) Output variation at 1.0 m/s, *u'* = 1.5%

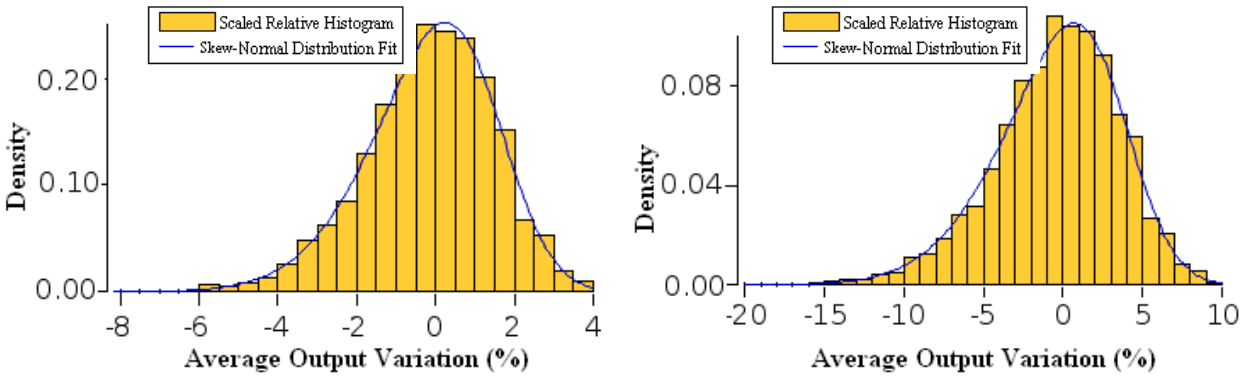

c) Output variation at 4.5 m/s, *u'* = 2.0% **d) Output variation at 7.5 m/s, *u'* = 4.0%**

Fig. 6.11: Probability density function of the average output variation w.r.t. the variation in the cornering stiffness parameters about their nominal values at different forward velocities; a) variation in cornering stiffness parameters, b) average output variation at 1.0 m/s, c) average output variation at 4.5 m/s, and d) average output variation at 4.5 m/s. Scaled relative frequency was used to represent the histograms so that the histograms also represented the probability distribution function.

The six state/output variables (Fig. 6.3) were used to calculate the effect of varying system parameter uncertainties about the nominal point on the system responses. In general, the parameter uncertainties and uncertainties in the system responses were related in a non-linear fashion (Fig. 6.12). The trend lines relating these uncertainties had r-squared values of 0.98 or more at each velocity.

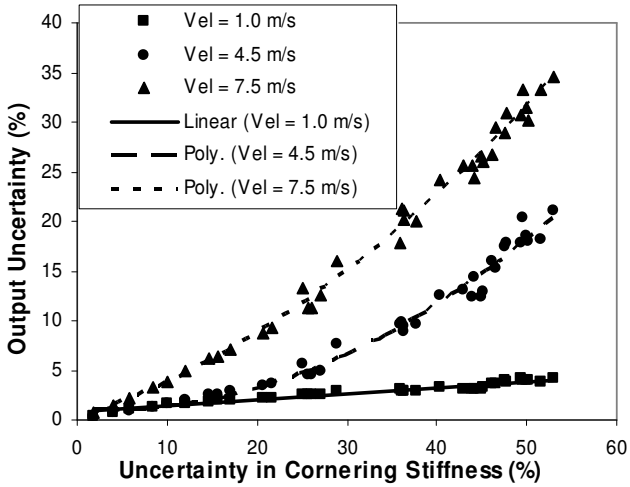

Fig. 6.12: The relationship between average uncertainty over the six output variables of the system and the uncertainty in cornering stiffness parameters. The variations were calculated at 1.0 m/s, 4.5 m/s and 7.5 m/s forward velocities.

Generally, the output uncertainties increased most rapidly at 7.5 m/s and least rapidly at 1.0 m/s forward velocities with the increasing input uncertainties. The average output uncertainty followed a second order polynomial relationship with the uncertainties in cornering stiffness parameters at 4.5 m/s and 7.5 m/s forward velocities. The same relationship was linear at 1.0 m/s forward velocity. At 4.5 m/s forward velocity, a 10% uncertainty in cornering stiffness parameters caused a 2% average uncertainty in the system responses whereas a 50% uncertainty in cornering stiffness parameters caused a 20% average uncertainty in the system responses. At 7.5 m/s, a 10% uncertainty in cornering stiffness parameter caused a 4% average output/state uncertainty whereas a 50% cornering stiffness uncertainty caused a 35% average output/state uncertainty. The result showed that if a 5% average uncertainty in system responses is acceptable, the cornering stiffness parameters must be estimated within 50%, 25% and 15% of actual/nominal values respectively at 1.0 m/s, 4.5 m/s and 7.5 m/s forward velocities.

6.4 Conclusions

Local and global sensitivities of a tractor and single axle grain cart system were calculated using a derivative-based method. Due to the complexity in deriving analytical sensitivity indices, a numerical analysis was performed using simulation-based dynamic system model responses. The work was important to understand the effect of parameter variations on the tractor and towed implement system responses. The system parameters were ranked based on the relative importance of the parameters to the system responses. It can be concluded from the work that there is a need for better estimates of the soil-tire interaction component of off-road vehicle dynamics simulation as it will play an important role in the vehicle responses. It was also determined that the changes in implement mass and moment of inertial will have little effect on the off-road vehicle responses. Specifically, the following conclusions were drawn from this work.

- Overall, cornering stiffness was the most influential parameter of the tractor and a single axle towed implement system dynamics. In terms of global sensitivity, the system was most sensitive to the tractor rear tire cornering stiffness followed by the tractor rear tire relaxation length at 1.0 m/s. At 4.5 m/s and 7.5 m/s, rear and front tire cornering stiffness were the most important two parameters. In terms of local sensitivity at the nominal point, the system was equally sensitive to both of the tractor front and rear tire cornering stiffness parameters. The system was least sensitive to the implement inertial parameters.

- In general, the cornering stiffness parameters influence the system dynamics more as the forward velocity increased whereas the tire relaxation length parameters were less influential with the increasing forward velocity.
- In general, uncertainty in system parameters and system outputs were related in a non-linear fashion. About the nominal values and 4.5 m/s forward velocity, a 10% uncertainty in the cornering stiffness parameters resulted to a 2% average output uncertainty where as a 50% cornering stiffness uncertainty resulted to a 20% output uncertainty.

Acknowledgements

This research was supported by Hatch Act and State of Iowa funds. Journal paper of the Iowa Agriculture and Home Economics Experiment Station, Ames, Iowa, Project No. 3612.

Notation and List of Variables

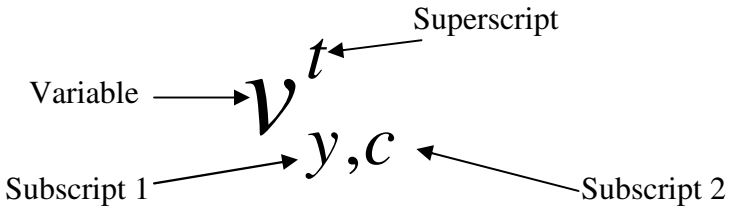

Variable: The variable itself.

Big or bold letter – vector or matrix, small letter – scalar

Superscript: Denotes whether the variable is related to tractor or implement.

t – tractor, i – implement

Subscript 1: Specifies the co-ordinate axis the variable corresponds to.

x – x axis, y – y axis, z – z axis

Subscript 2: Specifies the location the variable corresponds to.

f – front tire axle, r – rear tire axle, c – center of gravity, p – toe pin (hitch point)

List of variables

α	side slip angle or the angle between the direction the tire is going and the direction it is facing. The velocity vector to the right of the tire is positive and reverse is negative.
α_0	steady state side slip angle
γ	yaw rate
δ	steering angle
λ	angle between tractor heading and implement heading
σ	relaxation length
φ	heading angle
a	distance between front axle and CG of tractor
b	distance between rear axle and CG of tractor
c	distance between hitch point and CG of tractor
C_α	cornering stiffness
d	distance between hitch point and CG of implement
e	distance between rear axle and CG of implement
F	force
I_z	yaw moment of inertia
$\overline{M}'$	Global sensitivity measure
m	mass
p	parameter vector

S	local sensitivity measure
u	longitudinal velocity
v	lateral velocity
X-Y	world coordinates
x'-y'	vehicle coordinates
y	position of CG in y- axis of the world co-ordinate system

References

Bevly, D. M., J. C. Gerdes, and B. W. Parkinson (2002). A new yaw dynamic model for improved high speed control of a farm tractor. *Journal of Dynamic Systems, Measurement, and Control*, 124: 659-667.

Chen, C., and M. Tomizuka (1995). Dynamic modeling of tractor-semitrailer vehicles in automated highway systems. *Proc. of American Control Conference, Seattle, WA, June 21-23*.

Crolla, D. A., and A. S. A. El-Razaz (1987). A review of the combined lateral and longitudinal force generation of tyres on deformable surfaces. *Journal of Terramechanics*, 24(3): 199-225.

Crosetto, M., and S. Tarantola (2001). Uncertainty and sensitivity analysis: tools for GIS-based model implementation. *International Journal of Geographic Information Science,* 15(4): 415-437.

Cukier, R. I., C. M. Fortuin, K. E. Shuler, A. G. Petschek, and J. H. Schaibly (1973). Study of the sensitivity of coupled reaction system to uncertainties in rate coefficients - I: Theory. *Journal of Chemical Physics*, 59: 3873-3878.

Deng, W., and X. Kang (2003). Parametric study on vehicle-trailer dynamics for stability control. *SAE Transactions, Journal of Passenger Cars*, 411-1419.

Deif, A. S. (1986). Sensitivity analysis in linear systems. *Springer-Verlag*, Berlin, Heidelberg.

Eberhard, P., W. Schiehlen; and J. Sierts (2007). Sensitivity analysis of inertial parameters in multibody dynamics simulations. *Twelfth IFToMM World Congress*, Besancon, France, June 18-21.

Ellison, S. L. R., M. Rosslein, and A. Williams (2000). Quantifying Uncertainty in Analytical Measurement, *EURACHEM / CITAC Guide CG 4*.

Fales, R. (2004). Robust control design for an electrohydraulic wheel loader system with a human-in-the-loop assessment in virtual environment. *PhD dissertation*, Iowa State University.

Feng, L., Y. He Y. Bao, and H. Fang (2005). Development of trajectory model for a tractor-implement system for automated navigation applications. *Instrumentation and Measurement Technology Conference*, Ottawa, Canada, May 17-19.

Grau, C. A. (2002). A parametric study of the lateral dynamics of a nonlinear four-wheel road vehicle. *PhD dissertation*, University of Cincinnati.

Istvan, M. (1999). Introduction to the Monte-Carlo method. Budapest, Hungary: *Akademiai Kiado*.

Jang, J. H., and C. S. Han (1997). The state sensitivity analysis of the front wheel steering vehicle. *KSME International Journal,* 11(6): 595-604.

Karkee, M., and B. L. Steward. 2009. Study of the open and closed loop characteristics of a tractor and a single axle towed implement system. In review. *Journal of Terramechanics.*

Kim, Y. C., K. H. Yun, K. D. Min; Y. S. Byun; and J. K. Mok (2007). A lateral dynamic model of an all wheel steering bimodal vehicle. *International Conference on Control, Automation and Systems*, Seoul, Korea, Oct. 17-20.

Krick, G (1973). Behaviour of tyres driven in soft ground with side slip. *Journal of Terramechanics*, 9(4): 9-30.

Kioutsioukis, I., S. Tarantola; A. Saltelli; and D. Gatelli (2004). Uncertainty and global sensitivity analysis of road transport emission estimates. *Atmospheric Environment*, 38: 6609-6620.

Kucherenko, S., M. Rodriguez-Fernandez; C. Pantelides; N.Shah (2009). Monte Carlo evaluation of derivative-based global sensitivity measures. *Reliability Engineering and System Safety,* article in press.

McRae, G. J., J. W. Tilden, and J. H. Seinfield (1982). Global sensitivity analysis-a computational implementation of the Fourier amplitude sensitivity test (FAST). *Computational Chemical Engineering*, 6: 15-25.

Metz, L. D. (1993). Dynamics of four-wheel-steer off-highway vehicles. *SAE Paper No. 930765.* Warrendale, PA: SAE.

Morris, M. D. (1991). Factorial sampling plan for preliminary computational experiments. *Technometrics,* 33: 161-174.

Park, T. J., C. S. Han, and J. H. Jang (2003). Dynamic sensitivity analysis for the pantograph of a high-speed rail vehicle. *Journal of Sound and Vibration*, 266: 235-260.

Raheman, H., and R. Singh (2004). Steering forces on undriven tractor wheel. *Journal of Terramechanics,* 40: 161-178.

Rodriguez-Fernandez, M., and R. Banga (2009). Global sensitivity analysis of a biochemical pathway model. *Advances in Soft Computing, Springer-Verlag,* Berlin, Heidelberg.

Ruta, P., Z. Wojcicki (2003). Sensitivity analysis applied to a dynamic railroad model. *Journal of Sound and Vibration*, 266: 1-13.

Saltelli, A., S. Tarantola, and K. Chan (1999): A quantitative model-independent method for global sensitivity analysis of model output. *Technometrics,* 41(1): 39-56.

Schwanghart, H (1968). Lateral forces of steered tyres in loose soil. Journal of Terramechanics, 5(1): 9-29.

Schwanghart, H., and K. Rott (1984). The influence of the tire tread on the rolling resistance and steering forces on undriven wheels. *In Proc. 8th International Conference of the Society of Terrain Vehicle Systems,* 855-888. Cambridge, UK: ISTVS.

Sobol, I. M. (1993). Sensitivity estimates for nonlinear mathematical models. *Mathematical Modeling and Computational Experiment*, 1: 407-414.

Sobol, I. M. (2001). Global sensitivity indices for nonlinear mathematical models and their Monte Carlo estimates. *Mathematics and Computer Simulations*, 55: 271-280.

Xu, C., and G. Gertner (2007). Extending a global sensitivity analysis technique to models with correlated parameters. *Computational Statistics and Data Analysis*, 51: 5579-5590.

Wittwer, J. W. (2009). Monte Carlo Simulation Basics. Available at http://vertex42.com/ExcelArticles/mc/MonteCarloSimulation.html, accessed: 7/1/2009.

Wong, J. Y. (2001). Theory of ground vehicles. *John Wiley & Sons Ltd*, New York, N.Y., USA.

CHAPTER 7. PARAMETER ESTIMATION AND VALIDATION OF A TRACTOR AND SINGLE AXLE TOWED IMPLEMENT DYNAMIC SYSTEM MODEL

A paper to be submitted to *the Transactions of the ASABE*

Manoj Karkee, Brian L. Steward

Abstract

Developing models and estimating model parameters for a tractor and towed implement system is important for rapid development and improvement of precision implement guidance system, which is essential to take the optimum benefit from the agricultural automation technologies. Several field experiments were conducted to collect tractor and single axle grain cart trajectory data with various steering angle inputs. Three different replicates of the experimental trajectories were collected with each of the step, random and chirp steering inputs. The data was collected at 4.5 m/s forward velocity in two different fields. The experimental data and a prediction error minimization method were used to estimate cornering stiffness and relaxation length parameters of a dynamic system model and validate the time and frequency responses. The parameter estimation process was repeated with different replicates of the experimental data, and the individual estimates were combined using a weighted averaging method. The dynamic model with tire relaxation length dynamics and experimentally identified parameters represented the system responses with reasonable accuracy. With the different combinations two individual parameter

estimations, the tractor and implement CG trajectory calibration RMSEs varied from 0.05 m to 1.12 m. The validation RMSEs with the same parameter combinations varied from 0.05 m to 1.34 m. The model-based frequency responses also closely matched with the experimental frequency responses.

Keywords: implement guidance, system identification, parameter estimation, prediction error minimization, model validation

7.1 Introduction

Increased and sustained agricultural productivity is critical to meet the globally increasing demands for food and energy. Automation of agricultural machinery is one way to improve the efficiency and productivity of various field operations such as tillage, planting, pest control, nutrient management, and harvesting. Off-road vehicle automation technology has been studied and developed for several decades and has been commercialized in the past several years. However, the technology has been applied primarily to the agricultural tractors and combines. For automatic guidance of agricultural equipments to be widely acceptable in farm applications, its capability must be extended to field implements. Vehicle system models are very important in developing guidance controllers as mechatronic engineers are increasingly relying on model-based controller design. In addition, vehicle system models are used in virtual prototyping, real-time simulation, and hardware-and-operator-in-the-loop studies, all of which have the potential to decrease the product development time and cost (Cremer et al., 1996; Sastry and Boyd, 1998; Schulz et al., 1998; Fales et al., 2005; Antonya and Talaba, 2007; Howard and Vance, 2007; Karkee and Steward, 2009a).

Various tractor and towed implement models have been proposed in the literature for both on-road (Chen and Tomizuki, 1995; Deng and Kang, 2003; Kim et al., 2007) and off-road (Feng et al., 2005; Karkee and Steward, 2009a) operations. Chen and Tomizuka (1995) developed a nine degree of freedom non-linear model of an articulated highway vehicle using Lagrange's formulation. Linear analysis was performed to simplify the model for tracking controller design. Deng and Kang (2003) developed an all wheel drive vehicle-trailer dynamic bicycle model and used the model for vehicle stability analysis and control for on-road operations. Kim et al. (2003) developed a nonlinear as well as a linearized lateral dynamics model for a bimodal highway vehicle. For off-road applications, researchers have developed tractor and towed implement models with varying complexities. O'Connor et al. (1996), O'Connor (1997), Bell (1997) and Karkee et al. (2007) developed and used a kinematic model to design an automatic guidance controller. Feng et al. (2005) developed a bicycle model for a tractor and single axle towed implement system using the hitch point as a reference point. Karkee and Steward (2009a) developed a similar model using tractor and implement CGs as reference points. They also added tire relaxation length and steering unit dynamics to the model.

It is essential to test the accuracy of these analytical models in representing the physical system. Some effort has gone into validating these models. Hingwe et al. (2002) performed experimental spectral analysis for on-road operations in the forward velocity range from 9 m/s (20 mph) to 27 m/s (60 mph). In off-road applications, it is important to study the accuracy of these models in the velocity range up to ~8 m/s (Stombaugh et al., 1999). Feng et al. (2005) performed off-road experimental studies to validate a dynamic tractor and implement bicycle model over a limited range of forward velocities from 0.5 m/s

to 1.7 m/s. They found that the bicycle dynamic model-based trajectories may represent the actual trajectories of a tractor and towed implement system reasonably accurately achieving a RMSE as low as 0.01 m. The work also lacked frequency response analysis, which is useful for understanding the model accuracy over a range of input frequencies.

To accurately simulate the dynamics of a physical system, the dominant dynamics of the system must be represented in the model mathematics, and model parameters must be estimated to match with those of the physical system. In this regard, accuracy in both mathematical representation and parameter estimates play a collective role in determining the accuracy of the model-based responses. Agricultural vehicles and implements must be operated in a semi-controlled environment as compared with the controlled environment associated with a factory in a manufacturing context. This environment is highly variable along both temporal and spatial dimensions (Scarlett, 2001; Hall and Lima, 2001). Spatially, the environment varies in terms of farm relief, terrain conditions, soil type and soil conditions (Katupitiya and Eaton, 2008; Metz, 1993). Temporally, soil and terrain conditions can vary substantially depending on the history of weather and farming activities. The tractor and towed implement models developed in the literature contain various soil-tire parameters that are varying and difficult to measure accurately in the field. The inaccuracies in these parameters will affect the accuracy of the model-based responses as the responses are sensitive to these model parameters (Karkee and Steward, 2009b).

The trajectory of an off-road vehicle system depends on the lateral tire forces generated at the tire-soil interface, which is affected by the physical interactions at this interface governed by the phenomena such as tire soil friction, soil lateral deformation and soil sinkage (Metz, 1993). Because these phenomena depend highly on soil parameters such

as internal friction angle, cohesion, cone index, and tire-soil friction, off-road vehicle responses will vary spatially and temporally with different soil types (eg. clay, sand or loam), soil condition (e.g. density and moisture content), and soil surface cover (eg. bare soil, vegetation or stover) (Crolla and El-Razaz, 1987; Metz, 1993). The responses also vary with variation in tire deformation, which depends on tire construction, size, inflation pressure and normal load (Fig. 7.1) (Schwanghart, 1968; Krick, 1973; Schwanghart and Rott, 1984; Crolla and El-Razaz, 1987, Gillespie, 1992; Wong, 2001; Raheman and Singh, 2004).

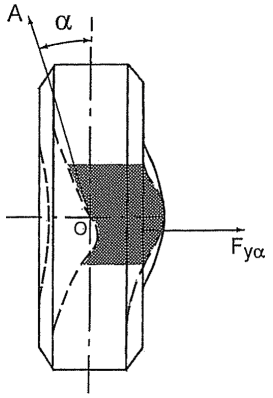

Fig. 7.1: Behavior of a tire subjected to a side force. The top view of the tire shows how a vehicle tire deforms under the application of a side force (Crolla and El-Razaz, 1987; Wong, 2001).

It may be difficult to estimate these variables accurately, and it is also difficult to find a widely accepted model to relate these variables to the tire lateral force. The cornering stiffness coefficient, which is the slope of the lateral tire force as a function of side slip angle at zero side slip, is the parameter often used to represent the combined effect of these variables (Metz, 1993) when the side slip angle is relatively small. Because soil-tire parameters are uncertain, varying, and/or inaccurate, the cornering stiffness parameter also tends to be varying and inaccurate. Vehicle tire relaxation length is often used to characterize

a first order lag required for the lateral force to build up. It is another parameter that could be varying and inaccurate (Rajamani, 2006; Bevly et al., 2002). These soil-tire parameters have to be estimated accurately to simulate vehicle steering dynamics reasonably accurately.

The overall goal of this work was to investigate how well estimated soil-tire parameters of a tractor and single axle towed implement dynamic system model could be used to accurately simulate experimental trajectory data collected with current commercial automatic guidance sensors. The specific objectives were to:

- investigate a method for estimating cornering stiffness and relaxation length parameters of a tractor and single axle towed implement steering dynamic model from experimental data and
- assess the model accuracy using the trajectory and frequency responses of the system

7.2 Materials and Methods

A field experiment was conducted to collect tractor and single axle grain cart trajectory data with various steering angle inputs at 4.5 m/s forward velocity. Based on the experimental data, soil-tire parameters of a tractor and single axle towed implement dynamic bicycle model were estimated using a parameter identification method. A weighted averaging method was used to improve the robustness and certainty of the estimated parameters when multiple sets of experimental data were available. The time and frequency responses of the model with estimated parameters were compared with the experimental responses to assess the model accuracy. A single axle grain cart was used as the towed implement because it represented the general behavior of a towed implement while offering a well defined system to be modeled. The study of this system will be important because various emerging

automation techniques such as coordinated guidance and autonomous guidance will need to incorporate knowledge of tractor and grain cart systems.

7.2.1 Field Data Collection

Tractor and towed implement trajectory data was collected on Sep 19, 2008 in the ISU Agronomy and Agricultural Engineering Research Center (AAERC) located about eight miles west of the ISU central campus. The experimental data was collected using commercially available general purpose GPS receivers (StarFire iTC, Deere and Co., Moline, IL), roll angle compensators, yaw-rate sensors and an integrated wheel angle sensor so that no special instrumentation was required. The field was planted to oats during the prior growing season and was harvested before the tests. A MFWD tractor (model 7930, Deere and Co., Moline, IL) and a single axle 18 m^3 (500 bu) grain cart (model 500, Alliance Product Group, Kalida, OH) were used in the experiment (Fig. 7.2).

Fig. 7.2: An experimental system with a John Deere 7930 tractor and Alliance Product Group Parker grain cart. Two RTK GPS receivers were mounted on the tractor and two were mounted on the implement.

Three types of inputs namely, step and random signals were applied to capture the responses over a wide range of input frequencies (Table 7.1). The experimental data

collection was repeated for three to five times with each input type whenever possible. These replicates or trials were completely randomized to avoid any systematic differences among the trials. The steering angle was less than 10° so that the small angle assumptions used in the vehicle model development would hold at typical farm velocities (<8.0 m/s). Data collection was performed at 4.5 m/s forward velocity, which was the highest possible velocity to safely operate the equipment on the uneven ground surface in the field. The trajectories were long enough to include both transient and steady state responses with both positive and negative steering angle inputs.

Table 7.1: Design of the experiments for the field data collection. The output variables recorded were the same in each replicate.

Input (-10°< Steering Angle <10°)	Replicate	Outputs
Step	1	-Steering Angle -Latitude, Longitude, Roll Angle, Heading Angle, Speed and Yaw-rate from Tractor Front, Tractor Rear, Implement Front and Implement Rear StarFire iTC units.
	2	
	3	
Chirp	1	
	2	
	3	
Random	1	
	2	
	3	

An RTK GPS base station was set up at the farm about 100 m away from the test field. Two roaming RTK GPS receivers were mounted in the front and back of the tractor and two more units were mounted in the front and back of the implement. The GPS receivers and the front wheel angle sensor were connected to a data collection computer through the tractor's implement bus. Various CAN messages such as latitude, longitude, compass

bearing, pitch angle, roll angle, forward velocity and yaw rate were logged at 5 Hz and the steering angle was logged at 50 Hz. Inertial and geometric parameters of the vehicle system were also measured (Table 7.2). Initial values of the cornering stiffness and relaxation length parameters were estimated based on the work of Schwanghart and Rott (1984), Metz (1993) and Bevly et al. (2002).

Table 7.2: Dynamic bicycle model parameters for the JD 7930 tractor and Parker 500 grain cart system.

	Tractor		Implement
Parameters	Nominal Values	Parameters	Nominal Values
a	1.7 m	d	3.62 m
b	1.2 m	e	0.1 m
c	2.1 m		
m^t	9391 kg	m^i	2127 kg
I_z^t	35709 kg-m^2	I_z^i	6402 kg-m^2
$C_{\alpha f}^t$	220 KN/rad*		
$C_{\alpha r}^t$	486 KN/rad*	$C_{\alpha r}^i$	167 KN/rad*
σ_f^t	1.1 m**	σ_r^i	1.1 m**
σ_r^t	1.5 m**		

**Values based on the work of Schwanghart and Rott (1984) and Metz (1993)*

***Values based on the work of Bevly et al. (2002)*

An additional field test was conducted on July 2, 2009 in another field located also at the ISU AAERC to perform the parameter identification method with the trajectory data collected with different soil type and condition. The same experimental design used in the first set of data collection was used in this data collection too. Based on the qualitative assessment, the soil moisture content in the new field was lower than that in the previous

field. The dry weight-based soil moisture content in this new field varied from 10% to 21% at five randomly selected locations around the test field and soil cone index varied from 450 KPa to 800 KPa at the same locations. The field was planted to alfalfa three growing seasons before the experiments were performed and had not been tilled since the season when it was planted to alfalfa. The field where the first set of data was collected will be called *first field,* and this new field will be called *second field* in the following text.

The GPS units used to collect the experimental data were mounted in the front and back of the tractor cab and the front and back of the grain cart. These RTK GPS receivers had a positional accuracy of 2.5 cm. Because the vehicle model discussed in Section 7.2.2 used the tractor and implement CG locations as the reference points, the tractor and implement CG positions in the world coordinate system were calculated using the GPS-unit positions in the world coordinate and vehicle coordinate systems, and the tractor and implement heading angle. The tractor and implement heading angles were calculated using the position of the front and rear GPS units instead of directly using the individual GPS compass bearing, which helped eliminate issues of drift in the vehicle attitude measurement (Ryu, 2004). For other variables such as vehicle forward velocity and yaw-rate, an average of the front and rear GPS unit-based measurements was used as the final measurement.

7.2.2 Vehicle Model

A tractor and single axle towed implement dynamic model was needed to estimate the soil-tire parameters of the system. Among the three models studied by Karkee and Steward (2009a), a dynamic bicycle model with tire relaxation length dynamics represented the system most accurately. In this work, their dynamic model was used to estimate the three tire cornering stiffness parameters and three tire relaxation length parameters. Common vehicle

dynamics symbols were used to describe the dynamics of the system (for notation, see the list of the variables). The following assumptions were made in developing the model:

- A "bicycle" approach was used meaning that the lateral forces in the left and right wheels were assumed to be equal and summed together.
- Longitudinal forces due to traction and rolling resistance were neglected since small steering angle operations will limit interaction with lateral forces.
- Roll, pitch and vertical dynamics were neglected assuming that the ground surface is flat, forward velocity is small and steering angle is small.
- The relationship between lateral tire force and tire side slip angle was assumed to be linear, which would hold for the small steering angles and low forward velocity operations.

This model is described by Eqs. 1 to 8:

$$\left(m^t + m^i\right)\dot{v}_c^t - m^i c\dot{\gamma}^t - m^i d\dot{\gamma}^i = -(m^i + m^t)u_c^t\gamma^t - C_{\alpha,f}^t\alpha_f^t - C_{\alpha,r}^t\alpha_r^t - C_{\alpha,r}^i\alpha_r^i \tag{7.1}$$

$$\left(I_z^t + m^i c^2\right)\dot{\gamma}^t - m^i c\dot{v}_c^t + m^i cd\dot{\gamma}^i = m^i cu_c^t\gamma^t - aC_{\alpha,f}^t\alpha_f^t + bC_{\alpha,r}^t\alpha_r^t + cC_{\alpha,r}^i\alpha_r^i \tag{7.2}$$

$$\left(I_z^i + m^i d^2\right)\dot{\gamma}^i - m^i d\dot{v}_c^t + m^i cd\dot{\gamma}^t = m^i du_c^t\gamma^t + (d+e)C_{\alpha,r}^i\alpha_r^i \tag{7.3}$$

$$\dot{\alpha}_f^t = \frac{v_c^t}{\sigma_f^t} + \frac{a\gamma^t}{\sigma_f^t} - \frac{u_c^t}{\sigma_f^t}\delta - \frac{u_c^t}{\sigma_f^t}\alpha_f^t \tag{7.4}$$

$$\dot{\alpha}_r^t = \frac{v_c^t}{\sigma_r^t} - \frac{b\gamma^t}{\sigma_r^t} - \frac{u_c^t}{\sigma_r^t}\alpha_r^t \tag{7.5}$$

$$\dot{\alpha}_r^i = \frac{v_c^t}{\sigma^i} - \frac{c\gamma^t}{\sigma^i} - \frac{(d+e)\gamma^i}{\sigma^i} + \frac{u_c^t}{\sigma^i}\varphi^t - \frac{u_c^t}{\sigma^i}\varphi^i - \frac{u_c^t}{\sigma^i}\alpha_r^i \tag{7.6}$$

$$\dot{\psi}^t = \gamma^t \tag{7.7}$$

$$\dot{\psi}^i = \gamma^i \tag{7.8}$$

Eqs. 1 – 8 can be represented in matrix form as,

$$M\dot{X} = NX + PU \tag{7.9}$$

where,

$X = \begin{bmatrix} v_c^t & \gamma^t & \gamma^i & \alpha_f^t & \alpha_r^t & \alpha_r^i & \varphi^t & \varphi^i \end{bmatrix}^T$ and the input, $U = [\delta]$.

The tractor CG trajectory was calculated as follows.

$$\dot{x}_c^t = u_c^t \cos(\varphi^t) - v_c^t \sin(\varphi^t) \tag{7.10}$$

$$\dot{y}_c^t = u_c^t \sin(\varphi^t) + v_c^t \cos(\varphi^t) \tag{7.11}$$

7.2.3 Parameter Identification

Parameter identification can be used to estimate various model parameters from the experimental data when a mathematical representation of the physical system is available or can be developed from first principles. As mentioned before, the front tire cornering stiffness $C_{\alpha f}^t$, rear-tire cornering stiffness $C_{\alpha r}^t$, implement tire cornering stiffness $C_{\alpha r}^i$, front tire relaxation length σ_f^t, rear tire relaxation length σ_r^t, and implement tire relaxation length σ_f^i were uncertain/varying and also difficult to estimate with direct instrumentation and were estimated in this work using the parameter identification method and the experimental data. Geometric and inertial parameters of the tractor and implement system were considered fixed as they can be known or sensed with reasonable accuracy (Table 7.2).

At first, experimental data was collected and preprocessed (see Section 7.2.1) to prepare the input output dataset required for the parameter identification (Fig. 7.3). Next, a dynamic tractor and single axle towed implement system model was acquired as discussed in Section 7.2.2. This parameter estimation method was based on the assumption that the model

represented the system reasonably accurately, all other parameters were accurate and the steering angle was measured accurately.

With the all six parameters, the parameter identification method would be a complex six-dimensional optimization problem, which had to work with noisy experimental data. To reduce the complexity of the optimization problem, a steady state analysis was first performed to estimate the cornering stiffness parameters. At steady state, the system equations (Eqs. 1 - 8) can be reduced to:

$$-\frac{1}{u_c^t}\left(C_{\alpha,f}^t + C_{\alpha,r}^t + C_{\alpha,r}^i\right)v_c^t - \left(\frac{aC_{\alpha,f}^t}{u_c^t} - \frac{bC_{\alpha,r}^t}{u_c^t} - \frac{cC_{\alpha,r}^i}{u_c^t} - \frac{(d+e)C_{\alpha,r}^i}{u_c^t} + m^i u_c^t + m^t u_c^t\right)\gamma^t \qquad (7.12)$$
$$-C_{\alpha,r}^i\lambda = -C_{\alpha,f}^t\delta$$

$$-\frac{1}{u_c^t}\left(aC_{\alpha,f}^t - bC_{\alpha,r}^t - cC_{\alpha,r}^i\right)v_c^t - \frac{1}{u_c^t}\left(a^2C_{\alpha,f}^t + b^2C_{\alpha,r}^t + c^2C_{\alpha,r}^i + c(d+e)C_{\alpha,r}^i\right)\gamma^t \qquad (7.13)$$
$$-m^i c u_c^{i^2} + cC_{\alpha,r}^i\lambda = -aC_{\alpha,f}^t\delta$$

$$\frac{(d+e)C_{\alpha,r}^i}{u_c^t}v_c^t - \left(\frac{c(d+e)C_{\alpha,r}^i}{u_c^t} + \frac{(d+e)^2C_{\alpha,r}^i}{u_c^t} - m^i du_c^t\right)\gamma^t + (d+e)C_{\alpha,r}^i\lambda = 0 \qquad (7.14)$$

At steady state, the relaxation length parameters dropped out of the system model (Eqs. 12 - 14), which simplified the parameter estimation method by providing a set of simpler algebraic equations with only three unknown parameters; $C_{\alpha,f}^t$, $C_{\alpha,r}^t$ and $C_{\alpha,r}^i$. Steady state tractor yaw-rate, tractor heading and implement heading measurements were used as the output variables in estimating these cornering stiffness parameters. Because yaw-rate and articulation angle (angle between the tractor and the implement) remain constant at steady state, these two outputs were used to define the following objective function:

$$f(\varepsilon_\gamma, \varepsilon_\lambda) = w_r * \varepsilon_\gamma^{\,2} + w_\lambda * \varepsilon_\lambda^{\,2} \qquad (7.15)$$

where, ε_{γ}^{2} = Mean Squared Error (MSE) of yaw-rate given by,

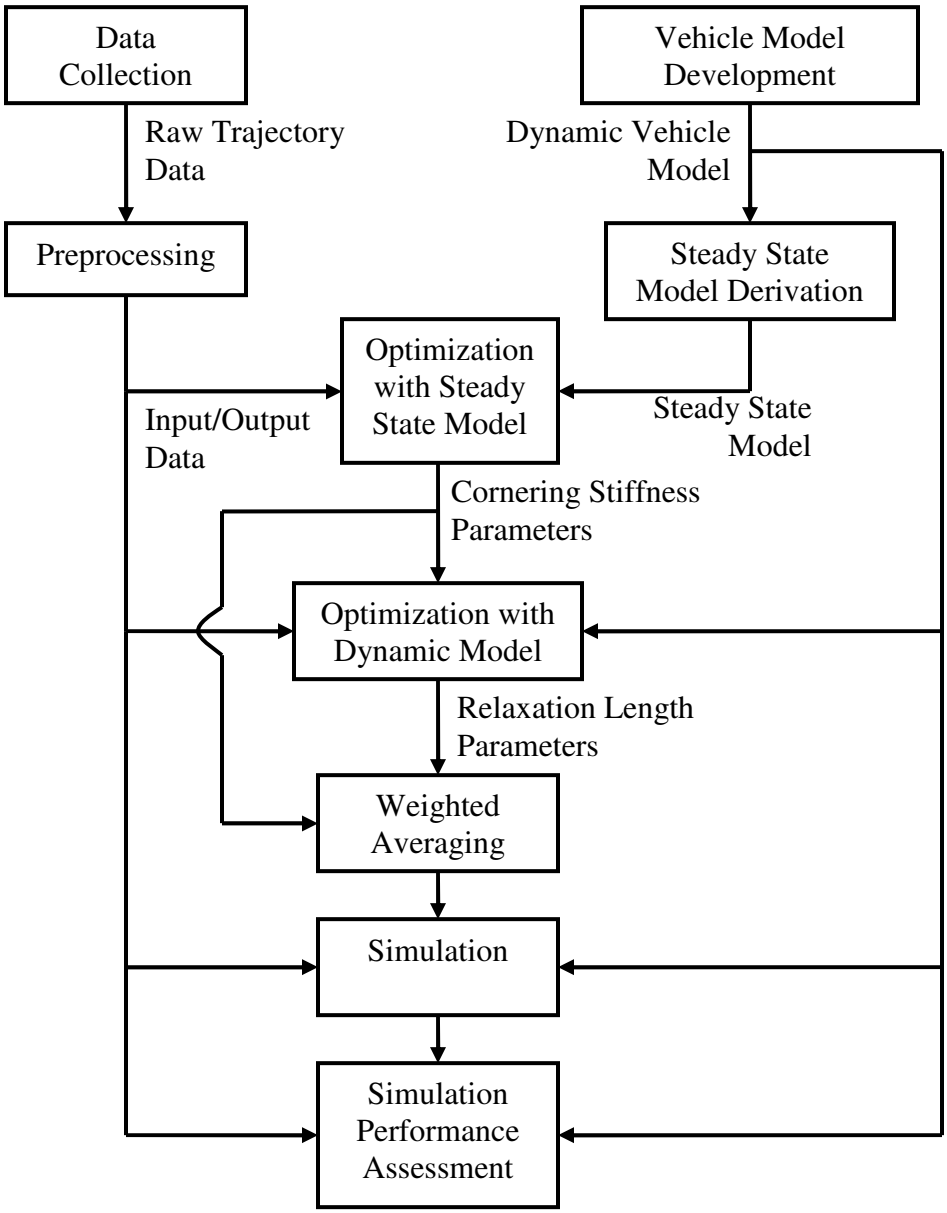

Fig. 7.3: Flowchart of the parameter identification process. Vehicle model and experimental data were supplied to an optimization routine to estimate the tire cornering stiffness and relaxation length parameters of a tractor and single axle grain cart dynamic system model.

$$\varepsilon_{\gamma}^{\ 2} = \frac{1}{N}\sum_{i=1}^{N}\left(\gamma_i^t - \hat{\gamma}_i^t\right)^2 \tag{7.16}$$

w_r = weight for yaw-rate MSE, ε_{λ}^2 = MSE of articulation angle defined similarly to Eq. 7.16, w_{λ} = weight for articulation angle MSE, and N = total number of data points. MSEs were used in the objective function definition so that the higher errors can be penalized more. The measured steering angle was the input to the steady state optimization routine, which used Levenberg-Marquardt search method to minimize the objective function. The MSEs were calculated using the actual outputs, and the model predicted outputs over a period of steady state field operation with step input trajectories collected in both the first and the second fields. Yaw-rate error was had a larger penalty than that of articulation angle (w_r = 4, w_{λ} = 1) because the error in the yaw-rate response will be integrated and propagated to the other model states/outputs.

Once the cornering stiffness parameters were estimated from the steady state model optimization, the second part of dynamic model optimization was also reduced to a three dimensional problem with three relaxation length parameters. The dynamic system model (Eq. 7.1 to Eq. 7.8) was represented as follows to perform this optimization:

$$\dot{x}(t) = Ax(t) + Bu(t) + Kw(t) \tag{7.17}$$

$$y(t) = Cx(t) + Du(t) + w(t) \tag{7.18}$$

where, *w(t)* is the noise model. A noise model was identified along with the relaxation length parameters to minimize the effect of un-modeled dynamics and the system and measurement noise. Steering angle was the input to the system and the tractor and implement yaw-rates and heading angles were the outputs. The Prediction Error Minimization (PEM)

method was used to minimize the objective function (which is the prediction error in this case) given below (Eq. 7.19). Gauss-Newton and Levenberg-Marquardt search methods were used in the PEM. The optimization technique resulted in a mean estimate and the standard deviation of the estimated parameter.

$$\varepsilon(t,\theta_*) = y(t) - \hat{y}(t \mid \theta_*) \tag{7.19}$$

Because of the possible variation in the operating condition and noise on the output data, the estimated parameters and their standard deviations varied with different sets of experimental data. To reduce the uncertainty in the estimates and avoid over-fitting to a particular dataset, multiple sets of experimental data with varying inputs were used in the optimization process. Three individual replicates of experimental trajectory data collected in the first field with step steering angles were used in the parameter estimation and weighted averaging process. Those three trials were called N_1, N_2 and N_3. In the beginning, various combinations of two individual trials were used to average the estimated parameters using the weighted averaging method proposed by Maybeck (1979). Finally, the results from all three individual parameter estimations were combined. In each case, the model accuracy was assessed on all three trials. With this method, two different estimates of a parameter were combined using,

$$\mu = \left(\frac{\sigma_{z_2}^2}{\sigma_{z_1}^2 + \sigma_{z_2}^2} \right) z_1 + \left(\frac{\sigma_{z_1}^2}{\sigma_{z_1}^2 + \sigma_{z_2}^2} \right) z_2 \tag{7.20}$$

and $$\sigma = \sqrt{\left(\frac{\sigma_{z_1}^2 \sigma_{z_2}^2}{\sigma_{z_1}^2 + \sigma_{z_2}^2} \right)} \tag{7.21}$$

where, z_1 and z_2 are the two individual estimates of a single parameter, σ_{z_1} and σ_{z_2} are the corresponding standard deviations, μ is the mean of the combined estimate and σ is the corresponding standard deviation. Eq. 7.21 indicated that the standard deviation of the combined estimate, which can also be viewed as the uncertainty in the estimated parameter (Karkee and Steward, 2009b), would decrease as multiple estimates are combined. The averaging process was repeated with three different estimates of each parameter of interest.

It was essential to assess the accuracy of the model after parameter estimation was performed. Qualitatively, the tractor and implement CG trajectories and tractor and implement yaw-rate frequency responses were compared with the experimental responses to assess the accuracy of the model-based responses in representing the experimental responses. The experimental frequency responses were calculated using the random input trajectory datasets collected in the first field. The accuracy of the model-based responses was assessed quantitatively using the Root Mean Squared Errors (RMSE) of the tractor and implement CG trajectories. The trajectory RMSE was calculated using the error distances between the corresponding points in the simulated and experimental trajectories at each simulation time step for a 30 s simulation time. For the parameters estimated with a single trajectory dataset, other two trajectories were used to calculate the validation RMSEs. When the parameters were combined from the two individual estimations, the third trajectory dataset was used to validate the model performance. Matlab, Simulink, symbolic math toolbox, system identification toolbox and optimization toolbox (The Mathworks Inc., Natick, MA) were used to implement the parameter identification method and perform the model performance analysis discussed in this section.

7.3 Results and Discussions

The experimental data showed a non-zero steering angle even when the tractor and implement system was going straight ahead (with zero yaw-rate). The estimated bias of 0.3° (left skewed) was removed from the recorded steering angle before performing parameter estimation and accuracy assessment studies. The experimental data was also affected by the unwanted signals and noise. Partially, the uneven ground surface formed by row cropping practice might have caused the oscillation in steady state yaw-rate responses. The sensor noise may be another cause of this oscillation. The analytical model did not capture these dynamics as the ground surface was assumed to be plane; that is; vertical, roll and pitch motion were not modeled (See Section 7.2.2). A noise model was identified in the parameter identification process to minimize the effect of these un-modeled dynamics.

The six soil-tire parameters of a tractor and single axle grain cart dynamic system model were estimated (Table 7.3). In the first field with a calibration dataset (second trial, or N_2, with step input), the cornering stiffness parameters were 101 KN/rad, 542 KN/rad and 90KN/rad respectively for the tractor front, tractor rear and implement tires. The same in the second field were 120 KN/rad, 650 KN/rad and 80 KN/rad. Generally, the cornering stiffness parameters in the second field were higher than those in the first field. This result was expected as the soil in the second field was drier and more firm than the first field based on the qualitative assessment of the two fields and recent cultural practices.

The rear tire cornering stiffness was approximately five times higher than the front

and implement tire cornering stiffness parameters. This higher cornering stiffness was caused by the higher normal load (54 kN compared with 38kN in the front) and larger size of the tractor rear tires (Gillespie, 1992). The relaxation length parameters were smaller in the second field than in the first field. The estimated parameter values were substantially different than the initial parameter values, which were calculated based on the work of Schwanghart and Rott (1984), Metz (1993) and Bevly et al. (2002). The differences and variations in soil type, soil condition and tire properties may have caused the differences in the initial and estimated parameters.

Table 7.3: Initial and estimated soil-tire parameters of a tractor and single axle grain cart dynamic system model. The parameter estimation was performed with the data collected in both the first and the second field at 4.5 m/s forward velocity.

Parameter	Initial Values	Estimated Values	
		First Field	Second Field
$C_{\alpha f}^{t}$ (KN/rad)	220	100	120
$C_{\alpha r}^{t}$ (KN/rad)	490	540	650
$C_{\alpha r}^{i}$ (KN/rad)	170	090	100
σ_{f}^{t} (m)	1.0	1.0	0.7
σ_{r}^{t} (m)	1.5	2.6	0.9
σ_{r}^{i} (m)	1.0	1.3	0.5

The simulated tractor and implement CG trajectories with parameters estimated from the calibration dataset closely matched the experimental trajectories (Fig. 7.4 a). The calibration RMSE (RMSEC) between the experimental and simulated tractor CG trajectories for a 30 s of field operation at 4.5 m/s forward velocity was 0.16 m. The same for the

implement CG trajectory was 0.21 m (Table 7.4). Partially, the error was caused by the effect of uneven ground surface, roll dynamics and noise in the experimental data that was not captured by the model. The spatial variation in the soil type and condition might also have caused some differences in the model-based and experimental responses.

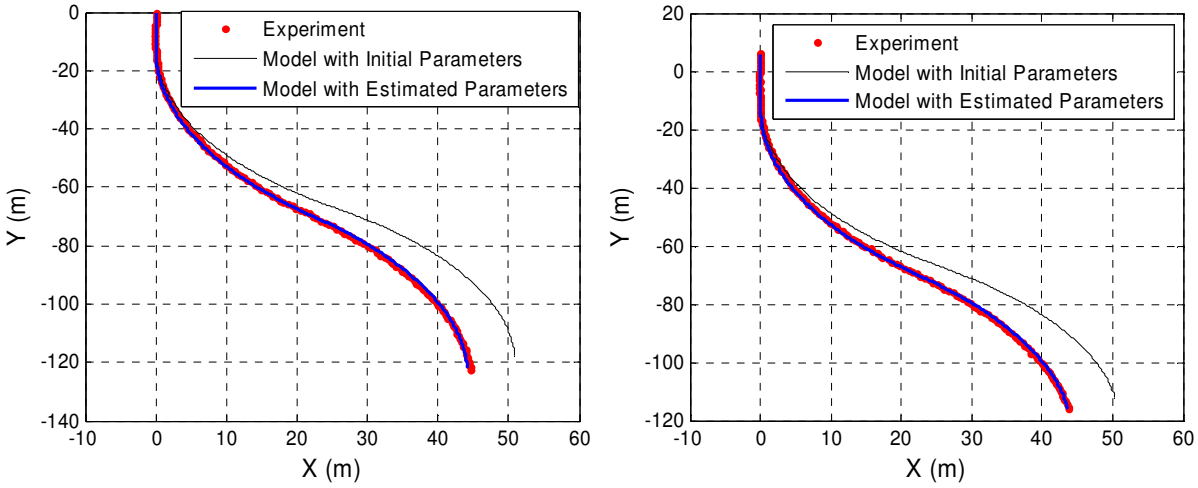

a) Tractor and implement CG trajectories with calibration dataset (N_2)

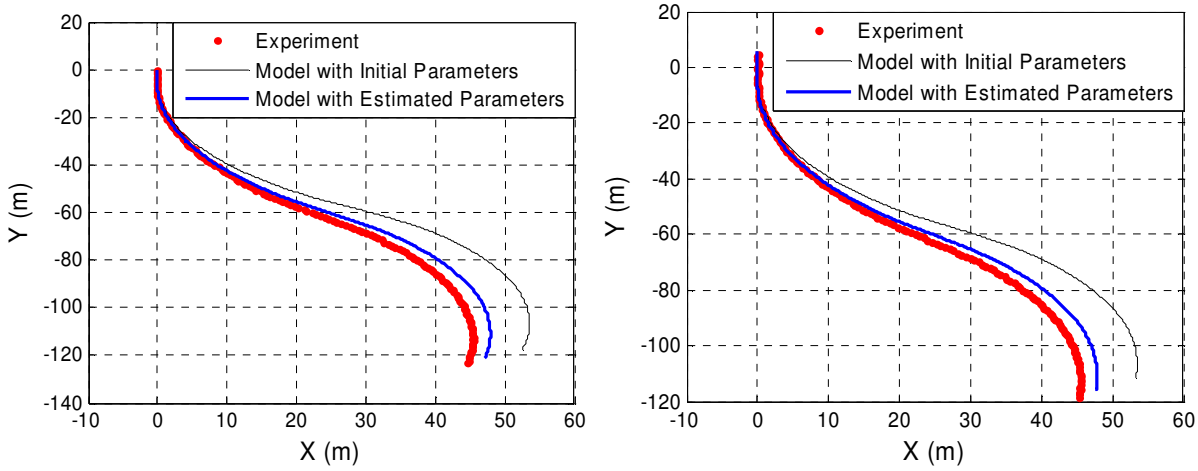

b) Tractor and implement CG trajectories with the first validation dataset (N_1)

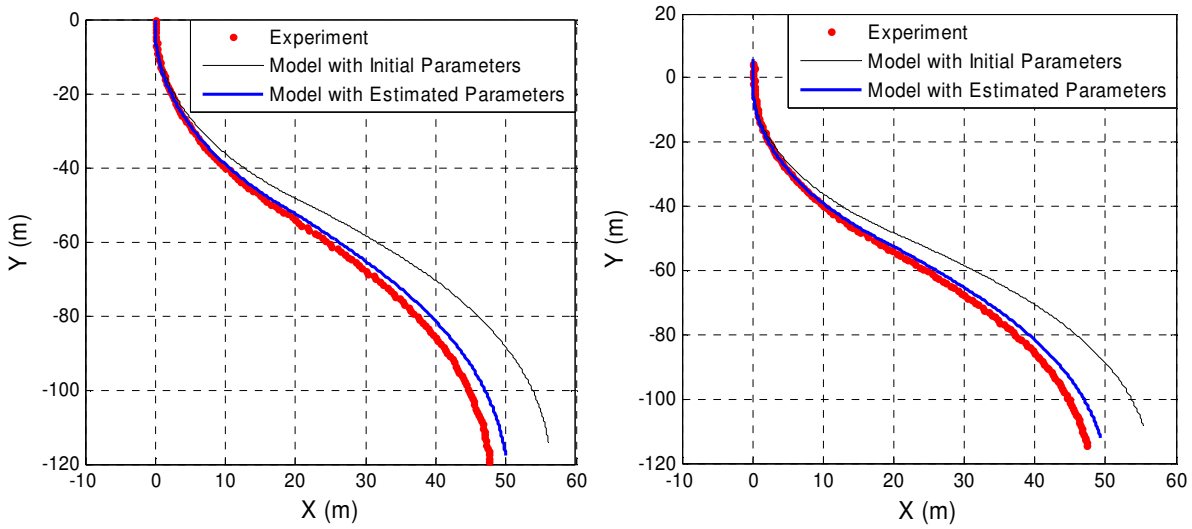

c) Tractor and implement CG trajectories with second validation dataset (N_3)

Fig. 7.4: Experimental and simulated tractor (left) and implement (right) CG trajectories with a) calibration dataset, b) first validation dataset and (c) second validation dataset. The experiment was conducted at 4.5 m/s forward velocity in the first field.

Simulated trajectories with the estimated parameters were also closer to the validation trajectories as compared to the simulated trajectories with initial parameters (Fig. 7.5). However, there was a substantial difference between the simulated and validation trajectories causing larger RMSEs between them. With the first validation dataset (N_1) (Fig. 7.4 b), the RMSEs were 5.68 m and 5.91 m respectively for tractor CG and implement CG trajectories (Table 7.4). The same with the second validation dataset (N_3) (Fig. 7.4 c) were 3.31 m and 4.18 m. This difference was expected as the parameters were optimized to the calibration dataset. Part of the error in both the calibration and validation trajectories could be due to the error in steering angle measurements. The RMSEs of the simulated trajectories with initial parameters were always more than 20.0 m.

Table 7.4: Tractor and implement CG trajectory RMSEs with calibration and validation trajectories. The data was collected in the first field at 4.5 m/s forward velocity.

Trajectory	RMSE (m)					
	Initial Parameters			Estimated Parameters		
	N_1	N_2	N_3	Calibration Dataset (N_2)	Validation Dataset 1 (N_1)	Validation Dataset 2 (N_2)
Tractor CG	24.0	57.0	50.0	0.2	2.0	1.5
Implement CG	37.0	25.0	21.0	0.2	1.9	1.1

The standard deviations of the estimated parameters decreased each time a new estimation was combined to the existing estimation (Table 7.5). With the weighted averaging of the parameters estimated from the combinations of two sets of experimental data, the standard deviation of the cornering stiffness parameters varied from 5% to 7% of the mean parameter estimates. The standard deviation of the tire relaxation length parameters varied from 15% to 52% for the same combinations of the estimated parameters.

When all three parameter estimations were combined, the cornering stiffness parameters had a standard deviation of 5% whereas the same was varying from 6% to 14% in the individual estimates (Table 7.5). The standard deviation of the estimated relaxation length parameters varied from 19% to 80% with individual estimates and varied from 16% to 36% after combining the three estimates. Relaxation length parameters were more difficult to estimate than the cornering stiffness parameters as indicated by the higher variance in these parameters. However, the effect of the uncertainty in relaxation length parameters on the system responses will be minimal as the system was less sensitive to the tire relaxation length parameters than to the tire cornering stiffness parameters (Karkee and Steward, 2009b).

Table 7.5: Weighted averaging of the estimated parameters. Three set of parameters were estimated from three different step input trajectories and combined together using the weighted averaging method. The data was collected in the first field at 4.5 m/s forward velocity.

Parameter	Estimated Parameter Values						
	First Trial (N_1)	Second Trial (N_2)	Third Trial (N_3)	N_1 and N_2 Combined	N1 and N_3 Combined	N_2 and N_3 Combined	N_1, N_2 and N_3 Combined
$C_{\alpha f}^{t}$ (KN/rad)	090±06*	100±10	090±07	090±05	090±05	090±05	090±05
$C_{\alpha r}^{t}$ (KN/rad)	600±40	550±70	560±40	590±40	580±30	550±40	580±30
$C_{\alpha r}^{i}$ (KN/rad)	070±05	090±10	060±05	070±05	059±05	060±05	062±05
σ_f^t (m)	1.5±0.4	1.0±0.8	2.1±.1.0	1.4±0.4	1.6±0.4	1.4±0.6	1.5±0.3
σ_r^t (m)	2.1±0.4	2.6±0.7	1.3±0.5	2.2±0.3	1.8±0.3	1.8±0.4	1.9±0.3
σ_r^i (m)	1.3±0.9	1.7±1.0	0.8±0.6	1.5±0.7	1.0±0.5	1.0±0.5	1.1±0.4

**Standard deviation of the estimates.*

After the weighted averaging of the estimated parameters, all three simulated trajectories closely matched with the experimental trajectories (Table 7.6, Fig. 7.5). Generally, the model-based trajectories represented the experimental trajectories with better accuracy when the parameters were estimated from the combination of the first and the third trials. Because there was more uncertainty in the parameters estimated from the second trial than those estimated from the first and the third trials, the combined parameters tended to fit the responses from first and the third trials more accurately than the responses from the second trial.

For the combinations of two individually estimated parameters, the model-based trajectory RMSEs were generally less than 0.5 m in the case of the first and the third trials

whereas it went up to 1.34 m in the case of second trial. When all three estimations were combined, the tractor CG RMSEs with improved parameters were 0.45 m, 0.83 m and 0.05 m respectively for the first, second and third trials. The same for the implement CG were 0.45, 0.76 m and 0.23 m.

Table 7.6: Tractor and implement CG trajectory RMSEs with different combinations of estimated parameters. Three set of parameters were estimated and combined using the weighted averaging method. The data was collected in the first field at 4.5 m/s velocity.

Parameter Combination	Dataset	Trajectory RMSE (m)	
		Tractor CG	Implement CG
First Trial (N_1) and Second Trial (N_2) Combined	N_1	0.29	0.53
	N_2	1.12	0.93
	N_3	0.05	0.53
First Trial (N_1) and Third Trial (N_3) Combined	N_1	0.19	0.49
	N_2	1.34	1.11
	N_3	0.09	0.61
Second Trial (N_2) and Third Trial (N_3) Combined	N_1	0.84	0.96
	N_2	0.54	0.43
	N_3	0.19	0.33
N_1, N_2 and N_3 Combined	N_1	0.45	0.45
	N_2	0.83	0.76
	N_3	0.05	0.23

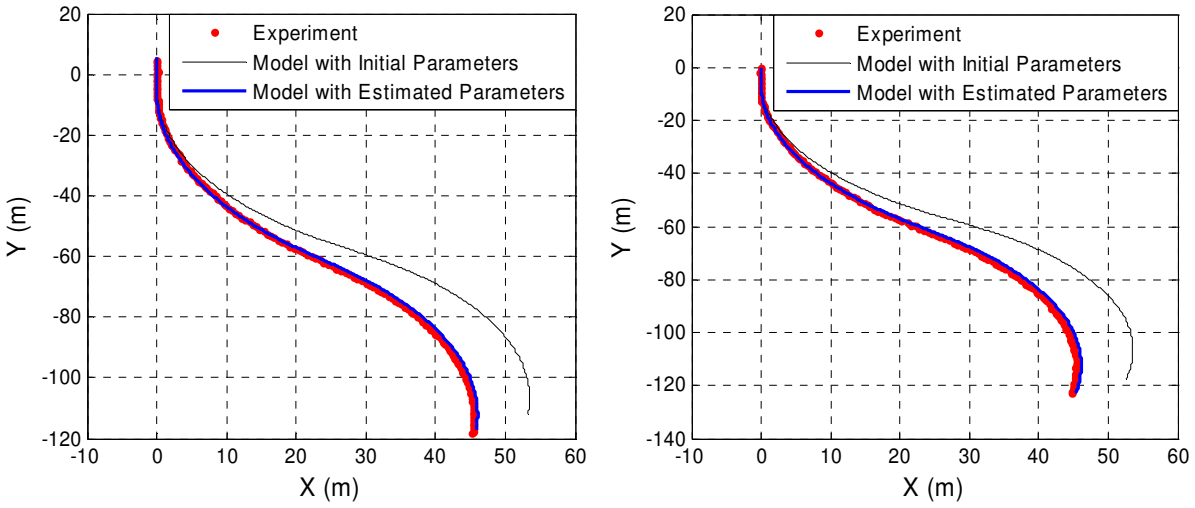

a) Tractor and implement CG trajectories with the first trajectory dataset (N_1)

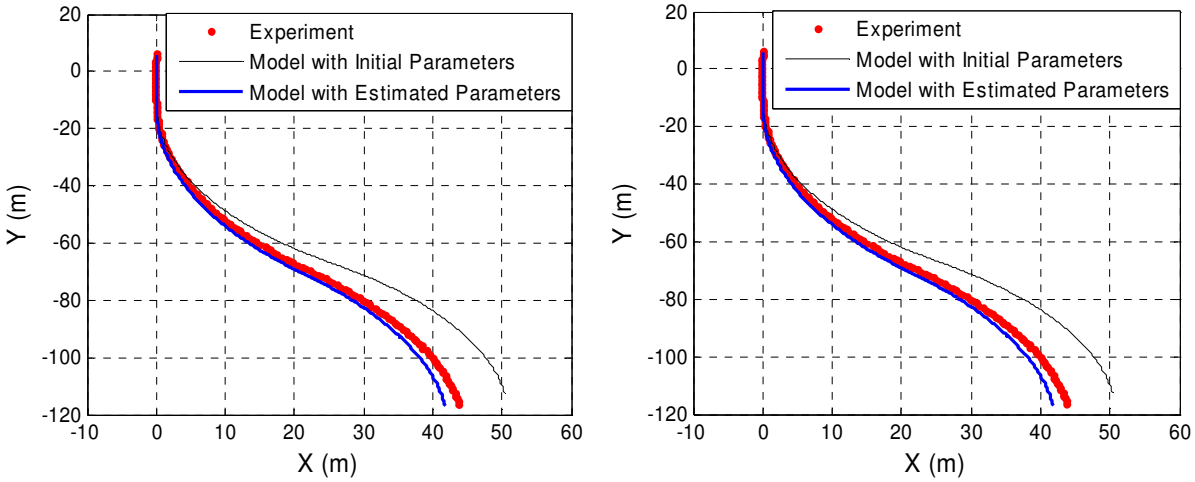

b) Tractor and implement CG trajectories with the second trajectory dataset (N_2)

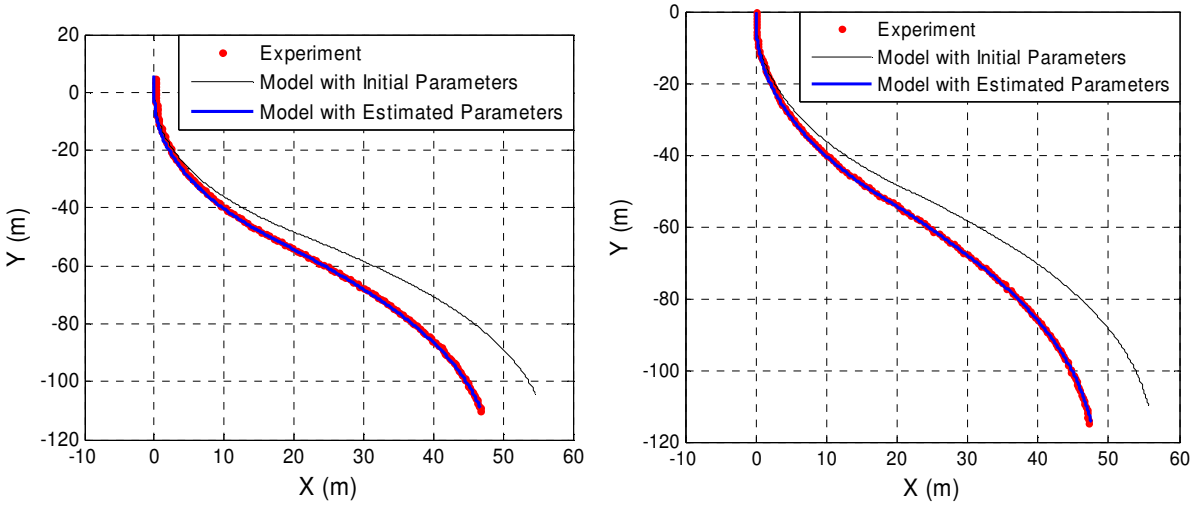

c) Tractor and implement CG trajectories with the third trajectory dataset (N_3)

Fig. 7.5: Experimental and model-based tractor and implement CG trajectories with combined parameters, a) first trial, b) second trial, and c) third trial. The experiment was conducted at 4.5 m/s forward velocity in the first field.

The weighted averaging method used to combine the individual parameter estimates provided a progressive update mechanism; meaning that the combined estimate can be updated as and when the new estimates are available. The approach allowed the robustness

and uncertainty of the parameter estimation to improve over time when repeated measurements were collected on the same field with similar soil and tire condition. This method of improving parameter estimation accuracy over the field operation may help improve the performance of an adaptive guidance controller, which depends on the accuracy of online parameter estimation method (Rekow, 2001).

The model-based frequency responses were calculated with the estimated (after weighted averaging) parameters and initial parameters. The experimental frequency responses were calculated with the random steering experimental data collected at 4.5 m/s forward velocity in the first field. The model-based frequency responses with the estimated parameters represented the experimental responses more accurately than the responses with initial parameters (Fig. 7.6). The steady state gain of the model-based yaw-rate responses with estimated parameters was smaller than the same with initial parameters. This reduced yaw-rate gain was required to match the model-based steady state turning radius to the experimental turning radius of the tractor and single axle grain cart system (Fig. 7.4 and Fig. 7.5).

The underdamped system responses caused by higher order dynamics of the system (Karkee and Steward, 2009a) was apparent in both experimental and model-based frequency responses. However, the cut-off frequency and resonance peak were generally smaller in the model-based responses with the estimated parameters than those with the initial parameters, which matched the experimental responses more closely as can be seen in the phase plots. These frequency responses presented second and sixth order dynamics dominating the tractor and implement yaw-rate responses. The experimental responses beyond ~8 rad/s frequency were noisy, which were caused by the band limited input excitation.

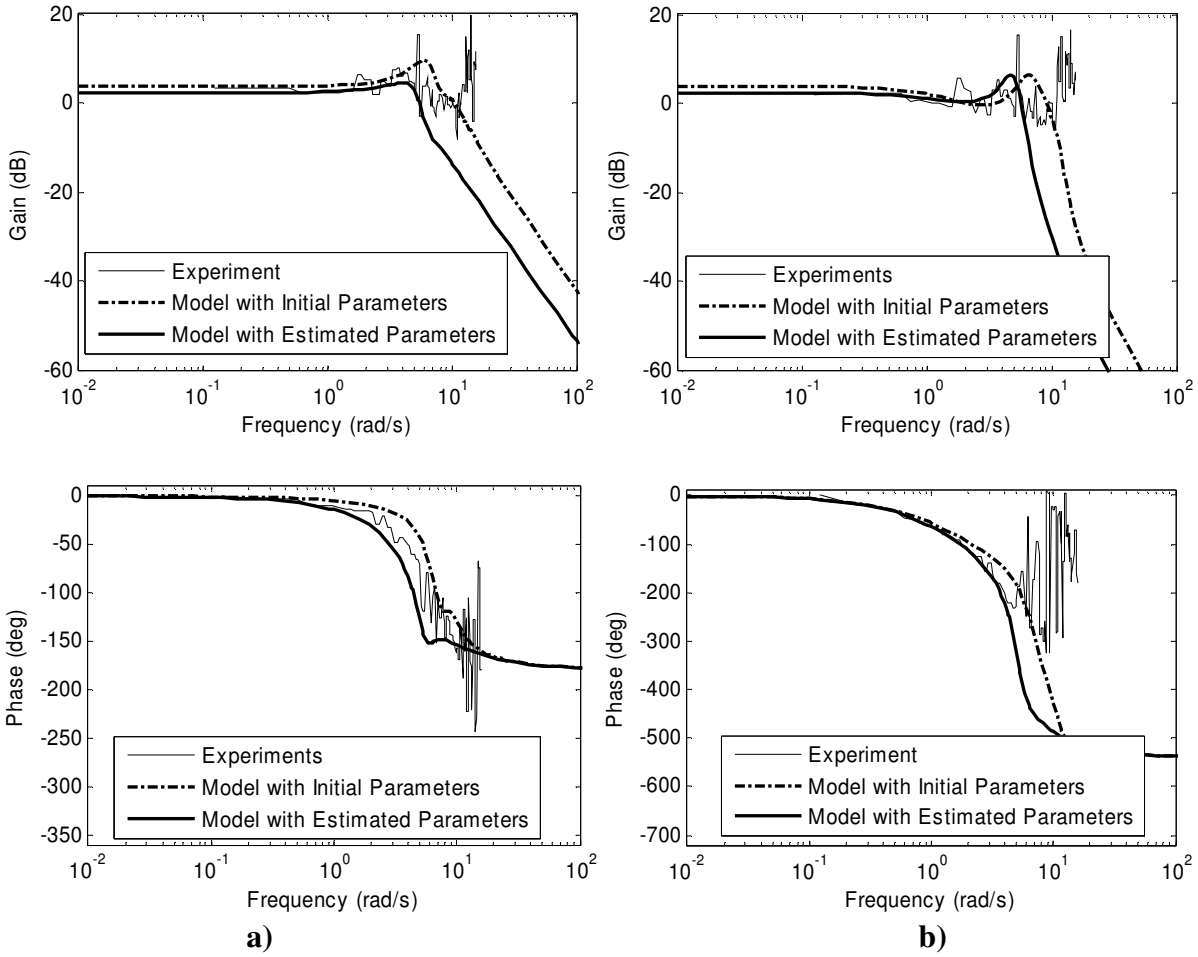

Fig. 7.6: Experimental and model-based frequency responses, a) tractor yaw-rate gain and phase shift, b) implement yaw-rate gain and phase shift. The random input experimental data collected at 4.5 m/s forward velocity in the first field was used in calculating the experimental frequency responses.

7.4 Conclusions

Experimental trajectory data collected with the commercially available RTK GPS receivers was used to estimate cornering stiffness and tire relaxation length parameters of a tractor and single axle towed implement dynamic system model and to validate the model.

From this research, it can be concluded that field level soil-tire interaction parameters of a dynamic off-road vehicle model can be estimated with reasonable accuracy when the soil parameters do not change substantially within the field boundary. This method can also be extended to online parameter estimation to improve the performance of adaptive tractor and towed implement guidance controllers. Specifically, the following conclusions can be made from this work:

- Trajectory data collected with commercially-available automatic guidance sensors can be used to identify tractor and single axle towed implement dynamic system model parameters.
- Assuming field conditions do not change, multiple sets of field trajectory data can be used to improve the robustness and reduce the uncertainty in the estimated parameters. After combining three different estimates, tire cornering stiffness parameter estimations had the standard deviations of about 5% of the mean value whereas the same varied from 16% to 36% of the mean value for the tire relaxation length parameters.
- A dynamic model with tire relaxation length dynamics and the parameters identified from the experimental trajectory data can represent the tractor and single axle towed implement dynamics reasonable accurately. With the different combinations two individual parameter estimations, the tractor and implement CG trajectory calibration RMSEs varied from 0.05 m to 1.12 m. The validation RMSEs with the same parameter combinations varied from 0.05 m to 1.34 m.

Acknowledgements

This research was supported by Hatch Act and State of Iowa funds. Journal paper of the Iowa Agriculture and Home Economics Experiment Station, Ames, Iowa, Project No. 3612.

Notation and List of Variables

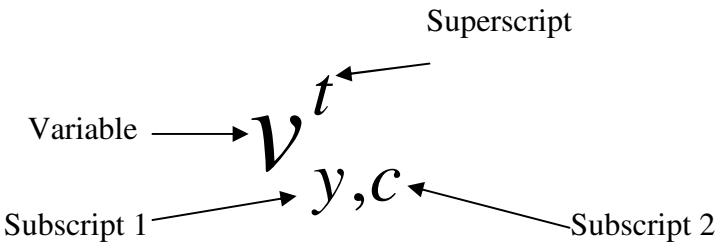

Variable: The variable itself.

Big or bold letter – vector or matrix, small letter – scalar

Superscript: Denotes whether the variable is related to tractor or implement

t – tractor, i – implement

Subscript 1: Specifies the co-ordinate axis the variable corresponds to.

x – x axis, y – y axis, z – z axis

Subscript 2: Specifies the location the variable corresponds to.

f – front tire axle, r – rear tire axle, c – center of gravity, p – toe pin (hitch point)

List of variables

α	side slip angle or the angle between the direction the tire is going and the direction it is facing. The velocity vector to the right of the tire is positive and reverse is negative.
α_0	steady state side slip angle
γ	yaw rate
δ	steering angle
φ	heading angle
λ	angle between tractor heading and implement heading
σ	relaxation length
a	distance between front axle and CG of tractor
b	distance between rear axle and CG of tractor
C_α	cornering stiffness
c	distance between hitch point and CG of tractor
d	distance between hitch point and CG of implement
e	distance between rear axle and CG of implement
F	force
I_z	yaw moment of inertia
m	mass
R	tire radius
u	longitudinal velocity
v	lateral velocity
y	position of CG in y- axis of the world co-ordinate system

References

Antonya, C., and D. Talaba (2007) Design evaluation and modification of mechanical systems in virtual environments. *Virtual Reality,* 11: 275-285

Bell, T. (1997). Precision robotic control of agricultural vehicles on realistic farm trajectory. *PhD Dissertation*, Stanford University.

Bevly, D. M., J. C. Gerdes, and B. W. Parkinson (2002). A new yaw dynamic model for improved high speed control of a farm tractor. *Journal of Dynamic Systems, Measurement, and Control* 124: 659-667.

Chen, C., and M. Tomizuka (1995). Dynamic modeling of tractor-semitrailer vehicles in automated highway systems. *Proc. of American Control Conference,* Seattle, WA, June 21-23.

Cremer, J., J. Kearney, Y. Papelis (1996) Driving simulation: challenges for VR technology. *IEEE Computer Graphics and Applications*, 16(5): 16-20.

Crolla, D. A.; A. S. A. El-Razaz (1987). A review of the combined lateral and longitudinal force generation of tyres on deformable surfaces. *Journal of Terramechanics*, 24(3): 199-225.

Deng, W., and X. Kang (2003). Parametric study on vehicle-trailer dynamics for stability control. *SAE Transactions, Journal of Passenger Cars*: 1411-1419.

Fales, R., E. Spencer, K. Chipperfield, F. Wagner, and A. Kelkar (2005). Modeling and Control of a Wheel Loader With a Human-in-the-Loop Assessment Using Virtual Reality. *Journal of Dynamic Systems, Measurement, and Control* 127: 415-423

Feng, L., Y. He, Y. Bao, and H. Fang (2005). Development of trajectory model for a tractor-implement system for automated navigation applications. *Instrumentation and Measurement Technology Conference*, Ottawa, Canada, May 17-19, .

Gillespie, T. D. (1992). Fundamentals of vehicle dynamics. Warrendale, P. A., USA: *Socienty of Automotive Engineers Inc*.

Hall, S. G. and M. Lima (2001). Problem-solving approaches and philosophies in biological engineering: challenges from technical, social, and ethical arenas. *Transactions of the ASAE*, 44(4): 1037-1041.

Hingwe, P., H. S. Tan, A. K. Packard, and M. Tomizuka (2002). Linear Parameter Varying Controller for Automated Lane Guidance: Experimental Study on Tractor-Trailers *IEEE Transactions on Control Systems Technology*, 10(6): 793-806

Howard, B. M., and J. M. Vance (2007). Desktop haptic virtual assembly using physically based modelling. *Virtual Reality,* 11: 207-215

Karkee, M., B. L. Steward, and S. A. Aziz (2007). Distributed virtual reality assisted steering controller design for Off-road vehicle and implement tracking. *ASABE Paper No. 073006*. ASABE, St. Joseph, MI.

Karkee, M., and B. L. Steward (2009a). Study of the open and closed loop characteristics of a tractor and a single axle towed implement system. In review. *Journal of Terramechanics.*

Karkee, M., and B. L. Steward (2009b). Local and global sensitivity analysis of a tractor and single axle grain cart dynamic system model. In review. *Biosystems Engineering.*

Katupitiya, J., and R. Eaton (2008). Precision autonomous guidance of agricultural vehicles for future autonomous farming. *ASAE Paper # 084687.* ASABE, St. Joseph, MI.

Kim, Y. C, K. H. Yun, K. D. Min, Y. S. Byun, and J. K. Mok (2007). A lateral dynamic model of an all wheel steering bimodal vehicle. *International Conference on Control, Automation and Systems*, Seoul, Korea, Oct. 17-20.

Krick, G. (1973). Behaviour of tyres driven in soft ground with side slip. *Journal of Terramechanics*, 9(4): 9-30.

Maybeck, P. S. (1979). Stochastic models, estimation, and control volume 1. New York, N.Y.: *Academy Press, Inc.*

Metz, L. D. (1993). Dynamics of four-wheel-steer off-highway vehicles. *SAE Paper No. 930765.* Warrendale, PA: SAE.

O'Connor, M., T. Bell, G. Elkaim, and B. Parkinson (1996). Automatic steering of farm vehicles using GPS. *Third International Conference on Precision Agriculture. Minneapolis*, MN, June 23–26.

O'Connor , M. L. (1997). Carrier-phase differential GPS for automatic control of land vehicles. *PhD Dissertation*, Stanford University.

Raheman, H., and R. Singh (2004). Steering forces on undriven tractor wheel. *Journal of Terramechanics*, 40: 161-178.

Rajamani, R. (2006). Vehicle dynamics and control. New York, N.Y., USA: *Springer.*

Reid, J. F., Q. Zhang, N. Noguchi, and M. Dickson (2000). Agricultural automatic guidance research in north America. *Computers and Electronics in Agriculture*, 25: 155-167.

Rekow, A. (2001). System identification, adaptive control and formation driving of farm tractors. *PhD Dissertation,* Stanford University, USA.

Ryu, J. (2004). State and parameter estimation for vehicle dynamics control using GPS. *PhD Dissertation*, Stanford University, USA.

Sastry, L, and D. R. S. Boyd, D. R. S. (1998) Virtual environments for engineering applications. Virtual Reality 3: 235-244

Scarlett, A. J. (2001). Integrated control of agricultural tractors and implements: a review of potential opportunities relating to cultivation and crop establishment. *Computers and Electronics in Agriculture*, 30: 167-191.

Schulz M., T. Reuding, and T. Ertl (1998) Analyzing engineering simulations in a virtual environment. *IEEE Computer Graphics and Applications*, 18(6): 46 – 52

Stombaugh, T. S., E. R. Benson, and J. W. Hummel (1999). Guidance control of agricultural vehicles at high field speeds. *Transactions of ASAE,* 42(2): 537-544.

Schwanghart, H. (1968). Lateral forces of steered tyres in loose soil. *Journal of Terramechanics*, 5(1): 9-29.

Schwanghart, H., and K. Rott (1984). The influence of the tire tread on the rolling resistance and steering forces on undriven wheels. *In Proc. 8th International Conference of the Society of Terrain Vehicle Systems*, 855-888. Cambridge, UK: ISTVS.

Wong, J. Y. (1993). Theory of ground vehicles. New York, N.Y., USA: *John Wiley & Sons Ltd.*

Chapter 8. General Conclusions and Recommendations

8.1 General Conclusions

This research investigated the responses of a tractor and single axle towed implement system through model-based and experimental studies. This work provides a basis for understanding the system behavior and sensitivity of the system to various system parameters at different forward velocities. The work also investigated the performance of a parameter identification method to estimate the soil-tire parameters of the system model.

The first objective of this work was to investigate the simulated steering responses of tractor and single axle towed implement system based on the three models of varying degrees of fidelity namely, a kinematic model, a dynamic model and a dynamic model with tire relaxation length dynamics. System eigenvalues were studied systematically to understand how the model-based responses would vary with different models as the forward velocity varied. The responses with different models were compared in both open and closed loop configurations to understand the similarities and difference among the models in repressing the physical system. In addition, Bode plots were studied to compare the models in frequency domain. Model-based frequency responses were compared with the experimental frequency responses to identify the strengths and weakness of each of the three models. The study was helpful to understand the advantages and limitations of using a particular tractor and implement system model in a specific application.

The second objective of this work was to investigate the dependence of system responses to the variations in the system parameters. Tire cornering stiffness, tire relaxation

length and implement inertial parameters were considered in the analysis as those were the most uncertain and/or varying parameters of the system. The work suggested that there is a need for better estimates of the soil-tire interaction component of off-road vehicle dynamics simulation as it will play an important role in the vehicle responses.

The third objective was to investigate a method to identify system parameters using the experimental trajectory data. The work concluded that a prediction error minimization technique can be used to estimate unknown vehicle model parameters such as tire cornering stiffness and relaxation length parameters reasonably accurately, which could be difficult to measure directly in the field. The method can be used to estimate and improve the model parameters over the successive field operations in near real-time so that the performance of adaptive tractor and implement guidance controller can be improved.

8.2 Recommendations for Future Work

There are several potential areas where this work can be improved and/or expanded. Some of the important areas are listed as follows.

- In this work, most of the model-based studies, sensitivity analysis, and model parameter estimation were carried out with linearized tractor and single axle towed implement model. It is recommended to perform non-linear model simulation and validation so that the applicability of the dynamic model and model-based studies can be extended to large (>10°) steering angle operations. The work can also be extended to study the behaviors of full six degree of freedom tractor and towed implement dynamic models, which is important to extend the model's applicability in sloped terrain.

- The experimental data was collected at 4.5 m/s or lower forward velocities because of the difficulty and potential risk in operating the vehicle system at higher forward velocities. It is recommended to perform the experiments in a field with minimum surface unevenness so that experimental data can be collected at higher forward velocities, which may improve the understanding about the higher order tractor and towed implement system dynamics. The commercially available equipments provided a sampling rate of 5Hz for most of the output signals acquired in the field experiments. It is recommended to explore and use sensors with higher sampling rate to acquire the wider range of frequency content in the output signals.
- Sensitivity analysis performed in this work was based on a dynamic vehicle model. Even though the model was validated using experimental data, it is recommended to validate the results of the sensitivity analysis through extended field experiments. The experimental system responses over a wide range of soil types, soil condition and implement load can be collected so that the analytical and experimental sensitivity results can be compared. It is also recommended to perform the sensitivity analysis in frequency domain to understand the system's dependence on model parameters over a range of input frequencies. Uncertainty analysis can be extended to relate the output uncertainties to the uncertainty in individual system parameters.
- Parameter estimation method was applied to the data collected at 4.5 m/s forward velocity. Further research at different forward velocities is recommended to widen the applicability of the parameter estimation method. The method may also be extended to estimate various other system parameters such as implement mass and moment of inertia which were assumed to be known in this study.